
# UNIVERSIDAD NACIONAL AUTÓNOMA DE MÉXICO

DOCTORADO EN CIENCIAS BIOMÉDICAS

FACULTAD DE MEDICINA

## EFECTO DE LAS LIPOPROTEÍNAS DE BAJA DENSIDAD (LDL) SOBRE LAS SUBPOBLACIONES DE MONOCITOS HUMANOS

TESIS
QUE PARA OPTAR POR EL GRADO DE:

DOCTOR EN CIENCIAS

PRESENTA:

MED. CIR. AARÓN NOÉ MANJARREZ REYNA

DIRECTOR DE TESIS

DR. EUSTACIO GALILEO ESCOBEDO GONZÁLEZ, FACULTAD DE MEDICINA

COMITÉ TUTOR:

DR. GILBERTO VARGAS ALARCÓN, FACULTAD DE MEDICINA

DRA. SONIA ANDREA LEÓN CABRERA, FACULTAD DE ESTUDIOS SUPERIORES IZTACALA

MÉXICO, CDMX, NOVIEMBRE 2022

# UNIVERSIDAD NACIONAL AUTÓNOMA DE MÉXICO

DOCTORADO EN CIENCIAS BIOMÉDICAS

FACULTAD DE MEDICINA

## EFECTO DE LAS LIPOPROTEÍNAS DE BAJA DENSIDAD (LDL) SOBRE LAS SUBPOBLACIONES DE MONOCITOS HUMANOS

TESIS

QUE PARA OPTAR POR EL GRADO DE:

DOCTOR EN CIENCIAS


PRESENTA:

MÉD. CIR. AARÓN NOÉ MANJARREZ REYNA

DIRECTOR DE TESIS

DR. EUSTACIO GALILEO ESCOBEDO GONZÁLEZ, FACULTAD DE MEDICINA

COMITÉ TUTOR:

DR. GILBERTO VARGAS ALARCÓN, FACULTAD DE MEDICINA

DRA. SONIA ANDREA LEÓN CABRERA, FACULTAD DE ESTUDIOS SUPERIORES IZTACALA


MÉXICO, CDMX, NOVIEMBRE 2022

AGRADECIMIENTOS

Agradezco al Programa de Doctorado en Ciencias Biomédicas, Facultad de Medicina, Universidad Nacional Autónoma de México por mi formación académica como Doctor en Ciencias.

Agradezco al Consejo Nacional de Ciencia y Tecnología por el apoyo número 473933, mediante el programa de becas nacionales, con número de becario 626423.

Agradezco de igual manera a los miembros de mi comité tutor conformado por el Dr. Gilberto Vargas Alarcón, la Dra. Sonia Andrea León Cabrera y el Dr. Galileo Escobedo.

*If I have seen further, it is by standing on the shoulders of giants*

*Sir Isaac Newton*

Agradecimientos

Agradezco a mi familia por haberme apoyado en todo momento, en especial a mi padre Moisés QEPD al cual le dedico esta tesis, sin tus consejos y tu apoyo no estaría donde estoy. A mi madre Soledad por estar siempre conmigo y apoyarme perpetuamente. A mis hermanos Samuel, Mauricio gracias por apoyarme, por compartir aventuras y momentos juntos, siempre iremos por más. A mis tías Zoila y Lupita por impulsarme a mejorar, en especial a mi Tía Zoila por ponerme el ejemplo como la primera doctora en la familia, así como apoyarme en mi vida académica y no académica, sin tu apoyo no estaría donde estoy. A mis abuelos *Mel* y qepd *Mamaque, Kino, Mamatere;* estarían muy orgullosos de su nieto y lo que lo logro con apoyo de su familia. A la familia Reyna García; tíos y primos por brindarme su apoyo. A mis padrinos Bernardo, Brisa, Ernesto y Esther, por su apoyo.

A mis amigos. Tobe, Quique, Horacio y Cesar por más años de amistad y viajes también. A Iván, Jhonny y Nydia gracias por escucharme, corregirme y compartir grandes momentos. A Mau García gracias por brindarme tu amistad y tus creaciones Tranceport y Deep Sessions un gran aliado para enfrentar mi examen de candidatura. A Lilo, Phillip, Jessy, Mariana, Tamara y Memo Tafoya ¡qué recuerdos! gracias por escucharme y apoyarme en diferentes etapas en mi formación médica. A Pablito, Andrés y *Pufus* que me distrajeron con momentos de diversión. A mis primos, que más que primos, amigos, *Brozz Stuff* y *Azmeden.* A Eli, tus consejos y apoyo fueron muy importantes para mí en esta etapa.

A mis compañeros de posgrado. A Camilo que más que compañero del doctorado se convirtió en un buen amigo y en un apoyo constante, tu crítica y tu visión me ayudo a finalizar este proyecto y muchos otros más. A Juan Carlos con el que compartí conocimiento y buenos momentos, espero que decida correctamente. Al maestro Jesús que me brido su amistad y apoyo no solo para realizar experimentos de esta tesis y otras si no en la vida. A Yunnuel, Isra, Diana, Marco, Mafer, Fernando, Ana, Salma y Rebeca gracias por ayudarme y enseñarme en esta etapa de mi vida y compartir buenos momentos en el Hospital.

A todos los trabajadores del banco de Sangre del HGM, a los trabajadores de la UME en especial a los del HIPAM y del Laboratorio de Patología experimental. A los trabajadores y colaboradores de la División de Investigación del Hospital General de México. A la Dra Lucia Méndez, por tus asesorías y tu amistad, al Dr Alfonso Olivos qepd, que nos brindó su espacio de trabajo, sus ideas y sobretodo su amistad, Ing Omar Agni por ser la primer persona en la UME que me abrió sus puertas y que cosechamos una amistad muy buena. A los doctores Oscar Perez y A mis tutores Dr. Gilberto Vargas Alarcón, la Dra. Sonia Andrea León Cabrera y el Dr. Galileo Escobedo por invertir su tiempo y hacer de mi un alumno mejor día con día En especial quiero agradecer al Dr. Galileo por darme una visión siempre diferente de las cosas, por apoyarme y acompañarme en mi crecimiento académico a través de estos 12 años, por tu amistad y consejos, gracias.

# ÍNDICE

## CONTENIDO

Índice ..... 1
Lista de abreviaturas ..... 2
Resumen ..... 4
Abstract ..... 5
Introducción ..... 6
Antecedentes ..... 7
Dislipidemia ..... 7
Lipoproteínas de baja densidad ..... 8
LDL nativo y oxidado ..... 12
Subpoblaciones de monocitos humanos ..... 14
Planteamiento del problema ..... 21
Hipótesis ..... 22
Objetivos ..... 23
Objetivo general ..... 23
Objetivos particulares ..... 23
Materiales y métodos ..... 24
Cultivo *in vitro* de monocitos humanos primarios ..... 24
Citometría de flujo para expresión de citocinas y receptores de quimiocinas ..... 25
Modelo con donadores ..... 26
Efectos de LDL sobre LBP e IL-1 beta en subpoblaciones de monocitos en el modelo con donadores ..... 27
Análisis estadístico ..... 28
Resultados ..... 29
Discusión ..... 43
Conclusión ..... 48
Perspectivas ..... 49
Referencias ..... 50
Anexo i: artículos generados durante los estudios de posgrado ..... 56

## LISTA DE ABREVIATURAS

| | |
|---|---|
| ACAT | Acil-CoA colesterol acil transferasa |
| ApoB100 | Apolipoproteina B100 |
| ATP III | Adult Treatment Panel III (Panel de tratamiento para adultos III) |
| CD14 | Cluster of differentiation 14, glicoproteína de membrana de expresada en monocitos/macrófagos |
| CD16 | Cluster of differentiation 16, FcγRIII, receptor tipo III para la fracción Fc de la IgG |
| CM | Monocitos clásicos |
| CCR2 | Receptor de quimiocinas C-C tipo 2, receptor de MCP-1 |
| $CX_3CR1$ | Receptor de quimiocinas C-X, receptor de fractalcina |
| ICAM-1 | Molécula de adhesión intercelular 1 |
| IDL | Lipoproteínas de densidad intermedia |
| IL-1 β | Interleucina 1 beta, citocina proinflamatoria |
| IM | Monocitos Intermedios |
| iPCSK9 | Inhibidores de la proproteína convertasa subtilisina/kexina tipo 9 |
| HF | Hipercolesterolemia familiar |
| HMGCR | 3-hidroxi-3-metilglutaril-CoA reductasa |
| LDL | Lipoproteínas de baja densidad |
| LDLr | Receptor de lipoproteínas de baja densidad |

| | |
|---|---|
| LPS | lipopolisacáridos |
| MCP-1 | Proteína quimioatrayente de monocitos 1 |
| NCEP | National Cholesterol Education Program |
| NCM | Monocitos no clásicos |
| NF-κB | Factor nuclear κB |
| nLDL | Lipoproteínas de baja densidad nativas |
| oxLDL | Lipoproteínas de baja densidad oxidadas |
| PCSK9 | Proproteína convertasa subtilisina/kexina tipo 9 |
| SREBP | Elementos regulatorios de esteroles |
| VCAM-1 | Molécula soluble de adhesión vascular |
| VLDL | Lipoproteínas de muy baja densidad |

## RESUMEN

Evidencia reciente muestra que las lesiones ateroscleróticas son ricas en lipoproteínas de baja densidad oxidadas (LDLox) y lipopolisacáridos (LPS). De manera sinérgica, estás moléculas promueven la acumulación *in situ* de macrófagos productores de moléculas con actividad proinflamatoria y quimiotáctica, como la interleucina (IL)-1 beta, el receptor de quimiocinas C-C tipo 2 (CCR2) y el receptor de quimiocinas CX3C 1 (CX3CR1). En el torrente circulatorio, las lipoproteínas de baja densidad se encuentran mayoritariamente en forma nativa (nLDL), en donde están en contacto con las subpoblaciones de monocitos y podrían alterar el reclutamiento de estas células a las placas ateromatosas para posteriormente diferenciarse en macrófagos. Sin embargo, el efecto de las nLDL en conjunto con el LPS sobre la expresión de IL-1 beta, CCR2 y CX3CR1 en las subpoblaciones de monocitos todavía no ha sido estudiado. Por esta razón, realizamos una estrategia complementaria *in vitro* y un modelo con donadores, en donde primeramente cultivamos células de sangre completa de donantes sanos (n = 20) en presencia o ausencia de 100 μg/ml de nLDL y/o 10 ng/ml de LPS durante 9 horas (h). Los ensayos de citometría de flujo revelaron que el nLDL por sí sólo redujo de forma significativa el porcentaje de monocitos clásicos (CM) y aumentó el porcentaje de monocitos no clásicos (NCM). Además, el nLDL en conjunto con el LPS aumentó de manera significativa el porcentaje de NCM que expresaron IL-1 beta y CCR2. Por el contrario, el número de NCM que expresaron CX3CR1 disminuyó de forma significativa. Para el modelo con donadores, reclutamos 150 participantes y medimos los niveles séricos de LDL ligado a colesterol (LDL-C) para dividir la población de estudio en dos: sujetos con LDL-C normal ≤100 mg/dL (*n* = 65), y donadores con LDL-C >100 mg/dL (*n* = 85). En comparación con el grupo control, los donadores con LDL-C >100 mg/dL mostraron mayores niveles séricos de LPS de manera significativa, que coincidió con un mayor porcentaje de NCM, en los niveles de IL-1 beta y en el índice de riesgo aterogénico II de Castelli. A través de una estrategia que combinó cultivos *in vitro* con estudios en donadores, este trabajo demuestra por primera vez que el nLDL actúa junto con el LPS para alterar el equilibrio de las subpoblaciones de monocitos humanos y su capacidad para producir citocinas inflamatorias y receptores de quimiocinas con funciones cruciales en la aterogénesis.

## ABSTRACT

Increasing evidence has demonstrated that oxidized low-density lipoproteins (oxLDL) and lipopolysaccharide (LPS) enhance accumulation of interleukin (IL)-1 beta-producing macrophages in atherosclerotic lesions. However, the potential synergistic effect of native LDL (nLDL) and LPS on the inflammatory ability and migration pattern of monocyte subpopulations remains elusive and is examined here. In vitro, whole blood cells from healthy donors (n = 20) were incubated with 100 g/mL nLDL, 10 ng/mL LPS, or nLDL + LPS for 9 h. Flow cytometry assays revealed that nLDL significantly decreases the classical monocyte (CM) percentage and increases the non-classical monocyte (NCM) subset. While nLDL + LPS significantly increased the number of NCMs expressing IL-1 beta and the C-C chemokine receptor type 2 (CCR2), the amount of NCMs expressing the CX3C chemokine receptor 1 (CX3CR1) decreased. In the model with patients, patients (n = 85) with serum LDL-cholesterol (LDL-C) >100 mg/dL showed an increase in NCM, IL-1 beta, LPS-binding protein (LBP), and Castelli's atherogenic risk index as compared to controls (n = 65) with optimal LDL-C concentrations (100 mg/dL). This work demonstrates for the first time that nLDL acts in together with LPS to alter the balance of human monocyte subsets and their ability to produce inflammatory cytokines and chemokine receptors with prominent roles in atherogenesis.

## INTRODUCCIÓN

El síndrome metabólico se ha convertido en una entidad de alto impacto en la población mundial, ya que no sólo predispone al desarrollo de enfermedades como *Diabetes Mellitus* tipo 2 o hipertensión, si no que por sí mismo es desencadenante de enfermedad cardiovascular catastrófica e incapacitante (Raúl Carrillo Esper, Martín De Jesús Sánchez Zúñiga, 2006). Uno de los componentes más frecuentes del síndrome metabólico en la población mexicana es la dislipidemia (Olaiz-Fernández G, Rivera-Dommarco J, Shamah-Levy T, Rojas R, Villalpando-Hernández S, Hernández-Avila M, 2006).

La dislipidemia se define como una elevación anormal de los niveles plasmáticos de triglicéridos, colesterol total y lipoproteínas de baja densidad (LDL), así como disminución en los valores de lipoproteínas de alta densidad (HDL) (S. Grundy et al., 2004). De manera particular, diversos estudios han demostrado que los niveles plasmáticos de LDL son un factor de riesgo para el desarrollo de aterosclerosis y de la cardiopatía isquémica asociada con esta condición (S. Grundy et al., 2004).

La aterosclerosis es una forma de inflamación no resolutiva, cuya trascendencia en la enfermedad cardiovascular y metabólica ha sido discutida recientemente (Libby et al., 2014; Viola & Soehnlein, 2015). La hiperinsulinemia está asociada con un aumento de LDL clase B que son partículas pequeñas y densas, y más susceptibles de ser oxidadas (LDLox) y por lo tanto más aterogénicas (Raúl Carrillo Esper, Martín De Jesús Sánchez Zúñiga, 2006). Los niveles elevados de LDL y LDLox están asociados con una alta expresión de moléculas de adhesión inducidas por el factor nuclear kappa B (NF-κB), tales como E-selectina, VCAM-1 e ICAM-1. Estas moléculas pueden mediar la infiltración de monocitos circulantes con capacidad de formar lesiones ateroscleróticas, una vez que se han diferenciado a macrófagos y posteriormente a células espumosas (Gerhardt & Ley, 2015; Hansson, 2005; Jackson et al., 2016; Tall & Yvan-Charvet, 2015; Witztum, 1994). Esta evidencia sugiere que el LDL no sólo es un componente de la dislipidemia, sino que podría jugar un papel crítico como agente inductor de respuestas inflamatorias asociadas con la aterosclerosis.

## ANTECEDENTES

### Dislipidemia

La dislipidemia está caracterizada por concentraciones anormales de lipoproteínas sanguíneas que cursan de manera asintomática y conforman uno de los componentes más frecuentes del síndrome metabólico.

La búsqueda intencionada de la dislipidemia es indispensable para un diagnóstico y tratamiento oportuno, así como para establecer tanto su etiología como el riesgo que confiere a un individuo de sufrir un evento cardiovascular (Consejo de Salubridad General, 2011).

El sobrepeso y la obesidad contribuyen fuertemente al desarrollo de dislipidemias. La pérdida del 5 al 10% del peso basal mejora el perfil de lípidos en sangre e influye favorablemente sobre otros factores de riesgo cardiovascular (Berrington de Gonzalez et al., 2010).

Para establecer el diagnóstico de dislipidemia se toman en cuenta las concentraciones elevadas de colesterol (>200 mg/dl) o de triglicéridos (> 150 mg/dl), así como el nivel bajo de colesterol HDL (< 40 mg/dl en hombres y < 50 mg/dl en mujeres) (Olaiz-Fernández G, Rivera-Dommarco J, Shamah-Levy T, Rojas R, Villalpando-Hernández S, Hernández-Avila M, 2006). La dislipidemia más frecuente en México es la hipoalfalipoproteinemia (colesterol HDL < 40 mg/dl). En todas las encuestas nacionales se ha informado que esta anormalidad afecta a cerca del 60% de los adultos (55.2% en la encuesta más reciente) (Olaiz-Fernández G, Rivera-Dommarco J, Shamah-Levy T, Rojas R, Villalpando-Hernández S, Hernández-Avila M, 2006; Romero-Martínez et al., 2016). La hipoalfalipoproteinemia es más común en los hombres, en el sur del país y se asocia con obesidad, diabetes y consumo de tabaco (Olaiz-Fernández G, Rivera-Dommarco J, Shamah-Levy T, Rojas R, Villalpando-Hernández S, Hernández-Avila M, 2006; Romero-Martínez et al., 2016).

Históricamente, la hipercolesterolemia es el tipo de dislipidemia que ha tenido un mayor aumento en su prevalencia. La frecuencia de hipercolesterolemia creció de 27.1% en 1994 a 43.6% en la actualidad (INSP, Encuesta-nacional-de-salud-1994-ensa-ii, 1994 recurso electr). De acuerdo con datos de la encuesta de salud más reciente, el uso creciente de estatinas se asoció con un decremento del 31% en la prevalencia de hipercolesterolemia en

nuestro país (Olaiz-Fernández G, Rivera-Dommarco J, Shamah-Levy T, Rojas R, Villalpando-Hernández S, Hernández-Avila M, 2006).

En un paciente con síndrome metabólico, la dislipidemia es un problema a gran escala, ya que aumenta el riesgo de desarrollar aterosclerosis subclínica. La aterosclerosis subclínica contribuye de manera importante con el riesgo de presentar un evento cardiovascular en 10 o 15 años. Por lo tanto, en las guías de la ATPIII para el síndrome metabólico, la meta principal es disminuir el nivel de LDL en pacientes dislipidémicos (S. Grundy et al., 2004; S. M. Grundy et al., 2001). La razón de esta meta es debida al efecto sinérgico que existe entre la dislipidemia y la aterosclerosis, mismo que aumenta considerablemente el riesgo de sufrir un evento cardiovascular.

**Lipoproteínas de baja densidad**

El LDL es una lipoproteína que se encarga de transportar colesterol preveniente de la dieta y de síntesis *de novo* a los tejidos periféricos (Michael S. Brown & Goldstein, 1986). El LDL está conformado por un componente proteico y uno lipídico (Figura 1).

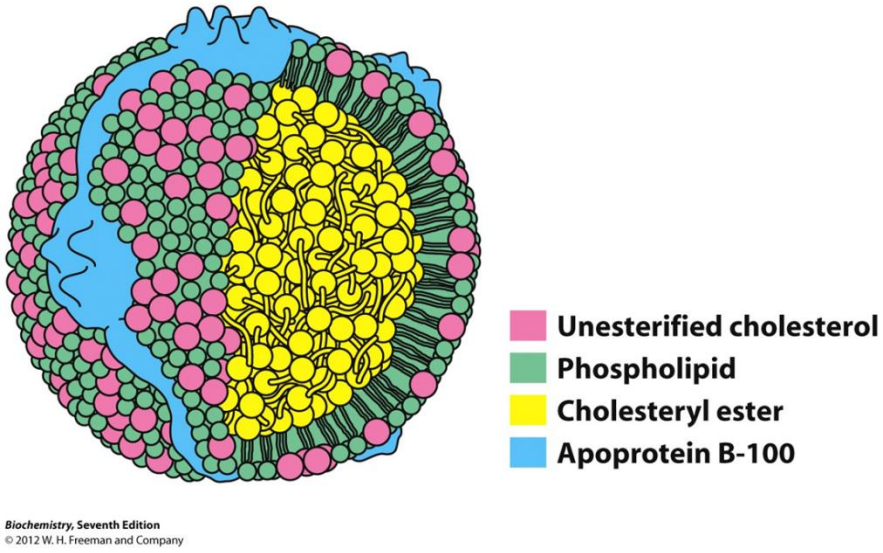


***Figura 1. Conformación de la LDL. Tomada de Biochemestry, seven Edition, 2012. W. H. Freeman and Company***

En azul se observa la apolipoproteína B100 (ApoB100) que constituye el componente proteico. El componente lipídico se encuentra formado principalmente por ésteres de

colesterol que se observan en amarillo; en verde podemos observar los fosfolípidos, mientras que en rosa el colesterol no esterificado. Adicionalmente, la molécula de LDL puede contener triglicéridos residuales.

Cada molécula de LDL solo tiene una partícula de apoB100 ubicada en forma extendida y que cubre la mitad de la superficie del LDL. La ApoB100 es la proteína responsable de la unión con el receptor de LDL (LDLr), a través del dominio C-terminal.

La apoB100 solo se expresa en el hígado y forma parte de las VLDL (lipoproteínas de muy baja densidad), IDL (lipoproteínas de densidad intermedia) y LDL. La apoB100 tiene un peso molecular de 513 KDa y consta de una sola cadena polipeptídica con 4536 residuos de aminoácidos, lo que la convierte en una de las proteínas monoméricas más grandes conocidas en el organismo. Debido a sus características fisicoquímicas, la LDL es muy hidrofóbica y sus porciones anfipáticas son consecuencia de sus escasas hélices alfa. El gen de la apoB está en el brazo corto del cromosoma 2 y tiene 43 kb, con 28 intrones y 29 exones.

Las mutaciones en la apoB100 pueden causar una enfermedad llamada hipercolesterolemia familiar (HF), la cual se trata de una dislipidemia hereditaria en la cual los niveles de LDL se encuentran elevados plasmáticamente. Los pacientes con HF tienen un riesgo mayor de debutar con enfermedades cardiovasculares a edad temprana.

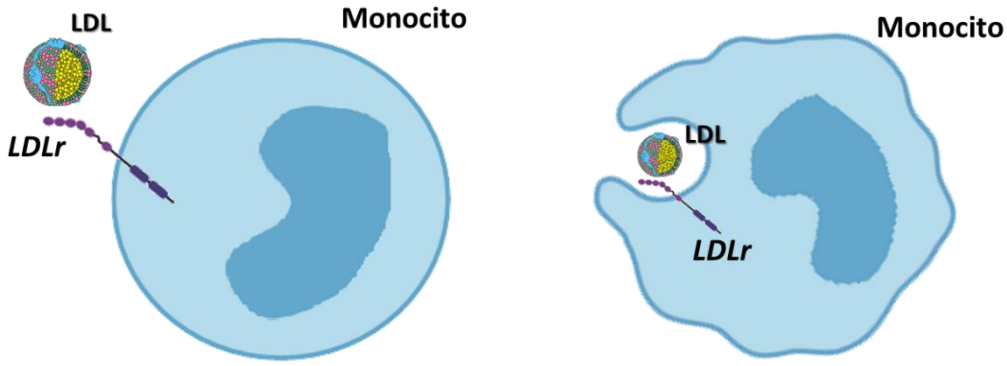


***Figura 2. Los monocitos interactúan e internalizan el LDL a través del LDLr.***

El LDLr es una glicoproteína ubicada en la membrana celular, la cual es encargada de la unión e internalización del LDL. El LDLr fue descrito por primera vez por Goldstein y a Brown en 1985, trabajo por el cual estos investigadores recibieron el premio nobel (M. S. Brown & Goldstein, 1984). El LDLr se expresa en la gran mayoría de las células (Figura 2). El gen del LDLr se encuentra en la región 13.2 del brazo corto del cromosoma 19 (Go & Mani, 2012). A través del LDLr se lleva a cabo el papel regulador del LDL en el metabolismo de los lípidos.

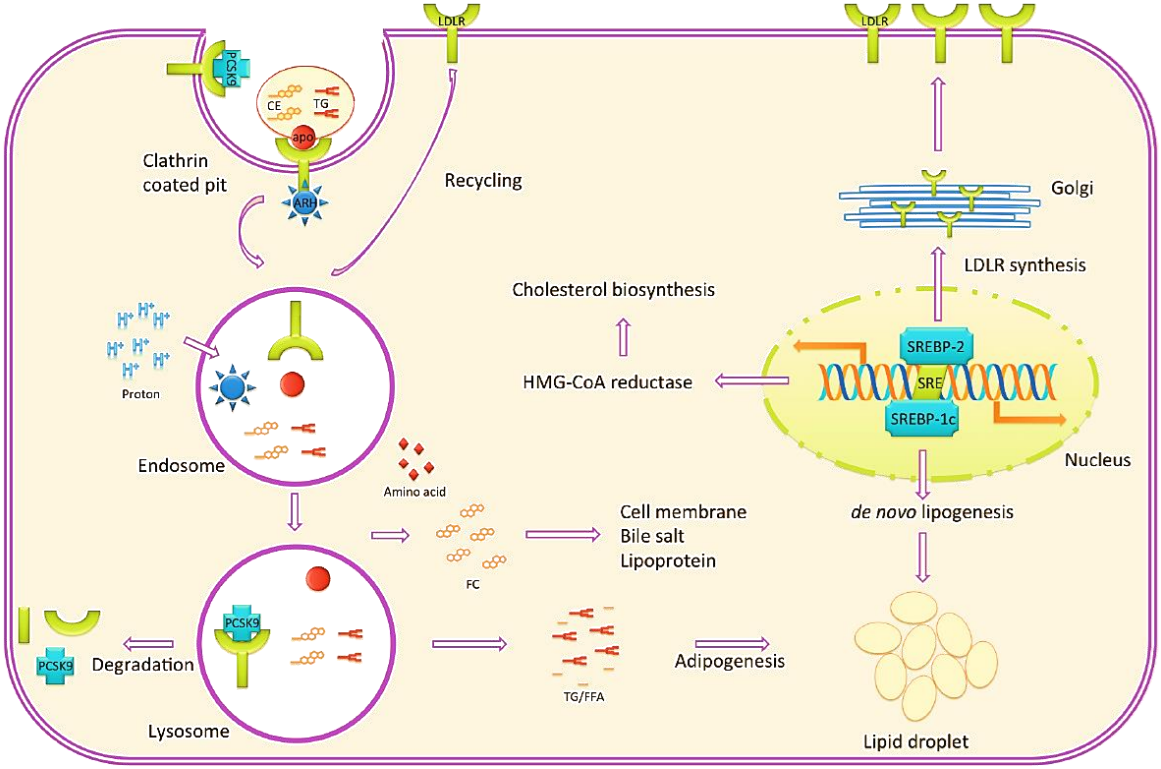


***Figura 3. Homeostasis celular del colesterol por medio de la interacción LDL-LDLr.***

En la Figura 3 se muestra que el primer paso para la endocitosis del LDL es el reconocimiento del dominio C-terminal de la proteína apoB100 por parte del LDLr y posteriormente se une con la proteína adaptadora de LDLr (ARH) en vesículas cubiertas de clatrina. Enseguida inicia la internalización del complejo lipoproteico a pH neutro. Después, las vesículas recubiertas de clatrina se fusionan con endosomas, donde el pH es menor, activando la liberación de ligandos internalizados desde el receptor desde donde llegan al

lisosoma donde se encuentran con enzimas que los catabolizan. Una vez finalizada la internalización, los receptores se reciclan direccionándose una vez más a la membrana celular.

Al entrar a la célula, el colesterol activa un sistema de retroalimentación negativa que reduce su biosíntesis, así como la transcripción de LDLr por medio de la inhibición de los elementos regulatorios de esteroles (SREBP-2). De manera paralela, la proteína convertasa subtilisina/kexina tipo 9 (PCSK9) se une a LDLr, desencadenando un proceso que lleva al LDLr al lisosoma para su degradación.

Otro proceso que ocurre en respuesta al ingreso del colesterol en la célula es la disminución de la lipogénesis *de novo* por medio de la inhibición de SREBP-1c, lo que lleva al almacenamiento de los triglicéridos en el tejido adiposo.

Como hemos visto, el proceso de captación vesicular del complejo LDL-LDLr es esencial en el metabolismo de los lípidos. En respuesta a una producción alta de lípidos el complejo LDL-LDLr induce la represión de la 3-hidroxi-3-metilglutaril-CoA reductasa (HMGCR) con la finalidad de evitar la biosíntesis de colesterol. Además, este proceso lleva al aumento de la actividad de la acil-CoA colesterol acil transferasa (ACAT) para reducir el colesterol libre. Finalmente, la síntesis de LDLr es suprimida para que a su vez se reduzca la captación de LDL a través del SREBP.

La regulación del LDLr es un proceso que se encuentra sometido a la acción de la proteína convertasa subtilisina/kexina tipo 9 (PCSK9) en los hepatocitos. Una vez secretada por los hepatocitos, PCSK9 experimenta una interacción proteína-proteína con LDLr, lo que resulta en su degradación (Lambert et al., 2017; Zhang et al., 2016). En humanos, la ganancia de peso corporal causa hipercolesterolemia, mientras que la pérdida de masa grasa se asocia con disminución del colesterol ligado a LDL (LDL-C) y protección contra la aterosclerosis. En este proceso, moléculas de ácido ribonucleico interferente (RNAi) son dirigidos a PCSK9 con la finalidad de reducir el LDL-C en plasma al prevenir la degradación de LDLr *in vivo* e *in vitro* (Duellman et al., 2017; Zhang et al., 2016). De manera similar, la inhibición de PCSK9 aumenta la expresión de LDLr en hígado y reduce el LDL-C en el plasma de ratones (Lambert et al., 2017). En resumen, LDLr es un receptor fundamental para la maquinaria endocítica y desempeña un papel fundamental en el mantenimiento de la homeostasis del

colesterol. El defecto en la función o expresión de LDLr desencadena niveles elevados de LDL-C y da como resultado el desarrollo de aterosclerosis subclínica que lleva a un aumento del riesgo cardiovascular, como veremos más adelante.

Por otro lado, dado que la regulación a la baja de PCSK9 es fundamental para aumentar la actividad de LDLr y disminuir el LDL-C, se han propuesto tres formas de inhibir la producción y/o el funcionamiento de esta proteína:

1. Manipulación genética a través de la inhibición del ARN mensajero encargado de la codificación de la proteína PCSK9.
2. Utilización de péptidos miméticos que compiten con la PCSK9 en el sitio de unión con los receptores de LDL-C.
3. Empleo de anticuerpos monoclonales contra PCSK9. Estos anticuerpos, también llamados iPCSK9, bloquean a PCSK9 y permiten que los receptores de LDL-C puedan transportarlo al interior del hepatocito, en donde el colesterol será metabolizado mientras que el receptor será reciclado para capturar nuevas moléculas de LDL-C en la superficie del hepatocito.

Así, muchas son las estrategias encaminadas a controlar los niveles plasmáticos de colesterol, reduciendo de esta forma el desarrollo de enfermedades como la aterosclerosis, que como hemos mencionado, eleva el riesgo cardiovascular en nuestra población.

**LDL nativo y oxidado**

En la circulación, el LDL se encuentra predominantemente de forma nativa (nLDL). Sin embargo, esta lipoproteína es susceptible a la oxidación en tejidos vasculares periféricos llevando a la formación de LDL mínimamente modificado (mmLDL) y posteriormente LDL oxidado (oxLDL), el cual pierde su función al no ser reconocido por el LDLr.

Existe una gran cantidad de estudios enfocados en el papel de oxLDL durante la aterosclerosis. Sin embargo, pocos estudios han sido enfocados en mmLDL y todavía muchos menos en nLDL (L. Chávez-Sánchez et al., 2010; Luis Chávez-Sánchez et al., 2014; Henning, 2014; Janabi et al., 2000; Levitan et al., 2009; Okura et al., 2000).

Como hemos mencionado, diversos estudios muestran que conforme aumenta el nivel de LDL-C, el riesgo cardiovascular también se incrementa de forma importante. En la Figura 4 observamos en el eje de las X los niveles de LDL, y en el eje de las Y el riesgo relativo para enfermedad coronaria y observamos que conforme los niveles de LDL-C se incrementan, el riesgo relativo para enfermedad coronaria aumenta, conforme a lo establecido por la NCEP (National Cholesterol Education Program Adult Treatment Panel III) (S. M. Grundy et al., 2001).

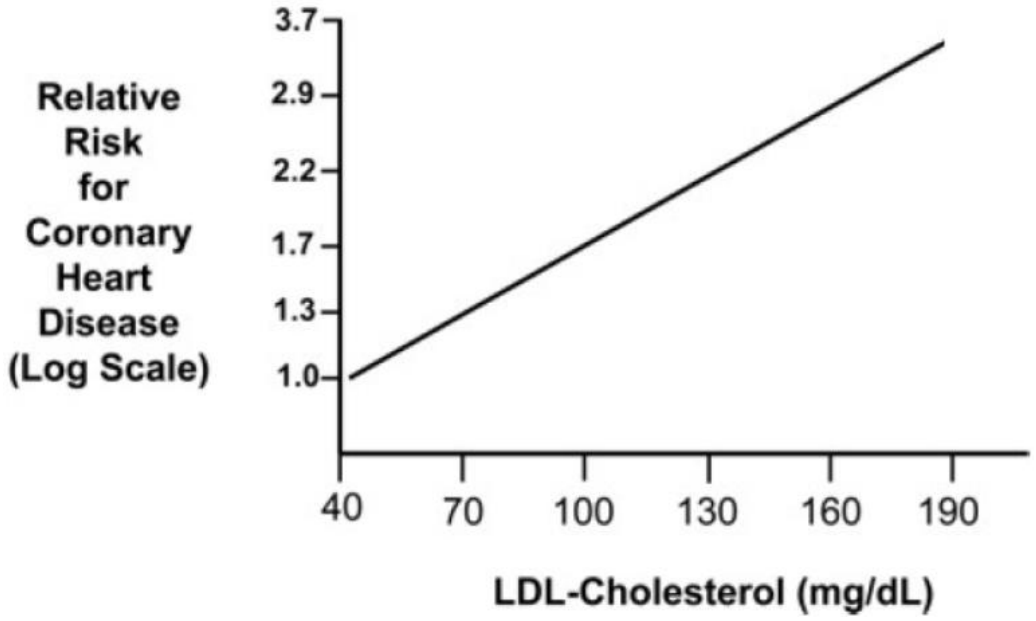


***Figura 4. Asociación entre los niveles de LDL-C y el riesgo para desarrollar enfermedad arterial coronaria. Tomada de S. M. Grundy et al., 2001.***

De acuerdo con la clasificación de la ATP III (S. M. Grundy et al., 2001), el objetivo terapéutico en un paciente es lograr un nivel de LDL-C menor o igual a 100 mg/dL. No obstante, de acuerdo con la Encuesta Nacional de Salud y Nutrición, el nivel promedio de LDL-C en México es de 131 mg/dL, encontrando un riesgo relativo de aproximadamente de 2.2 veces más para desarrollar enfermedad arterial coronaria. Aunado a esto, un número importante de estudios han mostrado que junto con el aumento de LDL-C existe un incremento de factores inflamatorios, particularmente aquellos asociados con las subpoblaciones de monocitos humanos (Al-Sharea et al., 2016; J. Han et al., 1997; Jackson

et al., 2016). De hecho, diversos estudios han reportado contacto directo entre el LDL-C y los monocitos en la circulación, lo cual ha llevado a plantear un escenario en el que los monocitos interactúan con el LDL-C, sinergia que podría contribuir con el progreso de la aterosclerosis. Sin embargo, esta posible interacción entre las lipoproteínas de baja densidad en estado nativo y las subpoblaciones de monocitos humanos todavía no ha sido estudiada.

**Subpoblaciones de monocitos humanos**

Los monocitos son células del sistema inmune que pueden llegar a medir hasta 18 micrómetros y representan del 4 al 8 % de los leucocitos totales en la sangre (Loems Ziegler-Heitbrock, 2015). Hace tiempo, se consideraba que esta población de células inmunes era homogénea. Sin embargo, adelantos en técnicas como la citometría de flujo nos permitieron desde el 2010 distinguir tres subpoblaciones de monocitos, de acuerdo con la expresión del correceptor para LPS (CD14) y de FcγRIII (CD16) (Woollard & Geissmann, 2010; Loems Ziegler-Heitbrock, 2015; Loems Ziegler-Heitbrock & Hofer, 2013).

Los monocitos clásicos expresan niveles altos de CD14 en la superficie celular y no expresan CD16. En segundo lugar, los monocitos intermedios expresan niveles altos de CD14 y ya expresan CD16. Por último, los monocitos no clásicos expresan niveles bajos de CD14 y conservan la expresión de CD16 (Woollard & Geissmann, 2010; Loems Ziegler-Heitbrock, 2015; Loems Ziegler-Heitbrock & Hofer, 2013). Además de distinguirse por la expresión estos marcadores de superficie celular, las subpoblaciones de monocitos tienen funciones diferenciales (Geissmann, 2010; L. Ziegler-Heitbrock et al., 2010; Loems Ziegler-Heitbrock, 2015). Tanto los monocitos clásicos como los monocitos intermedios tienen funciones orientadas hacia la migración celular debido a su alta producción de receptores de quimiocinas que les permiten migrar y posteriormente diferenciarse a macrófagos en tejidos periféricos en donde realizan funciones como la fagocitosis. Por el contrario, los monocitos no clásicos tienen funciones orientadas al patrullaje debido a que tienen la capacidad de permanecer en circulación donde pueden ser activados y una vez que esto ocurre, secretar citocinas proinflamatorias y orquestar el inicio de una respuesta inflamatoria. (Devevre et al., 2015; Gordon & Taylor, 2005; Jakubzick et al., 2017; Loems Ziegler-Heitbrock, 2015).

Los subtipos de monocitos no solamente han sido estudiados en condiciones normales, sino también en el contexto de alteraciones metabólicas como la dislipidemia, en donde parecen contribuir al desarrollo de enfermedades con un componente inflamatorio crítico como la aterosclerosis (Geng et al., 2014; Shi & Pamer, 2011; Woollard & Geissmann, 2010). En este sentido Al-Sharea y colaboradores (Al-Sharea et al., 2016) cultivaron monocitos en presencia de LPS + IFN-gama, en ausencia o presencia de nLDL (Figura 5). Posteriormente, ellos diferenciaron los monocitos a macrófagos y observaron que los macrófagos derivados de monocitos clásicos expresaban niveles mayores de TNF-alfa cuando el LPS y el IFN-gama estaban en combinación con el nLDL, en comparación con las células incubadas con LPS e IFN-gama sin nLDL.

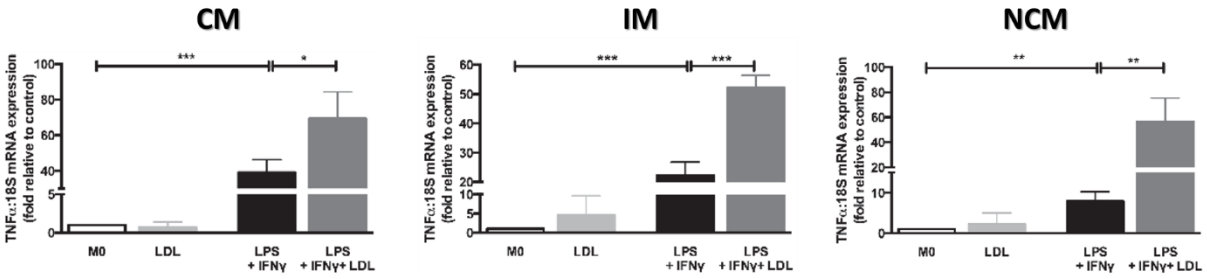


***Figura 5. Los macrófagos derivados de monocitos clásicos expresan niveles mayores de TNF-alfa en respuesta a nLDL, LPS e IFN-gama. Tomado de Al-Sharea (Al-Sharea et al., 2016)***

Cuando los autores estudiaron este efecto en macrófagos derivados de monocitos intermedios y no clásicos encontraron la misma tendencia, lo cual sugiere que el nLDL, junto con ligandos prototípicos como IFN-gama y LPS, es capaz de promover la expresión de TNF-alfa en macrófagos derivados de las tres subpoblaciones de monocitos.

Estudios posteriores han mostrado que el nLDL no sólo afecta la expresión de citocinas en macrófagos, sino también la producción de receptores de quimiocinas que son las moléculas que les permiten a los monocitos migrar a tejidos periférico o permanecer en circulación. Un estudio realizado por Han y colaboradores (K. H. Han et al., 1998) reveló

que los monocitos de sujetos con LDL-C menor a 100 mg/dL mostraban una expresión menor del receptor de quimiocinas C-C tipo 2 (CCR2) en comparación con sujetos con LDL mayor de 130 mg/dL (Figura 6). Este hallazgo sugiere que el LDL circulante podría estimular la expresión de receptores de quimiocinas implicados en la migración de los monocitos a tejido endotelial vascular durante la aterogénesis. Es importante recalcar que todavía no se sabe cuál es el efecto del LDL circulante sobre otros receptores de quimiocinas, específicamente en las subpoblaciones de monocitos.

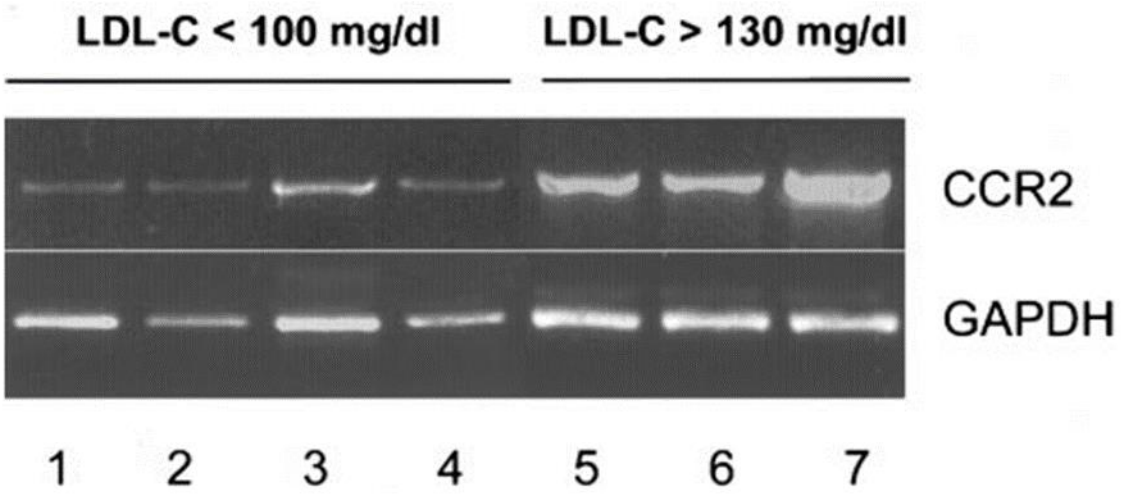


***Figura 6. Los monocitos de sujetos con LDL-C mayor de 130 mg/dL expresan más CCR2 que las células de sujetos con LDL menor de 100 mg/dL. Tomado de*** (K. H. Han et al., 1998)**.**

En otro estudio, Jackson y colaboradores en el 2016 (Jackson et al., 2016) cultivaron monocitos humanos en presencia de LDL y posteriormente tiñeron estas células con Lipidtox, el cual evidencia las vesículas lipídicas. Estos autores observaron que los monocitos CD16 negativos, que corresponden a los monocitos clásicos, incorporaron más lípidos a la célula en comparación con los monocitos CD16 positivos, que corresponden a los monocitos intermedios y no clásicos (Figura 7). Esta evidencia demuestra que los subtipos de monocitos incorporan de manera diferencial el LDL; sin embargo, aquí no se estudió el efecto de LDL de manera población-específica sino únicamente con base en la expresión de CD16.

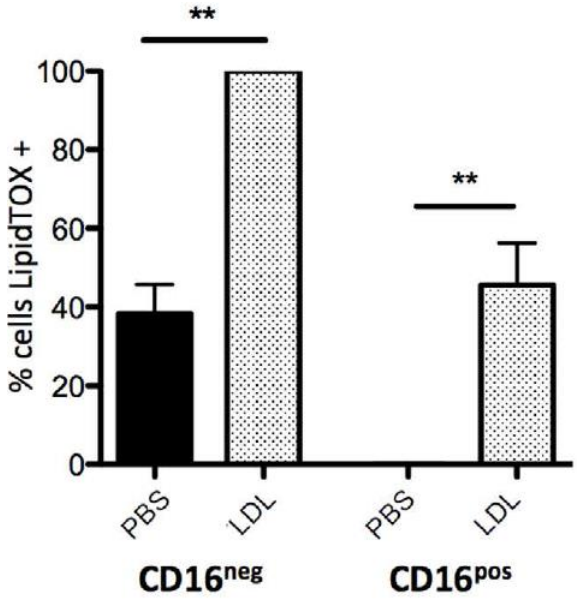


***Figura 7. La fracción de monocitos CD16- correspondiente a monocitos clásicos incorporan más LDL que los monocitos CD16+. Tomado de Jackson et al., 2016.***

Como se mencionó previamente, el LDL ingresa a las células principalmente por medio del LDLr. Sin embargo, evidencia reciente sugiere que este no es el único mecanismo por el cual el LDL puede incorporarse a la célula y ejercer sus funciones. En este sentido, Jackson y colaboradores (Jackson et al., 2016) estudiaron los monocitos de ratones deficientes de LDLr y encontraron que los monocitos clásicos $GR1^{high}$ y los no clásicos $GR1^{low}$ mantenían la incorporación de LDL, aun en ausencia del principal receptor de LDL descrito hasta ese momento (Figura 8). Esta noción ha llevado a la propuesta de otras moléculas que son capaces de mediar la incorporación de LDL independientemente del LDLr, como podría ser el caso de CD36.

CD36 es un receptor transmembranal tipo carroñero involucrado en la internalización de ácidos grasos en una gran variedad de células. En el estudio realizado por Feng y colaboradores (Feng et al., 2000), estos autores observaron la expresión de CD36 en una línea celular de macrófagos en respuesta a prostaglandinas y, de manera interesante, oxLDL.

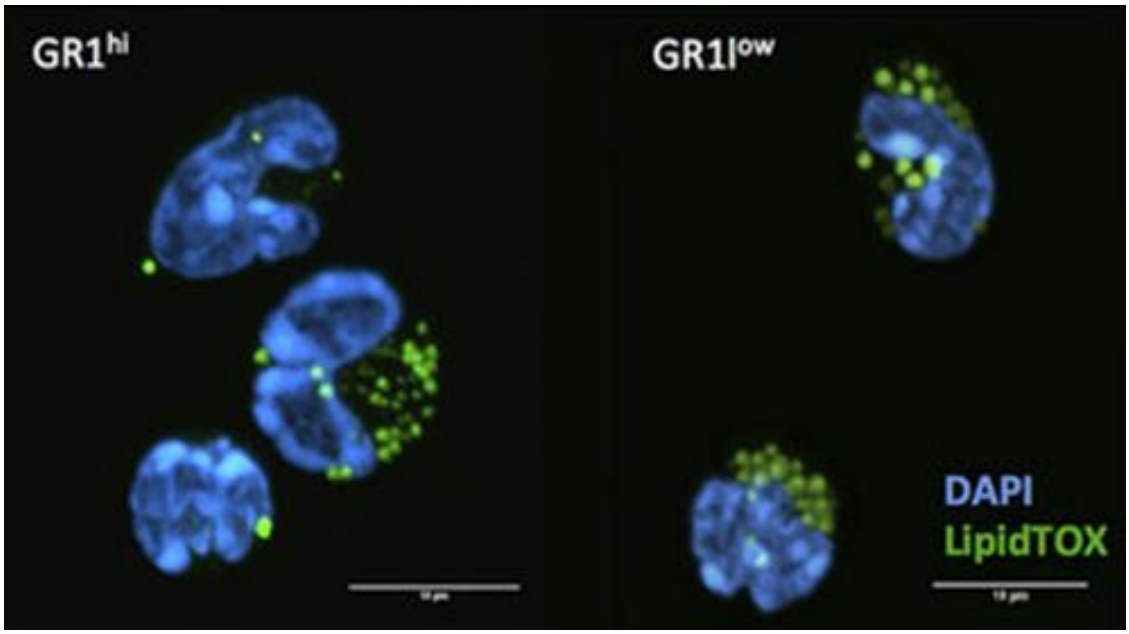


***Figura 8. Incorporación de LDL (verde) en monocitos que no expresan LDLr. Los núcleos se observan en azul. GR1, Marcador de diferenciación mieloide; DAPI, marcador de viabilidad; LipitTOX, marcador de gotas lipídicas. Tomado de Jackson et al., 2016***

Estos mismos autores encontraron que la expresión de CD36 en estos macrófagos aumentó de manera dependiente de la dosis de oxLDL con el que las células fueron incubadas. Sin embargo, cuando se usó nLDL, el incremento en la expresión de CD36 fue mucho más notorio en comparación con el observado con oxLDL. Estos hallazgos sugieren que CD36 podría comportarse como LDLr, quien pierde su capacidad de internalizar LDL cuando esta molécula está oxidada (Figura 9). Además, la regulación que ejerce el LDL sobre la expresión de CD36 hace recordar el mecanismo de retroalimentación negativa descrito para un sinnúmero de complejos ligando-receptor.

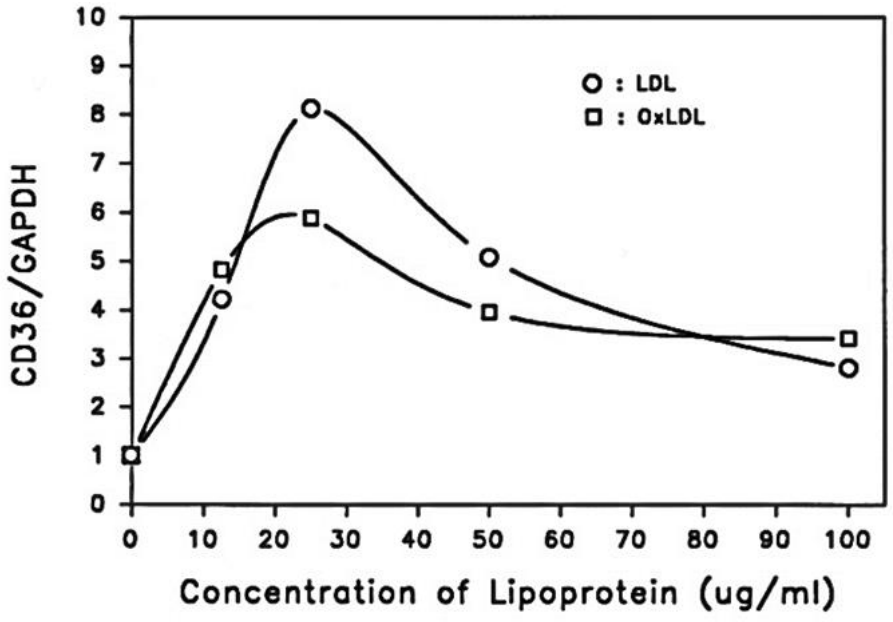


***Figura 9. La expresión de CD36 aumenta de manera dependiente de la dosis de oxLDL o nLDL en macrófagos de línea cultivados in vitro. Tomado de Feng et al., 2000***

Así mismo, Calvo y colaboradores (Calvo et al., 1998) realizaron un estudio en el que incubaron células Sf 9-CD36 que expresaban CD36 pero no LDLr en presencia de anticuerpos neutralizantes contra CD36 (Figura 10). A medida que la concentración de anticuerpo aumentaba, los autores observaron que la cantidad de LDL unido a CD36 disminuía, demostrando así la participación de CD36 en la unión a lipoproteínas, en específico a nLDL.

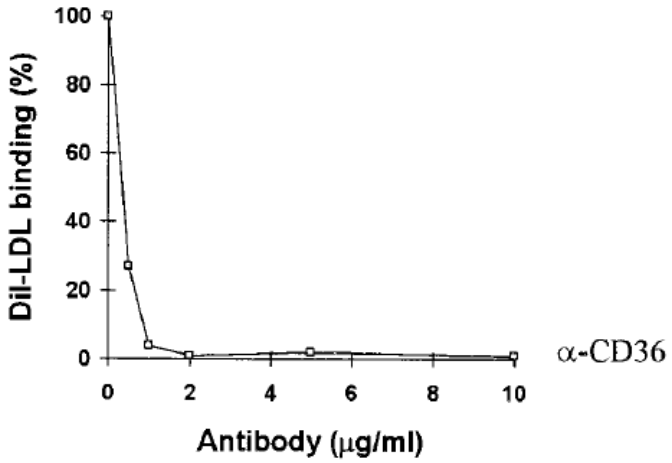


***Figura 10 Tomado de Calvo, Gómez-Coronado, Suárez, Lasunción, & Vega, 1998***

El conjunto de evidencias expuestas anteriormente demuestra que existe una relación entre el LDL y la función de los monocitos humanos. En específico, nosotros sugerimos que el LDL es capaz de cambiar la dinámica de las subpoblaciones de monocitos, alterando su capacidad de producir citocinas y receptores de quimiocinas involucrados en la infiltración de estas células al endotelio vascular durante el proceso aterogénico. Además, la información mostrada anteriormente nos hace suponer que los efectos del LDL podrían ser a través de CD36, y no necesariamente mediante la vía clásica regulada por LDLr. Sin embargo, estas hipótesis todavía no se han contrastado de forma experimental y hasta el momento, el papel del LDL y, en específico del nLDL, sobre la actividad inmunológica de los subtipos de monocitos humanos no está claro.

## PLANTEAMIENTO DEL PROBLEMA

La elevación en los niveles de nLDL es la forma más frecuente de dislipidemia en la población mexicana y uno de los factores más importantes en la elevación del riesgo cardiovascular. Sin embargo, a diferencia del oxLDL, el papel que el nLDL juega en el direccionamiento de monocitos circulantes hacia la placa ateromatosa todavía no es claro. Estudios realizados en nuestro grupo de trabajo y por otros grupos de investigación sugieren que existe una asociación entre el nLDL y la actividad de las subpoblaciones de monocitos humanos. Sin embargo, estas observaciones son sólo asociativas y actualmente se desconoce el efecto del nLDL sobre las subpoblaciones de monocitos humanos, su capacidad de estimular la producción de citocinas y receptores de quimiocinas, y la posible implicación de CD36 en estos efectos. Se ha encontrado evidencia que sugiere que sujetos obesos con cardiopatía esclerótica muestran un aumento del complejo LBP/LPS, los cuales muestran un proceso dislipidémico, por lo que no se ha estudiado si el complejo LBP/LPS tiene relación con el aumento de lipoproteínas de baja densidad.

Una estrategia combinada *in vitro* y con donadores puede ayudarnos a comprender el papel del nLDL sobre las subpoblaciones de monocitos humanos durante la aterogénesis, con miras a encontrar nuevos blancos terapéuticos que nos ayuden a disminuir el riesgo cardiovascular en nuestra población.

## HIPÓTESIS

En el primer escenario in vitro, el nLDL aumenta la subpoblación de monocitos no clásicos y disminuye a los monocitos intermedios y clásicos, incrementando los niveles de IL-1 beta, TNF alfa y CCR2, y disminuyendo la expresión de CX3CR1, mientras que aumenta la expresión de CD36. En el segundo escenario con donadores, el nLDL se asocia con un aumento de la subpoblación de monocitos no clásicos y con una disminución de los monocitos intermedios y clásicos, así como un aumento en los niveles séricos de IL-1 beta y LBP.

# OBJETIVOS

## Objetivo general

Evaluar el efecto del nLDL sobre las subpoblaciones de monocitos humanos *in vitro* y en donadores, estudiando su papel sobre el perfil de expresión de citocinas y receptores de quimiocinas, así como el posible mecanismo molecular involucrado.

## Objetivos particulares

1. Determinar el efecto del nLDL sobre el porcentaje de monocitos clásicos, intermedios y no clásicos de forma concentración-tiempo dependiente *in vitro*.
2. Estudiar el efecto del nLDL sobre la producción intracelular de IL-1 beta, TNF alfa, y los niveles de CCR2 y CX3CR1 en monocitos clásicos, intermedios y no clásicos *in vitro*.
3. Evaluar el efecto del nLDL en conjunto con LPS sobre la producción intracelular de IL-1 beta, TNF alfa, y los niveles de CCR2 y CX3CR1 en monocitos clásicos, intermedios y no clásicos *in vitro*.
4. Examinar el papel de CD36 como un posible mediador de los efectos del nLDL sobre los cambios en los monocitos clásicos, intermedios y no clásicos.
5. Comparar el porcentaje de las subpoblaciones de monocitos, y los niveles séricos de IL-1 beta y LBP, en sujetos con valores de LDL-C menores de 100 mg/dL y mayores de 130 mg/dL.

## MATERIALES Y MÉTODOS

### Diseño del estudio

Los participantes del estudio fueron varones de 28 a 45 años que acudieron como donadores al Banco de Sangre del Hospital General de México. Los participantes del estudio tenían un índice de masa corporal de 18.5-24.9 $kg/m^2$, sin evidencia clínica y bioquímica de resistencia a la insulina, *Diabetes Mellitus*, dislipidemia o alteraciones en la presión arterial. Los participantes del estudio no habían tomado medicamentos inmunomoduladores durante el último mes, y no habían consumido una cantidad elevada de alimentos ricos en lípidos dos días antes del estudio.

### Cultivo *in vitro* de monocitos humanos primarios

Veinte donantes de sangre, sanos, con niveles séricos de LDL-C inferiores a 100 mg/dl y valores séricos de proteína C reactiva de alta sensibilidad (hs-CRP) de 1.35 ± 0.26 mg/l, en promedio, se inscribieron en el estudio. Se realizaron ensayos independientes en los que cada participante acordó donar 8 ml de sangre, que se recolectó en un tubo que contenía heparina (VacutainerTM, BD Diagnostics, Franklin Lakes, NJ, EE. UU.). Posteriormente, las muestras de sangre total se dividieron individualmente y se colocaron en placas de cultivo celular de 6 pozos (Costar, Kennebunk, ME, EE. UU.), agregando 2 mL de sangre más 1 mL de RPMI-1640 (Sigma-Aldrich, St. Louis, MO , EE. UU.) suplementado con suero fetal bovino (FBS) al 5 %, L-glutamina 2 mM, HEPES 10 nM y gentamicina 50 μg/mL (GibcoTM, Grand Island, NY, EE. UU.) por pozo. La muestra de sangre contenida en el primer pozo se designó como control y recibió 300 μL de RPMI-1640 durante 9 h. El segundo pozo se incubó en presencia de 100 μg de nLDL (Sigma-Aldrich, St. Louis, MO, EE. UU.) disueltos en 300 μL de RPMI-1640 durante 9 h. El tercer pozo se incubó en presencia de 10 ng/mL de LPS (Sigma-Aldrich, St. Louis, MO, EE. UU.) disuelto en 300 μL de RPMI-1640 durante 9 h. La muestra contenida en el cuarto pozo se incubó en presencia de 100 μg de nLDL más 10 ng/mL de LPS disueltos en 300 μL de RPMI-1640 durante 9 h. El tiempo de exposición de los cultivos *in vitro* se seleccionó con base en las curvas de tiempo-respuesta a las 3, 6 y 9 h, encontrando que los monocitos muestran los cambios más significativos a las 9 h. Las placas de cultivo celular se incubaron a 37 °C en una atmósfera humidificada con $CO_2$ al 5 %. Para la tinción de citocinas

intracelulares, los glóbulos blancos (WBC) se trataron con Brefeldina A 1:1000 (BioLegend, Inc., San Diego, CA, EE. UU.) durante las últimas 2 h de cultivo *in vitro*. Todos los participantes brindaron su consentimiento informado por escrito, previamente aprobado por el comité de ética institucional del Hospital General de México (número de registro: DI/20/501/03/17), el cual garantizó que el estudio fuera conducido de manera rigurosa y de acuerdo a los principios descritos en la Declaración de Helsinki de 1964 y su posterior modificación en 2013.

**Citometría de flujo para expresión de citocinas y receptores de quimiocinas**

Después de la exposición a nLDL y/o LPS, colectamos las muestras de sangre completa y las centrifugamos a 500 × g durante 10 min. Después, los glóbulos blancos se separaron con una micropipeta y se resuspendieron en 1 ml de PBS1X (Sigma-Aldrich, St. Louis, MO, EE. UU.). Después de un paso de centrifugación adicional y la eliminación del sobrenadante, el botón celular se resuspendió en 50 µL de solución de tinción celular (BioLegend, Inc., San Diego, CA, EE. UU.). Los glóbulos blancos se incubaron con 5 µl de True-Stain Monocyte BlockerTM (BioLegend, Inc., San Diego, CA, EE. UU.) durante 10 min en hielo. Luego, los glóbulos blancos se incubaron con anti-CD14 PE/Cy7, anti-CD16 PE/Cy5, anti-CCR2 AF647, anti-CX3CR1 BV510, Zombie UVTM Fixable Viability Kit (BioLegend, Inc., San Diego, CA, EE. UU.), anti-CD36 PE y anti-HLA-DR BUV661 (BD Biosciences, San Jose, CA, EE. UU.) durante 20 min en la oscuridad a 4 °C. Posteriormente, los glóbulos blancos se incubaron con 100 µl de medio de fijación A (kit de permeabilización celular FIX & PERMTM) (InvitrogenTM, Carlsbad, CA, EE. UU.) durante 20 min a temperatura ambiente. Después de enjuagarse con Cell Staining Buffer (BioLegend, Inc., San Diego, CA, EE. UU.), las células mononucleares de sangre periférica (PBMC) se incubaron con 100 µL de medio de permeabilización B (FIX & PERMTM Cell Permeabilization Kit, InvitrogenTM, Carlsbad, CA, UU.) anti-TNF alfa FITC y anti-IL-1 beta Pacific Blue (BioLegend, Inc., San Diego, CA, EE. UU.) durante 20 min en la oscuridad a temperatura ambiente. Después de enjuagarse con Cell Staining Buffer (BioLegend, Inc., San Diego, CA, EE. UU.), las PBMC se adquirieron en un citómetro de flujo BD Influx (BD Biosciences, San Jose, CA, EE. UU.) utilizando el software BD SortwareTM 1.2, adquiriendo 20 000 eventos por ensayo por triplicado.

**Estrategia de análisis celular**

Para la estrategia de selección, los leucocitos se seleccionaron primero en un diagrama de densidad de dispersión temporal/lateral y, a continuación, se seleccionaron en la población de células negativas UV Zombie para la detección de células vivas. Posteriormente, las células vivas se seleccionaron para singletes en un diagrama de densidad de dispersión frontal (FS)/anchura de pulso de activación. Los monocitos fueron reconocidos en el cuadrante específico de HLA-DR. Luego, los monocitos se seleccionaron utilizando la estrategia de selección rectangular en la población CD14+/CD16+ para la identificación de monocitos clásicos (CM, CD14++CD16−), monocitos intermedios (IM, CD14++CD16+) y monocitos no clásicos (NCM, CD14+CD16+). La intensidad de fluorescencia mediana (MFI) para IL-1 beta, TNF alfa, CD36, CCR2 y CX3CR1 se obtuvo considerando poblaciones de células positivas y negativas para cada marcador. El porcentaje de células positivas para cada marcador se obtuvo utilizando controles de fluorescencia menos uno (FMO). Los controles de compensación se realizaron mediante UltraComp eBeadsTM (InvitrogenTM, Carlsbad, CA, EE. UU.) para cada fluorocromo. Los datos se analizaron mediante el software FlowJo 10.0.7 (TreeStar, Inc, Ashland, OR, EE. UU.).

**Modelo con donadores**

Se incluyeron en el estudio 150 voluntarios de ambos sexos, mayores de 18 años, con ayuno de 8 h que acudieron al Banco de Sangre y al Departamento de Medicina Interna del Hospital General de México. Se registraron el sexo, la edad, el índice de masa corporal (IMC), la circunferencia de la cintura, el porcentaje de grasa corporal y los niveles séricos de glucosa, insulina, proteína C reactiva (PCR), colesterol total, triglicéridos, HDL-C, y LDL-C en todos los participantes. El IMC resultó de dividir el peso corporal por la altura al cuadrado. La circunferencia de la cintura se midió en el punto medio entre el margen inferior de la costilla y la cresta ilíaca usando una cinta métrica. El porcentaje de grasa corporal se obtuvo mediante un analizador de composición corporal (TANITA® Body Composition Analyzer, Modelo TBF-300A, Tokio, Japón). La PCR se midió por triplicado mediante inmunoturbidimetría (Randox Laboratories, Meenmore, Irlanda). La glucosa sérica, el colesterol total, los

triglicéridos, el HDL-C y el LDL-C se midieron por triplicado mediante ensayos enzimáticos (Roche Diagnostics, Mannheim, Alemania). La insulina sérica se midió por triplicado mediante el ensayo inmunoabsorbente ligado a enzimas (ELISA) (Abnova, Corporation, Taipei, Taiwán). La estimación de la resistencia a la insulina se calculó individualmente utilizando la evaluación del modelo homeostático de la resistencia a la insulina (HOMA-IR) multiplicando la concentración de glucosa (mM) por la concentración de insulina (mU/L) y luego dividiéndola por 22.5. Todos los participantes recibieron una evaluación médica completa y dieron su consentimiento informado por escrito, previamente aprobado por el comité de ética institucional del Hospital General de México (número de registro del código de aprobación ética: DIC/11/UME/05/029), que garantizaba que el estudio se realizó siguiendo rigurosamente los principios descritos en la Declaración de Helsinki de 1964 y su posterior enmienda en 2013. Los voluntarios fueron excluidos del estudio si tenían un diagnóstico previo de diabetes tipo 1 (T1D), T2D, enfermedad coronaria, enfermedad hepática aguda o crónica, enfermedad renal aguda o crónica, cáncer, trastornos endocrinos, enfermedades infecciosas, enfermedades inflamatorias crónicas y/o trastornos autoinmunes. También excluimos del estudio a donadores seropositivos para el virus de la inmunodeficiencia humana (VIH), el virus de la hepatitis C (VHC) y/o el virus de la hepatitis B (VHB), a mujeres embarazadas o lactando y a sujetos bajo tratamiento con anti-inflamatorios o inmunomoduladores, incluidos los medicamentos antiinflamatorios no esteroideos (AINE).

**Efectos de LDL sobre LBP e IL-1 beta en subpoblaciones de monocitos en el modelo con donadores**

De acuerdo con las pautas clínicas del Panel de expertos sobre detección, evaluación y tratamiento del colesterol alto en sangre en adultos (Panel de tratamiento de adultos III) del Programa Nacional de Educación sobre el Colesterol (NCEP), los participantes del estudio se dividieron en dos grupos de concentración de LDL-C, de la siguiente manera: sujetos con concentración óptima de LDL-C $\leq$ 100 mg/dL e individuos con concentración elevada de LDL-C > 100 mg/dL [25]. Posteriormente, se cuantificaron y compararon entre ambos grupos el IMC, la circunferencia de la cintura, el porcentaje de grasa corporal, la glucosa, el HOMA-IR y el perfil lipídico. Además, se calculó el Índice de Riesgo de Castelli II a través

de la formula *CRI II = LDL/HDL*. Se obtuvieron muestras de sangre (6 ml) de todos los voluntarios para el posterior aislamiento de los glóbulos blancos. Los glóbulos blancos se incubaron con anti-CD14 PE/Cy7 y anti-CD16 FITC, adquiriendo 20 000 eventos por prueba por triplicado en un citómetro de flujo BD Influx (BD Biosciences, San Jose, CA, EE. UU.) utilizando el software BD SortwareTM 1.2 y FlowJo 10.0 .7 software (TreeStar, Inc, Ashland, OR, EE. UU.), como se describió anteriormente. En todos los participantes, la IL-1 beta sérica (Peprotech, Ciudad de México, México) y la proteína de unión a LPS (LBP) (InvitrogenTM, Carlsbad, CA, EE. UU.) se midieron por triplicado mediante ELISA y se analizaron según los niveles de LDL-C.

**Análisis estadístico**

La normalidad de la distribución de datos se estimó mediante la prueba de Shapiro-Wilk. Para los ensayos *in vitro*, se utilizó ANOVA de una cola, seguido de una prueba de Tukey post-hoc, para comparar los porcentajes de CM, IM y NCM, y la expresión de IL-1 beta, TNF alfa, CCR2, CX3CR1 y CD36 en los grupos celulares designados como control, nLDL, LPS y nLDL + LPS. Para los ensayos con donadores, se usó la prueba t de Student no pareada para comparar sujetos con LDL-C sérico $\leq$ 100 mg/dL e individuos con LDL-C sérico > 100 mg/dL en términos de sexo, edad, IMC, circunferencia de la cintura, porcentaje de grasa corporal, glucosa en ayunas, insulina, HOMA-IR, CRP, colesterol total, triglicéridos, HDL, porcentajes de CM, IM y NCM, IL-1 beta sérica y niveles de LBP circulante. Las diferencias se consideraron significativas cuando $p < 0.05$. Todos los análisis estadísticos se realizaron mediante el software GraphPad Prism 7 (GraphPad Software, San Diego, CA, EE. UU.).

## RESULTADOS

Para la estrategia de selección, los glóbulos blancos se seleccionaron primero en un gráfico de tiempo vs densidad de dispersión lateral (observando la complejidad o granularidad celular). Este gráfico fue necesario para observar que los eventos se hubieran leídos adecuadamente en el citometro de flujo. Posteriormente se seleccionó la población de células negativas a Zombie UV para la detección de glóbulos blancos vivos (Figura 11, panel superior). Posteriormente, los glóbulos blancos se seleccionaron en singletes en un diagrama de densidad de ancho de pulso de activación y dispersión frontal (FS). Después de eso, las células se seleccionaron en la población HLA-DR+ para el reconocimiento de monocitos. A continuación, los monocitos se seleccionaron en la población $CD14^{+}/CD16^{+}$ para la identificación de CM, IM y NCM. Luego, los subconjuntos de monocitos se seleccionaron en las poblaciones IL-1β+, TNFα+, CCR2+, $CX_3CR1$+ y CD36+ para evaluar los efectos de nLDL y LPS en la actividad inmunitaria de estas células (Figura 11, panel inferior).

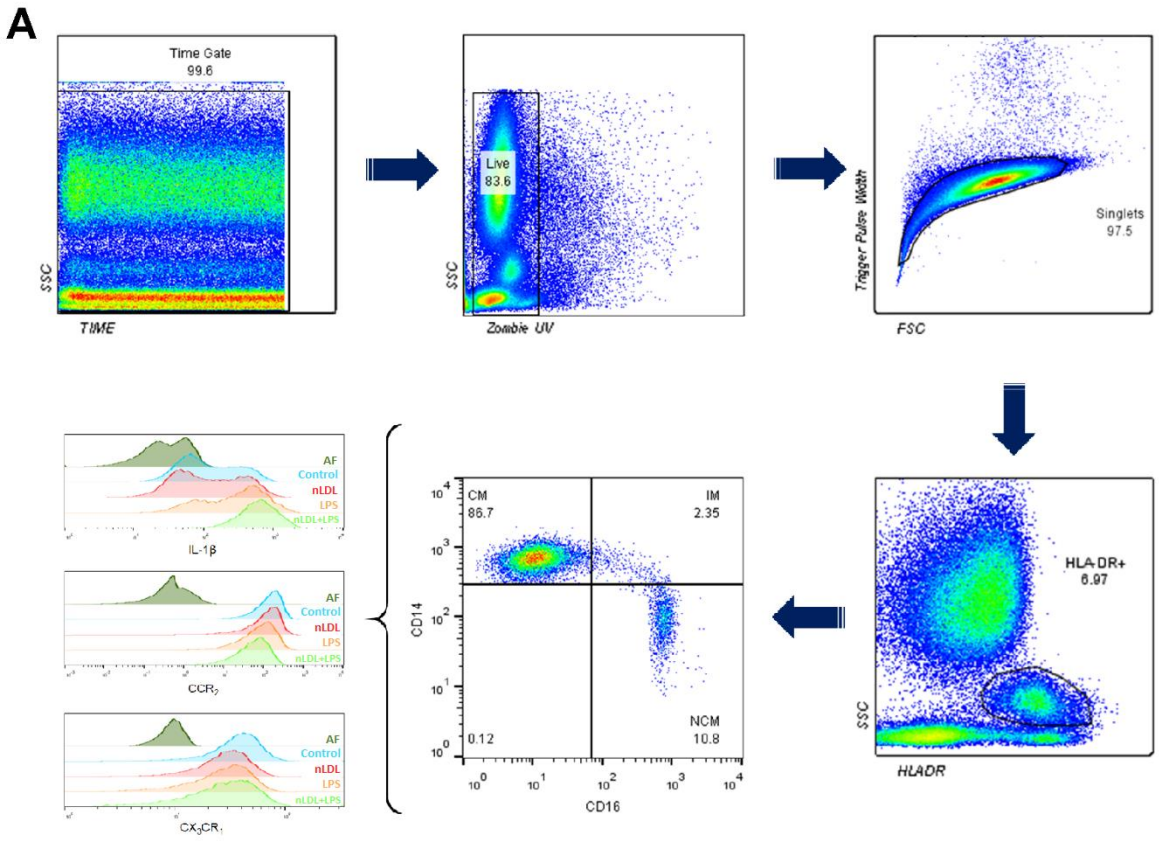


***Figura 11. Estrategia de activación para caracterizar subconjuntos de monocitos humanos. Los glóbulos blancos se seleccionaron primero en un diagrama de densidad de tiempo/dispersión lateral (SS), y luego se seleccionaron en la población de células negativas Zombie UV para la detección de células vivas. Posteriormente, las células vivas se seleccionaron para singletes en un diagrama de densidad de dispersión frontal (FS)/anchura de pulso de activación. Se reconocieron los monocitos en la selección HLA-DR+. Luego, los monocitos se seleccionaron en la población CD14+/CD16+ para la identificación de CM (CD14++CD16−), IM (CD14++CD16+) y NCM (CD14+CD16+). La expresión de IL-1 beta, CCR2 y CX3CR1 se midió en todos los subconjuntos de monocitos. SSC, dispersión lateral; FSC, dispersión frontal; HLA-DR, isotipo de antígeno leucocitario humano-DR; CM, monocitos clásicos; IM, monocitos intermedios; NCM, monocitos no clásicos; IL-1 beta, interleucina 1 beta; CCR2, receptor de quimiocinas C-C tipo 2; CX3CR1, receptor de quimiocinas CX3C 1.***

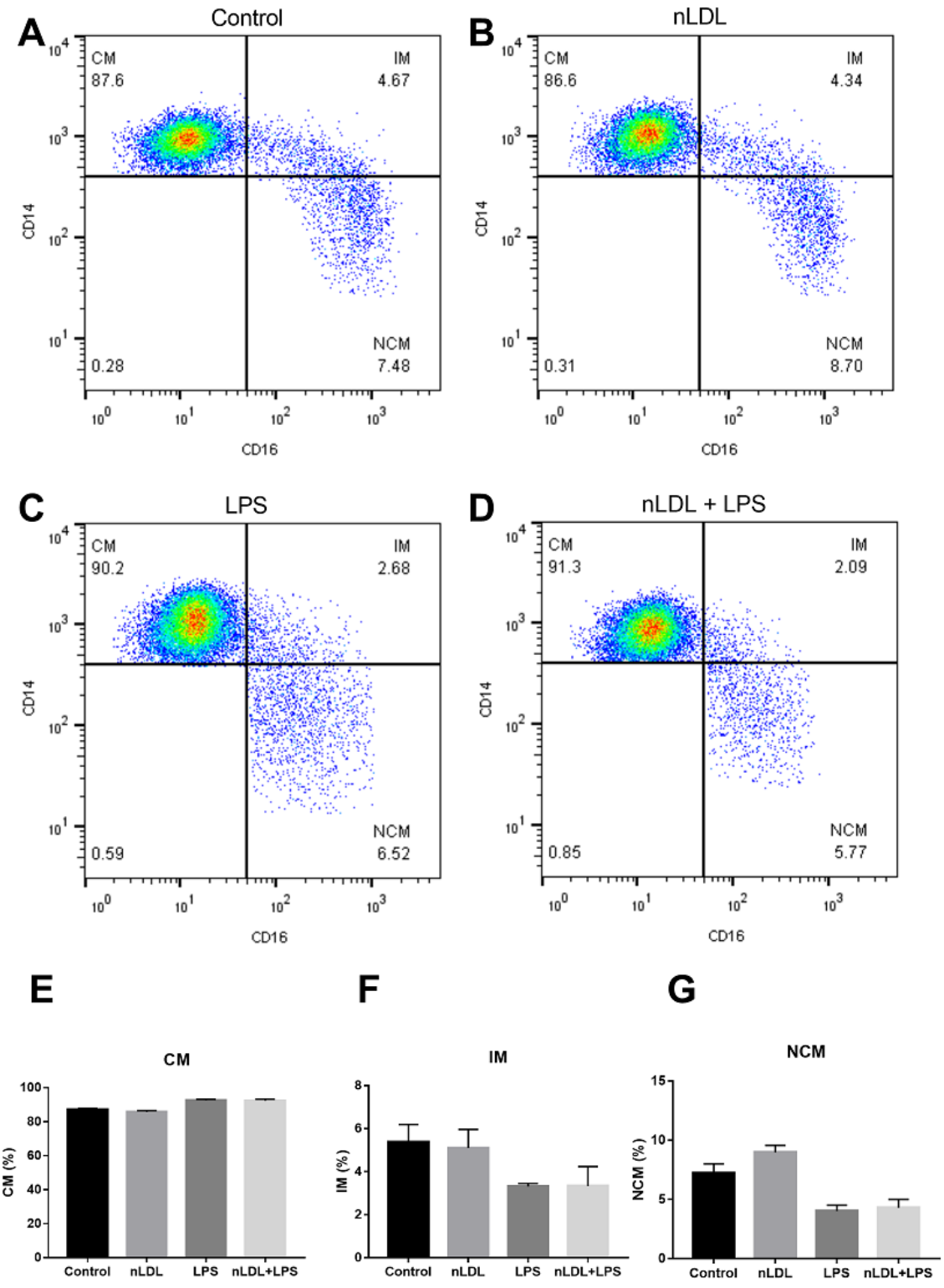
A
Control
CM
87.6
IM
4.67
0.28
NCM
7.48
B
nLDL
CM
86.6
IM
4.34
0.31
NCM
8.70
C
LPS
CM
90.2
IM
2.68
0.59
NCM
6.52
D
nLDL + LPS
CM
91.3
IM
2.09
0.85
NCM
5.77
CD14
CD16
E
CM
CM (%)
F
IM
IM (%)
G
NCM
NCM (%)
Control
nLDL
LPS
nLDL+LPS

***Figura 12. ← Efectos de nLDL y LPS sobre los porcentajes de las subpoblaciones de monocitos humanos. Se muestran gráficos de puntos que muestran de forma representativa los porcentajes de CM, IM y NCM en respuesta a las condiciones control (A), nLDL (B), LPS (C) o una combinación de nLDL + LPS (D). El nLDL disminuyó significativamente el porcentaje de CM y aumentó la cantidad de NCM en comparación con las células control (E y G, respectivamente). El LPS, solo o en combinación con el nLDL, aumentó significativamente el porcentaje de CM y disminuyó la cantidad de IM y NCM (E, F y G, respectivamente). Los datos se expresan como media ± desviación estándar. Los datos se compararon mediante ANOVA de una cola seguido de la prueba post-hoc de Tukey. Las diferencias se consideraron significativas cuando p < 0.05. * = p < 0.05; ** = p < 0.01; *** = p < 0.001; **** = p < 0.0001. CM, monocitos clásicos; IM, monocitos intermedios; NCM, monocitos no clásicos; nLDL, lipoproteínas de baja densidad nativas; LPS, lipopolisacárido.***

.

La Figura 12 muestra los gráficos representativos en donde se pueden observar los porcentajes de CM, IM y NCM tratados con nLDL o LPS (Figura 12A–D). En comparación con las células control, el porcentaje de CM se redujo significativamente cuando se trató con 100 μg/ml de nLDL (Figura 12E). Mientras que el porcentaje de IM no cambió (Figura 12F), el porcentaje de NCM exhibió un aumento significativo del 20% cuando se expuso a 100 μg/mL de nLDL con respecto al encontrado en células no tratadas (Figura 12G). Las subpoblaciones de monocitos también respondieron diferencialmente al LPS. El LPS, solo o en combinación con nLDL, aumentó de forma significativa el porcentaje de CM (Figura 12E). Por el contrario, IM y NCM no mostraron cambios significativos cuando se trataron con LPS o nLDL + LPS con respecto a lo encontrado en las células control (Figura 12F, G, respectivamente). Los porcentajes de CM, IM y NCM mostraron un comportamiento similar en respuesta a LPS o nLDL + LPS, lo que sugiere que este efecto fue mediado principalmente por LPS (Figura 12E-G, respectivamente).

La exposición de las células a nLDL y LPS no solo afectó el equilibrio entre las subpoblaciones de monocitos, sino también su capacidad para producir IL-1 beta, una citocina con acciones proinflamatorias muy importantes. La exposición de los monocitos a 100 μg/mL de nLDL no tuvo efectos significativos en la producción de IL-1 beta en todas las subpoblaciones de monocitos (Figura 13A). El LPS aumentó significativamente la producción de IL-1 beta en CM, IM y NCM, y este aumento fue aún más evidente cuando las células se expusieron a LPS en combinación con nLDL (Figura 13A). Paralelamente, los porcentajes de CM, IM y NCM que expresaron IL-1 beta también tendieron a disminuir en respuesta a nLDL (Figura 13B). El LPS, solo o en combinación con nLDL, aumentó significativamente el número de células IL-1 beta+ en todas las subpoblaciones de monocitos con respecto a las células no tratadas (Figura 13B). Similar a IL-1 beta, la exposición de los monocitos a 100 μg/mL de nLDL no tuvo efectos significativos en la producción de TNF alfa en todas las subpoblaciones de monocitos (Figura 13C). El LPS aumentó significativamente la producción de TNF alfa en CM, IM y NCM. Sin embargo, cuando las células se expusieron a LPS en combinación con nLDL se observó una disminución de la producción de TNF alfa, la cual solo fue significativa en los monocitos clásicos (Figura 13C panel izquierdo).

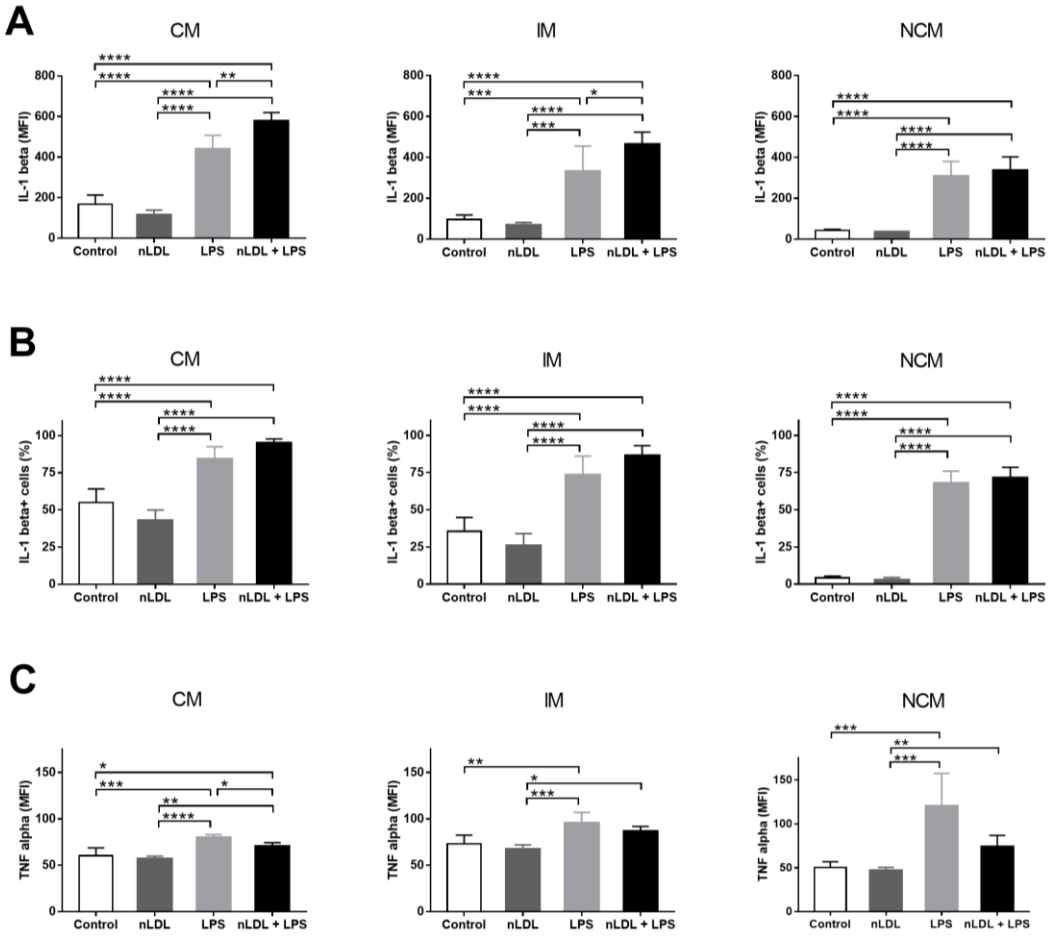


***Figura 13. Efectos del nLDL y LPS en la producción de IL-1 beta y TNF alfa en subpoblaciones de monocitos humanos. Aunque no se encontraron diferencias significativas, el nLDL tendió a disminuir la producción de IL-1 beta en CM, IM y NCM (paneles A, izquierdo, medio y derecho, respectivamente). El LPS, solo o en combinación con nLDL, aumentó significativamente la expresión de IL-1 beta en CM, IM y NCM (paneles A, izquierdo, medio y derecho, respectivamente). Aunque no se encontraron diferencias significativas, el nLDL tendió a disminuir los porcentajes de células IL-1 beta+ en todos los subconjuntos de monocitos (paneles B, izquierdo, medio y derecho, respectivamente). El LPS, solo o en combinación con nLDL, aumentó significativamente la cantidad de células IL-1 beta+ en todas las subpoblaciones de monocitos (paneles B, izquierdo, medio y derecho, respectivamente). El LPS en combinación con nLDL, disminuyo significativamente la expresión de TNF alfa en CM (panel C, izquierdo). Los datos se expresan como media ± desviación estándar. Los datos se compararon mediante ANOVA de una cola seguido de la prueba post-hoc de Tukey. Las diferencias se consideraron significativas cuando $p < 0.05$. * = $p < 0.05$; ** = $p < 0.01$; *** = $p < 0.001$; **** = $p < 0.0001$. CM, monocitos clásicos; IM, monocitos intermedios; NCM, monocitos no clásicos; nLDL, lipoproteínas de baja densidad nativas; LPS, lipopolisacárido; IL-1 beta, interleucina 1 beta; TNF alfa, Factor de necrosis tumoral alfa.***

Además de la expresión de IL-1 beta, también se ha demostrado que los subconjuntos de monocitos expresan diferencialmente los receptores de quimiocinas. En este sentido, la expresión de CCR2 fue claramente mayor en CM que en IM y NCM; sin embargo, CM no expresó diferencialmente CCR2 en respuesta a nLDL, solo o en combinación con LPS (Figura 14A). En general, el porcentaje de CM e IM que expresan CCR2 no cambió en respuesta a nLDL o LPS (Figura 14B, paneles izquierdo y central, respectivamente). Por el contrario, nLDL + LPS aumentó significativamente la cantidad de NCM que expresa CCR2 en comparación con la que se encontró cuando las células solo se expusieron a nLDL (Figura 14B, panel derecho). La expresión de CX3CR1 fue significativamente mayor en IM y NCM que en CM (Figura 14C). Además, el nLDL indujo una disminución en la expresión de CX3CR1 que fue incluso más evidente en NCM que en CM e IM (Figura 14C, panel derecho). La exposición de las células a LPS, solo o en combinación con nLDL, disminuyó la expresión de CX3CR1 en todas las subpoblaciones de monocitos (Figura 14C). Curiosamente, el porcentaje de NCM que expresó CX3CR1 disminuyó significativamente en respuesta al nLDL (Figura 14D, panel derecho), mientras que el LPS junto con el nLDL tuvieron el mismo efecto sobre IM y NCM (Figura 14D, paneles medio y derecho, respectivamente).

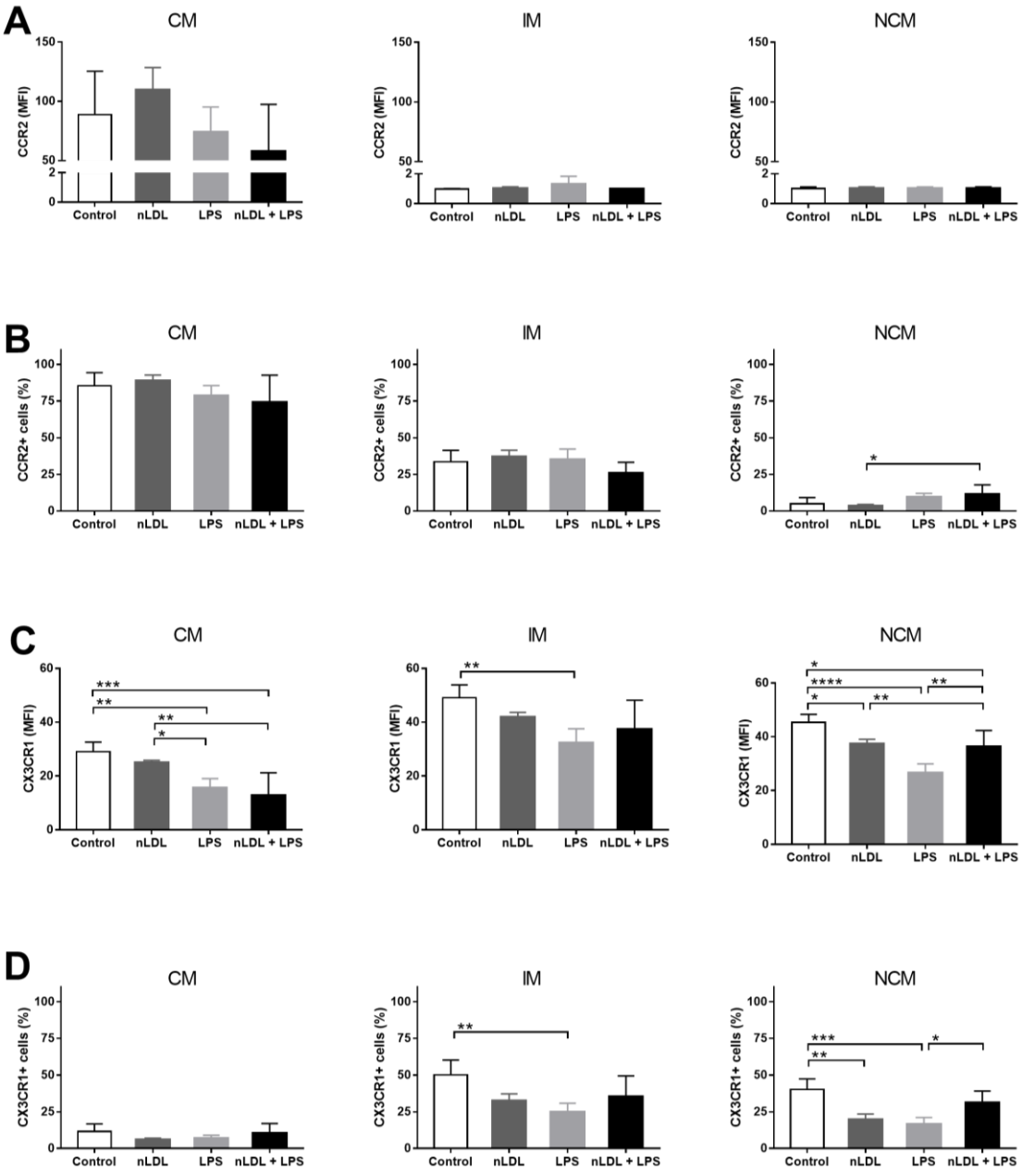
A
CM
IM
NCM
CCR2 (MFI)
150
100
50
2
0
Control
nLDL
LPS
nLDL + LPS
B
CM
IM
NCM
CCR2+ cells (%)
100
75
50
25
0
*
C
CM
IM
NCM
CX3CR1 (MFI)
60
40
20
0
***
**
*
****
D
CM
IM
NCM
CX3CR1+ cells (%)

***Figura 14. ←Efectos de nLDL y LPS en la expresión de CCR2 y CX3CR1 en las subpoblaciones de monocitos humanos. Aunque no se encontraron diferencias significativas entre las condiciones experimentales para cada condición, la expresión de CCR2 fue claramente mayor en CM que en IM y NCM (A, paneles izquierdo, medio y derecho, respectivamente). El porcentaje de células CCR2+ era mayor en el subconjunto CM en comparación con las subpoblaciones IM y NCM (paneles B, izquierdo, medio y derecho, respectivamente). En el subconjunto de NCM, el LPS actuó junto con nLDL para aumentar la cantidad de células CCR2+ en comparación con las células tratadas sólo con nLDL (B, panel derecho). La expresión de CX3CR1 era mayor en IM y NCM en comparación con CM (paneles C, izquierdo, medio y derecho, respectivamente). En NCM, el nLDL disminuyó significativamente la expresión de CX3CR1 en comparación con las células control (C, panel derecho). El LPS, solo o en combinación con nLDL, disminuyó la expresión de CX3CR1 en CM, IM y NCM (paneles C, izquierdo, medio y derecho, respectivamente). En IM, el LPS disminuyó el porcentaje de células CX3CR1+ en comparación con las células control (D, panel central). En NCM, el nLDL y el LPS disminuyó significativamente el porcentaje de células CX3CR1+ en comparación con las células control (D, panel derecho). Los datos se expresan como media ± desviación estándar. Los datos se compararon mediante ANOVA de una cola seguido de la prueba post-hoc de Tukey. Las diferencias se consideraron significativas cuando $p < 0.05$. * = $p < 0.05$; ** = $p < 0.01$; *** = $p < 0.001$; **** = $p < 0.0001$. CM, monocitos clásicos; IM, monocitos intermedios; NCM, monocitos no clásicos; nLDL, lipoproteínas de baja densidad nativas; LPS, lipopolisacárido; CCR2, receptor de quimiocinas C-C tipo 2; CX3CR1, receptor de quimiocinas CX3C 1.***

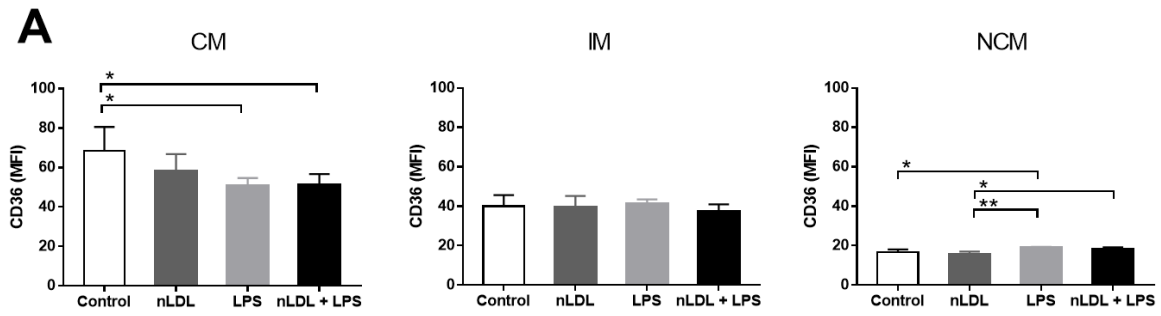


***Figura 15. Efectos de nLDL y LPS en la expresión de CD36 en las subpoblaciones de monocitos humanos. Se observaron diferencias significativas en la expresión de CD36, la cual disminuyó en presencia de LPS y LPS en combinación nLDL en CM (A, panel izquierdo). También, en NCM (A, panel derecho) la presencia de LPS incrementó los niveles de CD36 en comparación con la condición control, se observó una menor expresión de CD36 en nLDL en comparación con el LPS. Y al colocar LPS en combinación con nLDL se observó un aumento significativo de la expresión de CD36 en comparación de nLDL. Los datos se expresan como media ± desviación estándar. Los datos se compararon mediante ANOVA de una cola seguido de la prueba post-hoc de Tukey. Las diferencias se consideraron significativas cuando p < 0.05. * = p < 0.05; ** = p < 0.01; *** = p < 0.001; **** = p < 0.0001. CM, monocitos clásicos; IM, monocitos intermedios; NCM, monocitos no clásicos; nLDL, lipoproteínas de baja densidad nativas; LPS, lipopolisacárido; CD36, receptor scavenger tipo B.***

En búsqueda de otras moléculas que pudieran intervenir en la entrada de nLDL al interior de la célula examinamos a CD36 como un posible mediador de los efectos de LDL sobre los cambios en la proporción de monocitos clásicos, intermedios y no clásicos. De esta manera observamos que en presencia de nLDL había una tendencia a disminuir la expresión de CD36, pero sin cambios significativos, sobretodo en monocitos clásicos (Figura 15, panel izquierdo). En monocitos no clásicos se observan diferencias estadísticamente significativas cuando el LPS incrementó los niveles de CD36 en comparación con la condición control. De la misma forma se encontró una diferencia significativa, observando una menor expresión de CD36 en nLDL en comparación con el LPS. Asimismo, al colocar LPS en combinación con nLDL se observó un aumento significativo de la expresión de CD36 en comparación de nLDL por si solo (Figura 15, panel derecho).

*In vitro*, nLDL y LPS no sólo cambiaron el equilibrio de los subtipos de monocitos, sino también el patrón de expresión de moléculas que se han asociado previamente con la respuesta inflamatoria en la aterogénesis. Por lo tanto, decidimos confirmar estos resultados realizando experimentos similares, pero ahora con un modelo en donadores con niveles plasmáticos elevados de LDL-C. La Tabla 1 resume las diferencias en los factores de riesgo relacionados con el síndrome metabólico entre sujetos con niveles séricos de LDL-C normales y elevados (76.53 ± 4.1 contra 128.7 ± 3.6, respectivamente). No hubo diferencias significativas entre sujetos con valores de LDL-C por debajo y por encima de 100 mg/dL con respecto a la proporción de sexo, edad, IMC, circunferencia de cintura, porcentaje de grasa corporal, triglicéridos, HDL-C, insulina y glucosa en ayuno, HOMA-IR , y PCR (Tabla 1). Por el contrario, el colesterol total y el índice de riesgo cardiovascular II de Castelli son significativamente mayores en sujetos con LDL-C superior a 100 mg/dl (Tabla 1).

| | LDL | | |
|---|---|---|---|
| | **≤100 mg/dL** | **>100 mg/dL** | ***valor de P*** |
| Sexo (F,M) | 28/37 | 41/44 | 0.2650 |
| Edad (años) | 47.2 ± 1.056 | 49.49 ± 1.031 | 0.1913 |
| BMI (kg/m$^2$) | 28.22 ± 1.172 | 28.05 ± 0.9035 | 0.9155 |
| Circunferencia de cintura (cm) | 91.58 ± 2.94 | 96.73 ± 2.002 | 0.1696 |
| Porcentaje de grasa corporal (%) | 31.87 ± 1.696 | 31.91 ± 2.614 | 0.9909 |
| Colesterol (mg/dL) | 166.7 ± 7.079 | 220.7 ± 4.723 | <0.0001 |
| Triglicéridos (mg/dL) | 242.6 ± 41.08 | 186.4 ± 11.14 | 0.0769 |
| LDL (mg/dL) | 76.53 ± 4.156 | 128.7 ± 3.653 | <0.0001 |
| HDL (mg/dL) | 42.13 ± 3.44 | 47.06 ± 2.226 | 0.2332 |
| Insulina (µU/L) | 14.43 ± 1.057 | 13.52 ± 0.8046 | 0.5208 |
| Glucosa (mmol/L) | 5.104 ± 0.2653 | 5.346 ± 0.2502 | 0.5675 |
| HOMA-IR (a.u.) | 3.299 ± 0.3261 | 3.126 ± 0.1866 | 0.6290 |
| Índice de Riesgo de Castelli II | 1.966 ± 0.1827 | 2.892 ± 0.1294 | 0.0002 |

***Tabla 1. Parámetros antropométricos y bioquímicos de los sujetos de estudio. Los participantes del estudio se dividieron en dos grupos de concentración de LDL-C, de la siguiente manera: sujetos con concentración óptima de LDL-C ≤ 100 mg/dL e individuos con alta concentración de LDL-C > 100 mg/dL. El colesterol total y el índice de riesgo aterogénico de Castelli son significativamente mayores en donadores con LDL-C superior a 100 mg/dL. Abreviaturas: F, femenino; M, masculino; IMC, índice de masa corporal; LDL-C, lipoproteínas de baja densidad; HDL-C, lipoproteínas de alta densidad; HOMA-IR, modelo homeostático de evaluación de la resistencia a la insulina; PCR, proteína C reactiva; a.u., unidades arbitrarias. Los datos se presentan como media ± desviación estándar. Las diferencias se consideraron significativas cuando p < 0.05.***

Confirmando nuestros resultados *in vitro*, el porcentaje de CM fue significativamente menor en sujetos con LDL-C > 100 mg/dL (Figura 16A). Aunque el porcentaje de IM no mostró diferencias (Figura 16B), el porcentaje de NCM fue significativamente superior 1.5 veces más en individuos con LDL-C mayor a 100 mg/dL (Figura 16C). Los niveles séricos de IL-1 beta fueron significativamente mayores en sujetos con valores de LDL-C superiores a 100 mg/dL (Figura 16D). Además, los niveles de LBP fueron claramente mayores en sujetos con LDL-C > 100 mg/dL, lo que denota la presencia de valores séricos de LPS anormalmente altos en estos individuos (Figura 165E).

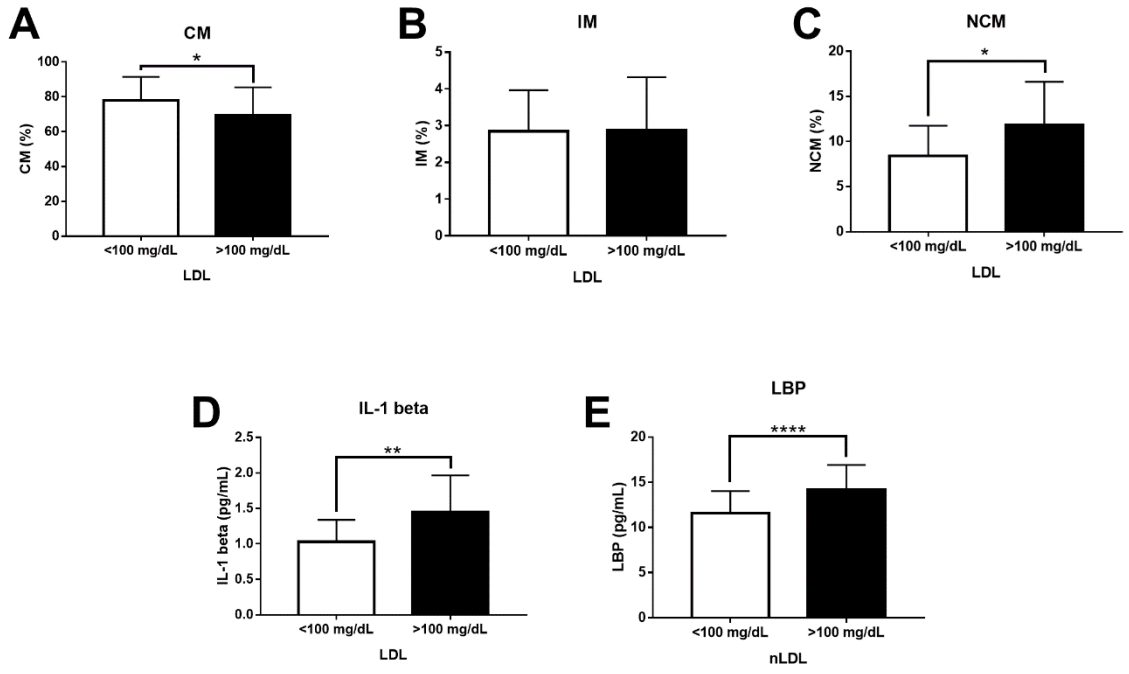

***Figura 16. ← Niveles de CM, IM, NCM, IL-1 beta y LBP en sujetos con niveles séricos óptimos y elevados de LDL-C. (A) El porcentaje de CM es significativamente menor en donadores con LDL-C sérico > 100 mg/dL (n = 85) en comparación con los controles (n = 65). (B) No hubo cambios significativos entre sujetos con concentración óptima y alta de LDL-C para el porcentaje de IM. (C) El porcentaje de NCM es significativamente mayor en donadores con LDL-C sérico > 100 mg/dl en comparación con los controles. (D) Los niveles séricos de IL-1 beta son significativamente superiores en donadores con LDL-C sérico > 100 mg/dl en comparación con los controles. (E) Los niveles séricos de LBP son significativamente mayores en donadores con LDL-C sérico > 100 mg/dl en comparación con los controles. Los datos se expresan como media ± desviación estándar. Los datos se compararon utilizando la prueba t de Student para datos no apareados. Las diferencias se consideraron significativas cuando p < 0.05. * = p < 0.05; ** = p < 0.01; **** = p < 0.0001. CM, monocitos clásicos; IM, monocitos intermedios; NCM, monocitos no clásicos; IL-1 beta, interleucina 1 beta; LBP, proteína de unión a LPS; LDL-C, lipoproteínas de baja densidad.***

## DISCUSIÓN

Se considera que los macrófagos y las LDLox son los principales contribuyentes a la formación de células espumosas y la infiltración de células inflamatorias en las lesiones ateroscleróticas [18]. Sin embargo, el hecho de que los monocitos y las nLDL puedan interactuar en el torrente sanguíneo ha planteado la cuestión de si estos precursores también podrían desempeñar un papel fundamental en la aterogénesis. En este sentido, la administración intraperitoneal de lipoproteínas ricas en triglicéridos disminuye el número de monocitos no clásicos Ly6C/Gr1low en ratones. Del mismo modo, la dislipidemia con niveles elevados de LDL o de lipoproteínas de muy baja densidad (VLDL) aumenta los subconjuntos de monocitos tanto Ly6C/Gr1high clásico como no clásico Ly6C/Gr1low en ratones alimentados con una dieta rica en grasas. De acuerdo con esta evidencia, nuestros resultados demuestran que nLDL puede alterar el equilibrio de las subpoblaciones de monocitos humanos al disminuir directamente a los monocitos clásicos y aumentar al subtipo de monocitos no clásicos *in vitro* y en nuestro modelo con donadores.

El mecanismo a través del cual las nLDL inducen el desequilibrio de los subconjuntos de monocitos aún no está claro y probablemente involucre la expresión de CD14 y CD16. Como se mencionó, la expresión de CD14 y CD16 es la característica principal que define las subpoblaciones de monocitos en humanos. CD14 es una proteína transmembrana que forma el complejo del receptor LPS junto con el receptor tipo Toll 4 (TLR4) y el factor de diferenciación mieloide 2 (MD-2). El complejo trimérico CD14/TLR4/MD-2 desencadena la vía de señalización dependiente del factor nuclear kappa B (NFκB) encargada de regular la expresión de citocinas inflamatorias como IL-6, TNF-alfa e IL-1 beta. La expresión de CD14 está regulada por la proteína de especificidad 1 (Sp1), un factor de transcripción que se activa a través del promotor del LDLr. Este cuerpo de evidencia apoya la idea de que nLDL podría disminuir la proporción de monocitos clásicos y aumentar el porcentaje de monocitos no clásicos al regular la expresión de CD14, probablemente a través de LDLr-Sp1. CD16 es un receptor Fc-gamma que reconoce microorganismos recubiertos de IgG y complejos inmunitarios. La evidencia reciente ha demostrado que la expresión de CD16 está bajo el control postranscripcional del microARN (miR)-218 en las células asesinas naturales (NK) humanas. *In vitro*, las oxLDL son capaces de disminuir la expresión de miR-218 en células

endoteliales microvasculares cardíacas de ratas. *In vivo*, la expresión de miR-218 se correlaciona inversamente con los niveles de oxLDL en pacientes con enfermedad arterial coronaria (EAC). En este sentido, el aumento de monocitos no clásicos CD14+CD16+ y la disminución de monocitos clásicos CD14+CD16− que encontramos pueden estar probablemente relacionados con la supresión de miR-218 que a su vez favorece la expresión de CD16, promoviendo la conversión de monocitos clásicos en monocitos no clásicos en respuesta a nLDL. Por lo tanto, la nLDL circulante puede inducir un desequilibrio de las subpoblaciones de monocitos humanos mediante mecanismos capaces de regular la expresión de CD14 y CD16, como los orquestados por LDLr, Sp1 y miR-218; sin embargo, esta hipótesis queda por dilucidar en estudios posteriores.

Diversas líneas de investigación han demostrado que los subconjuntos de monocitos humanos muestran acciones inflamatorias importantes expresando preferentemente IL-1 beta en respuesta a LPS. El LPS es un componente de la membrana externa de las bacterias Gram-negativas que puede translocarse a través de la pared intestinal hacia la circulación portal hepática, donde se une a LBP. El complejo LPS/LBP se considera un desencadenante inflamatorio clave para monocitos y macrófagos y se ha encontrado que está aumentado en sujetos obesos con cardiopatía aterosclerótica, entre los cuales también está aumentado el nLDL. Tras el reconocimiento, el LPS induce la síntesis de pro-IL-1 beta dependiente de NFκB, que a su vez es escindida proteolíticamente por el inflamasoma de la proteína 3 que contiene el dominio de pirina, NOD y LRR (NLRP3) para formar IL-1 beta en forma madura. La IL-1 beta tiene múltiples funciones en la aterogénesis. En las células endoteliales microvasculares humanas, la IL-1 beta estimula la expresión de la molécula de adhesión intracelular 1 (ICAM-1) y la molécula de adhesión de células vasculares 1 (VCAM-1), que tienen la capacidad de reclutar leucocitos en la capa interna de las arterias. En las células del músculo liso de la aorta humana, la IL-1 beta induce la expresión de la proteína quimioatrayente de monocitos-1 (MCP-1), que a su vez contribuye a la migración de células mononucleares hacia el endotelio vascular. La IL-1 beta también promueve directamente la formación de lesiones ateroscleróticas al estimular la producción de factor de crecimiento derivado de plaquetas, una molécula con la capacidad de inducir la proliferación de células de músculo liso vascular en el ateroma. Curiosamente, la exposición de las células endoteliales y las células del músculo liso vascular a LPS aumenta la liberación de IL-1 beta

en las placas ateroscleróticas de pacientes con niveles elevados de LDL. Nuestros datos amplían este cuerpo de evidencia al demostrar por primera vez que el LPS actúa en sinergia con el nLDL para aumentar la síntesis de IL-1 beta en monocitos humanos cultivados *in vitro*, especialmente en los subconjuntos de monocitos clásicos e intermedios.

En el modelo con donadores, nuestros resultados confirman que los sujetos con niveles elevados de LDL-C en suero también muestran un índice aterogénico elevado, así como niveles más altos de IL-1 beta y LBP que los que se encuentran en individuos con concentraciones óptimas de LDL-C. Sin embargo, vale la pena mencionar que aún necesitamos evaluar el efecto potencial del número y tamaño de partículas de LDL en la dinámica de las subpoblaciones de monocitos humanos y su capacidad para producir IL-1 beta, lo que puede ampliar el conocimiento sobre las múltiples acciones del nLDL en la respuesta inflamatoria asociada con la aterosclerosis.

Sorprendentemente encontramos que TNF alfa al contrario de lo que se espera, disminuyo en presencia de nLDL, pero solo en presencia LPS y nLDL y en monocitos clásicos fue cuando hallamos una diferencia estadísticamente significativa. Por otro lado, Mukherjee y colaboradores encontraron que disminuía la expresión de TNF alfa en monocitos no clásicos a las 6 horas de cultivo (Mukherjee et al., 2015); lo que nos habla de una dinámica muy diferente en comparación con IL-1 beta, camino que se debe continuar investigando.

Cuando examinamos a CD36 como un modificador en la entrada de nLDL al interior de la célula, nos enfrentamos a un resultado parcial; en el cual no se modifica la expresión de CD36 en presencia de nLDL, LPS y nLDL + LPS. Por lo que en un futuro es necesario evaluar la expresión de CD36 cuando se bloqueé el ingreso de nLDL a través de anticuerpos; 1) anti-LDLr, 2) anti-CD36, 3) anti- LDLr + anti-CD36. De manera paralela se deberá calcular la cantidad de nLDL que entro a la célula, así como la modificación de los porcentajes en las subpoblaciones de monocitos y la expresión de citosinas y quimiocinas por parte de estas.

El nLDL y el LPS no sólo mostraron efectos sinérgicos en la distribución de los subconjuntos de monocitos humanos y su capacidad para producir IL-1 beta, sino que

también afectaron el patrón de expresión de receptores de quimiocinas como CCR2 y CX3CR1. CCR2 es un receptor de quimiocinas C-C expresado principalmente en células mononucleares que media la migración de monocitos a tejidos inflamados en respuesta a MCP-1. CX3CR1 es el receptor celular de fractalcina, una quimioquina con la capacidad de inducir la retención de monocitos en circulación, preferiblemente aquellos que expresan CD16 como los monocitos intermedios y no clásicos. En nuestro estudio, el número de monocitos no clásicos CCR2+ aumentó en respuesta a nLDL y LPS, lo que puede actuar a favor de promover el reclutamiento de estas células al endotelio vascular. De acuerdo con estos hallazgos, un trabajo seminal realizado por Han et al. informó que la expresión de CCR2 aumenta en monocitos primarios de donadores con valores séricos de LDL-C elevados con respecto a los controles con niveles normales de colesterol. Además, la exposición de monocitos THP-1 a nLDL induce un aumento significativo tanto en la expresión de CCR2 como en la respuesta quimiotáctica *in vitro* a MCP-1, lo que sugiere que el nLDL podría incrementar el reclutamiento de monocitos a la lesión aterosclerótica.

En línea con la idea de un mayor reclutamiento celular, nuestros datos muestran que el nLDL y el LPS también redujeron la cantidad de monocitos no clásicos que expresaban CX3CR1. En este sentido, Nielsen y colaboradores encontraron una alteración en la expresión de TNF-alfa y CX3CR1 en monocitos primarios de pacientes con hipercolesterolemia familiar en comparación con sujetos con niveles normales de LDL-C. Curiosamente, la expresión de TNF-alfa y CX3CR1 se correlacionó positivamente con un mayor grosor de la íntima-media y la PCR de alta sensibilidad, ambos marcadores de aterosclerosis y riesgo cardiovascular. Paralelamente, Geng et al. demostraron que la administración de LPS a ratones ApoE-/- aumenta el reclutamiento de monocitos y la acumulación de macrófagos en las placas ateroscleróticas aórticas, lo que coincide con un aumento del depósito de lípidos en el ateroma. En conjunto, estos hallazgos respaldan la idea de que el nLDL y el LPS pueden contribuir directamente a la aterogénesis al alterar el patrón de expresión de las citocinas inflamatorias y los receptores de quimiocinas en los monocitos, lo que puede promover el reclutamiento de estas células hacia el ateroma. Sin embargo, esta idea aún debe probarse en enfoques experimentales *in vivo* centrados en caracterizar cómo el nLDL y el LPS afectan el patrón de reclutamiento de monocitos productores de IL-1 beta, CCR2 y CX3CR1 en lesiones ateroscleróticas.

Como hemos señalado aquí, el nLDL parece tener funciones proinflamatorias adicionales en la aterogénesis que difieren de las descritas clásicamente para el oxLDL. Además, los efectos del nLDL sobre la capacidad inflamatoria de las subpoblaciones de monocitos humanos se ven potenciados por el LPS, lo que confirma evidencia previa que sugiere que la nLDL y el LBP forman un círculo vicioso que contribuye a la aterosclerosis.

## CONCLUSIÓN

En conclusión, utilizando ensayos complementarios *in vitro* y en donadores, este trabajo demuestra por primera vez que el nLDL tiene un efecto directo sobre el equilibrio de los subconjuntos de monocitos humanos. Este efecto está dado por un aumento de la población de monocitos clásicos y la disminución de monocitos no clásicos, así como su capacidad para producir citocinas inflamatorias, evidenciado por el aumento intracelular de IL-1 beta, así como niveles séricos de IL-1 beta mayores en sujetos con valores de LDL-C superiores a 100 mg/dL. Asimismo, el efecto del nLDL podría estar mediado por un aumento en la expresión y el porcentaje de CX3CR1+ en NCM. Por otro lado, la expresión de CD36 no se ve afectada por nLDL. Estos efectos fueron potenciados por el LPS. Finalmente, se encontró que los niveles de LBP fueron claramente mayores en sujetos con LDL-C > 100 mg/dL, lo cual confirma los hallazgos *in vitro* sobre el efecto del nLDL sobre las subpoblaciones de monocitos humanos.

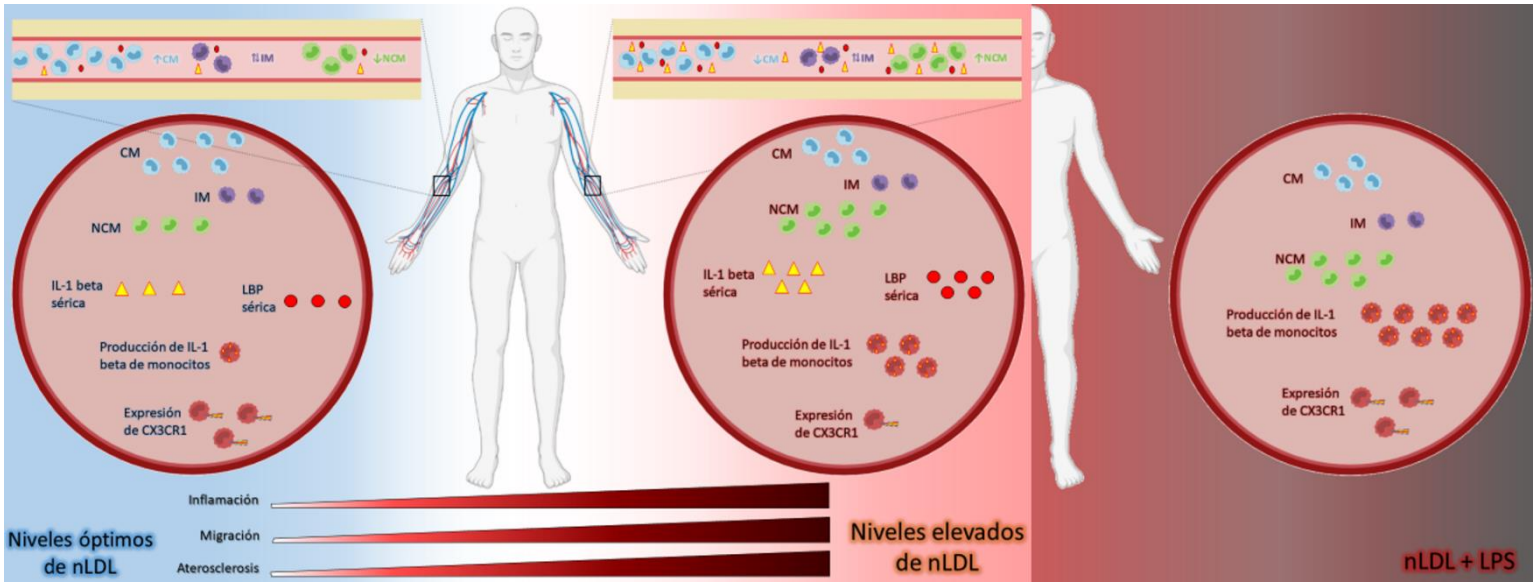


***Figura 17. ← Conclusión Grafica. CM, monocitos clásicos; IM, monocitos intermedios; NCM, monocitos no clásicos; nLDL, lipoproteínas de baja densidad nativas; LPS, lipopolisacárido; CX3CR1, receptor de quimiocinas CX3C 1; IL-1 beta, interleucina 1 beta; LBP, proteína de unión a LPS.***

## PERSPECTIVAS

A partir de los estudios y discusiones presentados en esta Tesis Doctoral, las perspectivas de trabajos futuros se dividen en observar no sólo el incremento de citocinas y de receptores de quimiocinas a tiempos cortos en cultivo, sino que también a tiempo largos (24 hrs en adelante) confirmando la presencia de estos por citometría de flujo y evaluando por medio de LipiodTox la incorporación de LDL después del cultivo. Además, aun es necesario evaluar la expresión de CD36 cuando se bloquee el ingreso de LDL. Además, estos resultados abren un panorama para el estudio de nuevos enfoques terapéuticos que disminuyan tanto los niveles de nLDL como de LPS/LBP, y así contribuyan a un menor desarrollo de aterosclerosis subclínica y clínica.

## REFERENCIAS


Al-Sharea, A., Lee, M. K. S., Moore, X.-L., Fang, L., Sviridov, D., Chin-Dusting, J., Andrews, K. L., & Murphy, A. J. (2016). Native LDL promotes differentiation of human monocytes to macrophages with an inflammatory phenotype. *Thrombosis and Haemostasis*, *115*(04), 762–772. https://doi.org/10.1160/TH15-07-0571

Berrington de Gonzalez, A., Hartge, P., Cerhan, J. R., Flint, A. J., Hannan, L., MacInnis, R. J., Moore, S. C., Tobias, G. S., Anton-Culver, H., Freeman, L. B., Beeson, W. L., Clipp, S. L., English, D. R., Folsom, A. R., Freedman, D. M., Giles, G., Hakansson, N., Henderson, K. D., Hoffman-Bolton, J., … Thun, M. J. (2010). Body-Mass Index and Mortality among 1.46 Million White Adults. *New England Journal of Medicine*, *363*(23), 2211–2219. https://doi.org/10.1056/nejmoa1000367

Brown, M. S., & Goldstein, J. L. (1984). How LDL receptors influence cholesterol and atherosclerosis. *Scientific American*, *251*(5), 58–66. https://doi.org/10.1038/scientificamerican1184-58

Brown, Michael S., & Goldstein, J. L. (1986). A receptor-mediated pathway for cholesterol homeostasis. *Science*, *232*(4746), 34–47. https://doi.org/10.1126/science.3513311

Calvo, D., Gómez-Coronado, D., Suárez, Y., Lasunción, M., & Vega, M. (1998). Human CD36 is a high affinity receptor for the native lipoproteins HDL, LDL, and VLDL. *Journal of Lipid Research*, *39*(4), 777–788. https://doi.org/Doi 10.1016/0013-4694(72)90178-2

Chávez-Sánchez, L., Madrid-Miller, A., Chávez-Rueda, K., Legorreta-Haquet, M. V., Tesoro-Cruz, E., & Blanco-Favela, F. (2010). Activation of TLR2 and TLR4 by minimally modified low-density lipoprotein in human macrophages and monocytes triggers the inflammatory response. *Human Immunology*, *71*(8), 737–744. https://doi.org/10.1016/j.humimm.2010.05.005

Chávez-Sánchez, Luis, Garza-Reyes, M. G., Espinosa-Luna, J. E., Chávez-Rueda, K.,

Legorreta-Haquet, M. V., & Blanco-Favela, F. (2014). The role of TLR2, TLR4 and CD36 in macrophage activation and foam cell formation in response to oxLDL in humans. *Human Immunology*, *75*(4), 322–329. https://doi.org/10.1016/j.humimm.2014.01.012

Consejo de Salubridad General. (2011). Guía de Referencia Rápida. Diagnóstico y Tratamiento de las Dislipidemias. *Catálogo Maestro de Guías de Práctica Clínica: IMSS-233-09*, 16. https://doi.org/10.1074/jbc.M000903200

Devevre, E. F., Renovato-Martins, M., Clément, K., Sautès-Fridman, C., Cremer, I., & Poitou, C. (2015). Profiling of the Three Circulating Monocyte Subpopulations in Human Obesity. *The Journal of Immunology*, *194*(8), 3917–3923. https://doi.org/10.4049/jimmunol.1402655

Duellman, S. J., Machleidt, T., Cali, J. J., & Vidugiriene, J. (2017). Cell-based, bioluminescent assay for monitoring the interaction between PCSK9 and the LDL receptor. *Journal of Lipid Research*, *58*(8), 1722–1729. https://doi.org/10.1194/jlr.D074658

Feng, J., Han, J., Pearce, S. F. A., Silverstein, R. L., Gotto, A. M., Hajjar, D. P., & Nicholson, A. C. (2000). Induction of CD36 expression by oxidized LDL and IL-4 by a common signaling pathway dependent on protein kinase C and PPAR-γ. *Journal of Lipid Research*, *41*(5), 688–698.

Geissmann, F. (2010). Development of Monocytes, Macrophages, and Dendritic Cells. *Science*, *656*(2010). https://doi.org/10.1126/science.1178331

Geng, Y., Zhang, L., Fu, B., Zhang, J., Hong, Q., Hu, J., Li, D., Luo, C., Cui, S., Zhu, F., & Chen, X. (2014). Mesenchymal stem cells ameliorate rhabdomyolysis-induced acute kidney injury via the activation of M2 macrophages. *Stem Cell Research and Therapy*, *5*(3), 1–14. https://doi.org/10.1186/scrt469

Gerhardt, T., & Ley, K. (2015). Monocyte trafficking across the vessel wall. *Cardiovascular Research*, *107*(3), 321–330. https://doi.org/10.1093/cvr/cvv147

Go, G. W., & Mani, A. (2012). Low-density lipoprotein receptor (LDLR) family orchestrates cholesterol homeostasis. *Yale Journal of Biology and Medicine*, *85*(1), 19–28. https://doi.org/10.1080/19440049.2011.569573

Gordon, S., & Taylor, P. R. (2005). Monocyte and macrophage heterogeneity. *Nature Reviews Immunology*, *5*(12), 953–964. https://doi.org/10.1038/nri1733

Grundy, S., Cleeman, J., Bairey, Merz, C., & et al. (2004). Coordinating Committee of the National Cholesterol Education Program. Implications of the recent clinical trials for the National Cholesterol Education Program Adult Treatment Panel III Guidelines. *Circulation*, *110*(Atp Iii), 227–239.

Grundy, S. M., Becker, D., Clark, L. T., Cooper, R. S., Denke, M. A., Howard, J., Hunninghake, D. B., Illingworth, R., Luepker, R. V, McBride, P., McKerney, J. M., Pasternak, R. C., Stone, N. J., & Van Horn, L. (2001). Executive Summary of the Third Report ( NCEP ) Expert Panel on Detection , Evaluation , and Treatment of High Blood Cholesterol in Adults ( Adult Treatment Panel III ). *Journal of American Medical Association*, *285*(19), 2486–2497.

Han, J., Hajjar, D. P., Febbraio, M., & Nicholson, A. C. (1997). Native and modified low density lipoproteins increase the functional expression of the macrophage class B scavenger receptor, CD36. *Journal of Biological Chemistry*, *272*(34), 21654–21659. https://doi.org/10.1074/jbc.272.34.21654

Han, K. H., Tangirala, R. K., Green, S. R., & Quehenberger, O. (1998). Chemokine Receptor CCR2 Expression and Monocyte Chemoattractant Protein-1–Mediated Chemotaxis in Human Monocytes. *Arteriosclerosis, Thrombosis, and Vascular Biology*, *18*(12), 1983–1991. https://doi.org/10.1161/01.ATV.18.12.1983

Hansson, G. K. (2005). Inflammation, Atherosclerosis, and Coronary Artery Disease. *New England Journal of Medicine*, 1685–1695.

Henning, A. L. (2014). *Monitoring Monocyte oxLDL Phagocytosis as a Cardiovascular Disease Risk Factor Following a High-Fat Meal*.

Jackson, W. D., Weinrich, T. W., & Woollard, K. J. (2016). Very-low and low-density lipoproteins induce neutral lipid accumulation and impair migration in monocyte subsets. *Scientific Reports*, *6*(January), 1–12. https://doi.org/10.1038/srep20038

Jakubzick, C. V, Randolph, G. J., & Henson, P. M. (2017). Monocyte differentiation and antigen-presenting functions. *Nature Reviews Immunology*, *17*(6), 349–362. https://doi.org/10.1038/nri.2017.28

Janabi, M., Yamashita, S., Hirano, K. I., Sakai, N., Hiraoka, H., Matsumoto, K., Zhang, Z., Nozaki, S., & Matsuzawa, Y. (2000). Oxidized LDL-induced NF-κB activation and subsequent expression of proinflammatory genes are defective in monocyte-derived macrophages from CD36-deficient patients. *Arteriosclerosis, Thrombosis, and Vascular Biology*, *20*(8), 1953–1960. https://doi.org/10.1161/01.ATV.20.8.1953

Lambert, G., Thedrez, A., Croyal, M., Ramin-Mangata, S., Couret, D., Diotel, N., Nobécourt-Dupuy, E., Krempf, M., LeBail, J. C., Poirier, B., Blankenstein, J., Villard, E. F., & Guillot, E. (2017). The complexity of lipoprotein (a) lowering by PCSK9 monoclonal antibodies. *Clinical Science*, *131*(4), 261–268. https://doi.org/10.1042/CS20160403

Levitan, I., Volkov, S., & Subbaiah, P. V. (2009). Oxidized LDL: Diversity, Patterns of Recognition, and Pathophysiology. *Antioxidants & Redox Signaling*. https://doi.org/10.1089/ars.2009.2733

Libby, P., Tabas, I., Fredman, G., & Fisher, E. A. (2014). Inflammation and its Resolution as Determinants of Acute Coronary Syndromes. *Circulation Research*, 1867–1879. https://doi.org/10.1161/CIRCRESAHA.114.302699

Mukherjee, R., Kanti Barman, P., Kumar Thatoi, P., Tripathy, R., Kumar Das, B., & Ravindran, B. (2015). Non-Classical monocytes display inflammatory features: Validation in Sepsis and Systemic Lupus Erythematous. *Scientific Reports*, *5*(May), 1–14. https://doi.org/10.1038/srep13886

Okura, Y., Brink, M., Itabe, H., Scheidegger, K. J., Kalangos, A., & Delafontaine, P.

(2000). Oxidized low-density lipoprotein is associated with apoptosis of vascular smooth muscle cells in human atherosclerotic plaques. *Circulation*. https://doi.org/10.1161/01.CIR.102.22.2680

Olaiz-Fernández G, Rivera-Dommarco J, Shamah-Levy T, Rojas R, Villalpando-Hernández S, Hernández-Avila M, S.-A. J. (2006). *Encuesta Nacional de Salud y Nutrición 2006*. Instituto Nacional de Salud Pública.

Raúl Carrillo Esper, Martín De Jesús Sánchez Zúñiga, S. E. A. (2006). Síndrome metabólico. *Rev Fac Med UNAM*, *49*.

Romero-Martínez, M., Shamah-Levy, T., Cuevas-Nasu, L., Gómez-Humarán, I. M., Gaona-Pineda, E. B., Gómez-Acosta, L. M., Rivera-Dommarco, J. Á., & Hernández-Ávila, M. (2016). [Methodological design of the National Health and Nutrition Survey 2016]. *Salud Publica de Mexico*, *59*(3), 299–305. https://doi.org/10.21149/8593

Shi, C., & Pamer, E. G. (2011). Monocyte recruitment during infection and inflammation. *Nature Reviews Immunology*, *11*(11), 762–774. https://doi.org/10.1038/nri3070

Tall, A. R., & Yvan-Charvet, L. (2015). Cholesterol, inflammation and innate immunity. *Nature Reviews Immunology*, *15*(2), 104–116. https://doi.org/10.1038/nri3793

Viola, J., & Soehnlein, O. (2015). Atherosclerosis – A matter of unresolved inflammation. *Seminars in Immunology*, 1–10. https://doi.org/10.1016/j.smim.2015.03.013

Witztum, J. L. (1994). The oxidation hypothesis of atherosclerosis. *The Lancet*. https://doi.org/10.1016/S0140-6736(94)92346-9

Woollard, K. J., & Geissmann, F. (2010). Monocytes in atherosclerosis: Subsets and functions. *Nature Reviews Cardiology*, *7*(2), 77–86. https://doi.org/10.1038/nrcardio.2009.228

Zhang, Y., Ma, K. L., Ruan, X. Z., & Liu, B. C. (2016). Dysregulation of the low-density lipoprotein receptor pathway is involved in lipid disorder-mediated organ injury. *International Journal of Biological Sciences*, *12*(5), 569–579.

https://doi.org/10.7150/ijbs.14027

Ziegler-Heitbrock, L., Leenen, P. J. M., Ancuta, P., Sozzani, S., Austyn, J. M., Crowe, S., Dalod, M., Grau, V., Hart, D. N., Shortman, K., Scherberich, J., Schmitz, J., Lutz, M. B., MacPherson, G., Zembala, M., & Liu, Y.-J. (2010). Nomenclature of monocytes and dendritic cells in blood. *Blood*, *116*(16), e74–e80. https://doi.org/10.1182/blood-2010-02-258558

Ziegler-Heitbrock, Loems. (2015). Blood monocytes and their subsets: Established features and open questions. *Frontiers in Immunology*, *6*(AUG), 1–5. https://doi.org/10.3389/fimmu.2015.00423

Ziegler-Heitbrock, Loems, & Hofer, T. P. J. (2013). Toward a refined definition of monocyte subsets. *Frontiers in Immunology*, *4*(FRB), 1–5. https://doi.org/10.3389/fimmu.2013.00023

# ANEXO I: ARTÍCULOS GENERADOS DURANTE LOS ESTUDIOS DE POSGRADO

Journal of
*Cardiovascular Development and Disease*

MDPI

*Article*

# The CCR2$^+$ Monocyte Subsets Increase in Obese Boys but Not Girls with Abnormally High Carotid Intima-Media Thickness: A Pilot Study

**María José Garcés-Hernández [1,*], Karen Pedraza-Escudero [1], Nayely Garibay-Nieto [1], Joselin Hernández-Ruiz [2], Jessica Lakshmi Prieto-Chávez [3], Lourdes Andrea Arriaga-Pizano [3], Eréndira Villanueva-Ortega [1], Galileo Escobedo [4], Aaron Noe Manjarrez-Reyna [4], Juan Carlos López-Alvarenga [5,6], José Luis Pérez-Hernández [7] and Gloria Queipo-García [8]**

1 Childhood Obesity Clinic, Hospital General de México Dr. Eduardo Liceaga, Ciudad de México 06720, Mexico
2 Clinical Pharmacology Unit, Hospital General de México Dr. Eduardo Liceaga, Dr. Balmis 148, Doctores, Cuauhtémoc, Ciudad de México 06720, Mexico
3 Flow Cytometry Laboratory, Instrumental Center, Health Investigation Coordination, Hospital de Especialidades del Centro Médico Siglo XXI, Instituto Mexicano del Seguro Social, Ciudad de México 06720, Mexico
4 Laboratory of Immunometabolism, Research Division, General Hospital of México "Dr. Eduardo Liceaga", Ciudad de México 06720, Mexico
5 Population Health and Biostatistics, School of Medicine, University of Texas Rio Grande Valley, Edinburg, TX 78539, USA
6 Research Department, Universidad México-Americana del Norte, Reynosa 88640, Mexico
7 Gastroenterology and Hepatology Department, Hospital General de México "Dr. Eduardo Liceaga", Ciudad de México 06720, Mexico
8 Department of Human Genetics, Hospital General de México "Dr. Eduardo Liceaga", Ciudad de México 06720, Mexico
* Correspondence: majogarces7@gmail.com

check for updates

**Citation:** Garcés-Hernández, M.J.; Pedraza-Escudero, K.; Garibay-Nieto, N.; Hernández-Ruiz, J.; Prieto-Chávez, J.L.; Arriaga-Pizano, L.A.; Villanueva-Ortega, E.; Escobedo, G.; Manjarrez-Reyna, A.N.; López-Alvarenga, J.C.; et al. The CCR2$^+$ Monocyte Subsets Increase in Obese Boys but Not Girls with Abnormally High Carotid Intima-Media Thickness: A Pilot Study. *J. Cardiovasc. Dev. Dis.* **2022**, *9*, 330. https://doi.org/10.3390/jcdd9100330

Academic Editor: Maria Grazia Andreassi

Received: 13 August 2022
Accepted: 23 September 2022
Published: 29 September 2022

**Publisher's Note:** MDPI stays neutral with regard to jurisdictional claims in published maps and institutional affiliations.



**Abstract:** The differential contribution of monocyte subsets expressing the C-C chemokine receptor 2 (CCR2) to subclinical atherosclerosis in girls and boys is unclear. In this pilot study, we compared classical, intermediate, and nonclassical monocyte subsets expressing CCR2 in 33 obese children of both sexes aged 8 to 16 divided by carotid intima-media thickness (IMT), considering values above the 75th percentile (p75) as abnormally high IMT. Obesity was defined as body mass index above the 95th percentile according to age and sex. Flow cytometry analyses revealed that boys but not girls with IMT $\geq$ p75 displayed increased CCR2$^+$ cell percentage and CCR2 expression in the three monocyte subsets, compared to boys with IMT < p75. The CCR2$^+$ cell percentage and CCR2 expression in the three monocyte subsets significantly correlated with increased IMT and insulin resistance in boys but not girls, where the CCR2$^+$ nonclassical monocyte percentage had the strongest associations ($r$ = 0.73 and $r$ = 0.72, respectively). The role of CCR2$^+$ monocyte subpopulations in identifying an abnormally high IMT shows a marked sexual dimorphism, where boys seem to be at higher subclinical atherosclerosis risk than girls.

**Keywords:** CCR2; nonclassical monocytes; children; intima-media thickness; insulin resistance; obesity

## 1. Introduction

Obesity is a risk factor for coronary heart disease. Cardiovascular diseases cause nearly 70% of deaths among persons with a high body mass index (BMI) [1]. Coronary artery disease, also known as atherosclerosis, is the most common heart disease characterized by the accumulation of cholesterol esters-ingesting macrophages in the subendothelial space of coronary arteries [2].

During obesity, cholesterol levels considerably increase and adhere to the vascular endothelium, triggering the local release of reactive oxygen species and the recruitment of

macrophages, which can expand vascular injury and promote atherogenesis [3,4]. Therefore, the atherosclerotic process originates with endothelial damage and dysfunction that lead to the recruitment of circulating monocytes with the ability to adhere to and infiltrate the injured arterial wall [5]. There, monocytes differentiate into macrophages that actively uptake cholesterol esters by phagocytosis, resulting in foam cell formation and further vessel wall inflammation. Foam cells contribute to intima-media thickening (IMT), a condition correlating with increased insulin resistance in children with obesity who can become individuals with advanced atherosclerosis in adult life [6–9]. In fact, insulin resistance that reflects the progressive loss of the action of insulin on target tissues is also an independent risk factor for developing systemic inflammation that often accompanies atherosclerotic cardiovascular disease [10].

Monocytes are divided into three subpopulations according to CD14 and CD16 expression as follows: classical monocytes ($CD14^{++}CD16^{-}$), intermediate monocytes ($CD14^{++}CD16^{+}$), and nonclassical monocytes ($CD14^{+}CD16^{+}$). The infiltration of monocyte subsets into artery vessels occurs in response to the C-C chemokine receptor 2 (CCR2), a G protein-coupled receptor whose ligands include the monocyte chemoattractant protein (MCP) family [11].

A recent study reported an increase in intermediate monocytes expressing CCR2 in adults with atherosclerosis [11]. CCR2 expression also elicits the adhesion of classical and nonclassical monocytes to the vascular endothelium during atherosclerosis [12]. Another study showed that these monocyte subsets could even help predict an impaired endothelial dysfunction in patients with atherosclerosis in a sex- and age-dependent fashion [13].

Currently, there is evidence of the influence of sex in the risk of developing atherosclerosis. Premenopausal women display less pro-atherogenic lipid profiles than men [14]. Ischemic cardiovascular disease resulting from atherosclerosis occurs more often in men than women. At an early age, male children and adolescents show higher IMT than girls [15]. Sexual dimorphism also influences the CCR2–MCP-1 axis. Petty and colleagues found that African American male adolescents present higher MCP-1 serum levels than females [16], confirming further evidence, indicating that MCP-1 is elevated only in male mice fed a high-fat diet (HFD) [17]. Verweij and coworkers expanded this body of evidence by showing that being a man significantly contributes to an elevated CCR2 expression in circulating monocytes, mostly classical monocytes [18].

Although increasing evidence in adults indicates that monocyte subsets expressing CCR2 contribute to atherosclerosis in a sex-dependent fashion, there is still scant information on girls and boys with obesity. Herein, we conducted a pilot study to analyze $CCR2^{+}$ monocyte subpopulations in children of both sexes with obesity, examining the association of these immune cells with cardiovascular risk factors, such as IMT and insulin resistance in a sex-dependent fashion.

## 2. Materials and Methods

### *2.1. Participants*

Initially, 40 children fulfilled the inclusion criteria. After the first biochemical analysis, we identified three volunteers with abnormally high blood cholesterol levels and removed them from the study. Another four volunteers did not agree to provide 6 mL of venous blood, and we withdrew them from the study. In the end, we enrolled 33 children with obesity aged 8 to 16 years in this pilot study. We included all study participants from the Childhood Obesity Clinic at the General Hospital of Mexico between 2017 and 2019. All volunteers agreed to participate in the study by signing the informed consent and assent letters. We excluded from the study participants with a diagnosis of familial hypercholesterolemia, hypertriglyceridemia, or diabetes mellitus, as well as children consuming alcohol or any drug interfering with metabolism and immune response to avoid potential confounding effects on parameters of subclinical atherosclerosis and CCR2 expression in monocyte subpopulations.

We conducted this study after getting approval from the Research, Ethics, and Biosafety Committees for Human Research of the General Hospital of Mexico (registration number: DI/17/311/03/028), following the ethical guidelines of the 1975 Declaration of Helsinki and its posterior amendment in 2013. According to the clinical practice guidelines of the Pediatric Endocrine Society, we used BMI $\geq$ 95th percentile according to age and sex to diagnose obesity in the studied children [19,20]. We calculated BMI by dividing weight in kilograms by the square of the height in meters.

### 2.2. Anthropometric Measurements

A group of two trained pediatricians and a nutritionist performed all anthropometric measurements in the study population. We measured body weight and composition using the Body Composition Analyzer Model IOI 353 scale (to 0.1 kg). Moreover, we used a stadiometer board mounted on the wall to register height (to the nearest 0.1 cm). We measured waist circumference (WC) using tape in a horizontal line at the midpoint between the lowest rib and the iliac crest. We registered blood pressure with a digital sphygmomanometer, following a fifteen-minute rest. We assessed pubertal development according to the Tanner stages.

### 2.3. Biochemical Markers

We obtained blood samples after 12 h fasting to measure metabolic markers, including glucose, insulin, uric acid, triglycerides, and liver function tests. We measured glucose, aminotransferases, total cholesterol, high density lipoprotein (HDL) cholesterol, low density lipoprotein (LDL) cholesterol, and triglycerides by enzymatic assays, using the Beckman Coulter DxC 700 AU Chemistry Analyzer (Beckman Coulter Inc., Brea, CA, USA). We determined serum insulin by ELISA (Abnova, Corporation, Taipei City, Taiwan).

We calculated the Homeostasis Model Assessment of insulin resistance (HOMA) by multiplying fasting glucose (mg/dL) by fasting insulin (mU/L) divided by 405. We considered children with insulin resistance as having HOMA values $\geq$ 3.4 [21,22].

### 2.4. Ultrasound Measurements

We used the Siemens Accuson 2000 ultrasound with high resolution (2 and 12 MHz) to get all ultrasound images. We measured abdominal fat by calculating the preperitoneal fat area (PFA). We placed a linear probe perpendicular to the skin of the median upper abdomen, moving the probe longitudinally from the xiphoid process to the umbilicus along with the midline to obtain an image that contained the maximum preperitoneal fat thickness. We considered the PFA as the full height of the triangular-shaped area in the transversal image. We measured the total preperitoneal area starting from the position of the maximum preperitoneal thickness over a distance of 20 mm in the caudal direction [23]. We evaluated the vascular structure as the intima-media thickness (IMT). We measured IMT in a supine position, with the neck extended and the probe in the anterolateral place in a longitudinal plane on the far wall of the left internal carotid artery 1 cm from the carotid bulb. A senior expert radiologist performed five measurements on each study volunteer, using the average IMT value for further analyses. We evaluated the inter-observer variability by calculating Cohen's kappa index, finding a $\kappa = 0.89$, which suggests a high reproducibility when measuring IMT. Depending on age and sex, we defined a high-risk IMT value when it fell above the 75th percentile (p75), based on Böhm et al. [15].

### 2.5. Total Leukocyte Isolation and Flow Cytometry

We obtained 6 mL of venous blood from all study participants and placed them in vacutainer tubes treated with EDTA. Immediately after, we centrifuged blood samples at 1200 rpm for 10 min and took the layer of white blood cells to transfer it to 2.5 mL Eppendorf tubes. We removed red blood cells using 1 mL ACK erythrocyte lysis buffer for 7 min at 4 °C. After centrifuging at 2000 rpm/4 °C for 5 min, we discarded the supernatant and obtained the leukocyte fraction. Later, we rinsed the cells with phosphate buffer saline

1X (PBS 1X), and after a centrifugation step at 2000 rpm/4 °C for 5 min, we transferred the cell pellet to 0.6 mL Eppendorf tubes. We counted cells using a Neubauer chamber by the Trypan blue exclusion test to determine the number of viable cells [20]. Next, we transferred leukocytes to an additional 0.6 mL Eppendorf tube at a density of $2 \times 10^6$ cells to incubate them with anti-CD14-PECy7 (BD Biosciences, Franklin Lakes, NJ, USA), anti-CD16-PECy5 (BD Biosciences, Franklin Lakes, NJ, USA), and anti-CCR2-Alexa Fluor 647 (BioLegend, San Diego, CA, USA) for 20 min at 4 °C in the absence of light. Then, we rinsed leukocytes with PBS1X and centrifuged samples at 2000 rpm/4 °C for 5 min. After that, we discarded the supernatant and suspended the cell pallet in 200 µL PBS. We acquired cells using the BD FACS Canto II, acquiring 10,000 monocyte events in triplicate. We categorized monocyte subsets according to CD14 and CD16 expression: $CD14^{++}CD16^{-}$, classical monocytes; $CD14^{++}CD16^{+}$, intermediate monocytes; $CD14^{+}CD16^{+}$, nonclassical monocytes (Figure 1). Whereas the percentage of positive cells reflects the number of cells expressing the target molecule, the mean fluorescence intensity (MFI) indicates how much the target molecule is produced in a specific cell population. For this reason, we obtained the MFI for CCR2, considering positive and negative cell populations for this marker. We obtained the percentage of positive cells for CCR2 using proper fluorescence minus one (FMO) controls, using UltraComp eBeads™ (Invitrogen™, Carlsbad, CA, USA) as compensation controls. We performed flow cytometry assays in the same controlled-temperature cell culture room between 9 and 11 in the morning to avoid procedural variations. We analyzed monocyte subpopulations using the FlowJo software version 10.0.

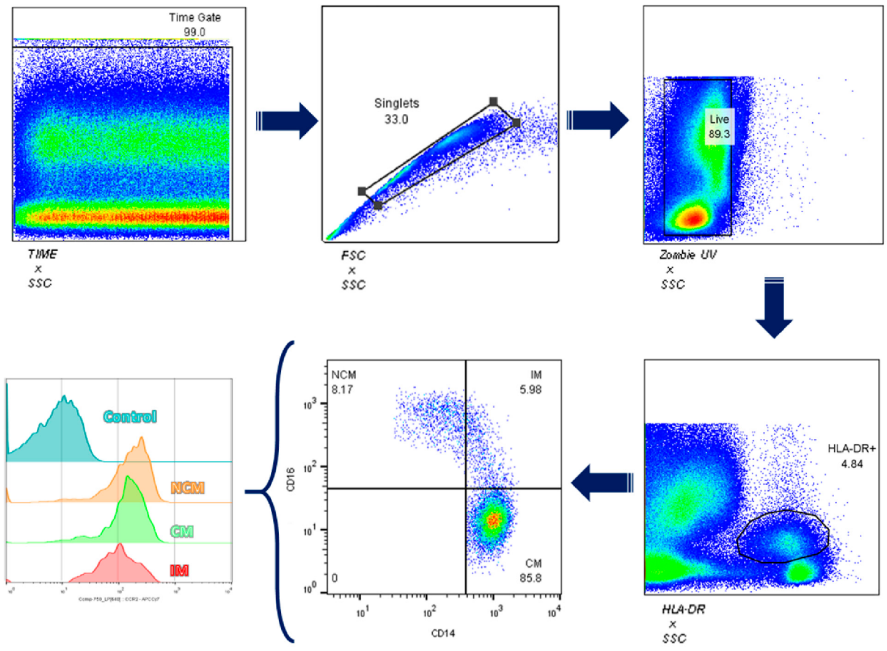


**Figure 1.** Gating Strategy. We first gated total leukocytes on a time/side scatter density plot and selected the Zombie UV negative cell population for detecting living cells. Next, we gated living cells for singlets on a forward scatter/trigger pulse width density plot. After recognizing cells by size and granularity, we selected monocytes on the HLA-DR gate. Then, we gated monocytes using the rectangular gating strategy on the $CD14^{+}/CD16^{+}$ cell population to identify $CD14^{++}CD16^{-}$ cells as

classical monocytes, $CD14^{++}CD16^{+}$ cells as intermediate monocytes, and $CD14^{+}CD16^{+}$ cells as nonclassical monocytes (Figure 1). We obtained the median fluorescence intensity (MFI) for CCR2 by considering both positive and negative cell populations. We got the $CCR2^{+}$ cell percentage using fluorescence minus one (FMO) control. For each fluorochrome, we used compensation controls through UltraComp eBeads™ (Invitrogen™, Carlsbad, CA, USA). We analyzed data by the FlowJo 10.0.7 software (TreeStar, Inc., Ashland, OR, USA).

### 2.6. Statistics

We show data as mean ± standard deviation (SD). According to IMT stratification, nine obese girls showed an IMT value above the p75, whereas IMT fell above the p75 in seven obese boys. We used the unpaired student *T*-test to compare demographic, cardiometabolic, and immune variables between girls and boys with and without increased IMT. We used the Pearson correlation test to calculate correlation coefficients with 95% confidence intervals between monocyte subsets and cardiometabolic outcomes. We used the rank-based inverse-normal transformation to estimate the interaction levels in the regression for sex, considering age and other metabolic and cellular variables. We adjusted data by sex, age, and sex–age interaction in multiple regression analysis, considering a minimum of ten subjects per variable to estimate regression coefficients, standard errors, and confidence intervals. Kappa calculation for IMT measurements was used to evaluate reproducibility of the data. We considered a $p$ value < 0.05 as significant. We analyzed data using SPSS version 22.0 and the GraphPad Prism 6.01 software (GraphPad Software, La Jolla, CA 92037, USA).

## 3. Results

### 3.1. Participants Characteristics

We enrolled 33 children with obesity with an average age of 10.9 ± 2.1, where 57.5% were females. According to sex, we found differences in body composition, where females showed a significant 4.6% increase in body fat percentage (BFP), compared to males ($p$ = 0.008). Conversely, males presented 33.4% more visceral fat adiposity (VFA), compared to females ($p$ = 0.002) (Table 1). There were no differences between females and males for BMI, WC, blood pressure, and PFA (Table 1). Children of both sexes presented similar pubertal stages and glucose homeostasis, showing similar blood glucose values, glycosylated hemoglobin, insulin, and HOMA (Table 1). Furthermore, there were no differences between females and males for uric acid, lipid profile, and liver function tests (Table 1). Children of both sexes also displayed similar IMT values, even after adjusting data by sex, age, or the interaction between these two variables (adjusted R square = 0.252).

**Table 1.** Demographic, anthropometric, biochemical, and cardiovascular characteristics of the study participants.

| | **All Participants ($n$ = 33)** | **Girls [a] ($n$ = 19)** | **Boys [b] ($n$ = 14)** | $p$ [a vs. b] |
|---|---|---|---|---|
| | Anthropometric variables | | | |
| Age (years) | 10.9 ± 2.1 | 11.0 ± 2.4 | 10.7 ± 1.7 | 0.741 |
| Weight (kg) | 59.1 ± 15.1 | 57.8 ± 14.9 | 60.9 ± 15.8 | 0.559 |
| Height (cm) | 147.6 ± 10.8 | 145.5 ± 11.32 | 150.4 ± 9.8 | 0.210 |
| BMI ($kg/m^2$) | 26.6 ± 3.3 | 26.8 ± 2.9 | 26.4 ± 3.8 | 0.786 |
| Waist (cm) | 86.5 ± 10.3 | 84.2 ± 8.3 | 89.7 ± 12.2 | 0.134 |
| SBP(mmHg) | 103.3 ± 9.8 | 101.5 ± 9.7 | 105.6 ± 9.8 | 0.247 |
| DBP (mmHg) | 68.7 ± 8.7 | 66.6 ± 7.0 | 71.5 ± 10.1 | 0.118 |
| BFP (%) | 31.4 ± 5.0 | 33.3 ± 3.8 | 28.7 ± 5.4 | **0.008** |
| VFA ($cm^3$) | 86.5 ± 34.5 | 71.3 ± 22.9 | 107.1 ± 37.5 | **0.002** |
| PFA ($cm^2$) | 4.6 ± 1.6 | 4.5 ± 1.9 | 4.6 ± 1.1 | 0.860 |

**Table 1.** *Cont.*

| | All Participants ($n$ = 33) | Girls [a] ($n$ = 19) | Boys [b] ($n$ = 14) | $p$ [a vs. b] |
|---|---|---|---|---|
| | Puberty Stages | | | |
| Tanner Stage | | | | |
| 1 | 43.3% | 33.3% | 58.3% | |
| 2 | 20% | 16.7% | 25% | 0.111 |
| 3 | 10% | 5.6% | 26.7% | |
| 4 | 23.3% | 38.9% | 0% | |
| 5 | 3.3% | 5.6% | 0% | |
| | Glucose Homeostasis | | | |
| Glucose (mg/dL) | 88.6 ± 8.4 | 88.9 ± 8.7 | 86.8 ± 8.2 | 0.493 |
| HbA1c | 5.3 ± 0.2 | 5.2 ± 0.1 | 5.3 ± 0.2 | 0.183 |
| Insulin (mg/dL) | 16.4 ± 1.4 | 16.9 ± 7.2 | 15.6 ± 10.2 | 0.687 |
| HOMA | 3.7 ± 1.9 | 4.0 ± 1.7 | 3.4 ± 2.3 | 0.403 |
| | Biochemical variables | | | |
| Uric acid (mg/dL) | 5.7 ± 1.0 | 5.8 ± 1.0 | 5.6 ± 1.1 | 0.958 |
| TG (mg/dL) | 138.5 ± 54.5 | 133.4 ± 45.3 | 145.4 ± 66.3 | 0.567 |
| ALT (UI/L) | 24.8 ± 1.8 | 22.8 ± 8.5 | 27.5 ± 13.3 | 0.235 |
| AST (UI/L) | 28.1 ± 7.2 | 26.3 ± 6.8 | 30.5 ± 6.8 | 0.105 |
| GGT (UI/L) | 16.2 ± 0.9 | 14.9 ± 3.7 | 18.0 ± 6.5 | 0.134 |
| | Cardiovascular variables | | | |
| Tot Chol (mg/dL) | 163.7 ± 21.0 | 162.0 ± 18.6 | 166.0 ± 24.5 | 0.603 |
| HDL (mg/dL) | 40.0 ± 7.8 | 40.0 ± 8.0 | 39.9 ± 7.8 | 0.965 |
| LDL (mg/dL) | 107.2 ± 17.9 | 107.0 ± 16.5 | 107.5 ± 20.3 | 0.938 |
| LDL/HDL Ratio | 2.7 ± 0.1 | 2.7 ± 0.6 | 2.7 ± 0.7 | 0.924 |
| IMT (mm) | 0.56 ± 0.1 | 0.58 ± 0.10 | 0.55 ± 0.11 | 0.399 |

Values are expressed as mean (standard deviation) for normal distribution. *T*-test analysis, Bold data are $p$ values < 0.05. BMI: body mass index, SDB: systolic blood pressure, DPB: diastolic blood pressure, Tot Chol: total cholesterol, HbA1c: glycated hemoglobin, HOMA: homeostasis model assessment, HDL: high density lipoprotein cholesterol, LDL: low density lipoprotein cholesterol, TG: triglycerides, ALT: alanine aminotransferase, AST: aspartate aminotransferase, GGT: gamma glutamyl transferase, BFP: body fat percentage, VFA: visceral fat adiposity, PFA: preperitoneal fat area, IMT: intima media thickness. "[a]" and "[b]" are placed to represent girls and boys and identify that the $p$ value is the result of the comparison of both.

### 3.2. $CCR2^+$ Monocyte Subsets in Boys and Girls with Obesity and High Risk IMT

Among all study participants, seven boys and nine girls showed IMT values above the p75. We found an overall increase in both $CCR2^+$ monocyte percentage (37.3 ± 17.4%, $p$ = 0.017) and CCR2 expression (20.2 ± 4.3%, $p$ = 0.017) in male obese children, compared to females. The $CCR2^+$ classical monocyte percentage was 14.7 ± 9.47% higher in male obese children with subclinical atherosclerosis risk than in boys with IMT < p75 ($p$ = 0.039). Moreover, CCR2 expression in this monocyte subset was 20.3% ± 1.02% higher in male obese children with IMT ≥ p75 than in boys with IMT values below the p75 ($p$ = 0.029) (Figure 2).

The intermediate monocyte subpopulation displayed similar behavior, where the $CCR2^+$ cell percentage was 50 ± 36.7% higher in male children with IMT ≥ p75 than in boys with IMT below the p75 ($p$ = 0.044). The CCR2 expression was 16.1% ± 6.5% higher in intermediate monocytes from boys with IMT ≥ p75 than in male children without subclinical atherosclerosis risk ($p$ = 0.047) (Figure 3).

The proportion of nonclassical monocyte expressing CCR2 was 92.3± 80.1% higher in male children with IMT ≥ p75 than in those without a high-risk IMT ($p$ = 0.037) (Figure 4). Moreover, the CCR2 MFI was 23.1 ± 8.4% higher in nonclassical monocytes from male children with high cardiovascular risk than in males with normal IMT ($p$ = 0.020) (Figure 4). We found no differences in obese girls with IMT below the p75.

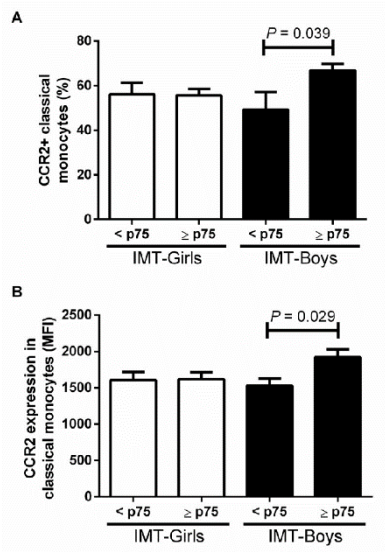


**Figure 2.** Evaluation of (**A**) the proportion of CCR2 in classical monocytes and intima media thickness (IMT) and (**B**) expression of CCR2 in classical monocytes and intima media thickness (IMT) by sex. We considered a high-risk IMT ≥ p75 and compared differences by the student *T*-test, considering a *p* value < 0.05 as significant.

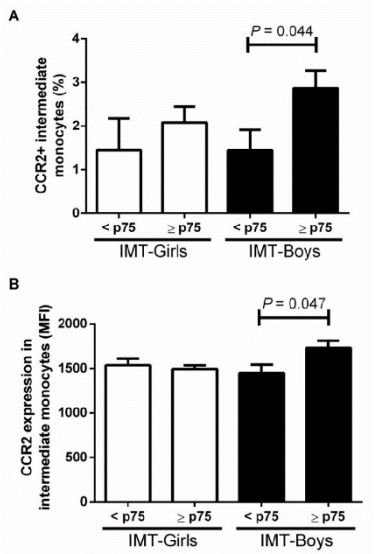


**Figure 3.** Evaluation of (**A**) the proportion of CCR2 in intermediate monocytes and intima media thickness (IMT) and (**B**) expression of CCR2 in intermediate monocytes and intima media thickness (IMT) by sex. We considered a high-risk IMT ≥ p75 and compared differences by the student *T*-test, considering a *p* value < 0.05 as significant.

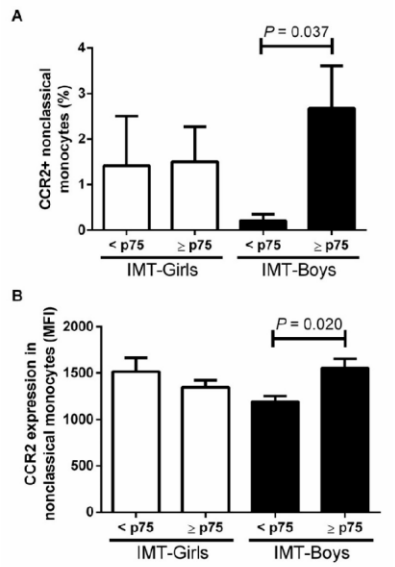


**Figure 4.** Evaluation of (**A**) the proportion of CCR2 in nonclassical monocytes and intima media thickness (IMT) and (**B**) expression of CCR2 in nonclassical monocytes and intima media thickness (IMT) by sex. We considered a high-risk IMT ≥ p75 and compared differences by the student *T*-test, considering a $p$ value < 0.05 as significant.

### *3.3. Correlation between CCR2⁺ Monocyte Subsets and Children with Obesity and High Risk IMT*

Furthermore, we explored potential associations of classical, intermediate, and nonclassical monocytes expressing CCR2 with cardiovascular and metabolic risk factors, such as HOMA and IMT. Interestingly, we noticed that males but not females displayed a strong positive correlation of CCR2⁺ circulating monocytes with IMT ≥ p75 (Table 2). We also found that CCR2⁺ classical, intermediate, and nonclassical monocyte percentage and CCR2 expression in these three monocyte subsets correlated with higher IMT values in males but not females (Table 2). The CCR2⁺ nonclassical monocyte percentage had the strongest association with IMT in males but not females ($r = 0.72$, $p < 0.01$). Additionally, we observed a strong correlation of CCR2⁺ nonclassical monocytes with insulin resistance ($r = 0.80$, $p < 0.01$) in males with IMT ≥ p75 but not females with the same criterion for subclinical atherosclerosis (Table 2). We did not observe significant correlations between monocyte subsets expressing CCR2⁺ with IMT or insulin resistance levels in female children, even those with IMT ≥ p75 (Table 2).

**Table 2.** Correlation of monocyte subsets expressing CCR2 with IMT and HOMA in boys and girls with obesity.

| | | CCR2 % | | CCR2 MFI | |
|---|---|---|---|---|---|
| | | **IMT ≥ p75** | **HOMA ≥ 3.4** | **IMT ≥ p75** | **HOMA ≥ 3.4** |
| CM | Boys ($n = 14$) | **$r = 0.56$ * (0.07–0.85)** | $r = 0.21$ (−0.45–0.72) | **$r = 0.61$ * (0.20–0.86)** | $r = 0.22$ (−0.45–0.70) |
| | Girls ($n = 19$) | $r = -0.05$ (−0.68–0.58) | $r = -0.11$ (−0.72–0.60) | $r = 0.22$ (−0.36–0.72) | $r = -0.21$ (−0.88–0.42) |
| IM | Boys ($n = 14$) | **$r = 0.62$ * (0.17–0.88)** | $r = 0.41$ (−0.12–0.88) | **$r = 0.62$ * (0.19–0.91)** | $r = 0.52$ (−0.00–0.86) |
| | Girls ($n = 19$) | $r = 0.27$ (−0.27–0.88) | $r = 0.03$ (−0.62–0.80) | $r = -0.04$ (−0.60–0.48) | $r = -0.07$ (−0.68–0.50) |

**Table 2.** *Cont.*

| | | CCR2 % | | CCR2 MFI | |
|---|---|---|---|---|---|
| | | **IMT ≥ p75** | **HOMA ≥ 3.4** | **IMT ≥ p75** | **HOMA ≥ 3.4** |
| NCM | Boys ($n$ = 14) | **$r$ = 0.72 ** (0.38–0.91)** | **$r$ = 0.80 ** (0.60–0.93)** | **$r$ = 0.73 ** (0.45–0.91)** | **$r$ = 0.70 ** (0.40–0.90)** |
| | Girls ($n$ = 19) | $r$ = 0.15 (−0.39–0.74) | $r$ = −0.22 (−0.71–0.40) | $r$ = −0.21 (−0.75–0.33) | $r$ = −0.20 (−0.69–0.37) |

CCR2 (%) indicates the percentage of monocytes expressing CCR2, while CCR2 (MFI) denotes how big CCR2 is expressed in each monocyte subset. We considered children with IMT ≥ p75 to have a higher risk for subclinical atherosclerosis. We considered HOMA ≥ 3.4 as a higher risk for insulin resistance. The number of girls we analyzed was 19, whereas we incorporated 14 boys into the study. The table shows correlation coefficient values ($r$) that we calculated by Pearson's correlation coefficient with 95% confidence intervals written between parentheses. We considered significant values when $p < 0.05$, indicating them in bold as follows: * $p < 0.05$, ** $p < 0.001$. CM, classical monocytes; IM, intermediate monocytes; NCM, nonclassical monocytes; MFI, mean fluorescent intensity; IMT, intima-media thickness; HOMA, homeostasis model assessment for insulin resistance.

## 4. Discussion

The contribution of sexual dimorphism in synergy with monocyte subpopulations expressing CCR2 to the development of atherosclerosis, since early ages is still unclear. Studies in animal models and human adults show that CCR2 expression in monocytes is associated with increased arterial wall inflammation and atherosclerosis progression, where males exhibit more robust CCR2 expression than females [15]. Herein, we used IMT ≥ p75 adjusted by sex and age as an early surrogate marker of subclinical atherosclerosis and cardiovascular risk in children with obesity instead of using a cutoff value of IMT that could lead us to bias and data misinterpretation [15]. In this scenario, we found that only boys with IMT ≥ p75 showed increased CCR2 expression in classical, intermediate, and nonclassical monocytes, compared to girls that also exhibited considerably high IMT values. In line with our results, two independent studies previously reported that compared to females, male adolescents display higher circulating levels of MCP-1, a CCR2 ligand whose interaction stimulates monocyte mobilization toward damaged tissues [16,24]. Simoes and coworkers observed that boys with obesity showed increased serum amyloid A (SAA) values, compared to girls; SAA induces MCP-1 production in monocytes and is associated with a higher risk of atherosclerosis [25,26]. These findings suggest that the atherosclerotic process may begin early in childhood in a sex-dependent fashion, resulting from the interaction between obesity, monocyte activation, and intima-media progressive thickening. As mentioned, the binding of the chemokine MCP-1 to CCR2 in circulating monocytes is one of the earliest steps in atherogenesis and is intimately linked to IMT continuing enlargement [27,28]. Okumoto and coworkers reported that monocytes expressing CCR2 correlate with increased IMT and are an independent risk factor promoting atherogenesis [29]. In this study, we observed a strong positive correlation of CCR2 expression in all monocyte subsets with IMT in male children but not in girls. Notably, nonclassical monocytes from boys with elevated IMT exhibited the highest increment in CCR2 expression, compared to male children with average IMT values and girls with and without IMT ≥ p75. Nonclassical and classical monocytes are recruited to vascular fatty streaks to form the atherosclerotic plaque, where classical monocytes migrate into the vascular wall, and nonclassical monocyte subsets remain in the lumen exerting patrolling functions [30]. It is feasible that the increase in nonclassical monocytes expressing CCR2 may reflect an attempt of these immune cells to repair the injured vascular endothelium, a notion suggesting the use of these cells as an early marker of subclinical atherosclerosis in obese boys.

The sexual dimorphism we saw in this work is supported by other studies in adults where monocyte subsets are linked to increased IMT in a sex-dependent fashion. Cannon and coworkers observed a positive correlation between IMT and nonclassical monocytes, where men showed a higher nonclassical monocyte percentage than women [31]. Feinstein and coworkers recently reported in male adults but not females that nonclassical monocytes correlate with IMT expansion during a ten-year follow-up [32]. Rogacev and coworkers found a higher classical monocyte percentage in male patients subjected to coronary angiography than in women facing the same procedure [33]. Altogether, this information

expands the knowledge behind the increased risk of developing atherosclerosis in males with obesity, compared to overweighed females, where monocyte subsets dynamically contribute to plaque formation. Studies in adult subjects found that classical and intermediate monocytes could predict adverse cardiovascular events [33,34]. Feinstein and coworkers reported that nonclassical monocytes could be an early biomarker of pre-atherosclerotic vascular lesion formation [32]. Larger studies in children are needed to evaluate the use of circulating monocyte subpopulations as accurate predictors of subclinical atherosclerosis.

Insulin resistance is defined as a reduce response of insulin-target tissues, such as the liver, skeletal muscle, and visceral fat to insulin action [35]. Insulin resistance leads to persistent hyperglycemia and is a risk factor intimately linked to atherosclerosis development. In an insulin-resistant setting, a reduced nitrite oxide (NO) bioavailability induces vascular damage, increasing the expression of adhesion molecules and inflammatory cytokines with the ability to promote monocyte recruitment and infiltration to the blood vessel wall [36]. It was our rationale behind estimating insulin resistance in our cohort of obese children, analyzing potential associations of monocyte subsets, expressing CCR2 with IMT and insulin resistance. Other studies in adult individuals looked for similar correlations between circulating monocytes and markers of altered glucose homeostasis associated with atherosclerosis progression. Poitou and coworkers observed that nonclassical monocytes were independently associated with fasting glycemia [37]. Mine and coworkers found increased CCR2 expression in circulating monocytes from diabetic patients, compared to control subjects, informing a direct correlation of CCL2 serum levels with glycated hemoglobin (HgA1c) [38]. Gallego-Suárez and coworkers reported a positive correlation of classical monocytes with HOMA in children with high BMI [39]. In line with these findings, we found a strong positive correlation of CCR2 expression in nonclassical monocytes with insulin resistance only in male children with IMT > p75. We encourage other research teams to assess whether the interaction between monocyte subsets expressing CCR2 and insulin resistance, as surrogate markers of subclinical atherosclerosis, can help understand the development of subclinical atherosclerosis early in life. Recently, research in this field is gaining attention because of novel therapeutic approach that blocks the CCL2–CCR2 axis and may improve atherosclerosis disease [40].

Due to the increasing obesity rates, cardiovascular events are still the leading cause of mortality worldwide, above all in men. Ischemic cardiovascular disease caused by atherosclerosis is more prevalent and often occurs earlier in men than in women [14]. Cardiovascular diseases are linked to insulin resistance and T2D, which are more prevalent in males than females [41]. Our findings in obese boys with IMT above average values indicate that sexual dimorphism can appear early in life. Sex differences in body composition exist even before exposure to gonadal hormones [42]. Males cumulate more visceral adipose tissue (VAT), whereas females amass more subcutaneous adipose tissue (SAT) [43]. Numerous lines of research have consistently reported that VAT gain triggers low-grade inflammation and monocyte activation, increasing the risk of developing insulin resistance, T2D, atherosclerosis, and ischemic heart disease [44]. In line with these findings, we observed that male children with obesity had more VAT than females, which could partially explain the increase in CCR2 expression in circulating monocytes from boys with IMT > p75.

This pilot study has some limitations. First, although statistically acceptable, the sample size appears small to estimate whether potentially confounding variables, such as sex or sexual development, may impact the measurement of intima-media thickness. To lessen the effect of this limitation, we adjusted data by age, sex, and the interaction of sex with age in multiple regression models, finding that only age but not sex appears to influence IMT. Another limitation of the study is that we analyzed body composition using a Body Composition Analyzer Model IOI 353 scale suitable for examining the pediatric population. However, if available, we would have liked to evaluate body composition using dual-energy X-ray absorptiometry (DEXA) or magnetic resonance imaging (MRI). Conversely, a strength of the work is that children enrolled in the study had no previous pharmacological treatment that could influence CCR2 expression, monocyte subset dy-

namic, or IMT values. We are now working on increasing the number of children enrolled in the study to clarify the contribution of circulating monocytes expressing CCR2 and other chemokine receptor repertoires to atherosclerosis development in a sex-dependent fashion.

## 5. Conclusions

In conclusion, CCR2 expression in circulating monocyte subsets is associated with elevated IMT and insulin resistance in male children with obesity. Circulating monocytes expressing CCR2, mostly nonclassical monocytes, may contribute to atherosclerotic plaque formation in a sex-dependent fashion, where boys appear to be at increased cardiovascular risk.

**Author Contributions:** Conceptualization, M.J.G.-H., J.H.-R. and G.E.; Data curation, M.J.G.-H., K.P.-E. and N.G.-N.; Formal analysis, M.J.G.-H., G.E. and J.C.L.-A.; Funding acquisition, N.G.-N. and G.Q.-G.; Investigation, M.J.G.-H.; Methodology, M.J.G.-H., K.P.-E., N.G.-N., J.H.-R. and E.V.-O.; Project administration, N.G.-N.; Resources, M.J.G.-H., J.H.-R. and G.Q.-G.; Software, M.J.G.-H., J.L.P.-C., L.A.A.-P., A.N.M.-R. and J.L.P.-H.; Supervision, G.Q.-G.; Validation, G.E. and G.Q.-G.; Visualization, G.Q.-G.; Writing—original draft, M.J.G.-H.; Writing—review and editing, G.E. All authors have read and agreed to the published version of the manuscript.

**Funding:** This research was supported by the Genetic Department and Investigation Department of the General Hospital of México "Dr. Eduardo Liceaga", by the Sertull Foundation: PS-17-SA-000510 and the Fondo sectorial de Investigación en salud y seguridad social: Fondo SALUD-2013-1-202499, CONACYT 2013.

**Institutional Review Board Statement:** The study was conducted in accordance with the Declaration of Helsinki, and approved by the Research, Ethics, and Biosafety Committees for Human Research of the General Hospital of Mexico (registration number: DI/17/311/03/028).

**Informed Consent Statement:** Informed consent and assent letters were obtained from all subjects involved in the study.

**Data Availability Statement:** Data are available on reasonable request to the corresponding author.

**Acknowledgments:** This work was supported by the Consejo Nacional de Ciencia y Tecnología (CONACYT), CVU number: 549440. This work is a component of the Ph.D. requirements of María José Garcés Hernández in the Programa de Doctorado en Ciencias Médicas, Odontológicas y de la Salud of the Universidad Nacional Autónoma de México.

**Conflicts of Interest:** The authors declare no conflict of interest. The funders had no role in the design of the study; in the collection, analyses, or interpretation of data; in the writing of the manuscript; or in the decision to publish the results.

## References

1. GBD 2015 Obesity Collaborators; Afshin, A.; Forouzanfar, M.H.; Reitsma, M.B.; Sur, P.; Estep, K.; Lee, A.; Marczak, L.; Mokdad, A.H.; Moradi-Lakeh, M.; et al. Health Effects of Overweight and Obesity in 195 Countries over 25 Years. *N. Engl. J. Med.* **2017**, *377*, 13–27. [CrossRef] [PubMed]
2. Medina-leyte, D.J.; Zepeda-garc, O.; Dom, M. Endothelial Dysfunction, Inflammation and Coronary Artery Disease: Potential Biomarkers and Promising Therapeutical Approaches. *Int. J. Mol. Sci.* **2021**, *22*, 3850. [CrossRef] [PubMed]
3. Hajjar, D.P.; Gotto, A.M. MINI-REVIEW Biological Relevance of In fl ammation and Oxidative Stress in the Pathogenesis of Arterial Diseases. *Am. J. Pathol.* **2013**, *182*, 1474–1481. [CrossRef]
4. Rocha, V.Z.; Libby, P. Obesity, inflammation, and atherosclerosis. *Nat. Rev. Cardiol.* **2009**, *6*, 399–409. [CrossRef]
5. Poznyak, A.; Grechko, A.V.; Poggio, P.; Myasoedova, V.A.; Alfieri, V.; Orekhov, A.N. The diabetes mellitus–atherosclerosis connection: The role of lipid and glucose metabolism and chronic inflammation. *Int. J. Mol. Sci.* **2020**, *21*, 1835. [CrossRef]
6. Powell-Wiley, T.M.; Poirier, P.; Burke, L.E.; Després, J.-P.; Gordon-Larsen, P.; Lavie, C.J.; Lear, S.A.; Ndumele, C.E.; Neeland, I.J.; Sanders, P.; et al. Obesity and Cardiovascular Disease: A Scientific Statement From the American Heart Association. *Circulation* **2021**, *143*, 89–91. [CrossRef] [PubMed]
7. McGill, H.C.; McMahan, C.A.; Herderick, E.E.; Zieske, A.W.; Malcom, G.T.; Tracy, R.E.; Strong, J.P. Obesity accelerates the progression of coronary atherosclerosis in young men. *Circulation* **2002**, *105*, 2712–2718. [CrossRef] [PubMed]
8. Giannini, C.; Santoro, N.; Caprio, S.; Kim, G.; Lartaud, D.; Shaw, M.; Pierpont, B.; Weiss, R. The triglyceride-to-HDL cholesterol ratio: Association with insulin resistance in obese youths of different ethnic backgrounds. *Diabetes Care* **2011**, *34*, 1869–1874. [CrossRef]

9. Drozdz, D.; Alvarez-Pitti, J.; Wójcik, M.; Borghi, C.; Gabbianelli, R.; Mazur, A.; Herceg-čavrak, V.; Lopez-Valcarcel, B.G.; Brzeziński, M.; Lurbe, E.; et al. Obesity and cardiometabolic risk factors: From childhood to adulthood. *Nutrients* **2021**, *13*, 4176. [CrossRef]
10. Di Pino, A.; Defronzo, R.A. Insulin Resistance and Atherosclerosis: Implications for Insulin-Sensitizing Agents. *Endocr. Rev.* **2019**, *40*, 1447–1467. [CrossRef]
11. Moroni, F.; Ammirati, E.; Norata, G.D.; Magnoni, M.; Camici, P.G. The role of monocytes and macrophages in human atherosclerosis, plaque neoangiogenesis, and atherothrombosis. *Med. Infl.* **2019**, *2019*, 7434376. [CrossRef] [PubMed]
12. França, C.N.; Izar, M.C.O.; Hortêncio, M.N.S.; do Amaral, J.B.; Ferreira, C.E.S.; Tuleta, I.D.; Fonseca, F.A.H. Monocyte subtypes and the CCR2 chemokine receptor in cardiovascular disease. *Clin. Sci.* **2017**, *131*, 1215–1224. [CrossRef] [PubMed]
13. Urbanski, K.; Ludew, D.; Filip, G.; Filip, M.; Sagan, A.; Szczepaniak, P.; Grudzien, G. CD14+CD16++ "nonclassical" monocytes are associated with Endothelial dysfunction in patients with coronary artery disease. *Thromb. Haemost.* **2017**, *117*, 971–980. [CrossRef] [PubMed]
14. Man, J.J.; Beckman, J.A.; Jaffe, I.Z. Sex as a Biological Variable in Atherosclerosis. *Circ. Res.* **2020**, *126*, 1297–1319. [CrossRef]
15. Böhm, B.; Hartmann, K.; Buck, M.; Oberhoffer, R. Sex differences of carotid intima-media thickness in healthy children and adolescents. *Atherosclerosis* **2009**, *206*, 458–463. [CrossRef]
16. Petty, K.H.; Li, K.; Dong, Y.; Fortenberry, J.; Stallmann-Jorgensen, I.; Guo, D.; Zhu, H. Sex dimorphisms in inflammatory markers ad adiposity in African American youth. *Int. J. Ped. Obes.* **2010**, *5*, 327–333. [CrossRef]
17. Dhanraj, P.; van Heerden, M.B.; Pepper, M.S.; Ambele, M.A. Sexual dimorphism in changes that occur in tissues, organs and plasma during the early stages of obesity development. *Biology* **2021**, *10*, 717. [CrossRef]
18. Verweij, S.L.; Duivenvoorden, R.; Stiekema, L.C.A.; Nurmohamed, N.S.; Van Der Valk, F.M.; Versloot, M.; Verberne, H.J.; Stroes, E.S.G.; Nahrendorf, M.; Bekkering, S.; et al. CCR2 expression on circulating monocytes is associated with arterial wall inflammation assessed by 18F-FDG PET/CT in patients at risk for cardiovascular disease. *Cardiovasc. Res.* **2018**, *114*, 468–475. [CrossRef]
19. Kuczmarski, R.J.; Ogden, C.L.; Guo, S.S.; Grummer-Strawn, L.M.; Flegal, K.M.; Mei, Z.; Wei, R.; Curtin, L.R.; Roche, A.F.; Johnson, C.L. 2000 CDC growth charts for the United States: Methods and development. *Vital Health Stat.* **2002**, *11*, 1–190.
20. Styne, D.M.; Arslanian, S.A.; Connor, E.L.; Farooqi, I.S.; Murad, M.H.; Silverstein, J.H.; Yanovski, J.A. Pediatric Obesity—Assessment, Treatment, and Prevention: An Endocrine Society Clinical Practice Guideline. *J. Clin. Endo. Metabo.* **2017**, *102*, 709–757. [CrossRef]
21. Lentferink, Y.E.; Elst, M.A.J.; Knibbe, C.A.J.; Vorst, M.M.J. Van Der. Predictors of Insulin Resistance in Children versus Adolescents with Obesity. *J. Obes.* **2017**, *2017*, 3793868. [CrossRef] [PubMed]
22. Van Der Aa, M.P.; Farsani, S.F.; Kromwijk, L.A.J.; De Boer, A.; Knibbe, C.A.J.; Van Der Vorst, M.M.J. How to Screen Obese Children at Risk for Type 2 Diabetes Mellitus? *Clin. Pediatr.* **2014**, *53*, 21–26. [CrossRef] [PubMed]
23. Mook-Kanamori, D.O.; Holzhauer, S.; Hollestein, L.M.; Durmus, B.; Manniesing, R.; Koek, M.; Boehm, G.; van der Beek, E.M.; Hofman, A.; Witteman, J.C.M.; et al. Abdominal Fat in Children Measured by Ultrasound and Computed Tomography. *Ultrasound Med. Biol.* **2009**, *35*, 1938–1946. [CrossRef] [PubMed]
24. Herder, C.; Schneitler, S.; Rathmann, W.; Haastert, B.; Schneitler, H.; Winkler, H.; Bredahl, R.; Hahnloser, E.; Martin, S. Low-grade inflammation, obesity, and insulin resistance in adolescents. *J. Clin. Endocrinol. Metab.* **2007**, *92*, 4569–4574. [CrossRef]
25. Lee, H.Y.; Kim, S.D.; Shim, J.W.; Lee, S.Y.; Lee, H.; Cho, K.-H.; Yun, J.; Bae, Y.-S. Serum Amyloid A Induces CCL2 Production via Formyl Peptide Receptor-Like 1-Mediated Signaling in Human Monocytes. *J. Immunol.* **2008**, *181*, 4332–4339. [CrossRef]
26. Simoes, E.; Correia-Lima, J.; Sardas, L.; Storti, F.; dos Santos Otani, T.Z.; Vasques, D.A.C.; Otani, V.H.O.; Bertolazzi, P.; Kochi, C.; Seelaender, M.; et al. Sex dimorphism in inflammatory response to obesity in childhood. *Int. J. Obes.* **2021**, *45*, 879–887. [CrossRef]
27. Kang, H.; Li, X.; Xiong, K.; Song, Z.; Tian, J.; Wen, Y.; Sun, A.; Deng, X. The Entry and Egress of Monocytes in Atherosclerosis: A Biochemical and Biomechanical Driven Process. *Cardiovas. Therap.* **2021**, *2021*, 6642927. [CrossRef]
28. Tan, C.; Liu, Y.; Li, W.; Deng, F.; Liu, X.; Wang, X.; Gui, Y.; Qin, L.; Hu, C.; Chen, L. Associations of matrix metalloproteinase-9 and monocyte chemoattractant protein-1 concentrations with carotid atherosclerosis, based on measurements of plaque and intima-media thickness. *Atherosclerosis* **2014**, *232*, 199–203. [CrossRef]
29. Okumoto, S.; Taniguchi, Y.; Nakashima, A.; Masaki, T.; Ito, T.; Ogawa, T.; Takasugi, N.; Kohno, N.; Yorioka, N. C-C chemokine receptor 2 expression by circulating monocytes influences atherosclerosis in patients on chronic hemodialysis. *Therap. Apher. Dial.* **2009**, *13*, 205–212. [CrossRef]
30. Narasimhan, P.B.; Marcovecchio, P.; Hamers, A.A.J.; Hedrick, C.C. Nonclassical Monocytes in Health and Disease. *Annu. Rev. Immunol.* **2019**, *37*, 439–456. [CrossRef]
31. Cannon, J.G.; Sharma, G.; Sloan, G.; Dimitropoulou, C.; Baker, R.R.; Mazzoli, A.; Kraj, B.; Mulloy, A.; Cortez-Cooper, M. Leptin regulates CD16 expression on human monocytes in a sex-specific manner. *Physiol. Rep.* **2014**, *2*, e12177. [CrossRef] [PubMed]
32. Feinstein, M.J.; Doyle, M.F.; Stein, J.H.; Sitlani, C.M.; Fohner, A.E.; Huber, S.A.; Landay, A.L.; Heckbert, S.R.; Rice, K.; Kronmal, R.A.; et al. Nonclassical Monocytes (CD14dimCD16+) Are Associated with Carotid Intima-Media Thickness Progression for Men but Not Women: The Multi-Ethnic Study of Atherosclerosis—Brief Report. *Arter. Thromb Vasc Biol.* **2021**, *41*, 1810–1817. [CrossRef] [PubMed]
33. Rogacev, K.S.; Cremers, B.; Zawada, A.M.; Seiler, S.; Binder, N.; Ege, P.; Große-Dunker, G.; Heisel, I.; Hornof, F.; Jeken, J.; et al. CD14++CD16+ monocytes independently predict cardiovascular events: A cohort study of 951 patients referred for elective coronary angiography. *J. Am. Coll. Cardiol.* **2012**, *60*, 1512–1520. [CrossRef] [PubMed]

34. Berg, K.E.; Ljungcrantz, I.; Andersson, L.; Bryngelsson, C.; Hedblad, B.; Fredrikson, G.N.; Nilsson, J.; Björkbacka, H. Elevated CD14++CD16-monocytes predict cardiovascular events. *Circ. Cardiovasc Gen.* **2012**, *5*, 122–131. [CrossRef]
35. Lee, S.H.; Park, S.Y.; Choi, C.S. Insulin Resistance: From Mechanisms to Therapeutic Strategies. *Diabetes Metab. J.* **2022**, *46*, 15–37. [CrossRef]
36. Di Pietrantonio, N.; Palmerini, C.; Pipino, C.; Baldassarre, M.P.A.; Bologna, G.; Mohn, A.; Giannini, C.; Lanuti, P.; Chiarelli, F.; Pandolfi, A.; et al. BBA—Molecular Basis of Disease Plasma from obese children increases monocyte-endothelial adhesion and affects intracellular insulin signaling in cultured endothelial cells: Potential role of mTORC1-S6K1. *BBA Mol. Basis Dis.* **2021**, *1867*, 166076. [CrossRef]
37. Poitou, C.; Dalmas, E.; Renovato, M.; Benhamo, V.; Hajduch, F.; Abdennour, M.; Kahn, J.-F.; Veyrie, N.; Rizkalla, S.; Fridman, W.-H.; et al. CD14dim CD16+ and CD14+CD16+Monocytes in obesity and During Weight Loss Relationships With Fat Mass and Subclinical Atherosclerosis. *Arter. Thromb. Vasc. Biol.* **2011**, *31*, 2322–2330. [CrossRef]
38. Mine, S.; Okada, Y.; Tanikawa, T.; Kawahara, C.; Tabata, T.; Tanaka, Y. Increased expression levels of monocyte CCR2 and monocyte chemoattractant protein-1 in patients with diabetes mellitus. *Biochem. Biophys. Res. Commun.* **2006**, *344*, 780–785. [CrossRef]
39. Gállego-Suárez, C.; Bulan, A.; Hirschfeld, E.; Wachowiak, P.; Abrishami, S.; Griffin, C.; Sturza, J.; Tzau, A.; Hayes, T.; Woolford, S.J.; et al. Enhanced Myeloid Leukocytes in Obese Children and Adolescents at Risk for Metabolic Impairment. *Front. Endocrinol.* **2020**, *11*, 327. [CrossRef]
40. Georgakis, M.K.; Bernhagen, J.; Heitman, L.H.; Weber, C.; Dichgans, M. Targeting the CCL2–CCR2 axis for atheroprotection. *Eur. Heart J.* **2022**, *43*, 1799–1808. [CrossRef]
41. McEwan, S.; Kwon, H.; Tahiri, A.; Shanmugarajah, N.; Cai, W.; Ke, J.; Huang, T.; Belton, A.; Singh, B.; Wang, L.; et al. Deconstructing the origins of sexual dimorphism in sensory modulation of pancreatic β cells. *Mol. Metab.* **2021**, *53*, 101260. [CrossRef] [PubMed]
42. Zore, T.; Palafox, M.; Reue, K. Sex differences in obesity, lipid metabolism, and inflammation—A role for the sex chromosomes? *Mol. Metab.* **2018**, *15*, 35–44. [CrossRef] [PubMed]
43. Chang, E.; Varghese, M.; Singer, K. Gender and Sex Differences in Adipose Tissue. *Curr. Diab. Rep.* **2018**, *18*, 69. [CrossRef] [PubMed]
44. Neeland, I.J.; Ross, R.; Després, J.-P.; Matsuzawa, Y.; Yamashita, S.; Shai, I.; Seidell, J.; Magni, P.; Santos, R.D.; Arsenault, B.; et al. Visceral and ectopic fat, atherosclerosis, and cardiometabolic disease: A position statement. *Lancet Diab. Endocrinol.* **2019**, *7*, 715–725. [CrossRef]

frontiers | Frontiers in Immunology

ORIGINAL RESEARCH
published: 01 July 2022
doi: 10.3389/fimmu.2022.897995

# *In Vitro* Exposure of Primary Human T Cells and Monocytes to Polyclonal Stimuli Reveals a Basal Susceptibility to Display an Impaired Cellular Immune Response and Develop Severe COVID-19

*Rebeca Viurcos-Sanabria[1,2], Aarón N. Manjarrez-Reyna[1], Helena Solleiro-Villavicencio[3], Salma A. Rizo-Téllez[1,2], Lucía A. Méndez-García[1], Victoria Viurcos-Sanabria[1], Jacquelina González-Sanabria[1], América Arroyo-Valerio[4], José D. Carrillo-Ruíz[4,5,6], Antonio González-Chávez[7], Jose I. León-Pedroza[6,8,9], Raúl Flores-Mejía[10], Octavio Rodríguez-Cortés[10] and Galileo Escobedo[1]**

[1] Laboratory of Immunometabolism, Research Division, General Hospital of Mexico "Dr. Eduardo Liceaga", Mexico City, Mexico, [2] PECEM, Facultad de Medicina, Universidad Nacional Autónoma de México, Mexico City, Mexico, [3] Posgrado de Ciencias Genómicas, Universidad Autónoma de la Ciudad de México, Mexico City, Mexico, [4] Research Directorate, General Hospital of Mexico "Dr. Eduardo Liceaga", Mexico City, Mexico, [5] Unit for Stereotactic and Functional Neurosurgery, General Hospital of Mexico "Dr. Eduardo Liceaga", Mexico City, Mexico, [6] Faculty of Health Sciences, Anahuac University, Mexico City, Mexico, [7] Clínica de Atención Integral para Pacientes con Diabetes y Obesidad, General Hospital of Mexico "Dr. Eduardo Liceaga", Mexico City, Mexico, [8] Departament of Intensive Medical Therapy, General Hospital of Mexico "Dr. Eduardo Liceaga", Mexico City, Mexico, [9] Facultad de Medicina, Universidad Nacional Autónoma de México, Mexico City, Mexico, [10] Laboratorio 103, Sección de Estudios de Posgrado e Investigación, Escuela Superior de Medicina, Instituto Politécnico Nacional, Plan de San Luis y Díaz Mirón, Casco de Santo Tomas, Ciudad de México, Mexico*

The contribution of the cellular immune response to the severity of coronavirus disease 2019 (COVID-19) is still uncertain because most evidence comes from patients receiving multiple drugs able to change immune function. Herein, we conducted a prospective cohort study and obtained blood samples from 128 unvaccinated healthy volunteers to examine the *in vitro* response pattern of CD4+ and CD8+ T cells and monocyte subsets to polyclonal stimuli, including anti-CD3, anti-CD28, poly I:C, severe acute respiratory syndrome coronavirus type 2 (SARS-CoV-2) recombinant spike S1 protein, and lipopolysaccharide. Then, we started a six-month follow-up and registered 12 participants who got SARS-CoV-2 infection, from whom we retrospectively analyzed the basal immune response pattern of T cells and monocytes. Of the 12 participants infected, six participants developed mild COVID-19 with self-limiting symptoms such as fever, headache, and anosmia. Conversely, six other participants developed severe COVID-19 with pneumonia, respiratory distress, and hypoxia. Two severe COVID-19 cases required invasive mechanical ventilation. There were no differences between mild and severe cases for demographic, clinical, and biochemical baseline characteristics. In response to polyclonal stimuli, basal production of interleukin-2 (IL-2) and interferon (IFN-) gamma significantly decreased, and the programmed cell death protein 1 (PD-1)

OPEN ACCESS

**Edited by:**
*Camilla Tincati, University of Milan, Italy*

**Reviewed by:**
*Leslie Chavez-Galan, Instituto Nacional de Enfermedades Respiratorias-México (INER), Mexico*
*Florence Larrous, Institut Pasteur, France*

***Correspondence:**
*Galileo Escobedo*
*gescobedog@msn.com*

**Specialty section:**
*This article was submitted to Viral Immunology, a section of the journal Frontiers in Immunology*

**Received:** *16 March 2022*
**Accepted:** *10 June 2022*
**Published:** *01 July 2022*

**Citation:**
*Viurcos-Sanabria R, Manjarrez-Reyna AN, Solleiro-Villavicencio H, Rizo-Téllez SA, Méndez-García LA, Viurcos-Sanabria V, González-Sanabria J, Arroyo-Valerio A, Carrillo-Ruíz JD, González-Chávez A, León-Pedroza JI, Flores-Mejía R, Rodríguez-Cortés O and Escobedo G (2022) In Vitro Exposure of Primary Human T Cells and Monocytes to Polyclonal Stimuli Reveals a Basal Susceptibility to Display an Impaired Cellular Immune Response and Develop Severe COVID-19. Front. Immunol. 13:897995. doi: 10.3389/fimmu.2022.897995*

increased in CD4+ and CD8+ T cells from participants who posteriorly developed severe COVID-19 compared to mild cases. Likewise, CD14++CD16- classical and CD14+CD16+ non-classical monocytes lost their ability to produce IFN-alpha in response to polyclonal stimuli in participants who developed severe COVID-19 compared to mild cases. Of note, neither the total immunoglobulin G serum titers against the virus nor their neutralizing ability differed between mild and severe cases after a month of clinical recovery. In conclusion, using *in vitro* polyclonal stimuli, we found a basal immune response pattern associated with a predisposition to developing severe COVID-19, where high PD-1 expression and low IL-2 and IFN-gamma production in CD4+ and CD8+ T cells, and poor IFN-alpha expression in classical and non-classical monocytes are linked to disease worsening. Since antibody titers did not differ between mild and severe cases, these findings suggest cellular immunity may play a more crucial role than humoral immunity in preventing COVID-19 progression.

**Keywords: T cell, monocyte, SARS-CoV-2, COVID-19, PD-1, IL-2, IFN-gamma, IFN-alpha**

## INTRODUCTION

The severe acute respiratory syndrome coronavirus type 2 (SARS-CoV-2) is the causal agent of coronavirus disease 2019 (COVID-19) (1). The clinical presentation of COVID-19 has caught the attention of the scientific community around the globe because of its enormous heterogeneity, ranging from mild and moderate self-limiting viral infection to severe and critical illness (2). However, the mechanisms involved in COVID-19 progression and severity are still a matter of debate (3). A growing body of evidence has pointed out advanced age, male gender, and comorbidities such as hypertension and type 2 diabetes (D) as leading risk factors for developing severe COVID-19 (4–7). Nevertheless, several studies have consistently reported that mild COVID-19 can present even in advanced-age men with comorbidities (2, 6), bringing to light the need to understand additional factors explaining how severe disease develops.

Numerous studies have informed that an exacerbated inflammatory response worsens the clinical course of SARS-CoV-2 infection by increasing the local and systemic levels of tumor necrosis factor-alpha (TNF-alpha), interleukin (IL-) 1 beta, and IL-6 (7–9). However, emerging evidence suggests that a defective cellular immunity may also accelerate COVID-19 progression (10). Compared to patients developing mild symptoms, CD4+ and CD8+ T cell populations from COVID-19 patients admitted to intensive care units (ICU) show reduced production of IL-2, a cytokine with major functions in enhancing T and B cell proliferation (11, 12). Furthermore, CD4+ T cells also express interferon-gamma (IFN-gamma), a cytokine able to inhibit viral replication; however, seriously ill COVID-19 patients show reduced IFN-gamma-producing CD4+ T cells compared to convalescent individuals (10). CD4+ and CD8+ T cell populations from COVID-19 patients in need of hospitalization also show increased expression of cell exhaustion markers, including the programmed cell death protein 1 (PD-1) (13–15). In parallel, the ability of classical and non-classical monocytes to release the antiviral cytokine interferon-alpha (IFN-alpha) decreases as COVID-19 severity increases in patients critically ill compared to those developing mild-to-moderate disease (16). Of note, even though T cells and monocytes appear to lose the capacity of producing key antiviral cytokines, patients with severe COVID-19 exhibit similar neutralizing antibody titers to those found in subjects with mild symptoms (10). This whole evidence emphasizes the idea that impairment in cellular immunity may play a crucial role in worsening SARS-CoV-2 infection.

Although this information suggests that cellular immunity plays a role in COVID-19 progression by stimulating T cells and monocytes to release crucial antiviral cytokines, most of this evidence comes from cross-sectional clinical studies with polytreated patients, making it challenging to correct data interpretation. We hypothesize that cytokine production mediated by cells such as T lymphocytes and monocytes against the SARS-CoV-2 has basal response patterns with the ability to predispose a patient towards the development of either mild or severe disease. However, this question is hard to respond to in infected patients receiving multiple drug schemes and therapeutic maneuvers able to modify the immune response pattern during the COVID-19 course.

For this reason, we conducted a prospective, longitudinal follow-up for six months in 105 family members of medical staff caring for COVID-19 patients, exploring their immune response pattern to *in vitro* polyclonal stimuli simulating the exposure to SARS-CoV-2. After grading disease severity in the participants resulting infected during that period, we retrospectively examined how CD4+ and CD8+ T cells and monocyte subpopulations responded *in vitro* to anti-CD3, anti-CD28, poly I:C, spike protein, and lipopolysaccharide (LPS) in seeking a basal immune pattern that could associate with the development of mild or severe COVID-19.

## MATERIALS AND METHODS

### Participants and Ethical Disclosures

We invited 128 healthy adult women and men to participate in the study. We enrolled participants if they met the following

inclusion criteria: family members of health care professionals working at a dedicated COVID-19 hospital in Mexico City, aging 18-65 years old, negative testing for SARS-CoV-2 by quantitative-polymerase chain reaction (qPCR), and seronegative to anti-SARS-CoV-2 IgG antibodies. We excluded subjects from the study if they had the previous diagnosis of the human immunodeficiency virus (HIV), hepatitis C virus (HCV), hepatitis B virus (HBV), chronic kidney or liver disease, cancer, autoimmune diseases, endocrine disorders, and infectious diseases. We also excluded pregnant or lactating women and patients taking immunomodulatory medication for the last six months. We eliminated participants from the study if they received any vaccine against COVID-19 within six months of enrollment. All study participants provided written informed consent previously approved by the institutional ethical committee of the General Hospital of Mexico (registration number of the ethical code approval: DI/20/501/03/17). The study rigorously met the principles described in the 1964 Declaration of Helsinki and its posterior amendment in 2013.

## Study Design

This prospective, longitudinal study with retrospective data analysis took place from December 2020 to September 2021. All family members of health care professionals who agreed to take part in the study signed the informed consent and received a full explanation of the purposes and procedures of the study. We collected demographic, clinical, and biochemical data from all 128 participants at the enrollment. Demographic and clinical data included sex, age, and previous diagnosis of obesity (body mass index (BMI) > 30 kg/m2), type 2 diabetes (D), hypertension, coronary heart disease (CHD), and hypercholesterolemia. Biochemical data included serum albumin, total proteins, blood glucose, lipid profile, liver and kidney function tests, hematic biometry, C-reactive protein (CRP), and lactate dehydrogenase (LDH). We measured all laboratory parameters using the Beckman Coulter DxC 700 AU Chemistry Analyzer (Beckman Coulter Inc., Brea, CA, USA), the Coulter LH 780 Hematology Analyzer (Beckman Coulter Inc., Brea, CA, USA), and the BCS® XP System (Siemens Healthcare GmbH, Erlangen, Germany). We collected 6 ml venous blood samples from all 128 healthy participants at the enrollment, using tubes containing sodium heparin (VacutainerTM, BD Diagnostics, NJ, USA). After whole blood *in vitro* exposure to polyclonal stimuli, we performed flow cytometry staining for cell surface and intracellular markers of T cells and monocytes, storing flow cytometry data. Polyclonal stimuli were used to simulate the exposure to SARS-CoV-2 in *in vitro* culture settings, using the SARS-CoV-2 recombinant spike S1 protein (the main surface antigen of the virus), Poly I:C (a double-stranded RNA widely used to mimic viral infections *in vitro*), anti-human CD3 and anti-human CD28 (co-stimulatory signals that enhance T cell expansion and activation *in vitro*), and LPS (an endotoxin that enhances monocyte activation). We weekly followed-up to all participants by phone calls for six months, asking for the occurrence of symptoms such as headache, fever (body temperature > 37.5°C), dry cough, tiredness, myalgia, arthralgia, nasal congestion, runny nose, anosmia, dysgeusia, sore throat, diarrhea, shortness of breath, chest pain, and blue-colored skin or lips. After reporting at least one of the above symptoms, participants attended the General Hospital of Mexico for SARS-CoV-2 infection confirmation by qPCR in nasopharyngeal swabs. Then, we started a daily follow-up on each participant confirmed for SARS-CoV-2 infection, recording relevant clinical and biochemical data at the symptom onset and seven days after, and categorizing the development of COVID-19 as mild-to-moderate or severe-to-critical disease. We classified the level of COVID-19 severity according to the World Health Organization (WHO) criteria as follows: mild COVID-19 cases showed headache, fever, dry cough, tiredness, myalgia, arthralgia, nasal congestion, runny nose, anosmia, dysgeusia, sore throat, and/or diarrhea that participants handled at home without needing of oxygen supply or hospitalization; severe COVID-19 cases presented at least one of the above symptoms plus oxygen saturation level ($SpO_2$) < 92% on room air, respiratory distress > 30 breath per minute, and/or >50% lung involvement on imaging that required either hospitalization or mechanical ventilation. Once we confirmed the clinical outcome of COVID-19, we retrospectively analyzed flow cytometry data for mild or severe groups in seeking a basal immune response pattern to *in vitro* polyclonal stimuli that could associate with the disease severity.

## Cell Cultures

We collected 6 ml venous blood samples from all participants at the enrollment, using tubes containing sodium heparin (VacutainerTM, BD Diagnostics, NJ, USA). Immediately after, we divided each whole blood sample into 24-well ultra-low attachment surface cell-culture plates (Costar, Kennebunk, ME, USA), adding 200 µl blood plus 400 µl RPMI-1640 (Sigma Aldrich, St. Louis, MO, USA) supplemented with 5% fetal bovine serum (FBS), 2 mM L-glutamine, and 10 nM HEPES buffer (GibcoTM, Grand Island, NY, USA) per well in triplicate. We designated the first three wells as unstimulated T cell culture control containing 200 µl blood plus 400 µl supplemented RPMI-1640 for 2 hours. The subsequent three wells had 200 µl blood plus 400 µl supplemented RPMI-1640 incubated in the presence of 0.5 µg/ml SARS-CoV-2 recombinant spike S1 protein (Arigo Biolaboratories, Hsinchu City, Taiwan), 100 µg/ml Poly I:C (Sigma Aldrich, St. Louis, MO, USA), and 10 ng/ml anti-human CD3 and anti-human CD28 (BioLegend, Inc., San Diego, CA, USA) for 2 hours. We designated the following three wells as unstimulated monocyte culture control containing 600 µl blood plus 1.2 ml supplemented RPMI-1640 for 2 hours. The last three wells had 600 µl blood plus 1.2 ml supplemented RPMI-1640 incubated in the presence of 0.5 µg/ml SARS-CoV-2 recombinant spike S1 protein (Arigo Biolaboratories, Hsinchu City, Taiwan), 100 µg/ml Poly I:C (Sigma Aldrich, St. Louis, MO, USA), and 10 ng/ml LPS (Sigma Aldrich, St. Louis, MO, USA) for 2 hours. We incubated cell cultures at 37°C in humidified 5% $CO_2$ atmosphere for 2 hours. We selected a 2-hour stimulation based on time-response curves (**Supplementary Figure 1**). We treated whole blood cultures for intracellular staining with 1:1000 Brefeldin A (BioLegend, Inc., San Diego, CA, USA) and 1 µg/ml monensin (BioLegend, Inc., San Diego, CA, USA) for 45 min before the culture's ending.

## Immunostaining and Flow Cytometry

After incubation, we collected whole blood samples into 5 ml falcon tubes (BD, Bedford, MA, USA), centrifuged tubes at 500 g for 10 min, and washed cell pellets with 200 µl PBS 1X (Sigma Aldrich, St. Louis, MO, USA) twice. Immediately after, we added 5 ml ammonium-chloride-potassium (ACK) lysing buffer to each cell pellet, mixed gently and incubated for 10 min at room temperature. After centrifuging each tube at 500 g for 10 min, we discarded the supernatant and resuspended the white blood cell (WBC) pellet in 1 ml PBS 1X (Sigma Aldrich, St. Louis, MO, USA). After an extra washing step, we resuspended $5x10^5$ WBCs in 50 µl cell staining buffer (BioLegend, Inc., San Diego, CA, USA). For monocyte cultures, we incubated WBCs with 5 µl True-Stain Monocyte Blocker™ (BioLegend, Inc., San Diego, CA, USA) for 10 min on ice. Then, we added anti-CD14 APC Fire 750, anti-CD16 PE/Cy5, and anti-HLA-DR PE (BD Biosciences, San Jose, CA, USA) for 20 min in darkness at 4°C. For T cell cultures, we incubated WBCs with anti-CD3 APC Fire 750, anti-CD4 BV 510, anti-CD8 APC, and anti-PD-1 PE for 20 min in darkness at 4°C. Afterward, we incubated WBCs with 100 µl Fixation Medium A (FIX & PERMTM Cell Permeabilization Kit) (Invitrogen™, Carlsbad, CA, USA) for 20 min at room temperature. After rinsing WBCs with Cell Staining Buffer (BioLegend, Inc., San Diego, CA, USA), we incubated cells with 100 µl Permeabilization Medium B (FIX & PERM TM Cell Permeabilization Kit, Invitrogen™, Carlsbad, CA, USA) plus anti-IFN-gamma Pacific Blue and anti-IL-2 PE/Cy7 for T cell cultures or IFN-alpha AF 647 (BioLegend, Inc., San Diego, CA, USA) for monocyte cultures during 20 min in darkness at room temperature. After rinsing the cell pellets with cell staining buffer (BioLegend, Inc., San Diego, CA, USA), we acquired cells on a BD FACS Canto II Flow Cytometer (BD Biosciences, San Jose, CA, USA), acquiring 10,000 events per test on CD3+ or HLA-DR+ cells, respectively in three different and individual staining.

## Gating Strategy

After we confirmed the severity of COVID-19, we retrospectively analyzed flow cytometry data for mild COVID-19 cases or severe COVID-19 participants. For T cells, we first gated single cells on a forward scatter (FSC-H)/side scatter (SSC-A) density plot. Afterward, we gated cells on a time/side scatter density plot to visualize how well the flow of cells was during acquisition. We recognized the lymphocyte population on a side scatter (SSC-A)/forward scatter (FSC-A) plot. Then, we gated lymphocytes using the CD3 expression, acquiring 10,000 events on this gate for posterior analyses. After that, we obtained CD4+ and CD8+ T cells through a rectangular gating strategy using CD4 and CD8 expression. Finally, we analyzed IFN-gamma, IL-2, and PD-1 expression on the CD4+ and CD8+ T cell populations (**Supplementary Figures 2A, B**, respectively). For monocytes, we first gated single cells on a forward scatter (FSC-H)/side scatter density plot. Then, we gated cells on a time/side scatter density plot. Afterward, we recognized monocytes using HLA-DR expression, acquiring 10,000 events on this gate for posterior analyses. Then, we obtained total monocytes on a CD14/CD16 density plot and subsequently identified gates for classical monocytes (CD14++CD16-), intermediate monocytes (CD14++CD16+), and non-classical monocytes (CD14+CD16+). Finally, we analyzed IFN-alpha expression on each monocyte subset (**Supplementary Figure 3**). We obtained the Median Fluorescence Intensity (MFI) for IL-2, IFN-gamma, PD-1, and IFN-alpha, considering both positive and negative cell populations for each marker, as shown in **Supplementary Figure 4**. We obtained the percentage of positive cells for each marker using proper fluorescence minus one (FMO) controls. We performed compensation controls for each fluorochrome by UltraComp eBeads™ (Invitrogen™, Carlsbad, CA, USA). We analyzed data using the FlowJo 10.0.7 software (TreeStar, Inc, Ashland, OR, USA).

## Total IgG and Neutralizing Antibodies Anti-SARS-CoV-2

One month after clinical recovery of the twelve patients who developed mild or severe COVID-19, we collected venous blood samples for posterior serum isolation and measurement of anti-SARS-CoV-2 IgG total antibodies and neutralizing antibody percentage in triplicate by the Enzyme Linked-ImmunoSorbent Assay (ELISA). For total antibodies, we measured IgG antibody serum levels against the SARS-CoV-2 nucleocapsid (N) protein using a kit from Abcam (Abcam, ab274339, Cambridge, UK) and a microplate reader at 450 nm. For neutralizing antibody percentage, we used the anti-SARS-CoV-2 Neutralizing Antibody ELISA Kit and a microplate reader at 450 nm (Thermo Fisher Scientific, BMS2326, Vienna, Austria). We calculated the neutralization percentage for unknown samples as follows: neutralization (%) = 1 − (absorbance of unknown sample/absorbance of negative control) × 100.

## Statistics

We evaluated the normality of data by the Shapiro-Wilk test. For *in vitro* assays, we compared the basal expression of IL-2, PD-1, IFN-gamma, and IFN-alpha between mild COVID-19 cases and severe COVID-19 cases by the unpaired Student's T test. We compared the amount of IFN-gamma+IL-2+ double-positive cells in helper and cytotoxic T cells expressing or not PD-1 from mild COVID-19 cases and severe COVID-19 cases by two-way ANOVA. We compared the anti-SARS-CoV-2 IgG total antibodies and neutralizing antibody percentage between mild COVID-19 cases and severe COVID-19 cases by the unpaired Student's T test. We considered differences significant when $P < 0.05$. We performed all statistical analyses using the GraphPad Prism 7 software.

# RESULTS

## Demographic, Clinical, and Laboratory Parameters in the Study Population

We show the selection process of participants enrolled in the study in **Figure 1**. After meeting inclusion and exclusion criteria, we eliminated 23 participants from the study because they

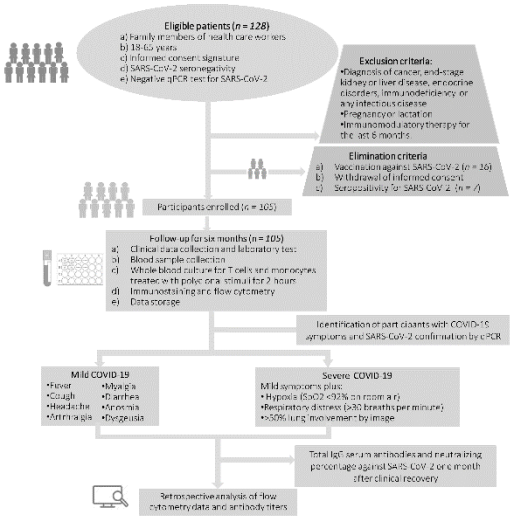


**FIGURE 1** | Schematic flow chart showing the selection process of eligible participants. SpO2, oxygen saturation level; SARS CoV 2, severe acute respiratory syndrome coronavirus type 2; qPCR, quantitative polymerase chain reaction; COVID-19, coronavirus disease 2019.

exhibited specific IgG serum antibody titers against the SARS-CoV-2 N protein ($n$ = 7) or got the Pfizer-BioNTech COVID-19 vaccine ($n$ = 16). One hundred and five volunteers completed the six-month follow-up without getting vaccinated (**Figure 1**). At the beginning of the follow-up, the whole study population consisted of 41 women and 64 men that were 41.6 ± 11.2 years on average and showed a low prevalence of comorbidities such as obesity, type 2 diabetes, hypertension, coronary heart disease and average values of routine biochemical tests (**Table 1**). After grading COVID-19 severity in participants who got SARS-CoV-2 infection during the six-month follow-up, we registered two women and four men only experiencing a self-limiting disease with mild symptoms such as fever, anosmia, headache, myalgia, and arthralgia, resolved without specific drug treatment after 9-12 days (**Table 2**). Conversely, one woman and five men developed severe COVID-19 characterized by the symptoms mentioned above, plus respiratory distress (36.6 ± 3.1 breaths per minute), hypoxia (74.0 ± 7.6%), and pneumonia (**Table 2**). Two participants developing severe COVID-19 required ICU admission for invasive ventilatory support (**Table 2**). Of note, the baseline clinical characteristics did not differ between participants who developed mild or severe COVID-19 during the follow-up (**Table 1**). Except for neutrophil and lymphocyte percentages, ALP, and serum albumin, there were no differences between participants who developed mild or severe COVID-19 for the values of hematic biometry, blood glucose, lipid profile, renal parameters, and liver function tests seven days after symptom onset (**Table 2**). As we have outlined here, neither baseline characteristics nor the clinical presentation of COVID-19 allowed predicting the disease severity in the participants who got SARS-CoV-2 infection during the follow-up.

## IL-2, IFN-Gamma, and PD-1 Production in Helper T Cells

Supplementary **Figure 2A** illustrates the gating strategy for analyzing IL-2, IFN-gamma, and PD-1 expression in CD3+CD4+ T cells stimulated with anti-CD3, anti-CD28, poly I:C, and SARS-CoV-2 recombinant spike S1 protein in whole blood *in vitro* cultures at the beginning of the follow-up, when all healthy participants were initially enrolled in the study (**Supplementary Figure 2A**). Representative dot-plots illustrate the comparison of CD3+CD4+ T cells expressing IL-2 in blood samples treated with polyclonal stimuli from participants who developed mild or severe COVID-19 during the follow-up (**Figure 2A**). In response to polyclonal *in vitro* stimulation, the percentage of CD3+CD4+IL-2+ T cells showed a significant 4-fold decrease in the group that during the follow-up developed severe COVID-19 compared to participants experiencing mild symptoms ($P$ = 0.0085) (**Figure 2B**). IL-2 expression behaved in the same way as observed in cell percentage, displaying a significant 2-fold diminution in helper T cells from participants that after SARS-CoV-2 infection developed severe COVID-19 compared to the mild disease group ($P$ = 0.0075) (**Figure 2C**). Representative dot-plots exemplify the contrast of CD3+CD4+ T cells expressing IFN-gamma in whole blood samples exposed to polyclonal molecules from participants who experienced mild or

**TABLE 1** | Baseline characteristics of the study participants.

| Parameter | Baseline characteristics in the entire study population | Baseline characteristics only in participants who developed COVID-19 | | Reference ranges | *P* value[a vs b] |
|---|---|---|---|---|---|
| | | Mild[a] | Severe[b] | | |
| Gender (W/M) | 41/64 | 2/4 | 1/5 | - | 0.505 |
| Age (years) | 41.6 ± 11.2 | 47.3 ± 10.3 | 45 ± 9.6 | - | 0.343 |
| BMI (kg/m$^2$) | 27.3 ± 4.8 | 26 ± 1.6 | 25.5 ± 1.1 | <25.0 | 0.458 |
| Obesity (W/M) | 14/10 | 0/0 | 0/1 | - | 1.000 |
| D prevalence (%) | 6 | 0 | 0 | - | 1.000 |
| Hypertension prevalence (%) | 8.6 | 0 | 0 | - | 1.000 |
| Coronary heart disease (%) | 1.7 | 0 | 0 | - | 1.000 |
| Heart rate (beats per minute) | 75.4 ± 10.8 | 72.5 ± 5.9 | 70.5 ± 5.2 | 60-100 | 0.550 |
| Breathing rate (bpm) | 15.7 ± 3.3 | 16.5 ± 2.5 | 15.6 ± 2.8 | 15-20 | 0.609 |
| Body temperature (°C) | 36.2 ± 0.2 | 36.1 ± 0.2 | 36.1 ± 0.1 | ≤37.5 | >0.999 |
| Systolic blood pressure (mmHg) | 128.6 ± 18.3 | 124.5 ± 11.5 | 125.8 ± 7.2 | <130 | 0.816 |
| Diastolic blood pressure (mmHg) | 82.1 ± 11.3 | 78.5 ± 9.3 | 80.1 ± 6.3 | <85 | 0.725 |
| Peripheral oxygen saturation (%) | 95.8 ± 2.2 | 95.6 ± 1.0 | 96.1 ± 2.7 | >91 | 0.682 |
| Leukocytes (x10$^3$/µl) | 6.3 ± 1.2 | 6.1 ± 0.8 | 6.9 ± 1.8 | 4.00-11.00 | 0.213 |
| Neutrophil percentage (%) | 58.3 ± 8.6 | 55.2 ± 10.4 | 57.2 ± 7.2 | 37.00-80.00 | 0.367 |
| Lymphocyte percentage (%) | 31.5 ± 7.2 | 33.8 ± 9.6 | 27.4 ± 4.1 | 10.00-50.00 | 0.106 |
| Monocyte percentage (%) | 5.8 ± 0.9 | 6.3 ± 0.3 | 7.4 ± 1.6 | 0.00-8.00 | 0.084 |
| Band cells (%) | 0.04 ± 0.03 | 0.08 ± 0.08 | 0.00 ± 0.00 | 0.00-7.00 | 0.216 |
| Hemoglobin (g/dl) | 16.7 ± 1.0 | 16.2 ± 1.4 | 16.9 ± 0.7 | 13.1-18.00 | 0.173 |
| Platelets (x10$^3$/µl) | 219.3 ± 24.6 | 180 ± 22.9 | 208.6 ± 26.5 | 150 -400 | 0.053 |
| Glucose (mg/dl) | 96.3 ± 7.4 | 83.4 ± 6.1 | 92 ± 9.7 | 70.0-126.0 | 0.447 |
| Urea (mg/dl) | 30.2 ± 8.6 | 28.6 ± 4.9 | 39.2 ± 10.5 | 20.00-40.00 | 0.059 |
| Creatinine (mg/dl) | 1.1 ± 0.2 | 0.9 ± 0.1 | 0.8 ± 0.1 | 0.60-1.30 | 0.180 |
| Total Cholesterol (mg/dl) | 207.9 ± 48.0 | 178.8 ± 18.3 | 171.4 ± 37.5 | 50.0-200.0 | 0.350 |
| Triglycerides (mg/dl) | 180.5 ± 82.6 | 196.8 ± 104 | 134.8 ± 59.1 | 30.0-200.0 | 0.140 |
| HDL (mg/dl) | 44.7 ± 8.5 | 40.6 ± 10.8 | 41 ± 9.4 | ≤45.00 | 0.475 |
| LDL (mg/dl) | 110.6 ± 34.2 | 114. 6 ± 33.3 | 117.8 ± 28.4 | <116.00 | 0.437 |
| Total bilirubin (mg/dl) | 0.9 ± 0.1 | 0.7 ± 0.2 | 0.7 ± 0.2 | 0.00-1.00 | 0.423 |
| Direct bilirubin (mg/dl) | 0.2 ± 0.1 | 0.2 ± 0.1 | 0.1 ± 0.06 | 0.00-0.30 | 0.211 |
| Indirect bilirubin (mg/dl) | 0.5 ± 0.2 | 0.5 ± 0.2 | 0.6 ± 0.2 | 0.20-1.00 | 0.421 |
| ALT (IU/l) | 30.4 ± 8.9 | 27.6 ± 9.6 | 24 ± 9.9 | 30-65 | 0.288 |
| AST (IU/l) | 28.2 ± 5.6 | 23.6 ± 6.8 | 19.4 ± 3.6 | 15-37 | 0.129 |
| ALP (IU/l) | 51.5 ± 14.1 | 17.6 ± 16.8 | 59.2 ± 15.7 | 50-136 | 0.116 |
| GGT (IU/l) | 31.2 ± 19.7 | 36.4 ± 31.0 | 35.7 ± 17.4 | 5-40 | 0.485 |
| Total Protein (mg/dl) | 7.1 ± 0.1 | 7.2 ± 0.1 | 7.1 ± 0.2 | 6.50-8.20 | 0.275 |
| Albumin (mg/dl) | 4.8 ± 0.4 | 4.29 ± 0.2 | 4.4 ± 0.3 | 3.50-5.00 | 0.267 |
| LDH (IU/l) | 194.2 ± 17.0 | 179.2 ± 4.7 | 162.6 ± 25.0 | 100-190 | 0.118 |
| Amylase (IU/l) | 51.3 ± 15.6 | 45.5 ± 13.2 | 47.4 ± 17.1 | 25-115 | 0.430 |
| Lipase (IU/l) | 37.4 ± 14.8 | 28.5 ± 12.5 | 24.8 ± 10.8 | 12-70 | 0.324 |

*Reference values are shown according to the Clinical Laboratory of the General Hospital of Mexico. We expressed data as mean ± standard deviation. We retrospectively compared baseline characteristics between mild and severe groups using the chi-square test or the unpaired Student's T-test and considered differences significant when P < 0.05. COVID-19, coronavirus disease 2019; W, women; M, men; BMI, body mass index; D, type 2 diabetes; bpm, breaths per minute; HDL, high-density lipoproteins; LDL, low-density lipoproteins; ALT, alanine aminotransferase; AST, aspartate aminotransferase; ALP, alkaline phosphatase; GGT, gamma glutamyl transferase; LDH, lactate dehydrogenase.*
*We show demographic, clinical, and biochemical baseline parameters in all participants and those who developed COVID-19 during the six-month follow-up.*

severe COVID-19 throughout the follow-up (**Figure 2D**). The percentage of CD3+CD4+IFN-gamma+ T cells displayed a significant 4-fold reduction in the severe COVID-19 group compared to participants developing a mild disease ($P$ = 0.0034) (**Figure 2E**). Likewise, IFN-gamma production significantly decreased in helper T cells from participants experiencing severe COVID-19 compared to those found in individuals with mild symptoms ($P$ = 0.0369) (**Figure 2F**). Representative dot-plots illustrate the comparison of CD3+CD4+ T cells expressing PD-1 in blood samples treated with polyclonal stimuli from participants who developed mild or severe COVID-19 during the follow-up (**Figure 2G**). The percentage of CD3+CD4+ T cells expressing PD-1 exhibited a significant 2-fold increase in the severe COVID-19 group compared to the mild disease group ($P$ = 0.0416) (**Figure 2H**). There were no significant changes between severe and mild COVID-19 participants for PD-1 expression in the population of helper T cells (**Figure 2I**). Representative dot-plots exemplify the contrast of CD3+CD4+ T cells simultaneously expressing IL-2, IFN-gamma, and PD-1 in whole blood samples exposed to polyclonal molecules from participants who experienced mild or severe COVID-19 throughout the follow-up (**Figure 2J**). Interestingly, PD-1 expression was intimately related to IL-2 and

**TABLE 2** | Clinical and biochemical characteristics of participants who developed mild or severe COVID-19 during the six-month follow-up.

| Parameter | Onset of symptoms | | | *P* value |
|---|---|---|---|---|
| | Mild COVID-19[a] | Severe COVID-19[b] | Reference ranges | [a] vs [b] |
| Fever (Yes/No) | 4/2 | 5/1 | <37.5°C | 1.000 |
| Anosmia (Yes/No) | 4/2 | 3/3 | - | 1.000 |
| Headache (Yes/No) | 6/0 | 6/0 | - | 1.000 |
| Myalgia (Yes/No) | 4/2 | 5/1 | - | 1.000 |
| Arthralgia (Yes/No) | 2/4 | 1/5 | - | 1.000 |
| Diarrhea (Yes/No) | 3/3 | 2/4 | - | 1.000 |
| ICU admission (Yes/No) | 0/6 | 2/4 | - | 0.227 |
| Clinical characteristics seven days after symptom onset | | | | |
| Heart rate (beats per minute) | 69.1 ± 6.3 | 81.3 ± 8.9 | 60-100 | 0.021 |
| Breathing rate (bpm) | 19.8 ± 3.0 | 36.6 ± 3.1 | 15-20 | <0.0001 |
| Peripheral oxygen saturation (%) | 95.1 ± 1.7 | 74.0 ± 7.6 | >91 | <0.0001 |
| Leukocytes ($\times10^3$/µl) | 5.6 ± 1.4 | 11.0 ± 5.6 | 4.00-11.00 | 0.066 |
| Neutrophil percentage (%) | 48.6 ± 14.2 | 80.1 ± 15.6 | 37.00-80.00 | 0.044* |
| Lymphocyte percentage (%) | 40.9 ± 13.0 | 13.8 ± 14.8 | 10.00-50.00 | 0.043* |
| Monocyte percentage (%) | 7.3 ± 0.1 | 5.8 ± 1.7 | 0.00-8.00 | 0.200 |
| Band cells (%) | 0.0 ± 0.0 | 0.0 ± 0.0 | 0.00-7.00 | >0.999 |
| Hemoglobin (g/dl) | 16.7 ± 0.7 | 14.5 ± 1.7 | 13.1-18.00 | 0.088 |
| Platelets ($\times10^3$/µl) | 273.5 ± 16.2 | 283.4 ± 112.5 | 150-400 | 0.444 |
| Glucose (mg/dl) | 89.0 ± 12.7 | 208.9 ± 92.1 | 70.00-100.00 | 0.088 |
| Urea (mg/dl) | 34.8 ± 12.5 | 58.9 ± 68.6 | 20.00-40.00 | 0.355 |
| Creatinine (mg/dl) | 0.9 ± 0.0 | 1.6 ± 2.3 | 0.80-1.30 | 0.354 |
| Total Cholesterol (mg/dl) | 194.0 ± 42.4 | 116.7 ± 21.1 | 50.00-200.00 | 0.071 |
| Triglycerides (mg/dl) | 344.5 ± 86.9 | 162.8 ± 81.6 | 30.00-150.00 | 0.142 |
| HDL (mg/dl) | 32.5 ± 7.7 | 27.0 ± 8.2 | ≤45.00 | 0.428 |
| LDL (mg/dl) | 118.0 ± 26.8 | 79.3 ± 27.7 | ≤115.00 | 0.142 |
| Total bilirubin (mg/dl) | 0.8 ± 0.3 | 0.5 ± 0.1 | 0.00-1.00 | 0.500 |
| Direct bilirubin (mg/dl) | 0.1 ± 0.0 | 0.1 ± 0.0 | 0.00-0.30 | >0.999 |
| Indirect bilirubin (mg/dl) | 0.6 ± 0.2 | 0.4 ± 0.1 | 0.20-1.00 | 0.500 |
| ALT (IU/l) | 37.5 ± 27.5 | 49.2 ± 37.8 | 30-65 | 0.711 |
| AST (IU/l) | 23.5 ± 6.3 | 48.5 ± 32.5 | 15-37 | 0.133 |
| ALP (IU/l) | 60.0 ± 2.8 | 99.3 ± 17.0 | 50-136 | 0.044* |
| GGT (IU/l) | 46.0 ± 24.4 | 56.7 ± 27.3 | 5-40 | 0.755 |
| Total Protein (mg/dl) | 7.4 ± 0.0 | 6.7 ± 0.6 | 6.50-8.20 | 0.166 |
| Albumin (mg/dl) | 4.6 ± 0.0 | 3.6 ± 0.4 | 3.50-5.00 | 0.044* |
| LDH (IU/l) | 162.5 ± 38.8 | 354.6 ± 146.5 | 100-190 | 0.088 |
| Amylase (IU/l) | 45.0 ± 9.8 | 65.0 ± 66.8 | 25-115 | 0.700 |
| Lipase (IU/l) | 41.0 ± 14.1 | 45.3 ± 45.6 | 12-70 | 0.810 |

*We recorded data from all COVID-19 participants at the onset of symptoms and seven days after. Reference values are shown according to the Clinical Laboratory of the General Hospital of Mexico. We expressed data as mean ± standard deviation. We compared clinical and biochemical data between mild and severe groups using the chi-square test or the unpaired Student's T-test and considered differences significant when P < 0.05. The asterisks represent significant differences. COVID-19, coronavirus disease 2019; ICU, intensive care unit; bpm, breaths per minute; HDL, high-density lipoproteins; LDL, low-density lipoproteins; ALT, alanine aminotransferase; AST, aspartate aminotransferase; ALP, alkaline phosphatase; GGT, gamma glutamyl transferase; LDH, lactate dehydrogenase.*

IFN-gamma production in the population of helper T cells. In this sense, participants who developed mild symptoms showed that PD-1+ T cells expressing both IL-2 and IFN-gamma decreased 4-fold compared to PD-1 negative helper T lymphocytes ($P$ = 0.0001), indicating that PD-1 expression inversely associated with IL-2 and IFN-gamma production (**Figure 2K**). Nevertheless, we did not observe this expected behavior in participants developing severe COVID-19 after SARS-CoV-2 infection, whose helper T cells exhibited similar IL-2 and IFN-gamma expression patterns independently of expressing or not PD-1 (**Figure 2K**). Additionally to cell percentages, we show the corresponding absolute numbers of CD3+CD4+ T cells expressing IL-2, IFN-gamma, and PD-1 in **Supplementary Figure 5**. We found no detectable IL-2, IFN-gamma, and PD-1 expression in CD3+CD4+ T cells cultured in the absence of anti-CD3, anti-CD28, poly I:C, and SARS-CoV-2 recombinant spike S1 protein (data not shown).

## IL-2, IFN-Gamma, and PD-1 Production in Cytotoxic T Cells

Supplementary figure 2B shows the gating strategy for examining IL-2, IFN-gamma, and PD-1 expression in CD3+CD8+ T cells exposed to polyclonal stimuli *in vitro* (**Supplementary Figure 2B**). Representative dot-plots illustrate the comparison of CD3+CD8+ T cells expressing IL-2 in blood samples treated with polyclonal stimuli from participants who developed mild or severe COVID-19 during the follow-up (**Figure 3A**). In response to anti-CD3, anti-CD28, poly I:C, and SARS-CoV-2 recombinant spike S1 protein, whole blood cultures revealed that the percentage of CD3+CD8+IL-2+ T cells exhibited a significant 5-fold decrease in the group that posteriorly developed severe COVID-19 compared to participants with mild symptoms ($P$ = 0.0085) (**Figure 3B**). As expected, IL-2 production significantly reduced in cytotoxic T cells from

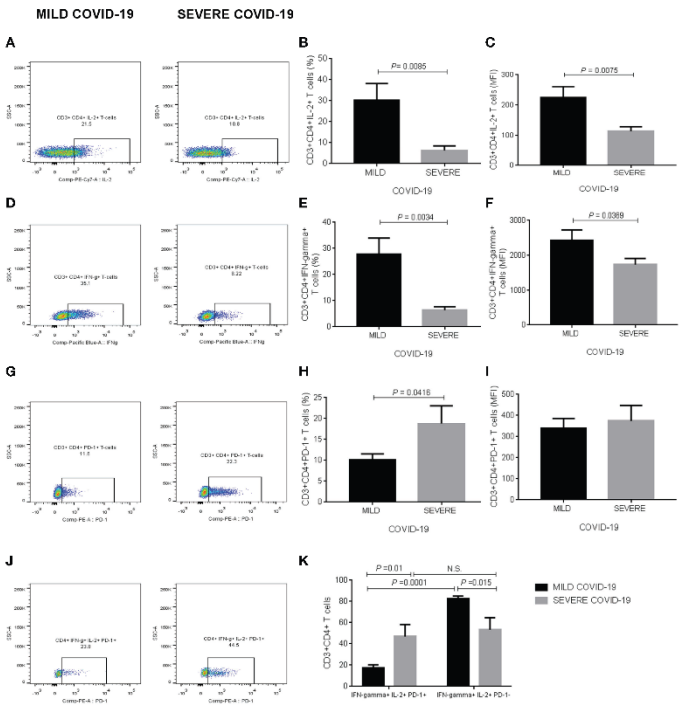


**FIGURE 2** | IL-2, IFN-gamma, and PD-1 expression in CD3+CD4+ T cells in response to polyclonal stimuli *in vitro*. **(A)** Representative dot-plots illustrating the comparison of CD3+CD4+ T cells expressing IL-2 in blood samples treated with polyclonal stimuli from participants who developed mild or severe COVID-19 during the follow up. **(B)** Percentage of CD3+CD4+ T cells expressing IL 2. **(C)** Mean fluorescence intensity of IL 2 in CD3+CD4+ T cells. **(D)** Representative dot plots exemplifying the contrast of CD3+CD4+ T cells expressing IFN-gamma in whole blood samples exposed to polyclonal molecules from participants who experienced milo or severe COVID-19 throughout the follow up. **(E)** Percentage of CD3+CD4+ T cells expressing IFN-gamma. **(F)** Mean fluorescence intensity of IFN-gamma in CD3+CD4+ T cells. **(G)** Representative dot-plots illustrating the comparison of CD3+CD4+ T cells expressing PD-1 in blood samples treated with polyclonal stimuli from participants who developed mild or severe COVID-19 during the follow-up. **(H)** Percentage of CD3+CD4+ T cells expressing PD-1. **(I)** Mean fluorescence intensity of PD-1 in CD3+CD1+ T cells. **(J)** Representative dot-plots exemplifying the contrast of CD3+CD1+ T cells simultaneously expressing IL-2, IFN-gamma, and PD-1 in whole blood samples exposed to polyclonal molecules from participants who experienced mild or severe COVID-19 throughout the follow-up. **(K)** Percentage of CD3+CD4+ T cells producing both IL 2 and IFN gamma depending on PD 1 expression. Prior to infection, we obtained whole blood samples from all participants enrolled in the study and cultured them with polyclonal stimuli, including anti-CD3, anti-CD28, poly I:C, and SARS-CoV-2 recombinant spike S1 protein for two hours. We then acquired CD3+CD4+ T cells on a BD FACS Canto II Flow Cytometer, acquiring 10,000 events per test in triplicate and storing data until a participant got SARS-CoV-2 infection. Upon infection and depending on the clinical course of the disease, we analyzed flow cytometry data as part of the mild or severe COVID-19 groups. Black bars represent the milo COVID-19 group. Gray bars represent the severe COVID-19 group. We expressed data as mean ± standard deviation. We compared data using the unpaired Student's T-test or two-way ANOVA and considered differences significant when $P < 0.05$. IL-2, interleukin-2; IFN-gamma, interferon-gamma; PD-1, programmed cell death protein 1; MFI, mean fluorescence intensity; COVID-19, coronavirus disease 2019; SARS-CoV-2, severe acute respiratory syndrome coronavirus type 2.

participants developing severe COVID-19 compared to those found in subjects experiencing mild disease ($P$ = 0.0002) (**Figure 3C**). Representative dot-plots exemplify the contrast of CD3+CD8+ T cells expressing IFN-gamma in whole blood samples exposed to polyclonal molecules from participants who experienced mild or severe COVID-19 throughout the follow-up (**Figure 3D**). The percentage of CD3+CD8+IFN-gamma+ T cells showed a significant 3-fold diminution in the severe COVID-19 group compared to participants experiencing mild symptoms ($P$ = 0.0025) (**Figure 3E**). In parallel, IFN-gamma expression significantly decreased in the cytotoxic T cell population of participants who developed severe COVID-19 compared to that found in subjects with mild symptoms ($P$ = 0.0232) (**Figure 3F**). Representative dot-plots illustrate the

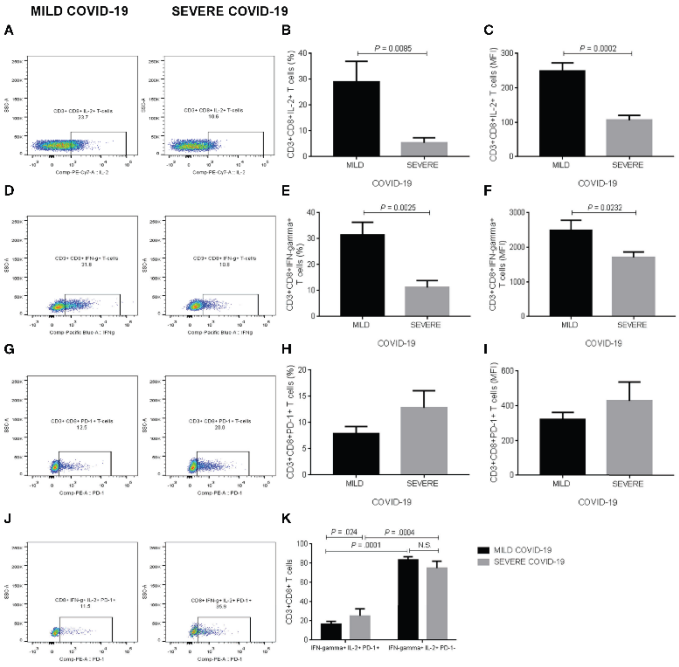


**FIGURE 3** | IL-2, IFN-gamma, and PD-1 expression in CD3+CD8+ T cells in response to polyclonal stimuli *in vitro*. **(A)** Representative dot-plots illustrating the comparison of CD3+CD8+ T cells expressing IL-2 in blood samples treated with polyclonal stimuli from participants who developed mild or severe COVID-19 during the follow-up. **(B)** Percentage of CD3+CD8+ T cells expressing IL-2. **(C)** Mean fluorescence intensity of IL-2 in CD3+CD8+ T cells. **(D)** Representative dot-plots exemplifying the contrast of CD3+CD8+ T cells expressing IFN-gamma in whole blood samples exposed to polyclonal molecules from participants who experienced milo or severe COVID-19 throughout the follow-up. **(E)** Percentage of CD3+CD8+ T cells expressing IFN-gamma. **(F)** Mean fluorescence intensity of IFN-gamma in CD3+CD8+ T cells. **(G)** Representative dot-plots illustrating the comparison of CD3+CD8+ T cells expressing PD-1 in blood samples treated with polyclonal stimuli from participants who developed mild or severe COVID-19 during the follow-up. **(H)** Percentage of CD3+CD8+ T cells expressing PD-1. **(I)** Mean fluorescence intensity of PD-1 in CD3+CD8+ T cells. **(J)** Representative dot-plots exemplifying the contrast of CD3+CD8+ T cells simultaneously expressing IL-2, IFN-gamma, and PD-1 in whole blood samples exposed to polyclonal molecules from participants who experienced mild or severe COVID-19 throughout the follow-up. **(K)** Percentage of CD3+CD8+ T cells producing both IL-2 and IFN-gamma depending on PD-1 expression. Prior to infection, we obtained whole blood samples from all participants enrolled in the study and cultured them with polyclonal stimuli, including anti-CD3, anti-CD28, poly I:C, and SARS-CoV-2 recombinant spike S1 protein for two hours. We then acquired CD3+CD8+ T cells on a BD FACS Canto II Flow Cytometer, acquiring 10,000 events per test in triplicate and storing data until a participant got SARS-CoV-2 infection. Upon infection and depending on the clinical course of the disease, we analyzed flow cytometry data as part of the mild or severe COVID-19 groups. Black bars represent the milo COVID-19 group. Gray bars represent the severe COVID-19 group. We expressed data as mean ± standard deviation. We compared data using the unpaireo Student's T test or two-way ANOVA and considered differences significant when $P < 0.05$. IL-2, interleukin-2; IFN-gamma, interferon-gamma; PD-1, programmed cell death protein 1; MFI, mean fluorescence intensity; COVID-19, coronavirus oisease 2019; SARS-CoV-2, severe acute respiratory syndrome coronavirus type 2.

comparison of CD3+CD8+ T cells expressing PD-1 in blood samples treated with polyclonal stimuli from participants who developed mild or severe COVID-19 during the follow-up (**Figure 3G**). Contrary to what we expected, neither the percentage of CD3+CD8+PD-1+ T cells nor PD-1 production itself exhibited significant differences between the mild and severe COVID-19 groups (**Figures 3H, I**, respectively). Representative dot-plots exemplify the contrast of CD3+CD8+ T cells simultaneously expressing IL-2, IFN-gamma, and PD-1 in whole blood samples exposed to polyclonal molecules from participants who experienced mild or severe COVID-19 throughout the follow-up (**Figure 3J**). However, PD-1 expression conditioned IL-2 and IFN-gamma production in cytotoxic T cells, which expressed higher IL-2 and IFN-gamma levels in PD-1 negative cells than CD3+CD8+PD-1+ T cells independently of having been analyzed in participants that

posteriorly developed either mild or severe COVID-19 (**Figure 3K**). In addition to cell percentages, we provide the corresponding absolute numbers of CD3+CD8+ T cells expressing IL-2, IFN-gamma, and PD-1 in **Supplementary Figure 5**. We observed no detectable IL-2, IFN-gamma, and PD-1 expression levels in CD3+CD8+ T cells cultured without anti-CD3, anti-CD28, poly I:C, and recombinant spike S1 protein (data not shown).

## IFN-Alpha Production in Monocyte Subpopulations

**Supplementary Figure 3** illustrates the gating strategy for evaluating IFN-alpha expression in classical, intermediate, and non-classical monocytes exposed to SARS-CoV-2 recombinant spike S1 protein, poly I:C and LPS in whole blood *in vitro* cultures (**Supplementary Figure 3**). Representative dot-plots illustrate the comparison of CD14++CD16- classical monocytes expressing IFN-alpha in blood samples treated with polyclonal stimuli from participants who developed mild or severe COVID-19 during the follow-up (**Figure 4A**). In response to polyclonal *in vitro* stimulation, the percentage of classical monocytes expressing IFN-alpha showed a significant 3-fold decrease in the group who developed severe COVID-19 during the follow-up compared to participants with mild symptoms ($P = 0.0013$) (**Figure 4B**). There were no significant changes between mild and severe COVID-19 group for IFN-alpha expression in this monocyte subset (**Figure 4C**). Representative dot-plots exemplify the contrast of CD14++CD16+ intermediate monocytes expressing IFN-alpha in whole blood samples exposed to polyclonal molecules from participants who experienced mild or severe COVID-19 throughout the follow-up (**Figure 4D**). Neither the percentage

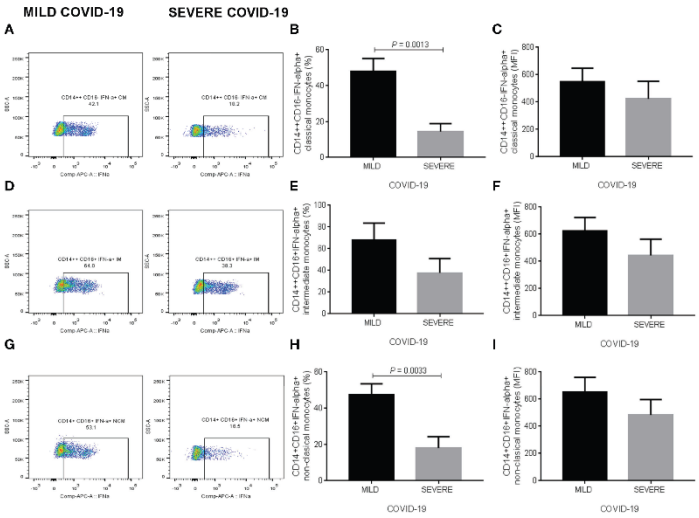


**FIGURE 4** | IFN-alpha expression in classical, intermediate, and non-classical monocyte subpopulations in response to polyclonal stimuli *in vitro*. **(A)** Representative dot-plots illustrating the comparison of CD14++CD16- classical monocytes expressing IFN-alpha in blood samples treated with polyclonal stimuli from participants who developed milo or severe COVID-19 during the follow-up. **(B)** Percentage of CD14++CD16- classical monocytes expressing IFN-alpha. **(C)** Mean fluorescence intensity of IFN-alpha in CD14++CD16- classical monocytes. **(D)** Representative dot-plots exemplifying the contrast of CD14++CD16+ intermediate monocytes expressing IFN-alpha in whole blood samples exposed to polyclonal molecules from participants who experienced mild or severe COVID-19 throughout the follow-up. **(E)** Percentage of CD14++CD16+ intermediate monocytes expressing IFN alpha. **(F)** Mean fluorescence intensity of IFN alpha in CD14++CD16+ intermediate monocytes. **(G)** Representative dot-plots illustrating the comparison of CD14+CD16+ non-classical monocytes expressing IFN-alpha in blood samples treated with polyclonal stimuli from participants who developed mild or severe COVID 19 during the follow up. **(H)** Percentage of CD14+CD16+ non classical monocytes expressing IFN-alpha. **(I)** Mean fluorescence intensity of IFN-alpha in CD14+CD16+ non-classical monocytes. Prior to infection, we obtained whole blood samples from all participants enrolled in the study and cultured them with polyclonal stimuli, including poly I:C. SARS CoV 2 recombinant spike S1 protein, and LPS. for two hours. We then acquired monocyte cells on a BD FACS Canto II Flow Cytometer, acquiring 10,000 events per test in triplicate and storing data until a participant got SARS-CoV-2 infection. Upon infection and deepening on the clinical course of the disease, we analyzed flow cytometry data as part of the mild or severe COVID-19 groups. Black bars represent the mild COVID-19 group. Gray bars represent the severe COVID-19 group. We expressed data as mean ± standard deviation. We compared data using the unpaired Student's T-test and considered differences significant when $P < 0.05$. We defined classical monocytes as CD14++CD16-, intermediate monocytes as CD14++CD16+, and non classical monocytes as CD14+CD16+. IFN alpha, interferon alpha; MFI, mean fluorescence intensity; COVID-19, coronavirus disease 2019, LPS, lipopolysaccharide; SARS-CoV-2, severe acute respiratory syndrome coronavirus type 2.

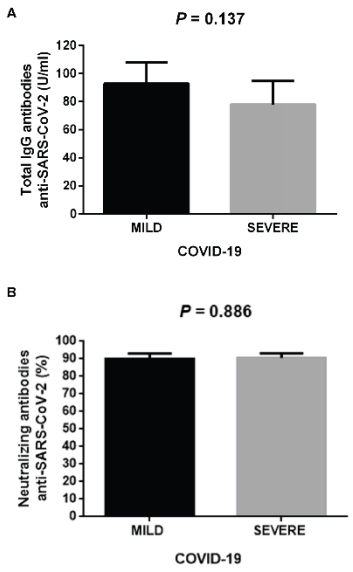


**FIGURE 5** | Total IgG and neutralizing antibodies anti-SARS-CoV-2 in the stuoy participants. **(A)** Total IgG serum antibodies against the N protein of the SARS-CoV-2 in participants who developeo mild or severe COVID-19 during the follow-up. **(B)** Percentage of neutralizing antibodies anti-SARS-CoV-2 in participants who developed mild or severe COVID-19 during the follow-up. We measureo total IgG or neutralizing antibooies one month after clinical recovery of participants. Black bars represent the mild COVID-19 group. Gray bars represent the severe COVID-19 group. We expressed data as mean ± standard deviation. We compared data using the unpaireo Student's T-test ano considered differences significant when $P < 0.05$. IgG, immunoglobulin G; SARS-CoV-2, severe acute respiratory syndrome coronavirus type 2; COVID-19, coronavirus disease 2019.

of intermediate monocytes expressing IFN-alpha nor IFN-alpha production itself displayed significant differences between the mild and severe COVID-19 groups (**Figures 4E, F**, respectively). Representative dot-plots illustrate the comparison of CD14 +CD16+ non-classical monocytes expressing IFN-alpha in blood samples treated with polyclonal stimuli from participants who developed mild or severe COVID-19 during the follow-up (**Figure 4G**). The percentage of non-classical monocytes expressing IFN-alpha exhibited a significant 2.5-fold reduction in participants developing severe COVID-19 compared to that found in individuals experiencing mild symptoms ($P = 0.0033$) (**Figure 4H**). Conversely, there were no significant changes between mild and severe COVID-19 groups for IFN-alpha expression in this monocyte subset (**Figure 4I**). Besides showing cell percentages, we present the corresponding absolute numbers of classical, intermediate, and non-classical monocytes expressing IFN-alpha in **Supplementary Figure 5**. We found no detectable IFN-alpha expression in classical, intermediate, and non-classical monocytes cultured without recombinant spike S1 protein, poly I:C, and LPS (data not shown).

## Total IgG and Neutralizing Antibodies Anti-SARS-CoV-2

The production pattern of IL-2, IFN-gamma, and IFN-alpha suggested that helper and cytotoxic T cells and monocyte subpopulations show a basal defective cellular response against polyclonal stimuli, which is probably associated with predisposing to the development of severe COVID-19 after SARS-CoV-2 infection. To know whether a possible impairment in the cellular immune response led to defective antibody production, we decided to measure the total concentration of IgG serum antibodies and the percentage of neutralizing antibodies against the SARS-CoV-2 in participants who developed either mild or severe COVID-19. Unexpectedly, the total IgG serum titers against the N protein of the SARS-CoV-2 showed no significant changes between participants developing mild or severe COVID-19 ($\bar{x} = 92.8 \pm 15.1$ and $\bar{x} = 77.9 \pm 16.8$, $P = 0.137$, respectively) (**Figure 5A**). Likewise, the neutralizing antibody percentage against the virus did not differ between participants who developed mild or severe COVID-19 ($\bar{x} = 89.6 \pm 7.1$ and $\bar{x} = 90.2 \pm 6.4$, respectively, $P = 0.886$) (**Figure 5B**). Thus, defective expression of IL-2, IFN-gamma, and IFN-alpha in T lymphocytes and monocytes did not affect the production of either total IgG or neutralizing antibodies against the SARS-CoV-2.

## DISCUSSION

The mechanisms of the cell-mediated immunity contributing to worsening the severity of COVID-19 remain unclear (17, 18). For this reason, we formed a cohort of healthy individuals who were family members of health care professionals working at a dedicated COVID-19 hospital and obtained more than 120 whole blood samples. Then, we exposed T cells and monocytes to polyclonal stimuli *in vitro* to characterize a cytokine response pattern that we could link to the severity of COVID-19 only in those participants resulting infected during a six-month follow-up. We found that participants who got infected and posteriorly experienced mild COVID-19 symptoms exhibit a different immune expression pattern in response to polyclonal stimuli than that observed in subjects that developed severe COVID-19. Participants that responded to polyclonal stimuli by increasing IL-2 and IFN-gamma production and decreasing PD-1 expression in CD4+ and CD8+ T cells tended to develop mild COVID-19 symptoms. Conversely, subjects with decreased IL-2 and IFN-gamma expression and increased PD-1 production in CD4+ and CD8+ T cells in response to polyclonal stimuli tended to display the most severe form of COVID-19, including respiratory distress and mechanical ventilatory support needing. These findings reveal a basal immune response pattern to polyclonal stimuli intimately associated with COVID-19 progression, wherein CD4+ and CD8+ T cells fail

to produce IL-2 and IFN-gamma but show an increased ability to express PD-1.

At the pandemic's beginning, most studies informed that more than 80% of patients seriously ill with COVID-19 tended to exhibit a marked lymphocytopenia at hospital admission (19–21). After that, several lines of evidence confirmed that severe COVID-19 was not only related to a reduced number of circulating lymphocytes but also decreased T cell activity, especially cytokine production such as IL-2 and IFN-gamma (22, 23). IL-2 plays a decisive role in preventing lymphocytopenia by promoting CD4+ T cell proliferation *via* the Janus kinase 1/Signal transducer and activator of transcription 5 (JAK1/STAT5) (21, 24). In fact, the use of recombinant IL-2 stimulates lymphocyte count recovery and systemic inflammatory response amelioration in patients with severe COVID-19 pneumonia (25). This body of evidence makes it feasible to think that subjects with a low number of IL-2-producing CD4+ T cells in response to *in vitro* polyclonal stimuli display increased susceptibility to severe COVID-19 after SARS-CoV-2 infection. IFN-gamma's primary function in the anti-viral response is acting directly on CD8+ T cells to boost their abundance and reduce viral load (26). IFN-gamma-producing CD8+ T cells considerably decrease in patients with severe COVID-19 compared to patients experiencing mild symptoms (27). What is also relevant is that IFN-gamma is considered an independent risk factor of mortality in COVID-19 patients (28). All this information concurs with our findings and supports the idea that a basal deficiency in IFN-gamma-producing CD8+ T cells, as revealed when we used unspecific polyclonal stimuli, may increase the risk of exacerbating viral load and developing severe COVID-19 after SARS-CoV-2 infection. However, CD8+ T cells are not only able to secrete IFN-gamma but also molecules with potent cytotoxic activity such as granzyme and perforin, which are crucial components in the recognition and lysis of infected cells. Therefore, we still must characterize the production of cytotoxic molecules in CD8+ T cells exposed to polyclonal stimuli to draw significant conclusions regarding the possible role of the cytotoxic activity of CD8+ T lymphocytes in COVID-19 progression.

PD-1 has a pivotal role in preventing exacerbation of immune responses by modulating the activity of T cells *via* apoptosis promotion, cell proliferation arrest, and cytokine secretion inhibition (29). In COVID-19, the function of PD-1 is still a matter of debate because some research teams have consistently reported that CD4+ and CD8+ T cells from COVID-19 patients express high PD-1 levels and are exhausted (13, 30). In contrast, other working groups have informed that cytotoxic T cells retain their anti-viral functions against the SARS-CoV-2 despite expressing PD-1 (31). We may attribute these controversial findings to the fact that most investigations assessing PD-1 expression in COVID-19 have studied patients treated with several drug cocktails, including cyclooxygenase (COX)-inhibitors, dexamethasone, anticoagulants, among others (32, 33). These drug schemes aim to treat and prevent COVID-19 complications but can also alter the expression of cytokines such as IL-2 and IFN-gamma and immune checkpoints as occurs with PD-1. For instance, Kailin Xing and colleagues previously demonstrated that dexamethasone increases PD-1 expression and decreases IL-2 and IFN-gamma production in human primary T cells in a dose-dependent fashion (34). Likewise, celecoxib and aspirin, two COX-inhibitors widely used in COVID-19 patients, can increase PD-1 expression in CD4+ and CD8+ chimeric antigen receptor T cells *in vitro* (35). This information illustrates why trying to clarify the contribution of immune cells and mediators such as CD4+ T cells, CD8+ T cells, IL-2, IFN-gamma, and PD-1 to COVID-19 progression is extremely hard in polytreated patients already hospitalized. From a different perspective, our strategy involving unspecific polyclonal stimuli prior to infection allows us to expand on the body of evidence supporting that PD-1 expression increases as IL-2 and IFN-gamma production decreases in severe COVID-19. In other words, our results suggest that a group of individuals may have CD4+ and CD8+ T cells with a basal predisposition to express high PD-1 levels and low IL-2 and IFN-gamma amounts in response to either polyclonal stimuli or SARS-CoV-2. This notion might partially explain why participants that showed helper and cytotoxic T cells with increased PD-1 expression and decreased IL-2 and IFN-gamma production in response to polyclonal stimuli tended to develop severe COVID-19 once infected. Furthermore, these findings support the idea that failure in mounting an adequate T cell-mediated immune response at the beginning of the SARS-CoV-2 infection is associated with increased viral load, systemic inflammatory response occurrence, and death (36, 37). The molecular mechanisms behind this intriguing hypothesis remain to be elucidated, which will positively contribute to expanding our knowledge regarding the very heterogeneous immune responses of humans to pathogens, above all if they are emerging public threats as occurred with SARS-CoV-2.

Besides the response mediated by CD4+ and CD8+ T cells, monocyte subpopulations play a crucial role in the anti-viral immune response by providing the first cell-virus interaction that will lead to antigen presentation and cytokine release (38). Several research teams have shown that monocyte subsets display dynamic changes in COVID-19, including an increase in classical and non-classical monocyte subpopulations and impaired cell ability to express cytokines with anti-viral functions (16, 39, 40). In response to polyclonal stimuli, we did not observe any alteration in the monocyte subset balance; however, we found that classical and non-classical monocytes lost their ability to produce IFN-alpha in subjects that once infected developed severe COVID-19. A study conducted in COVID-19 patients reported that IFN-alpha serum levels considerably decreased as the severity of the disease increased (16). Vanessa Chilunda and coworkers characterized the transcriptional profile of CD16+ monocyte subsets from COVID-19 patients. They informed that intermediate and non-classical monocytes exhibited down-regulation of numerous interferon response-related genes in severe cases compared to subjects that experienced the mild disease (41). In line with these reports, our findings indicate that an apparent susceptibility of classical and non-classical monocytes to express

low IFN-alpha levels in response to polyclonal stimuli might be associated with a higher risk of developing severe COVID-19 after SARS-CoV-2 exposure.

Cellular immunity mediated by monocytes and T cells provides the first immediate response to pathogens *via* antigen presentation and cytokine release while stimulating B cells to initiate humoral immunity through antibody production. Often, a defective cellular immunity leads to decreased memory B cell expansion and impaired antibody production, as occurs with H1N1/09 influenza vaccine non-responders where failure in CD4+ T cell stimulation and IL-2 secretion concurs with a low percentage of IgG antibody-secreting cells (42). However, the apparent link between cellular and humoral immune responses is still not clear in COVID-19. A recent study reported that PBMCs from severe COVID-19 patients show less CD4+ and CD8+ T cell activation and IFN-gamma production than PBMCs from mild cases in response to *in vitro* stimulation with M, N, and S viral proteins (43). Nevertheless, the neutralizing ability of anti-SARS-CoV-2-specific antibodies remained the same between severe and mild COVID-19 patients after a month of having been diagnosed by PCR test (43). Likewise, Irene Cassaniti and colleagues informed that CD4+ and CD8+ T cells from mild COVID-19 patients produce higher IFN-gamma concentrations than those found in T cells from severe cases in response to viral peptides (44). However, the authors reported no correlation between the *in vitro* T cell response and anti-SARS-CoV-2 antibody titers (44). In line with this body of evidence, we observed a group of subjects with a robust cellular immunity mediated by T cells and monocytes in response to polyclonal stimuli. This immune response pattern concurred with the development of mild COVID-19 symptoms after SARS-CoV-2 exposure. Conversely, we found another group of individuals that responded to polyclonal stimuli by showing a defective cellular immune activation associated with the development of severe COVID-19 once infection took place. Of note, we detected no changes between mild and severe COVID-19 patients for serum anti-SARS-CoV-2 IgG antibody titers or their neutralizing ability after a month of the symptom onset. Altogether, these findings lead us to suppose that a basal impairment in cellular immunity activation may play a more critical role in preventing COVID-19 worsening than the humoral response mediated by antibodies. We are now working on characterizing the possible mechanisms involved in stimulating PD-1 expression and impairing IL-2 and IFN-gamma production in CD4+ and CD8+ T cells and IFN-alpha secretion in classical and non-classical monocyte subsets, including differential methylation patterns and polymorphic variants.

Finally, we found a SARS-CoV-2 infection rate of around 11% in our study population, among who 50% developed a severe form of COVID-19. The Mexican government officially reported an accumulated number of SARS-CoV-2 positive cases of 725,346 for Mexico City from December 2020 to September 2021 (https://datos.covid-19.conacyt.mx). The official number of inhabitants in Mexico City was around 9,209,944 in 2021. These numbers suggest that about 8% of the general population living in Mexico City got SARS-CoV-2 infection when we conducted the study. Moreover, a recent study indicated that nearly 39% of SARS-CoV-2 positive cases in Mexico were hospitalized due to the COVID-19 severity (45). These data reflect, to some extent, what we found in our study if we consider the limited number of SARS-CoV-2 detection tests available during that period and the remarkable underestimation of the most severe COVID-19 cases in Mexico.

In conclusion, using *in vitro* polyclonal stimuli, we found two basal immune response patterns associated with a predisposition to developing mild or severe COVID-19 once SARS-CoV-2 infection occurs. The pattern linked to severe COVID-19 is characterized by high PD-1 expression, low IL-2 and IFN-gamma production in CD4+ and CD8+ T cells, and poor IFN-alpha expression in classical and non-classical monocytes. Conversely, low PD-1 synthesis and high IL-2 and IFN-gamma expression in helper and cytotoxic T cells and an increased IFN-alpha production in classical and non-classical monocyte subsets are related to a basal predisposition to developing mild COVID-19 symptoms after SARS-CoV-2 exposure. Since the serum anti-SARS-CoV-2 IgG antibody titers or their neutralizing ability did not differ between mild and severe COVID-19 cases, these findings suggest that cellular immunity may play a more crucial function than humoral immunity in preventing COVID-19 progression.

## DATA AVAILABILITY STATEMENT

The raw data supporting the conclusions of this article will be made available by the authors, without undue reservation.

## ETHICS STATEMENT

The studies involving human participants were reviewed and approved by Institutional ethical committee of the General Hospital of Mexico (registration number of the ethical code approval: DI/20/501/03/17). The patients/participants provided their written informed consent to participate in this study.

## AUTHOR CONTRIBUTIONS

Conceptualization, GE; Methodology, RV-S, AM-R, HS-V, SR-T, LM-G, VV-S, JG-S, AG-C, JIL-P, RF-M, and OR-C; Patient Enrolment, RV-S, SR-T, LM-G, VV-S, JG-S, AA-V, JC-R, AG-C, and JL-P; DATA CURATION, RV-S, AM-R, HS-V, SR-T, LM-G, VV-S, JG-S, AA-V, and JC-R; Formal Analysis, RV-S, AA-V, JC-R, AG-C, JL-P, RF-M, OR-C, and GE; Writing—Original Draft Preparation, RV-S and GE; Writing—Review And Editing, RV-S, AM-R, HS-V, SR-T, LM-G, VV-S, JS-G, AA-V, JC-R, AG-C, JL-P, RF-M, and OR-C; Funding Acquisition, GE. All authors contributed to the article and approved the submitted version.

## FUNDING

This work was supported by grants no. CB-2016-286209 from the Fondo Sectorial de Investigación para la Educación SEP-CONACYT-México and SALUD-2017-02-290345 from the Fondo Sectorial de Investigación y Desarrollo en Salud y Seguridad Social SS/IMSS/ISSSTE/CONACYT-México to GE.

## ACKNOWLEDGMENTS

We thank the subjects who bravely took part in the study and all the medical and nursery staff of the General Hospital of México "Dr. Eduardo Liceaga". RV-S is a doctoral student from the Plan de Estudios Combinados en Medicina, Licenciatura y Doctorado (PECEM) of the Universidad Nacional Autónoma de México (UNAM) and has received CONACYT fellowship 762613.

## SUPPLEMENTARY MATERIAL

The Supplementary Material for this article can be found online at: https://www.frontiersin.org/articles/10.3389/fimmu.2022.897995/full#supplementary-material

**Supplementary Figure 1 |** Time-response curves. **(A)** Based on time-response curves, we selected the earliest *in vitro* culture time to detect IL-2 production in CD3 + T cells. IL-2 production peaked after 2 hours on *in vitro* culture and showed no significant differences at 6, 12, and 24 hours. **(B)** Based on time-response curves, we selected the earliest *in vitro* culture time to detect IFN-gamma production in CD3 + T cells. IFN-gamma production peaked after 2 hours on *in vitro* culture and showed no significant differences at 6, 12, and 24 hours. **(C)** Based on time-response curves, we selected the earliest *in vitro* culture time to detect IFN-alpha production in CD14+ monocytes. IFN-alpha production peaked after 2 hours on *in vitro* culture and showed no significant differences at 6, 12, and 24 hours. We expressed data as mean ± standard deviation. We compared the production of IL-2, IFN-gamma, and IFN-alpha at 0, 1, 2, 6, 12, and 24 hours using one-way ANOVA and considered differences significant if $P < 0.05$. IL-2, interleukin-2; IFN-gamma, interferon-gamma; IFN-alpha, interferon-alpha; MFI, mean fluorescence intensity.

**Supplementary Figure 2 |** Gating strategy for T cells. **(A)** Gating strategy for selecting primary human CD3+CD4+ lymphocyte subsets and measuring IL-2, IFN-gamma, and PD-1 precisely. **(B)** Gating strategy for selecting primary human CD3+CD8 + lymphocyte subsets and measuring IL-2, IFN-gamma, and PD-1 precisely. FSC-H, forward scatter height; FSC-A, forward scatter area; SSC-A, side scatter area; IL-2, interleukin-2; IFN-gamma, interferon-gamma; PD-1, programmed cell death protein 1.

**Supplementary Figure 3 |** Gating strategy for monocyte subsets. Gating strategy for selecting primary human HLA-DR+ monocyte subsets and measuring IFN-alpha precisely. FSC-H, forward scatter height; FSC-A, forward scatter area; SSC-A, side scatter area; HLA-DR, human leukocyte antigen-DR isotype; IFN-alpha.

**Supplementary Figure 4 |** Representative spectra of mean fluorescence intensity for IL-2, IFN-gamma, PD-1, and IFN-alpha in T cells and monocyte subsets. **(A)** Representative histograms show the comparison of CD3+CD4+ T cells expressing IL-2 in blood samples treated with polyclonal stimuli from participants who developed mild or severe COVID-19 during the follow-up. **(B)** Representative histograms show the comparison of CD3+CD8+ T cells expressing IL-2 in blood samples treated with polyclonal stimuli from participants who developed mild or severe COVID-19 throughout the follow-up. **(C)** Representative histograms show the comparison of CD3+CD4+ T cells expressing IFN-gamma in blood samples treated with polyclonal stimuli from participants who developed mild or severe COVID-19 during the follow-up. **(D)** Representative histograms show the comparison of CD3+CD8+ T cells expressing IFN-gamma in blood samples treated with polyclonal stimuli from participants who developed mild or severe COVID-19 throughout the follow-up. **(E)** Representative histograms show the comparison of CD3+CD4+ T cells expressing PD-1 in blood samples treated with polyclonal stimuli from participants who developed mild or severe COVID-19 during the follow-up. **(F)** Representative histograms show the comparison of CD3+CD8+ T cells expressing PD-1 in blood samples treated with polyclonal stimuli from participants who developed mild or severe COVID-19 throughout the follow-up. **(G)** Representative histograms show the comparison of CD14++CD16- classical monocytes expressing IFN-alpha in blood samples treated with polyclonal stimuli from participants who developed mild or severe COVID-19 throughout the follow-up. **(H)** Representative histograms show the comparison of CD14++CD16+ intermediate monocytes expressing IFN-alpha in blood samples treated with polyclonal stimuli from participants who developed mild or severe COVID-19 during the follow-up. **(I)** Representative histograms show the comparison of CD14+CD16 + non-classical monocytes expressing IFN-alpha in blood samples treated with polyclonal stimuli from participants who developed mild or severe COVID-19 throughout the follow-up. In all cases, control indicates the spectra of MFI from unstimulated cells. IL-2, interleukin-2; IFN-gamma, interferon-gamma; PD-1, programmed cell death protein 1; IFN-alpha, interferon-alpha; MFI, mean fluorescence intensity; COVID-19, coronavirus disease 2019.

**Supplementary Figure 5 |** Absolute cell numbers for percentages of T cells and monocyte subsets. We show absolute cell numbers for percentages of CD3+CD4+ T cells expressing IL-2, IFN-gamma, and PD-1 on top. We show absolute cell numbers for percentages of CD3+CD8+ T cells expressing IL-2, IFN-gamma, and PD-1 in the middle. We show absolute cell numbers for percentages of classical, intermediate, and non-classical monocytes expressing IFN-alpha on the bottom. We defined classical monocytes as CD14++CD16-, intermediate monocytes as CD14++CD16+, and non-classical monocytes as CD14+CD16+. We expressed data as mean ± standard deviation. We compared data using the unpaired Student's T-test and considered differences significant when $P < 0.05$. IL-2, interleukin-2; IFN-gamma, interferon-gamma; PD-1, programmed cell death protein 1; IFN-alpha, interferon-alpha; COVID-19, coronavirus disease 2019.

## REFERENCES

1. Hu B, Guo H, Zhou P, Shi ZL. Characteristics of SARS-CoV-2 and COVID-19. *Nat Rev Microbiol* (2020) 19:141–54. doi: 10.1038/s41579-020-00459-7
2. Li J, Huang DQ, Zou B, Yang H, Hui WZ, Rui F, et al. Epidemiology of COVID-19: A Systematic Review and Meta-Analysis of Clinical Characteristics, Risk Factors, and Outcomes. *J Med Virol* (2021) 93:1449–58. doi: 10.1002/jmv.26424
3. Li X, Xu S, Yu M, Wang K, Tao Y, Zhou Y, et al. Risk Factors for Severity and Mortality in Adult COVID-19 Inpatients in Wuhan. *J Allergy Clin Immunol* (2020) 146:110–8. doi: 10.1016/j.jaci.2020.04.006
4. Nandy K, Salunke A, Pathak SK, Pandey A, Doctor C, Puj K, et al. Coronavirus Disease (COVID-19): A Systematic Review and Meta-Analysis to Evaluate the Impact of Various Comorbidities on Serious Events. *Diabetes Metab Syndr Clin Res Rev* (2020) 14:1017–25. doi: 10.1016/j.dsx.2020.06.064
5. Viurcos-Sanabria R, Escobedo G. Immunometabolic Bases of Type 2 Diabetes in the Severity of COVID-19. *World J Diabetes* (2021) 12:1026–41. doi: 10.4239/WJD.V12.I7.1026
6. Salinas-Escudero G, Carrillo-Vega MF, Granados-García V, Martínez-Valverde S, Toledano-Toledano F, Garduño-Espinosa J. A Survival Analysis of COVID-19 in the Mexican Population. *BMC Public Health* (2020) 20:1–8. doi: 10.1186/s12889-020-09721-2
7. Chi Y, Ge Y, Wu B, Zhang W, Wu T, Wen T, et al. Serum Cytokine and Chemokine Profile in Relation to the Severity of Coronavirus Disease 2019 in China. *J Infect Dis* (2020) 222:746–54. doi: 10.1093/infdis/jiaa363
8. Conti P, Ronconi G, Caraffa A, Gallenga CE, Ross R, Frydas I, Kritas SK. Induction of Pro-Inflammatory Cytokines (IL-1 and IL-6) and Lung Inflammation by Coronavirus-19 (COVI-19 or SARS-CoV-2): Anti-Inflammatory Strategies. *J Biol Regul Homeost Agents* (2020) 34:327–31. doi: 10.23812/CONTI-E

9. Zhang C, Wu Z, Li JW, Zhao H, Wang GQ. Cytokine Release Syndrome in Severe COVID-19: Interleukin-6 Receptor Antagonist Tocilizumab may be the Key to Reduce Mortality. *Int J Antimicrob Agents* (2020) 55:105954. doi: 10.1016/j.ijantimicag.2020.105954
10. Ni L, Cheng ML, Feng Y, Zhao H, Liu J, Ye F, et al. Impaired Cellular Immunity to SARS-CoV-2 in Severe COVID-19 Patients. *Front Immunol* (2021) 12:603563/BIBTEX. doi: 10.3389/FIMMU.2021.603563/BIBTEX
11. Chen G, Wu D, Guo W, Cao Y, Huang D, Wang H, et al. Clinical and Immunological Features of Severe and Moderate Coronavirus Disease 2019. *J Clin Invest* (2020) 130:2620–9. doi: 10.1172/JCI137244
12. Zheng HY, Zhang M, Yang CX, Zhang N, Wang XC, Yang XP, et al. Elevated Exhaustion Levels and Reduced Functional Diversity of T Cells in Peripheral Blood may Predict Severe Progression in COVID-19 Patients. *Cell Mol Immunol* (2020) 17:541–3. doi: 10.1038/s41423-020-0401-3
13. Diao B, Wang C, Tan Y, Chen X, Liu Y, Ning L, et al. Reduction and Functional Exhaustion of T Cells in Patients With Coronavirus Disease 2019 (COVID-19). *Front Immunol* (2020) 11:827. doi: 10.3389/fimmu.2020.00827
14. Freeman GJ, Long AJ, Iwai Y, Bourque K, Chernova T, Nishimura H, et al. Engagement of the PD-1 Immunoinhibitory Receptor by a Novel B7 Family Member Leads to Negative Regulation of Lymphocyte Activation. *J Exp Med* (2000) 192:1027–34. doi: 10.1084/JEM.192.7.1027
15. Barber DL, Wherry EJ, Masopust D, Zhu B, Allison JP, Sharpe AH, et al. Restoring Function in Exhausted CD8 T Cells During Chronic Viral Infection. *Nature* (2006) 439:682–7. doi: 10.1038/NATURE04444
16. Hadjadj J, Yatim N, Barnabei L, Corneau A, Boussier J, Smith N, et al. Impaired Type I Interferon Activity and Inflammatory Responses in Severe COVID-19 Patients. *Sci (80- )* (2020) 369:718–24. doi: 10.1126/science.abc6027
17. Brodin P. Immune Determinants of COVID-19 Disease Presentation and Severity. *Nat Med 2021 271* (2021) 27:28–33. doi: 10.1038/s41591-020-01202-8
18. Velikova TV, Kotsev SV, Georgiev DS, Batselova HM. Immunological Aspects of COVID-19: What do We Know? *World J Biol Chem* (2020) 11:14–29. doi: 10.4331/WJBC.V11.I2.14
19. Tan L, Wang Q, Zhang D, Ding J, Huang Q, Tang Y-Q, et al. Lymphopenia Predicts Disease Severity of COVID-19: A Descriptive and Predictive Study. *Signal Transduct Target Ther 2020 51* (2020) 5:1–3. doi: 10.1038/s41392-020-0148-4
20. Lombardi A, Trombetta E, Cattaneo A, Castelli V, Palomba E, Tirone M, et al. Early Phases of COVID-19 Are Characterized by a Reduction in Lymphocyte Populations and the Presence of Atypical Monocytes. *Article* (2019) 11:560330. doi: 10.3389/fimmu.2020.560330
21. Shi H, Wang W, Yin J, Ouyang Y, Pang L, Feng Y, et al. The Inhibition of IL-2/IL-2R Gives Rise to CD8+ T Cell and Lymphocyte Decrease Through JAK1-STAT5 in Critical Patients With COVID-19 Pneumonia. *Cell Death Dis 2020 116* (2020) 11:1–8. doi: 10.1038/s41419-020-2636-4
22. Tjan LH, Furukawa K, Nagano T, Kiriu T, Nishimura M, Arii J, et al. Early Differences in Cytokine Production by Severity of Coronavirus Disease 2019. *J Infect Dis* (2021) 223:1145–9. doi: 10.1093/infdis/jiab005
23. Kim M-H, Salloum S, Wang JY, Wong LP, Regan J, Lefteri K, et al. Type I, II, and III Interferon Signatures Correspond to COVID-19 Disease Severity. *J Infect Dis* (2021) 224:777–782. doi: 10.1093/infdis/jiab288
24. Hope JC, Campbell F, Hopkins SJ. Deficiency of IL-2 or IL-6 Reduces Lymphocyte Proliferation, But Only IL-6 Deficiency Decreases the Contact Hypersensitivity Response. *Eur J Immunol* (2000) 30:197–203. doi: 10.1002/1521-4141
25. Zhu M-E, Wang Q, Zhou S, Wang B, Ke L, He P. Recombinant Interleukin-2 Stimulates Lymphocyte Recovery in Patients With Severe COVID-19. *Exp Ther Med* (2021) 21:1–1. doi: 10.3892/ETM.2021.9658
26. Whitmire JK, Tan JT, Whitton JL. Interferon-γ Acts Directly on CD8+ T Cells to Increase Their Abundance During Virus Infection. *J Exp Med* (2005) 201:1053–9. doi: 10.1084/JEM.20041463
27. Zheng M, Gao Y, Wang G, Song G, Liu S, Sun D, et al. Functional Exhaustion of Antiviral Lymphocytes in COVID-19 Patients. *Cell Mol Immunol 2020 175* (2020) 17:533–5. doi: 10.1038/s41423-020-0402-2
28. Gadotti AC, de Castro Deus M, Telles JP, Wind R, Goes M, Garcia Charello Ossoski R, de Padua AM, de Noronha L, et al. IFN-γ is an Independent Risk Factor Associated With Mortality in Patients With Moderate and Severe COVID-19 Infection. *Virus Res* (2020) 289:198171. doi: 10.1016/J.VIRUSRES.2020.198171
29. Dong Y, Sun Q, Zhang X. PD-1 and its Ligands are Important Immune Checkpoints in Cancer (2017) (Accessed April 27, 2021).
30. Bellesi S, Metafuni E, Hohaus S, Maiolo E, Marchionni F, D'Innocenzo S, et al. Increased CD95 (Fas) and PD-1 Expression in Peripheral Blood T Lymphocytes in COVID-19 Patients. *Br J Haematol* (2020) 191:207–11. doi: 10.1111/BJH.17034
31. Rha MS, Jeong HW, Ko JH, Choi SJ, Seo IH, Lee JS, et al. PD-1-Expressing SARS-CoV-2-Specific CD8 + T Cells Are Not Exhausted, But Functional in Patients With COVID-19. *Immunity* (2021) 54:44–52.e3. doi: 10.1016/J.IMMUNI.2020.12.002
32. van de Veerdonk FL, Giamarellos-Bourboulis E, Pickkers P, Derde L, Leavis H, van Crevel R, Engel JJ, Wiersinga WJ, Vlaar APJ, et al. A Guide to Immunotherapy for COVID-19. *Nat Med 2022 281* (2022) 28:39–50. doi: 10.1038/s41591-021-01643-9
33. Baghaki S, Yalcin CE, Baghaki HS, Aydin SY, Daghan B, Yavuz E. COX2 Inhibition in the Treatment of COVID-19: Review of Literature to Propose Repositioning of Celecoxib for Randomized Controlled Studies. *Int J Infect Dis* (2020) 101:29. doi: 10.1016/J.IJID.2020.09.1466
34. Xing K, Gu B, Zhang P, Wu X. Dexamethasone Enhances Programmed Cell Death 1 (PD-1) Expression During T Cell Activation: An Insight Into the Optimum Application of Glucocorticoids in Anti-Cancer Therapy. *BMC Immunol* (2015) 16:1–9. doi: 10.1186/S12865-015-0103-2/FIGURES/6
35. Yang M, Wang L, Ni M, Neuber B, Wang S, Gong W, et al. Dual Effects of Cyclooxygenase Inhibitors in Combination With CD19.CAR-T Cell Immunotherapy. *Front Immunol* (2021) 12:670088. doi: 10.3389/FIMMU.2021.670088
36. Hasan A, Al-Ozairi E, Al-Baqsumi Z, Ahmad R, Al-Mulla F. Cellular and Humoral Immune Responses in Covid-19 and Immunotherapeutic Approaches. *ImmunoTargets Ther* (2021) 10:63–85. doi: 10.2147/ITT.S280706
37. Melenotte C, Silvin A, Goubet AG, Lahmar I, Dubuisson A, Zumla A, et al. Immune Responses During COVID-19 Infection. *Oncoimmunology* (2020) 9:1807836. doi: 10.1080/2162402X.2020.1807836
38. Nikitina E, Larionova I, Choinzonov E, Kzhyshkowska J. Monocytes and Macrophages as Viral Targets and Reservoirs. *Int J Mol Sci 2018 Vol 19 Page 2821* (2018) 19:2821. doi: 10.3390/IJMS19092821
39. Qin S, Jiang Y, Wei X, Liu X, Guan J, Chen Y, et al. Dynamic Changes in Monocytes Subsets in COVID-19 Patients. *Hum Immunol* (2021) 82:170–6. doi: 10.1016/J.HUMIMM.2020.12.010
40. Matic S, Popovic S, Djurdjevic P, Todorovic D, Djordjevic N, Mijailovic Z, et al. SARS-CoV-2 Infection Induces Mixed M1/M2 Phenotype in Circulating Monocytes and Alterations in Both Dendritic Cell and Monocyte Subsets. *PloS One* (2020) 15:e0241097. doi: 10.1371/JOURNAL.PONE.0241097
41. Chilunda V, Martinez-Aguado P, Xia LC, Cheney L, Murphy A, Veksler V, et al. Transcriptional Changes in CD16+ Monocytes May Contribute to the Pathogenesis of COVID-19. *Front Immunol* (2021) 12:665773. doi: 10.3389/FIMMU.2021.665773
42. Pallikkuth S, Kanthikeel SP, Silva SY, Fischl M, Pahwa R, Pahwa S. Innate Immune Defects Correlate With Failure of Antibody Responses to H1N1/09 Vaccine in HIV-Infected Patients. *J Allergy Clin Immunol* (2011) 128:1279–85. doi: 10.1016/J.JACI.2011.05.033
43. Lafon E, Diem G, Witting C, Zaderer V, Bellmann-Weiler RM, Reindl M, et al. Potent SARS-CoV-2-Specific T Cell Immunity and Low Anaphylatoxin Levels Correlate With Mild Disease Progression in COVID-19 Patients. *Front Immunol* (2021) 12:684014. doi: 10.3389/FIMMU.2021.684014
44. Cassaniti I, Percivalle E, Bergami F, Piralla A, Comolli G, Bruno R, et al. SARS-CoV-2 Specific T-Cell Immunity in COVID-19 Convalescent Patients and Unexposed Controls Measured by Ex Vivo ELISpot Assay. *Clin Microbiol Infect* (2021) 27:1029–34. doi: 10.1016/J.CMI.2021.03.010
45. Martínez-Martínez MU, Alpízar-Rodríguez D, Flores-Ramírez R, Portales-Pérez DP, Soria-Guerra RE, Pérez-Vázquez F, et al. An Analysis COVID-19 in Mexico: A Prediction of Severity. *J Gen Intern Med* (2022) 37:624–31. doi: 10.1007/s11606-021-07235-0


**Conflict of Interest:** The authors declare that the research was conducted in the absence of any commercial or financial relationships that could be construed as a potential conflict of interest.

the publisher, the editors and the reviewers. Any product that may be evaluated in this article, or claim that may be made by its manufacturer, is not guaranteed or endorsed by the publisher.

*microorganisms*

MDPI

*Article*

# The Combined Use of Cytokine Serum Values with Laboratory Parameters Improves Mortality Prediction of COVID-19 Patients: The Interleukin-15-to-Albumin Ratio

**Salma A. Rizo-Téllez [1,2], Lucia A. Méndez-García [1], Ana C. Rivera-Rugeles [3], Marcela Miranda-García [1], Aarón N. Manjarrez-Reyna [1], Rebeca Viurcos-Sanabria [1,2], Helena Solleiro-Villavicencio [4], Enrique Becerril-Villanueva [5], José D. Carrillo-Ruíz [6,7,8], Julian M. Cota-Arce [9], Angélica Álvarez-Lee [9], Marco A. De León-Nava [9,*] and Galileo Escobedo [1,*]**

1 Laboratory of Immunometabolism, Research Division, General Hospital of Mexico "Dr. Eduardo Liceaga", Mexico City 06720, Mexico; sart.17.04@gmail.com (S.A.R.-T.); angelica.mendez.86@hotmail.com (L.A.M.-G.); mm.mirandha7416@gmail.com (M.M.-G.); aaron.manjarrez@gmail.com (A.N.M.-R.); viurcos.reb@hotmail.com (R.V.-S.)
2 PECEM, Facultad de Medicina, Universidad Nacional Autónoma de México, Coyoacán, Mexico City 04510, Mexico
3 Laboratory of Oncoimmunology, Biomedical Research Unit, Universidad Nacional Autónoma de México, Tlalnepantla 54090, Mexico; acriverar@unal.edu.co
4 Posgrado de Ciencias Genómicas, Universidad Autónoma de la Ciudad de México, Mexico City 03100, Mexico; helena.solleiro@uacm.edu.mx
5 Laboratory of Psychoimmunology, National Institute of Psychiatry "Ramón de la Fuente", Mexico City 14370, Mexico; lusenbeve@yahoo.com
6 Research Directorate, General Hospital of Mexico "Dr. Eduardo Liceaga", Mexico City 06726, Mexico; josecarrilloruiz@yahoo.com
7 Department of Neurology and Neurosurgery, General Hospital of Mexico "Dr. Eduardo Liceaga", Mexico City 06726, Mexico
8 Facultad de Ciencias de la Salud, Universidad Anáhuac, Campus Norte, Huixquilucan 52786, Mexico
9 Department of Biomedical Innovation, Center for Scientific Research and Higher Education of Ensenada (CICESE), Ensenada 22860, Mexico; jmcotaarce@gmail.com (J.M.C.-A.); ibeth@cicese.mx (A.Á.-L.)
* Correspondence: madeleon@cicese.mx (M.A.D.L.-N.); gescobedog@msn.com (G.E.); Tel.: +52-(55)-2789-2000 (ext. 5646) (M.A.D.L.-N. & G.E.)

check for updates

**Citation:** Rizo-Téllez, S.A.; Méndez-García, L.A.; Rivera-Rugeles, A.C.; Miranda-García, M.; Manjarrez-Reyna, A.N.; Viurcos-Sanabria, R.; Solleiro-Villavicencio, H.; Becerril-Villanueva, E.; Carrillo-Ruíz, J.D.; Cota-Arce, J.M.; et al. The Combined Use of Cytokine Serum Values with Laboratory Parameters Improves Mortality Prediction of COVID-19 Patients: The Interleukin-15-to-Albumin Ratio. *Microorganisms* **2021**, *9*, 2159. https://doi.org/10.3390/microorganisms9102159

Academic Editor: Sofia Costa-de-Oliveira

Received: 8 September 2021
Accepted: 13 October 2021
Published: 16 October 2021

**Publisher's Note:** MDPI stays neutral with regard to jurisdictional claims in published maps and institutional affiliations.



**Abstract:** Laboratory parameters display limited accuracy in predicting mortality in coronavirus disease 2019 (COVID-19) patients, as with serum albumin. Emerging evidence suggests that cytokine serum values may enhance the predictive capacity of albumin, especially interleukin (IL)-15. We thus investigated whether the use of the IL-15-to-albumin ratio enables improving mortality prediction at hospital admission in a large group of COVID-19 patients. In this prospective cross-sectional study, we enrolled and followed up three hundred and seventy-eight patients with a COVID-19 diagnosis until hospital discharge or death. Two hundred and fifty-five patients survived, whereas one hundred and twenty-three died. Student's *T*-test revealed that non-survivors had a significant two-fold increase in the IL-15-to-albumin ratio compared to survivors ($167.3 \pm 63.8$ vs. $74.2 \pm 28.5$), a difference that was more evident than that found for IL-15 or albumin separately. Likewise, mortality prediction considerably improved when using the IL-15-to-albumin ratio with a cut-off point > 105.4, exhibiting an area under the receiver operating characteristic curve of 0.841 (95% Confidence Interval, 0.725–0.922, $p < 0.001$). As we outlined here, this is the first study showing that combining IL-15 serum values with albumin improves mortality prediction in COVID-19 patients.

**Keywords:** IL-15; albumin; COVID-19; SARS-CoV-2; mortality; prognosis

## 1. Introduction

Severe acute respiratory syndrome coronavirus-2 (SARS-CoV-2) is the causal agent of coronavirus disease 2019 (COVID-19), a global pandemic that has affected more than

two hundred and thirty-five countries with nearly four million deaths up to June 2021 [1]. Clinical manifestations of COVID-19 are highly heterogeneous, ranging from asymptomatic or mild disease to severe or critical illness in patients who develop acute respiratory distress syndrome (ARDS), sepsis, and multiple organ failure [2]. Case fatality rates of COVID-19 vary depending on the geographical area; however, the vast majority of countries report mortality rates of around 2–4% [3]. Conversely, the case fatality rate of COVID-19 in Mexico is as high as 9.2%, revealing the deep need for novel markers to identify patients at higher risk of death in a timely manner [4].

The combined use of laboratory parameters with inflammatory markers increases the ability to identify COVID-19 patients at a higher mortality risk, as with serum albumin, C-reactive protein (CRP), and neutrophilia. In this sense, the CRP-to-albumin ratio better predicts the severity of COVID-19 than CRP or serum albumin separately [5]. Likewise, the combination of the neutrophil count with serum albumin values improves the area under the receiver operating characteristic (ROC) curve for predicting mortality in COVID-19 patients compared to those found when the neutrophil count or serum albumin are used separately [6]. However, emerging evidence suggests that combining laboratory parameters with markers significantly involved in the cytokine storm may also help to predict the mortality risk in COVID-19 patients, mainly albumin and interleukin (IL)-15 [7–9].

Albumin is a plasma protein produced in the liver that exerts multiple physiological functions in blood transport and anticoagulation. Serum albumin is also related to the severity of COVID-19; in fact, patients with the most severe forms of SARS-CoV-2 infection display lower albumin values than patients with the mild-to-moderate disease [10]. Serum albumin is also associated with increased mortality in COVID-19 patients [11]. However, most studies concur that the accuracy of albumin as a mortality predictor in SARS-CoV-2 infection is still limited.

IL-15 is a pleiotropic cytokine expressed by numerous immune and non-immune cells, including monocytes, macrophages, dendritic cells, neurons, epithelial cells, and fibroblasts [12]. IL-15 has a significant role in initiating inflammatory responses against microbial pathogens by modulating innate and adaptive immune cells [13]. A recent study showed that IL-15 serum levels increase in the same proportion as COVID-19 mortality [14]. The use of neutralizing antibodies anti-IL-15 as a potential immunotherapy for patients with severe SARS-CoV-2 infection was recently proposed [15]. Nevertheless, the combined use of IL-15 values with albumin to predict mortality in COVID-19 is unexplored, even though hypoalbuminemia is a common laboratory finding in patients with severe illness, and IL-15 belongs to the cytokine storm that is frequently associated with disease lethality. Thus, the purpose of this study was to examine whether the use of the IL-15-to-albumin ratio allows predicting mortality at hospital admission in a large group of patients with severe SARS-CoV-2 infection.

## 2. Materials and Methods

### *2.1. Patients*

Three hundred and seventy-eight patients admitted to the Emergency Department of the General Hospital of Mexico from 30 November 2020 to 9 July 2021, were enrolled in this prospective cross-sectional study. Patients of both sexes were enrolled in the study if they met the following inclusion criteria: 18 years and older, COVID-19 diagnosis confirmed by detection of SARS-CoV-2 specific ribonucleic acid (RNA) in nasopharyngeal swabs using quantitative polymerase chain reaction (qPCR), respiratory distress (>30 breaths per minute), hypoxia (peripheral oxygen saturation <92% on room air), or $\geq$50% lung involvement on imaging. Patients were excluded from the study if they had a previous diagnosis of human immunodeficiency virus (HIV), hepatitis C virus (HCV), hepatitis B virus (HBV), cancer, endocrine disorders, or autoimmune disease. Pregnant or lactating women and patients under long-term immunomodulatory medication, including non-steroidal anti-inflammatory drugs, were also excluded from the study. All study participants provided written informed consent previously approved by the institutional

ethical committee of the General Hospital of Mexico (registration number of the ethical code approval: DI/20/501/03/17). The study rigorously met the principles described in the 1964 Declaration of Helsinki and its posterior amendment in 2013. This cross-sectional study met the Strengthening the Reporting of Observational Studies in Epidemiology (STROBE) Statement: guidelines for reporting observational studies.

### 2.2. Data Collection

We collected demographic and clinical data from the Emergency Department of the General Hospital of Mexico at admission. We also recorded clinical evolution, drug regimen, and inpatient days up to hospital discharge or death. Demographic and clinical data included sex, age, and previous diagnosis of obesity (body mass index (BMI) > 30 $kg/m^2$), type 2 diabetes (T2D), hypertension, coronary heart disease (CHD), chronic kidney disease (CKD), and chronic liver disease (CLD).

### 2.3. Laboratory Parameters

We collected laboratory data at admission using the digital version of the electronic health record of the General Hospital of Mexico. Laboratory parameters included albumin, blood glucose, lipid profile, liver function tests, kidney function tests, coagulation markers, hematic biometry, CRP, troponin I, ferritin, procalcitonin, myoglobin, and D-dimer. We measured all laboratory parameters within sixty minutes of the patient's arrival in the hospital using the Beckman Coulter DxC 700 AU Chemistry Analyzer (Beckman Coulter Inc., Brea, CA, USA), the Coulter LH 780 Hematology Analyzer (Beckman Coulter Inc., Brea, CA, USA), and the BCS® XP System (Siemens Healthcare GmbH, Erlangen, Germany), following standard operating procedures.

### 2.4. IL-15 Serum Levels

At hospital admission, 4 mL blood samples were drawn from all participants and collected in pyrogen-free tubes (Vacutainer™, BD Diagnostics, NJ, USA) at room temperature. After a centrifugation step at 1000 g/4 °C for 30 min, we obtained serum samples for measuring IL-15 in triplicate by the Enzyme-Linked ImmunoSorbent Assay (ELISA) (PeproTech, Cranbury, NJ, USA). We measured IL-15 serum levels within 180 min of the patient's arrival in the hospital.

### 2.5. Statistics

We collected all demographic, clinical, laboratory, and immune parameters at hospital admission. We followed up with patients until hospital discharge or death. Then, we formed two groups of patients according to the primary outcome: survival or non-survival. In this way, we analyzed and compared all demographic, clinical, and laboratory parameters retrospectively. We used the Shapiro–Wilk test to estimate the normality of data distribution for numerical variables. We compared numerical variables between survival and non-survival groups using unpaired Student's *T*-tests, showing data as mean ± standard deviation. We used the chi-squared test to analyze categorical variables, showing data as absolute values and percentages. We analyzed ROC curves by obtaining the area under the ROC curve (AUROC) and 95% confidence interval (95% CI), sensitivity, specificity, and odds ratio (OR) for IL-15, serum albumin, and the IL-15-to-albumin ratio as potential mortality predictors. We used the Youden index to calculate optimal cut-off points for IL-15, serum albumin, and the IL-15-to-albumin ratio as potential mortality predictors. The IL-15-to-albumin ratio resulted from dividing the serum levels of IL-15 by albumin. We detected and removed outliers using Grubbs' test. We considered a $p$ value < 0.05 as significant. We used the GraphPad Prism 6.01 software (GraphPad Software, La Jolla, CA 92037, USA), the MedCalc Software (New York, NY 10003, USA), and the IBM SPSS Statistics version 25.0 (IBM, Armonk, NY, USA) for statistical analyses.

## 3. Results

Figure 1 shows an overview of the selection process of eligible participants. After applying the inclusion and exclusion criteria, we enrolled three hundred-sixteen patients in the study. After hospital discharge or death, we retrospectively assigned COVID-19 patients to survival ($n$ = 255) or non-survival ($n$ = 123) groups (Figure 1).

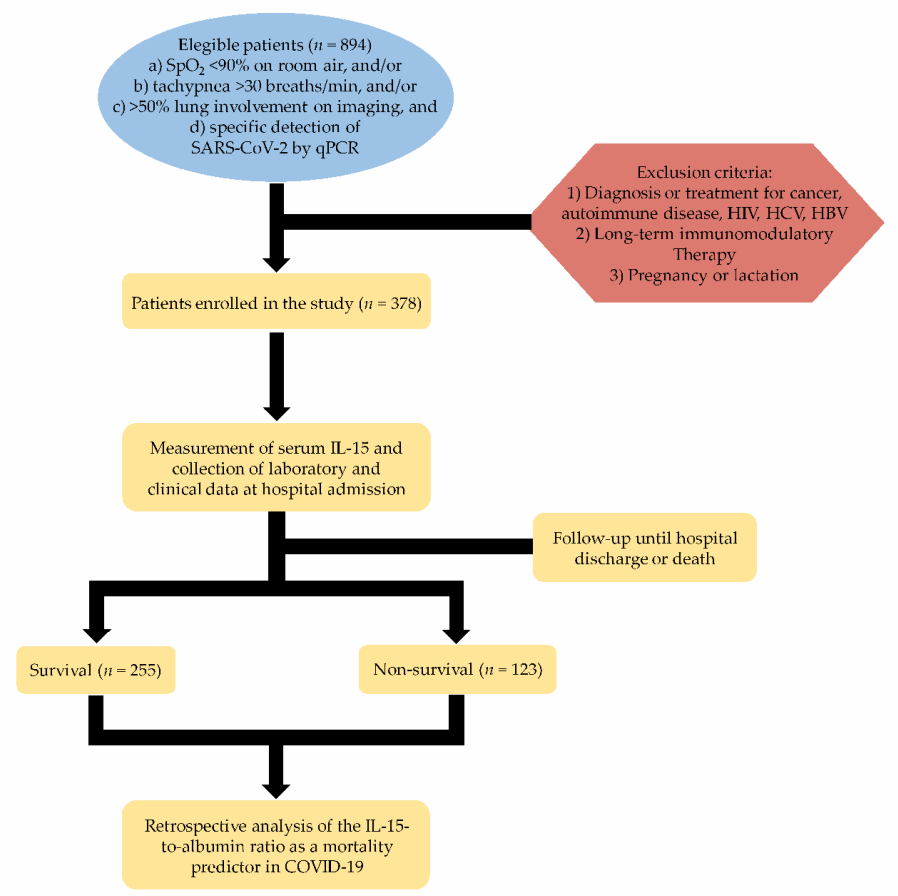


**Figure 1.** Schematic flow chart illustrating the selection process of eligible patients. SpO2, peripheral oxygen saturation; SARS-CoV-2, severe acute respiratory syndrome coronavirus-2; qPCR, quantitative polymerase chain reaction; HIV, human immunodeficiency virus; HCV, hepatitis C virus; HBV, hepatitis B virus; COVID-19, coronavirus disease 2019.

There were no significant differences between survivors and non-survivors concerning the proportion of women and men ($p$ = 0.3) and BMI ($p$ = 0.35) (Table 1). Patients in the survival group were, on average, seven years younger than those in the non-survival group (51.4 ± 13.2 versus 58.9 ± 13.7 years, $p$ < 0.0001, respectively) (Table 1). There were no significant differences between survivors and non-survivors with respect to the prevalence of obesity, T2D, hypertension, CHD, CKD, and CLD ($p$ = 0.8, $p$ = 0.1, $p$ = 0.5, $p$ = 0.3, $p$ = 0.6, and $p$ = 0.3, respectively). Body temperature and mean arterial pressure showed no changes

between survivors and non-survivors ($p = 0.3$ and $p = 0.1$, respectively). Conversely, there were significant differences between survivors and non-survivors for heart rate, breathing rate, and peripheral oxygen saturation ($p = 0.005$, $p = 0.001$, and $p < 0.001$, respectively) (Table 1). Sixty-eight percent ($n = 84$) of non-survivors required admission to the intensive care unit (ICU) for invasive mechanical ventilation, whereas only 23.5% ($n = 60$) of survivors needed ICU admission ($p < 0.001$) (Table 1). The number of inpatient days was, on average, greater for survivors than non-survivors (14.7 ± 9.9 vs. 7.3 ± 5.2 days, $p = 0.014$, respectively) (Table 1). All patients enrolled in the study received the same drug regimen: azithromycin, ceftriaxone, oseltamivir, enoxaparin sodium, dexamethasone, and acetaminophen.

**Table 1.** Demographic and clinical characteristics of patients enrolled in the study. Data are expressed as media ± standard deviation or absolute values and percentages. * Differences were considered significant when $p < 0.05$. We only show clinical data that significantly differed between groups. W, women; M, men; BMI, body mass index; T2D, type 2 diabetes; ICU, intensive care unit.

| Parameters | Total ($n = 378$) | Survival ($n = 255$) | Non-Survival ($n = 123$) | $p$ Value |
|---|---|---|---|---|
| Gender (W/M) | 137/241 | 97/158 | 40/83 | 0.3 |
| Age (years) | 54 ± 13.7 | 51.4 ± 13.2 | 58.9 ± 13.7 | <0.001 * |
| BMI (kg/m$^2$) | 26.7 ± 4.8 | 25.8 ± 6.7 | 27.5 ± 4.4 | 0.3 |
| Heart rate (bpm) | 89 ± 13.2 | 87.7 ± 12.9 | 92 ± 13.5 | 0.005 * |
| Breathing rate (bpm) | 24.1 ± 4.1 | 23.6 ± 3.9 | 25.2 ± 4.5 | 0.001 * |
| Oxygen saturation (%) | 83 ± 9.5 | 84.5 ± 8.7 | 79.8 ± 12.5 | <0.001 * |
| ICU needing (%) | 143 (37.8) | 60 (23.5) | 84 (68.3) | <0.001 * |
| Inpatient days | 12.1 ± 9.2 | 14.7 ± 9.9 | 7.3 ± 5.2 | 0.014 * |

Hematological parameters had no significant differences between survivors and non-survivors, except for the neutrophil count, which was 1.7-fold higher in the non-survival group ($p < 0.001$) (Table 2). Overall, there were no significant differences between survivors and non-survivors for most laboratory parameters, including CRP, procalcitonin, fibrinogen, ferritin, and D-dimer. As compared to survivors, non-survivors showed substantial increases in the values of urea, uric acid, aspartate aminotransferase (AST), alkaline phosphatase (ALP), lactate dehydrogenase (LDH), creatinine kinase-MB (CK-MB), and brain natriuretic peptide (BNP) (Table 2).

**Table 2.** Laboratory parameters of patients enrolled in the study. Data are expressed as media ± standard deviation. Differences were considered significant when $p < 0.05$. We only show laboratory parameters that significantly differed between groups. AST, aspartate aminotransferase; ALP, alkaline phosphatase; LDH, lactate dehydrogenase; CK-MB, creatinine kinase myocardial band; BNP, brain natriuretic peptide.

| Parameters | Total ($n = 378$) | Survival ($n = 255$) | Non-Survival ($n = 123$) | $p$ Value |
|---|---|---|---|---|
| Neutrophils ($\times 10^3$/mL) | 8.6 ± 5.6 | 6.7 ± 3.9 | 12 ± 6.7 | <0.001 |
| Urea (mg/dL) | 59.8 ± 54.7 | 35.1 ± 14.1 | 96.8 ± 70.8 | <0.001 |
| Uric Acid (mg/dL) | 6.2 ± 3.1 | 5.2 ± 1.7 | 8 ± 4.3 | 0.001 |
| AST (IU/L) | 37.2 ± 19 | 33 ± 15.3 | 46 ± 23 | 0.008 |
| ALP (IU/L) | 93.3 ± 33.2 | 84.8 ± 28.3 | 109.9 ± 36.4 | 0.003 |
| LDH (IU/L) | 393.3 ± 224.9 | 311.2 ± 144.4 | 539 ± 268.2 | 0.001 |
| CK-MB (IU/L) | 22.1 ± 7.8 | 19.8 ± 5.6 | 27 ± 9.9 | 0.002 |
| BNP (pg/mL) | 151.2 ± 304.6 | 19.1 ± 11.5 | 291.4 ± 396.4 | 0.004 |

Non-survivors exhibited significantly lower serum values of albumin than those found in survivors (3 ± 0.5 versus 3.6 ± 0.6 g/dL, respectively, $p = 0.004$) (Figure 2A). IL-15 serum levels showed a significant 1.8-fold increase in non-survivors as compared to survivors (488.7 ± 242.8 versus 261.7 ± 137.6 pg/mL, respectively, $p < 0.001$) (Figure 2B). However, it is worth mentioning that differences between survivors and non-survivors were more evident when circulating values of IL-15 were divided by serum albumin. The

IL-15-to-albumin ratio was 2.2-fold higher in non-survivors than in survivors (167.3 ± 63.8 vs. 74.2 ± 28.5, respectively, $p < 0.001$) (Figure 2C).

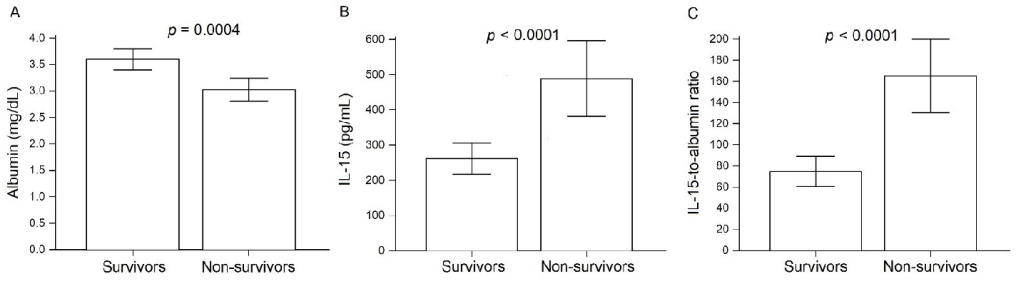


**Figure 2.** Serum levels of IL-15 and albumin in COVID-19 patients. (**A**) Serum albumin levels in survivors and non-survivors. (**B**) Serum IL-15 levels in survivors and non-survivors. (**C**) The IL-15-to-albumin ratio in survivors and non-survivors. The IL-15-to-albumin ratio resulted from dividing IL-15 serum values by serum albumin. Data are presented as mean ± standard deviation. We considered a $p$ value < 0.05 as significant.

The AUROC for albumin was 0.797 (95% CI, 0.678–0.915, $p < 0.001$), with a cut-off point ≤ 3.3 g/dL, a sensitivity of 90.91%, a specificity of 61.54%, and an OR of 11.31 (95% IC, 2.84–45.06) (Figure 3A). The AUROC for IL-15 was 0.797 (95% CI, 0.675–0.889, $p < 0.001$), with a cut-off point ≤ 364.6 pg/mL, a sensitivity of 68.18%, a specificity of 84.60%, and an OR of 9.79 (95% IC, 2.91–32.98) (Figure 3B). Conversely, a combination between the values of IL-15 and albumin significantly improved the ability to predict mortality in COVID-19 patients. In fact, the AUROC for the IL-15-to-albumin ratio was 0.841 (95% CI, 0.725–0.922, $p < 0.001$), with a cut-off point > 105.4, a sensitivity of 72.73%, a specificity of 87.18%, and an OR of 18.13 (95% IC, 4.81–68.37) (Figure 3C).

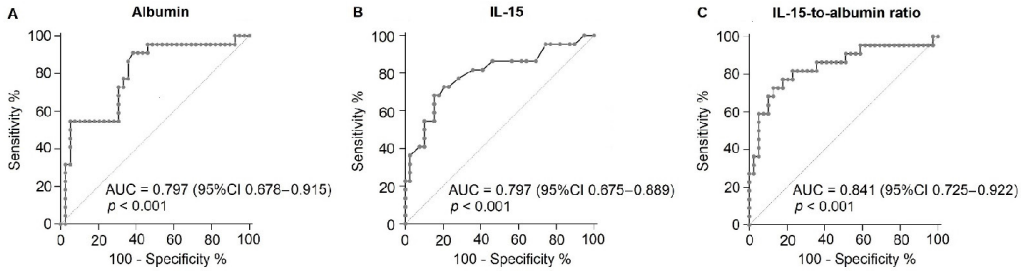


**Figure 3.** The area under the receiver operating characteristic curves for albumin, IL-15, and the IL-15-to-albumin ratio. (**A**) AUROC for albumin. (**B**) AUROC for IL-15. (**C**) AUROC for the IL-15-to-albumin ratio. We considered a $p$ value < 0.05 as significant. AUROC, area under the receiver operating characteristic curves; AUC, area under the curve; CI, confidence interval.

The use of IL-15 serum values improved the predictive accuracy of albumin and several clinical and laboratory parameters. For instance, oxygen saturation showed an AUROC of 0.795 (95% CI, 0.647–0.902) for mortality prediction (Figure 4A); however, the combined use of IL-15 values with oxygen saturation exhibited an AUROC of 0.823 (95% IC, 0.705–0.909) (Figure 4B). Likewise, the use of IL-15 significantly increased the AUROC values of the neutrophil count, blood urea, AST, and CRP, among others (Figure 4).

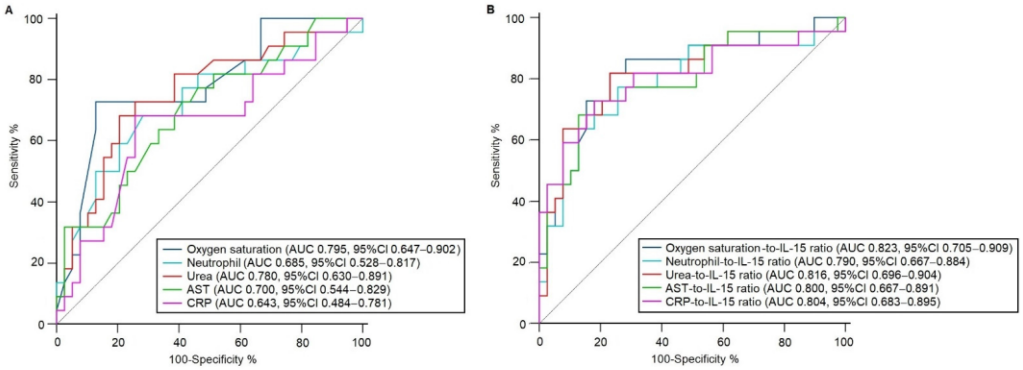


**Figure 4.** IL-15 serum values improved the area under the receiver operating characteristic curves of clinical and laboratory parameters. (**A**) AUROCs for oxygen saturation, the neutrophil count, blood urea, AST, and CRP. (**B**) AUROCs for the IL-15-to-oxygen saturation ratio, IL-15-to-neutrophil ratio, IL-15-to-urea ratio, IL-15-to-AST ratio, and IL-15-to-CRP ratio. We considered a $p$ value < 0.05 as significant. AUROC, area under the receiver operating characteristic curves; AUC, area under the curve; CI, confidence interval; AST, aspartate aminotransferase; CRP, C-reactive protein.

## 4. Discussion

The case fatality rate of COVID-19 has continued to increase in the last few months, especially in countries with slow vaccination rates, such as Mexico [1,4]. Thus, there is still a deep sense of urgency to find novel strategies to help improve our ability to identify COVID-19 patients at high mortality risk. Routine laboratory tests can be measured easily, quickly, and at a low cost, making them good candidates to estimate prognosis after hospital admission. However, the accuracy of laboratory parameters to predict mortality in COVID-19 patients remains limited [16,17]. In this sense, we show that combining laboratory markers' values with serum cytokines is an excellent strategy to improve the early recognition of COVID-19 patients with an increased risk of death, mainly albumin and IL-15.

Combining cytokine serum values with laboratory parameters recently emerged as a promising approach to estimate prognosis in patients with SARS-CoV-2 infection. A recent study conducted on COVID-19 patients from China demonstrated that the use of IL-2R enhances the accuracy of the lymphocyte count to predict the risk of developing severe-to-critical illness [18]. Likewise, the combined ratio between IL-6 and the T CD8 cell count improves mortality prediction in COVID-19 patients, performing better than other clinical prediction tools, such as the CURB-65 score [19]. In line with previous evidence, we now report for the first time that combining IL-15 with albumin in a single prognostic ratio considerably improved our ability to identify COVID-19 patients at a much higher mortality risk. This trend was observed not only for albumin but also for other clinical and laboratory parameters. In terms of accuracy, the use of IL-15 seemed to enhance the predictive accuracy of albumin concerning that reported using other clinical and inflammatory parameters. A study conducted in 144 COVID-19 patients showed that the neutrophil count-to-albumin ratio (NAR) is an independent predictor of mortality with an AUROC of 0.736 [6]. In parallel, a study conducted in a large group of COVID-19 patients reported that the blood urea nitrogen-to-albumin ratio (BAR) could predict mortality with an AUROC of 0.809 [20]. Likewise, the CRP-to-albumin ratio (CAR) can predict mortality in COVID-19 patients with an AUROC of 0.807 [5]. As we have shown here, the IL-15-to-albumin ratio can predict mortality in COVID-19 patients with an AUROC of 0.841, which improves the predictive accuracy of NAR, BAR, and CAR. Nevertheless, it is crucial to consider that although the IL-15-to-albumin ratio appears to have higher predictive accuracy than other scales, the

measurement of routine laboratory parameters is more accessible than IL-15 quantification. We will discuss this notion as part of the limitations of this study.

Since the combined use of the IL-15-to-albumin ratio acts as an accurate mortality predictor, we believe that it is of great importance to discuss the possible mechanisms through which these molecules may contribute to the progression and severity of COVID-19. Decreased serum albumin is one of the most common laboratory alterations in COVID-19 patients that require hospitalization [16,17]. Hypoalbuminemia is also a central component of multiple conditions, such as cancer, cirrhosis, trauma, and sepsis [21–24]. As a matter of fact, low serum albumin is a mortality predictor in critically ill patients with sepsis and septic shock [25]. Thus, we believe it is crucial to understand the possible mechanisms by which some pathophysiological elements of COVID-19 may down-regulate serum albumin levels. First, decreased hepatic albumin production is associated with increased release of proinflammatory mediators belonging to the COVID-19-related cytokine storm, such as IL-6 and tumor necrosis factor-alpha (TNF-alpha) [26]. Interestingly, injection of Chinese hamster ovary cells transfected with the human gene encoding TNF-alpha into nude mice decreases albumin synthesis [27]. In SARS-CoV-2 infection, Huang and coworkers reported an inverse correlation between IL-6 and serum albumin in patients with poorer survival probability [16]. Moreover, human recombinant IL-6 induces a dose- and time-dependent decrease in the mRNA levels of albumin in in vitro cultured HepG2 cells [28]. This information becomes more significant in patients with COVID-19, wherein increased levels of TNF-alpha and IL-6 may directly decrease albumin production and lead to hypoalbuminemia. In the second place, several acute inflammatory diseases show that serum content of albumin can be redistributed to the interstitial space due to increased vascular permeability and capillary leakage, leading to decreased serum albumin values [26,29]. This information is in line with the fact that COVID-19 is characterized by the release of potent vascular permeability mediators such as arachidonic acid metabolites, IL-8, and monocyte chemoattractant protein-1 (MCP-1), all of which might contribute to the transvascular leakage of albumin [30]. As we have outlined here, the cytokine storm and vascular permeability may act in synergy with SARS-CoV-2 to decrease serum albumin levels in COVID-19 patients, information that might partially explain why hypoalbuminemia appears to be an excellent contributor to mortality prediction in this disease.

In parallel, there is little evidence supporting the possible role of IL-15 in the progression and mortality of COVID-19. After binding to the high-affinity IL-2Rβ/IL-15Rα receptor, IL-15 induces the release of IL-8 and MCP-1 in human monocytes [31]. In severe SARS-CoV-2 infection, IL-8 and MCP-1 can recruit neutrophils and monocytes to the bronchoalveolar space and contribute to tissue damage and respiratory insufficiency [32,33]. In human macrophages, IL-15 can autocrinally promote the release of TNF-alpha, which in turn can induce apoptosis of human coronary artery endothelial cells and bovine pulmonary artery endothelial cells [34,35]. TNF-alpha-induced endothelial cell apoptosis is also associated with endothelial injury, vascular permeability, and systemic capillary leak syndrome, all of which contribute to the progression of COVID-19 [36–38]. Thus, IL-15 appears to orchestrate a two-hit deleterious action characterized by an exaggerated inflammatory response and increased endothelial cell apoptosis that together may contribute to the severity of COVID-19. Consistent with this idea, the analysis of 66 soluble biomarkers in 175 patients with severe SARS-CoV-2 infection revealed that IL-15 increases in the same proportion as mortality [14]. A recent cross-sectional study showed that COVID-19 patients with increased serum levels of IL-15 at admission experience a longer duration of hospitalization [39]. Altogether, this information reveals a pivotal role of IL-15 in the progression of SARS-CoV-2 infection and supports using this cytokine as a mortality predictor in COVID-19 patients. As we have outlined here, hypoalbuminemia and IL-15 may share a common pathophysiological mechanism mediated by the cytokine storm, which in turn appears to favor vascular permeability and neutrophil infiltration and leads to increased mortality risk. However, we should further explore the exact molecular mechanism through which albumin and IL-15 worsen survival prognosis in COVID-19.

Another phenomenon captured in our study involves the unexpected finding that there was no difference between survivors and non-survivors for gender and BMI. Most studies have documented that the COVID-19 case fatality rate is commonly higher in men than women [40]. However, a few studies have found that once severe COVID-19 occurs, the risk of dying is similar in women and men. We found no significant differences in the case fatality rate between female and male patients in line with this evidence. Men are more likely to be hospitalized than women; however, mortality is similar in both sexes once severe disease occurs. Likewise, although we noticed that BMI and obesity prevalence tended to be higher in non-survivors than survivors, we found no significant effects on the COVID-19 case fatality rate. Concurring with our findings, several studies have reported that BMI or obesity are not necessarily independent predictors of in-hospital mortality in COVID-19 [41–43]. We can explain these controversial findings since, at the time of hospitalization, all patients enrolled in this study had developed the most severe form of COVID-19, including respiratory distress and pneumonia. As mentioned above, most of the studies concur that once severe COVID-19 occurs, the potential contribution of variables such as gender and BMI to mortality rates tends to decrease [40,43]. However, we should consider these findings with caution, and further research is needed to understand the roles of gender and obesity in COVID-19 mortality in a population-specific manner.

Limitations of the study include: (1) the exclusion of HIV, HCV, or HBV seropositive individuals and COVID-19 patients with mild-to-moderate disease, which restricts our findings to a specific group of patients, and (2) the measurement of IL-15 serum levels may not be as easy in primary care. To improve these limitations, we are now conducting additional prospective studies to enroll patients with infectious diseases and other comorbidities. We are also developing rapid IL-15 tests to measure the levels of this cytokine quickly and affordably.

## 5. Conclusions

As we have outlined here, as far as we know, this is the first study demonstrating that the combined use of the IL-15-to-albumin ratio improves mortality prediction in COVID-19 patients that meet hospitalization criteria. Overall, the combination of IL-15 serum values with other clinical and laboratory parameters significantly increased our ability to identify patients at higher mortality risk. The mechanisms through which IL-15 and albumin contribute to mortality in COVID-19 remain to be elucidated. Although albumin measurement appears to be easier than IL-15 quantification in primary care, IL-15 serum levels can be detected quickly and affordably in tertiary healthcare centers, where most patients with severe COVID-19 are admitted. For this reason, we suggest the use of the IL-15-to-albumin ratio with cut-off point >105.4 to triage COVID-19 patients with increased mortality risk, which becomes more relevant in countries with slow vaccination rates. We encourage other research groups to study the impact of combining cytokine serum values with laboratory parameters in the early identification of COVID-19 patients at a much higher mortality risk.

**Author Contributions:** Conceptualization, S.A.R.-T., L.A.M.-G. and G.E.; methodology, S.A.R.-T., L.A.M.-G., A.C.R.-R., M.M.-G., A.N.M.-R., R.V.-S., H.S.-V., E.B.-V., J.D.C.-R., J.M.C.-A., A.Á.-L. and M.A.D.L.-N.; software data acquisition, R.V.-S., E.B.-V., J.M.C.-A., A.Á.-L. and M.A.D.L.-N.; formal analysis, S.A.R.-T., L.A.M.-G., A.C.R.-R., M.M.-G., A.N.M.-R., R.V.-S., H.S.-V., E.B.-V., J.D.C.-R., J.M.C.-A., A.Á.-L. and G.E.; data curation, S.A.R.-T., L.A.M.-G. and G.E.; writing—original draft preparation, M.A.D.L.-N. and G.E.; writing—review and editing, S.A.R.-T., L.A.M.-G., A.C.R.-R., M.M.-G., A.N.M.-R., R.V.-S., H.S.-V., E.B.-V., J.D.C.-R., J.M.C.-A., A.Á.-L., M.A.D.L.-N. and G.E.; funding acquisition, M.A.D.L.-N. and G.E. All authors have read and agreed to the published version of the manuscript.

**Funding:** This work was supported by grant no. CB-2016-01-286209 from the Fondo Sectorial de Investigación para la Educación-CONACYT-México and grant no. SALUD-2017-02-290345 from the Fondo Sectorial de Investigación y Desarrollo en Salud y Seguridad Social SS/IMSS/ISSSTE/CONACYT-México to GE.

**Institutional Review Board Statement:** The study was conducted in rigorous adherence to the principles described in the 1964 Declaration of Helsinki and its posterior amendment in 2013 and approved by the Ethics Committee of the General Hospital of Mexico with registration number of the ethical code approval DI/20/501/03/17 (22 April 2020).

**Informed Consent Statement:** Informed consent was obtained from all subjects involved in the study.

**Data Availability Statement:** The data presented in this study are available upon request.

**Acknowledgments:** S.A.R.-T. is a doctoral student from the Plan de Estudios Combinados en Medicina, Licenciatura y Doctorado (PECEM) of the Universidad Nacional Autónoma de México (UNAM) and has received CONACYT fellowship 762603.

**Conflicts of Interest:** The authors declare no conflict of interest.

## References

1. Karlinsky, A.; Kobak, D. Tracking excess mortality across countries during the COVID-19 pandemic with the World Mortality Dataset. *eLife* **2021**, *10*, e69336. [CrossRef] [PubMed]
2. Guan, W.-J.; Ni, Z.-Y.; Hu, Y.; Liang, W.-H.; Ou, C.-Q.; He, J.-X.; Liu, L.; Shan, H.; Lei, C.-L.; Hui, D.S.; et al. Clinical Characteristics of Coronavirus Disease 2019 in China. *N. Engl. J. Med.* **2020**, *382*, 1708–1720. [CrossRef]
3. Chaibakhsh, S.; Pourhoseingholi, A.; Vahedi, M. Global Incidence and Mortality Rate of COVID-19; Special Focus on Iran, Italy and China. *Arch. Iran. Med.* **2020**, *23*, 455–461. [CrossRef]
4. Dahal, S.; Banda, J.M.; Bento, A.I.; Mizumoto, K.; Chowell, G. Characterizing all-cause excess mortality patterns during COVID-19 pandemic in Mexico. *BMC Infect. Dis.* **2021**, *21*, 1–10. [CrossRef]
5. Özdemir, I.H.; Özlek, B.; Özen, M.B.; Gündüz, R.; Çetin, N.; Özlek, E.; Yıldız, B.S.; Bilge, A.R. Prognostic value of C-reactive protein/albumin ratio in hypertensive COVID-19 patients. *Clin. Exp. Hypertens.* **2021**, *43*, 1–7. [CrossRef]
6. Varim, C.; Yaylaci, S.; Demirci, T.; Kaya, T.; Nalbant, A.; Dheir, H.; Senocak, D.; Kurt, R.; Cengiz, H.; Karacaer, C. Neutrophil count to albumin ratio as a new predictor of mortality in patients with COVID-19 infection. *Rev. Assoc. Médica Bras.* **2020**, *66*, 77–81. [CrossRef] [PubMed]
7. Angioni, R.; Sánchez-Rodríguez, R.; Munari, F.; Bertoldi, N.; Arcidiacono, D.; Cavinato, S.; Marturano, D.; Zaramella, A.; Realdon, S.; Cattelan, A.; et al. Age-severity matched cytokine profiling reveals specific signatures in Covid-19 patients. *Cell Death Dis.* **2020**, *11*, 1–12. [CrossRef]
8. Masselli, E.; Vitale, M. NK cells on the ViP stage of COVID-19. *EBioMedicine* **2021**, *69*, 103458. [CrossRef] [PubMed]
9. Soraya, G.V.; Ulhaq, Z.S. Crucial laboratory parameters in COVID-19 diagnosis and prognosis: An updated meta-analysis. *Med. Clín.* **2020**, *155*, 143–151. [CrossRef] [PubMed]
10. Huang, J.; Cheng, A.; Kumar, R.; Fang, Y.; Chen, G.; Zhu, Y.; Lin, S. Hypoalbuminemia predicts the outcome of COVID-19 independent of age and co-morbidity. *J. Med. Virol.* **2020**, *92*, 2152–2158. [CrossRef] [PubMed]
11. Violi, F.; Cangemi, R.; Romiti, G.F.; Ceccarelli, G.; Oliva, A.; Alessandri, F.; Pirro, M.; Pignatelli, P.; Lichtner, M.; Carraro, A.; et al. Is Albumin Predictor of Mortality in COVID-19? *Antioxid. Redox Signal.* **2021**, *35*, 139–142. [CrossRef]
12. Perera, P.-Y.; Lichy, J.H.; Waldmann, T.A.; Perera, L.P. The role of interleukin-15 in inflammation and immune responses to infection: Implications for its therapeutic use. *Microbes Infect.* **2012**, *14*, 247–261. [CrossRef]
13. Jabri, B.; Abadie, V. IL-15 functions as a danger signal to regulate tissue-resident T cells and tissue destruction. *Nat. Rev. Immunol.* **2015**, *15*, 771–783. [CrossRef] [PubMed]
14. Abers, M.S.; Delmonte, O.M.; Ricotta, E.E.; Fintzi, J.; Fink, D.L.; de Jesus, A.A.A.; Zarember, K.A.; Alehashemi, S.; Oikonomou, V.; Desai, J.V.; et al. An immune-based biomarker signature is associated with mortality in COVID-19 patients. *JCI Insight* **2021**, *6*. [CrossRef] [PubMed]
15. Kandikattu, H.K.; Venkateshaiah, S.U.; Kumar, S.; Mishra, A. IL-15 immunotherapy is a viable strategy for COVID-19. Cytokine Growth Factor Rev. **2020**, *54*, 24–31. [CrossRef]
16. Huang, W.; Li, C.; Wang, Z.; Wang, H.; Zhou, N.; Jiang, J.; Ni, L.; Zhang, X.A.; Wang, D.-W. Decreased serum albumin level indicates poor prognosis of COVID-19 patients: Hepatic injury analysis from 2,623 hospitalized cases. *Sci. China Life Sci.* **2020**, *63*, 1–10. [CrossRef] [PubMed]
17. Zhang, Z.-L.; Hou, Y.-L.; Li, D.-T.; Li, F.-Z. Laboratory findings of COVID-19: A systematic review and meta-analysis. *Scand. J. Clin. Lab. Investig.* **2020**, *80*, 1–7. [CrossRef] [PubMed]
18. Hou, H.; Zhang, B.; Huang, H.; Luo, Y.; Wu, S.; Tang, G.; Liu, W.; Mao, L.; Wang, F.; Sun, Z. Using IL-2R/lymphocytes for predicting the clinical progression of patients with COVID-19. *Clin. Exp. Immunol.* **2020**, *201*, 76–84. [CrossRef]
19. Luo, M.; Liu, J.; Jiang, W.; Yue, S.; Liu, H.; Wei, S. IL-6 and CD8+ T cell counts combined are an early predictor of in-hospital mortality of patients with COVID-19. *JCI Insight* **2020**, *5*, 5. [CrossRef]
20. Küçükceran, K.; Ayrancı, M.K.; Girişgin, A.S.; Koçak, S.; Dündar, Z.D. The role of the BUN/albumin ratio in predicting mortality in COVID-19 patients in the emergency department. *Am. J. Emerg. Med.* **2021**, *48*, 33–37. [CrossRef]

21. Hu, W.-H.; Eisenstein, S.; Parry, L.; Ramamoorthy, S. Preoperative malnutrition with mild hypoalbuminemia associated with postoperative mortality and morbidity of colorectal cancer: A propensity score matching study. *Nutr. J.* **2019**, *18*, 1–7. [CrossRef] [PubMed]
22. Carvalho, J.R.; Machado, M.V. New Insights About Albumin and Liver Disease. *Ann. Hepatol.* **2018**, *17*, 547–560. [CrossRef] [PubMed]
23. Egbert, R.C.; Bouck, T.T.; Gupte, N.; Pena, M.M.; Dang, K.H.; Ornell, S.S.; Zelle, B.A. Hypoalbuminemia and Obesity in Orthopaedic Trauma Patients: Body Mass Index a Significant Predictor of Surgical Site Complications. *Sci. Rep.* **2020**, *10*, 1953–1957. [CrossRef]
24. Wiedermann, C.J. Hypoalbuminemia and the Risk of Acute Kidney Injury in Sepsis. *Crit. Care Med.* **2019**, *47*, e377–e378. [CrossRef]
25. Furukawa, M.; Kinoshita, K.; Yamaguchi, J.; Hori, S.; Sakurai, A. Sepsis patients with complication of hypoglycemia and hypoalbuminemia are an early and easy identification of high mortality risk. *Intern. Emerg. Med.* **2019**, *14*, 539–548. [CrossRef]
26. Nicholson, J.; Wolmarans, M.; Park, G. The role of albumin in critical illness. *Br. J. Anaesth.* **2000**, *85*, 599–610. [CrossRef] [PubMed]
27. Brenner, A.D.; Buck, M.; Feitelberg, S.P.; Chojkier, M. Tumor necrosis factor-alpha inhibits albumin gene expression in a murine model of cachexia. *J. Clin. Investig.* **1990**, *85*, 248–255. [CrossRef]
28. Bartalena, L.; Farsetti, A.; Flink, I.L.; Robbins, J. Effects of interleukin-6 on the expression of thyroid hormone-binding protein genes in cultured human hepatoblastoma-derived (Hep G2) cells. *Mol. Endocrinol.* **1992**, *6*, 935–942. [CrossRef]
29. Franch-Arcas, G. The meaning of hypoalbuminaemia in clinical practice. *Clin. Nutr.* **2001**, *20*, 265–269. [CrossRef]
30. Alunno, A.; Carubbi, F.; Rodríguez-Carrio, J. Storm, typhoon, cyclone or hurricane in patients with COVID-19? Beware of the same storm that has a different origin. *RMD Open* **2020**, *6*, e001295. [CrossRef]
31. Badolato, R.; Ponzi, A.N.; Millesimo, M.; Notarangelo, L.D.; Musso, T. Interleukin-15 (IL-15) Induces IL-8 and Monocyte Chemotactic Protein 1 Production in Human Monocytes. *Blood* **1997**, *90*, 2804–2809. [CrossRef]
32. Cavalcante-Silva, L.H.A.; Carvalho, D.C.M.; Lima, É.D.A.; Galvão, J.G.F.M.; Silva, J.S.D.F.D.; de Sales-Neto, J.M.; Rodrigues-Mascarenhas, S. Neutrophils and COVID-19: The road so far. *Int. Immunopharmacol.* **2020**, *90*, 107233. [CrossRef] [PubMed]
33. Knoll, R.; Schultze, J.L.; Schulte-Schrepping, J. Monocytes and Macrophages in COVID-19. *Front. Immunol.* **2021**, *12*, 2952. [CrossRef]
34. Chen, J.; Li, D.; Zhang, X.; Mehta, J.L. Tumor Necrosis Factor-α-Induced Apoptosis of Human Coronary Artery Endothelial Cells: Modulation by the Peroxisome Proliferator-Activated Receptor-γ Ligand Pioglitazone. *J. Cardiovasc. Pharmacol. Ther.* **2004**, *9*, 35–41. [CrossRef] [PubMed]
35. Polunovsky, V.A.; Wendt, C.H.; Ingbar, D.H.; Peterson, M.S.; Bitterman, P.B. Induction of Endothelial Cell Apoptosis by TNFα: Modulation by Inhibitors of Protein Synthesis. *Exp. Cell Res.* **1994**, *214*, 584–594. [CrossRef]
36. Munshi, N.; Fernandis, A.Z.; Cherla, R.P.; Park, I.-W.; Ganju, R.K. Lipopolysaccharide-Induced Apoptosis of Endothelial Cells and Its Inhibition by Vascular Endothelial Growth Factor. *J. Immunol.* **2002**, *168*, 5860–5866. [CrossRef] [PubMed]
37. Assaly, R.; Olson, D.; Hammersley, J.; Fan, P.-S.; Liu, J.; Shapiro, J.I.; Kahaleh, M.B. Initial Evidence of Endothelial Cell Apoptosis as a Mechanism of Systemic Capillary Leak Syndrome. *Chest* **2001**, *120*, 1301–1308. [CrossRef]
38. de Chambrun, M.P.; Cohen-Aubart, F.; Donker, D.W.; Cariou, P.-L.; Luyt, C.-E.; Combes, A.; Amoura, Z. SARS-CoV-2 Induces Acute and Refractory Relapse of Systemic Capillary Leak Syndrome (Clarkson's Disease). *Am. J. Med.* **2020**, *133*, e663–e664. [CrossRef]
39. Singh, A.K.; Kasarpalkar, N.; Bhowmick, S.; Paradkar, G.; Talreja, M.; Shah, K.; Tiwari, A.; Palav, H.; Kaginkar, S.; Kul-Karni, R.; et al. IL-15 and sMAdCAM: Novel roles in COVID-19 pathogenesis. *medRxiv* **2021**. [CrossRef]
40. Raimondi, F.; Novelli, L.; Ghirardi, A.; Russo, F.M.; Pellegrini, D.; Biza, R.; Trapasso, R.; Giuliani, L.; Anelli, M.; Amoroso, M.; et al. Covid-19 and gender: Lower rate but same mortality of severe disease in women—an observational study. *BMC Pulm. Med.* **2021**, *21*, 1–11. [CrossRef]
41. Nyabera, A.; Lakhdar, S.; Li, M.; Trandafirescu, T.; Tall, S.O. The Association Between BMI and Inpatient Mortality Outcomes in Older Adults With COVID-19. *Cureus* **2020**, *12*. [CrossRef] [PubMed]
42. Deng, L.; Zhang, J.; Wang, M.; Chen, L. Obesity is associated with severe COVID-19 but not death: A dose−response meta-analysis. *Epidemiol. Infect.* **2021**, *149*, 1–27. [CrossRef] [PubMed]
43. Chu, Y.; Yang, J.; Shi, J.; Zhang, P.; Wang, X. Obesity is associated with increased severity of disease in COVID-19 pneumonia: A systematic review and meta-analysis. *Eur. J. Med. Res.* **2020**, *25*, 1–15. [CrossRef] [PubMed]

biomolecules

MDPI

Article

# Native Low-Density Lipoproteins Act in Synergy with Lipopolysaccharide to Alter the Balance of Human Monocyte Subsets and Their Ability to Produce IL-1 Beta, CCR2, and CX3CR1 In Vitro and In Vivo: Implications in Atherogenesis

**Aarón N. Manjarrez-Reyna [1], Camilo P. Martínez-Reyes [1], José A. Aguayo-Guerrero [1], Lucia A. Méndez-García [1], Marcela Esquivel-Velázquez [1], Sonia León-Cabrera [2,3], Gilberto Vargas-Alarcón [4], José M. Fragoso [4], Elizabeth Carreón-Torres [4], Oscar Pérez-Méndez [4,5], Jessica L. Prieto-Chávez [6] and Galileo Escobedo [1,*]**

1 Laboratory of Immunometabolism, Research Division, General Hospital of Mexico "Dr. Eduardo Liceaga", Mexico City 06720, Mexico; aaron.manjarrez@gmail.com (A.N.M.-R.); nava111222@hotmail.com (C.P.M.-R.); jose.aguayo01@iest.edu.mx (J.A.A.-G.); angelica.mendez.86@hotmail.com (L.A.M.-G.); esquivel.marcela@gmail.com (M.E.-V.)

2 Unidad de Biomedicina, Facultad de Estudios Superiores-Iztacala, Universidad Nacional Autónoma de México, Tlalnepantla, Edo. De Mexico 54090, Mexico; soleon81@gmail.com

3 Carrera de Médico Cirujano, Facultad de Estudios Superiores-Iztacala, Universidad Nacional Autónoma de México, Tlalnepantla, Edo. De Mexico 54090, Mexico

4 Department of Molecular Biology, Instituto Nacional de Cardiología "Ignacio Chávez", Juan Badiano 1, Sección XVI, Tlalpan, Mexico City 14080, Mexico; gvargas63@yahoo.com (G.V.-A.); mfragoso1275@yahoo.com.mx (J.M.F.); qfbelizabethcm@yahoo.es (E.C.-T.); opmendez@yahoo.com (O.P.-M.)

5 School of Engineering and Sciences Campus CDMX, Tecnológico de Monterrey, Calle Puente 222, Tlalpan, Mexico City 14380, Mexico

6 Laboratorio de Citometría de Flujo, Centro de Instrumentos, Coordinación de Investigación en Salud, Hospital de Especialidades del Centro Médico Siglo XXI, Instituto Mexicano del Seguro Social, Mexico City 06720, Mexico; lakshmi.litmus@hotmail.com

* Correspondence: gescobedog@msn.com or gescobedo@unam.mx; Tel.: +52-(55)-2789-2000 (ext. 5646)



Citation: Manjarrez-Reyna, A.N.; Martínez-Reyes, C.P.; Aguayo-Guerrero, J.A.; Méndez-García, L.A.; Esquivel-Velázquez, M.; León-Cabrera, S.; Vargas-Alarcón, G.; Fragoso, J.M.; Carreón-Torres, E.; Pérez-Méndez, O.; et al. Native Low-Density Lipoproteins Act in Synergy with Lipopolysaccharide to Alter the Balance of Human Monocyte Subsets and Their Ability to Produce IL-1 Beta, CCR2, and CX3CR1 In Vitro and In Vivo: Implications in Atherogenesis. *Biomolecules* **2021**, *11*, 1169. https://doi.org/10.3390/biom11081169

Academic Editors: Alessandro Mattina, Giuseppe Mandraffino and Roberto Scicali

Received: 11 June 2021
Accepted: 4 August 2021
Published: 7 August 2021

**Abstract:** Increasing evidence has demonstrated that oxidized low-density lipoproteins (oxLDL) and lipopolysaccharide (LPS) enhance accumulation of interleukin (IL)-1 beta-producing macrophages in atherosclerotic lesions. However, the potential synergistic effect of native LDL (nLDL) and LPS on the inflammatory ability and migration pattern of monocyte subpopulations remains elusive and is examined here. In vitro, whole blood cells from healthy donors (n = 20) were incubated with 100 µg/mL nLDL, 10 ng/mL LPS, or nLDL + LPS for 9 h. Flow cytometry assays revealed that nLDL significantly decreases the classical monocyte (CM) percentage and increases the non-classical monocyte (NCM) subset. While nLDL + LPS significantly increased the number of NCMs expressing IL-1 beta and the C-C chemokine receptor type 2 (CCR2), the amount of NCMs expressing the CX3C chemokine receptor 1 (CX3CR1) decreased. In vivo, patients (n = 85) with serum LDL-cholesterol (LDL-C) >100 mg/dL showed an increase in NCM, IL-1 beta, LPS-binding protein (LBP), and Castelli's atherogenic risk index as compared to controls (n = 65) with optimal LDL-C concentrations (≤100 mg/dL). This work demonstrates for the first time that nLDL acts in synergy with LPS to alter the balance of human monocyte subsets and their ability to produce inflammatory cytokines and chemokine receptors with prominent roles in atherogenesis.

**Keywords:** atherogenesis; monocyte subpopulations; native LDL; LPS; IL-1 beta; CCR2; CX3CR1; LBP

## 1. Introduction

Atherosclerosis is a chronic inflammatory disease of the arteries and a leading cause of death worldwide [1]. Atherogenesis is the pathological process through which atheromatous plaque is formed in the inner layer of the arteries, leading to vessel thickening, arterial remodeling, and potential obstruction of blood flow at the site of the lesion [2].

Atherosclerotic plaque formation is a highly dynamic process involving the adhesion of circulating monocytes to the tunica intima, wherein these cells differentiate into macrophages [3]. Then, monocyte-derived macrophages can migrate to the subendothelial space and turn into foam cells after ingesting oxidized low-density lipoproteins (oxLDL), triggering an inflammatory response that injures endothelial cells and promotes arterial remodeling [4]. In this scenario, the role of macrophages and oxLDL in atherogenesis appears to be clear [5]; however, monocytes and native LDL (nLDL) might also contribute to atherosclerosis by mechanisms that are not yet fully understood.

In the blood stream, human monocytes are sorted into three subsets based on the cell surface expression of CD14 and CD16 [6]. Classical monocytes (CMs) express high CD14 levels but do not express CD16 (CD14++CD16−). Intermediate monocytes (IMs) exhibit CD16 expression and high CD14 levels (CD14++CD16+), while non-classical monocytes (NCMs) also express CD16 but show low CD14 levels (CD14+CD16+) [7]. Upon lipopolysaccharide (LPS) stimulation, human monocyte subpopulations differentially respond to produce interleukin (IL)-1 beta, a proinflammatory cytokine with key roles in atherosclerosis [8]. Monocyte subsets also differentially express the C-C chemokine receptor type 2 (CCR2) and the CX3C chemokine receptor 1 (CX3CR1), each of which are chemokine receptors with prominent functions in cell migration and endothelial adhesion during atherosclerosis [9,10].

The immune function of monocyte subpopulations is regulated by prototypical factors such as LPS, double-stranded ribonucleic acid (dsRNA), and tumor necrosis factor alpha (TNF-alpha) [11,12]. However, emerging evidence suggests that non-prototypical immunometabolic ligands can also influence the cytokine and chemokine expression profile in these cells. In this sense, excess glucose increases TNF-alpha expression in in vitro cultured primary human monocytes [13]. Free-fatty acids induce IL-1 beta secretion in in vitro cultured THP-1 cells and primary human monocytes [14]. Furthermore, immunometabolic agents can also act in synergy with prototypical immune factors to regulate the activity of monocyte subsets. In this regard, low concentration of high-density lipoproteins (HDL) increases IL-1 beta expression in NCMs stimulated with LPS and in subjects with high serum levels of LPS-binding protein (LBP) [15–17]. On the contrary, the study of the action of LDL in monocytes has been restricted to its role as oxLDL [4,5], even though accumulating evidence also suggests that monocytes and nLDL could interact in circulation, thus contributing to atherosclerotic plaque formation [18,19]. In this sense, elevated circulating nLDL levels are associated with an increment in the percentage of CMs that can migrate into endothelial tissue by mainly expressing CX3CR1 and CCR2 in *ApoE*$^{-/-}$ mice, an animal model of atherosclerosis [20]. In parallel, LPS directly increases lipid deposition in primary human adventitial fibroblasts, inducing secretion of molecules with prominent roles in atherosclerosis such as monocyte chemoattractant protein 1 (MCP-1), the main ligand for CCR2 [21]. Interestingly, consumption of Western-style high-fat diets is associated with increased serum LPS levels in humans [22,23]. However, the potential contribution of nLDL and LPS to the inflammatory activity of human monocyte subsets during atherogenesis remains unclear.

The main goal of this study was to examine the effect of nLDL on the immune function of human monocyte subpopulations in in vitro LPS-stimulated primary monocytes and in patients with high LDL-cholesterol (LDL-C) and LBP serum levels.

## 2. Materials and Methods

### *2.1. In Vitro Culture of Primary Human Monocytes*

Twenty healthy blood donors with LDL-C serum levels less than 100 mg/dL and high-sensitive C-reactive protein (hs-CRP) serum values of 1.35 ± 0.26 mg/L, on average, were enrolled in the study. Each participant agreed to donate 8 mL of blood, which was collected into a tube containing heparin (Vacutainer$^{TM}$, BD Diagnostics, Franklin Lakes, NJ, USA). Subsequently, whole blood samples were individually divided and placed in 6-well cell-culture plates (Costar, Kennebunk, ME, USA), adding 2 mL of blood plus 1 mL of

RPMI-1640 (Sigma-Aldrich, St. Louis, MO, USA) supplemented with 5% fetal bovine serum (FBS), 2 mM L-glutamine, 10 nM HEPES buffer, and 50 µg/mL gentamicin (Gibco™, Grand Island, NY, USA) per well. The blood sample contained in the first well was designated as the control and received 300 µL of RPMI-1640 for 9 h. The second well was incubated in the presence of 100 µg nLDL (Sigma-Aldrich, St. Louis, MO, USA) dissolved in 300 µL of RPMI-1640 for 9 h. The third well was incubated in the presence of 10 ng/mL LPS (Sigma-Aldrich, St. Louis, MO, USA) dissolved in 300 µL of RPMI-1640 for 9 h. The sample contained in the fourth well was incubated in the presence of 100 µg nLDL plus 10 ng/mL LPS dissolved in 300 µL of RPMI-1640 for 9 h. Exposure time of in vitro cultures was selected based on time-response curves at 3, 6, and 9 h, finding that monocytes show the most significant changes at 9 h. The cell-culture plates were incubated at 37 °C in humidified 5% $CO_2$ atmosphere. For intracellular cytokine stain, white blood cells (WBCs) were treated with 1:1000 Brefeldin A (BioLegend, Inc., San Diego, CA, USA) for the last 2 h of in vitro culture. All of the participants provided written informed consent, previously approved by the institutional ethical committee of the General Hospital of Mexico (registration number of ethical approval code: DI/20/501/03/17), which guaranteed that the study was conducted in rigorous adherence to the principles described in the 1964 Declaration of Helsinki and its posterior amendment in 2013.

### 2.2. *Flow Cytometry*

After incubation, whole blood samples were collected and centrifuged at 500× *g* for 10 min. Immediately afterwards, WBCs were separated using a micropipette and resuspended in 1 mL PBS1X (Sigma-Aldrich, St. Louis, MO, USA). After an additional centrifugation step and removal of the supernatant, each cell pellet was resuspended in 50 µL cell staining buffer (BioLegend, Inc., San Diego, CA, USA). WBCs were incubated with 5 µL True-Stain Monocyte Blocker™ (BioLegend, Inc., San Diego, CA, USA) for 10 min on ice. Then, WBCs were incubated with anti-CD14 PE/Cy7, anti-CD16 PE/Cy5, anti-CCR2 AF647, anti-CX3CR1 BV510, Zombie ultraviolet (UV) Fixable Viability Kit (BioLegend, Inc., San Diego, CA, USA), and anti-human leukocyte antigen-DR (HLA-DR) BUV661 (BD Biosciences, San Jose, CA, USA) for 20 min in darkness at 4 °C. Afterwards, WBCs were incubated with 100 µL Fixation Medium A (FIX & PERM™ Cell Permeabilization Kit) (Invitrogen™, Carlsbad, CA, USA) for 20 min at room temperature. After being rinsed using Cell Staining Buffer (BioLegend, Inc., San Diego, CA, USA), peripheral blood mononuclear cells (PBMCs) were incubated with 100 µL Permeabilization Medium B (FIX & PERM™ Cell Permeabilization Kit, Invitrogen™, Carlsbad, CA, USA) and anti-IL-1 beta Pacific Blue (BioLegend, Inc., San Diego, CA, USA) for 20 min in darkness at room temperature. After being rinsed using Cell Staining Buffer (BioLegend, Inc., San Diego, CA, USA), PBMCs were acquired on a BD Influx flow cytometer (BD Biosciences, San Jose, CA, USA) using the BD Sortware™ software 1.2, acquiring 20,000 events per test in triplicate. For the gating strategy, WBCs were first gated on a time/side scatter density plot, and then gated on the Zombie UV negative cell population for detection of living cells. Afterwards, living cells were gated for singlets on a forward scatter (FS)/Trigger Pulse Width density plot. Monocytes were recognized on the HLA-DR gating. Then, monocytes were selected using the rectangular gating strategy on the CD14+/CD16+ population for identification of CMs (CD14++CD16−), IMs (CD14++CD16+), and NCMs (CD14+CD16+), as previously reported [24]. The median fluorescence intensity (MFI) for IL-1 beta, CCR2, and CX3CR1 was obtained by considering both positive and negative cell populations for each marker. The percentage of positive cells for each marker was obtained using proper fluorescence minus one (FMO) controls. Compensation controls were performed by means of UltraComp eBeads™ (Invitrogen™, Carlsbad, CA, USA) for each fluorochrome. Data were analyzed by means of the FlowJo 10.0.7 software (TreeStar, Inc., Ashland, OR, USA).

### 2.3. Subjects for In Vivo Assays

One hundred fifty volunteers from both sexes, aged 18 years or older, with 8 h fasting who attended the Blood Bank and the Department of Internal Medicine of the General Hospital of Mexico were included in the study. A group of three trained physicians registered gender, age, body mass index (BMI), waist circumference, body fat percentage, and the serum levels of glucose, insulin, C-reactive protein (CRP), total cholesterol, triglycerides, HDL-C, and LDL-C in all participants. BMI resulted from dividing weight by height squared. Waist circumference was measured at the midpoint between the lower rib margin and the iliac crest using a tape. Body fat percentage was obtained by means of a body composition analyzer (TANITA® Body Composition Analyzer, Model TBF-300A, Tokyo, Japan). CRP was measured in triplicate by immunoturbidimetry (Randox Laboratories, Meenmore, Ireland). Serum glucose, total cholesterol, triglycerides, HDL-C, and LDL-C were measured in triplicate by enzymatic assays (Roche Diagnostics, Mannheim, Germany). Serum insulin was measured in triplicate by the Enzyme-Linked Immunosorbent Assay (ELISA) (Abnova, Corporation, Taipei City, Taiwan). The estimate of insulin resistance was individually calculated using the homeostatic model assessment of insulin resistance (HOMA-IR) by multiplying glucose concentration (mM) by insulin concentration (mU/L) and then dividing by 22.5. All of the participants received full medical evaluation and provided written informed consent, previously approved by the institutional ethical committee of the General Hospital of Mexico (registration number of ethical approval code: DIC/11/UME/05/029), which guaranteed that the study was conducted in rigorous adherence to the principles described in the 1964 Declaration of Helsinki and its posterior amendment in 2013. Volunteers were excluded from the study if they had a previous diagnosis of type 1 diabetes (T1D), T2D, coronary disease, acute or chronic liver or renal disease, cancer, endocrine disorders, infectious diseases, chronic inflammatory disease, and/or autoimmune disorders. We also excluded from the study human immunodeficiency virus (HIV), hepatitis C virus (HCV), and hepatitis B virus (HBV)-seropositive patients, pregnant or lactating woman, and subjects with anti-inflammatory or immunomodulatory medication, including non-steroidal anti-inflammatory drugs (NSAIDs).

### 2.4. Effects of LDL and LBP on Monocyte Subpopulations and IL-1 Beta In Vivo

According to clinical guidelines of the National Cholesterol Education Program (NCEP) Expert Panel on Detection, Evaluation and Treatment of High Blood Cholesterol in Adults (Adult Treatment Panel III), the study participants were divided in two groups of LDL-C concentration, as follows: subjects with optimal concentration of LDL-C $\leq$ 100 mg/dL, and individuals with high concentration of LDL-C > 100 mg/dL [25]. Then, BMI, waist circumference, body fat percentage, glucose metabolism, HOMA-IR, and lipid profile were registered and compared between both groups. Blood samples (6 mL) were obtained from all volunteers for posterior isolation of WBCs. WBCs were incubated with anti-CD14 PE/Cy7 and anti-CD16 FITC, acquiring 20,000 events per test in triplicate on a BD Influx flow cytometer (BD Biosciences, San Jose, CA, USA) using the BD Sortware™ software 1.2 and the FlowJo 10.0.7 software (TreeStar, Inc., Ashland, OR, USA), as described above. In all participants, serum IL-1 beta (Peprotech, Mexico City, Mexico) and LBP (Invitrogen™, Carlsbad, CA, USA) were measured in triplicate by ELISA and analyzed according to LDL-C levels.

### 2.5. Statistics

Normality of data distribution was estimated by the Shapiro–Wilk test. For in vitro assays, one-way ANOVA, followed by a post-hoc Tukey test, was used to compare percentages of CMs, IMs, and NCMs, and expression of IL-1 beta, CCR2, and CX3CR1 in the cell groups designated as control, nLDL, LPS, and nLDL + LPS. For in vivo assays, the unpaired Student's *t*-test was used to compare subjects with serum LDL-C $\leq$ 100 mg/dL and individuals with serum LDL-C > 100 mg/dL in terms of gender, age, BMI, waist circumference, body fat percentage, fasting glucose, insulin, HOMA-IR, CRP, total cholesterol,

triglycerides, HDL, percentages of CMs, IMs, and NCMs, serum IL-1 beta, and circulating LBP levels. Differences were considered significant when $p < 0.05$. All of the statistical analyses were performed by means of the GraphPad Prism 7 software (GraphPad Software, La Jolla, CA 92037, USA).

## 3. Results

For the gating strategy, WBCs were first gated on a time/side scatter (SS) density plot, and then gated on the Zombie UV negative cell population for detection of living WBCs (Figure 1, top panel). Afterwards, WBCs were gated for singlets on a forward scatter (FS)/Trigger Pulse Width density plot, and after that gated on the HLA-DR+ population for monocyte recognition. Monocytes were then gated on the CD14+/CD16+ population for identification of CMs (CD14++CD16−), IMs (CD14++CD16+), and NCMs (CD14+CD16+). Monocyte subsets were then gated on the IL-1 beta+, CCR2+, and CX3CR1+ populations for assessing the effects of nLDL and LPS on the immune activity of these cells (Figure 1, bottom panel).

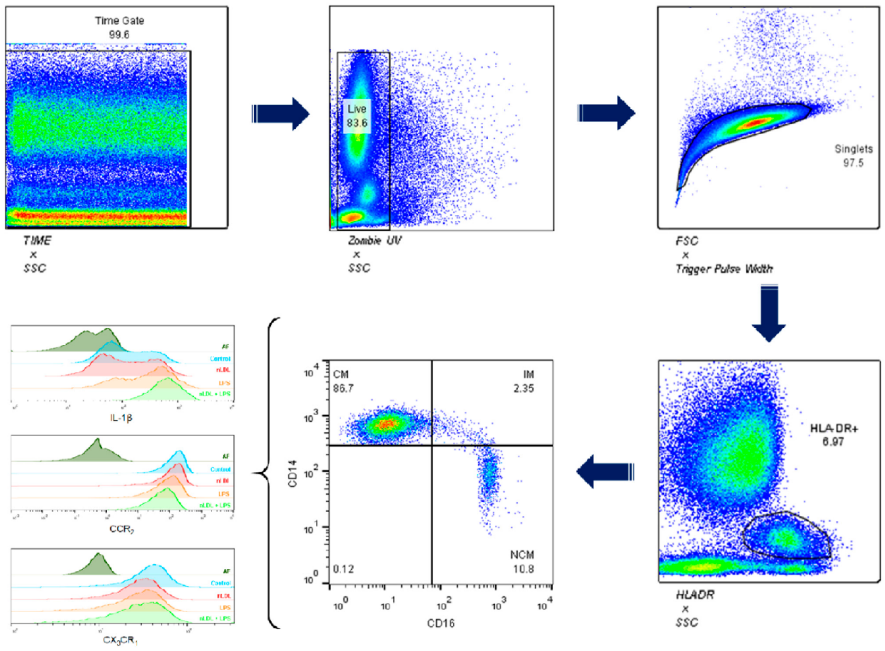


**Figure 1.** Gating strategy for characterizing human monocyte subsets. White blood cells were first gated on a time/side scatter (SS) density plot, and then gated on the Zombie UV negative cell population for detection of living cells. Afterwards, living cells were gated for singlets on a forward scatter (FS)/Trigger Pulse Width density plot. Monocytes were recognized on the HLA-DR gating. Then, monocytes were gated on the CD14+/CD16+ population for identification of CMs (CD14++CD16−), IMs (CD14++CD16+), and NCMs (CD14+CD16+). Expression of IL-1 beta, CCR2, and CX3CR1 was measured in all monocyte subsets. SSC, side scatter; FSC, forward scatter; HLA-DR, human leukocyte antigen-DR isotype; CM, classical monocytes; IM, intermediate monocytes; NCM, non-classical monocytes; IL-1 beta, interleukin 1 beta; CCR2, C-C chemokine receptor type 2; CX3CR1, CX3C chemokine receptor 1.

Figure 2 illustrates representative plots showing the percentages of CMs, IMs, and NCMs treated with nLDL and/or LPS (Figure 2A–D). As compared to control cells, the percentage of CMs was significantly reduced when treated with 100 µg/mL nLDL (Figure 2E). While the percentage of IMs did not change (Figure 2F), the percentage of NCMs exhibited

a significant 20% increase when exposed to 100 µg/mL nLDL with respect to that found in untreated cells (Figure 2G). Monocyte subpopulations also differentially responded to LPS. LPS, alone or in combination with nLDL, induced a significant 10% increase in CMs (Figure 2E). Conversely, IMs and NCMs showed significant reductions when treated with LPS or nLDL + LPS with respect to that found in control cells (Figure 2F,G, respectively). The percentages of CMs, IMs, and NCMs showed similar behavior in response to LPS or nLDL + LPS, suggesting that this effect was mainly mediated by LPS (Figure 2E–G, respectively).

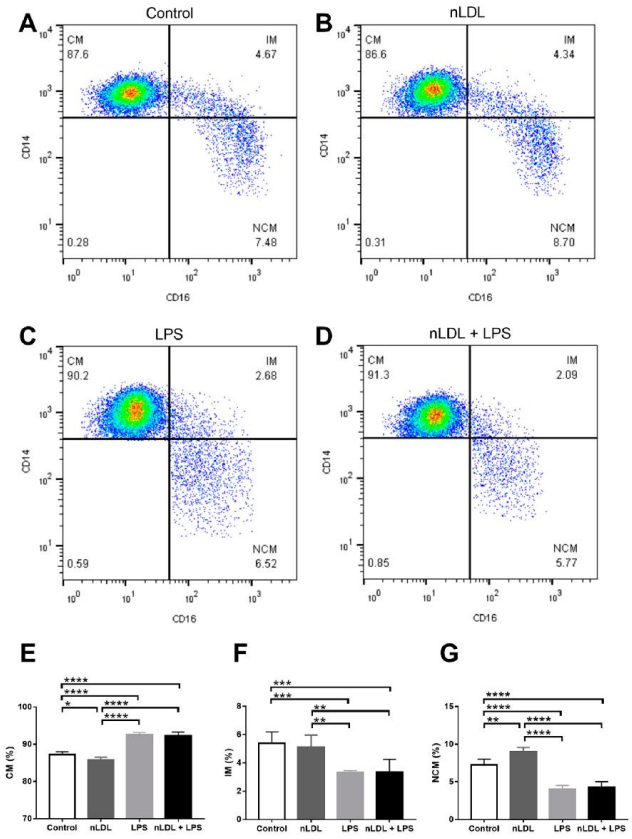


**Figure 2.** Effects of nLDL and LPS on the dynamics of human monocyte subpopulations. Representative plots showing the percentages of CMs, IMs, and NCMs in response to control conditions (**A**), nLDL (**B**), LPS (**C**), or a combination of nLDL + LPS (**D**). nLDL significantly decreased the CM percentage and increased the amount of NCMs as compared to control cells (**E**,**G**, respectively). LPS, alone or in combination with nLDL, significantly increased the CM percentage and decreased the amount of IMs and NCMs (**E**–**G**, respectively). Cells were incubated in the presence or absence of 100 µg/mL nLDL and/or 10 ng/mL LPS for 9 h. Data are expressed as mean ± standard deviation. Data were compared using one-way ANOVA followed by the post-hoc Tukey test. Differences were considered significant when $p < 0.05$. * = $p < 0.05$; ** = $p < 0.01$; *** = $p < 0.001$; **** = $p < 0.0001$. CM, classical monocytes; IM, intermediate monocytes; NCM, non-classical monocytes; nLDL, native low-density lipoproteins; LPS, lipopolysaccharide.

Exposure of cells to nLDL and LPS not only affected the balance among monocyte subpopulations but also their ability to produce IL-1 beta, a cytokine with key proinflammatory actions. Exposure of monocytes to 100 μg/mL nLDL had no significant effects on IL-1 beta production in all monocyte subpopulations (Figure 3A). LPS significantly increased IL-1 beta production in CMs, IMs, and NCMs, and this increase was even more evident when cells were exposed to LPS in combination with nLDL (Figure 3A). In parallel, the percentages of CMs, IMs, and NCMs that expressed IL-1 beta also tended to decrease in response to nLDL (Figure 3B). LPS, alone or in combination with nLDL, significantly increased the number of IL-1 beta+ cells in all monocyte subpopulations with respect to untreated cells (Figure 3B).

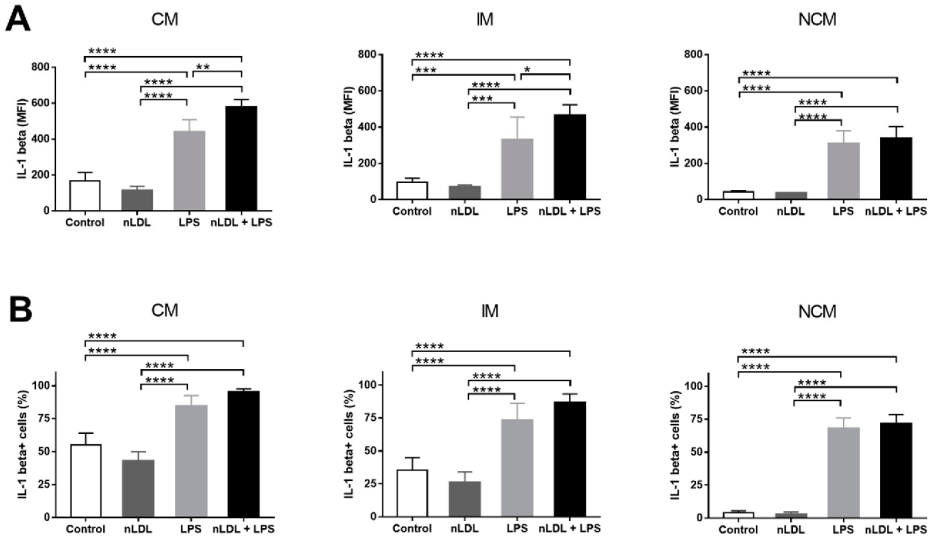


**Figure 3.** Effects of nLDL and LPS on IL-1 beta production in human monocyte subpopulations. Although no significant differences were found, nLDL tended to decrease IL-1 beta production in CMs, IMs, and NCMs (**A**, left, middle, and right panels, respectively). LPS, alone or in combination with nLDL, significantly increased IL-1 beta expression in CMs, IMs, and NCMs (**A**, left, middle, and right panels, respectively). Although no significant differences were found, nLDL tended to decrease the percentages of IL-1 beta+ cells in all monocyte subsets (**B**, left, middle, and right panels, respectively). LPS, alone or in combination with nLDL, significantly increased the amount of IL-1 beta+ cells in all monocyte subpopulations (**B**, left, middle, and right panels, respectively). Cells were incubated in the presence or absence of 100 μg/mL nLDL and/or 10 ng/mL LPS for 9 h. Data are expressed as mean ± standard deviation. Data were compared using one-way ANOVA followed by the post-hoc Tukey test. Differences were considered significant when $p < 0.05$. * = $p < 0.05$; ** = $p < 0.01$; *** = $p < 0.001$; **** = $p < 0.0001$. CM, classical monocytes; IM, intermediate monocytes; NCM, non-classical monocytes; nLDL, native low-density lipoproteins; LPS, lipopolysaccharide; IL-1 beta, interleukin 1 beta; MFI, median fluorescence intensity.

Besides IL-1 beta expression, monocyte subsets have also been shown to differentially express chemokine receptors. In this sense, CCR2 expression was clearly higher in CMs than IMs and NCMs; however, CMs did not differentially express CCR2 in response to nLDL, alone or in combination with LPS (Figure 4A). Overall, the percentage of CMs and IMs expressing CCR2 did not change in response to nLDL or LPS (Figure 4B, left and middle panels, respectively). Conversely, nLDL + LPS significantly increased the amount of NCMs expressing CCR2 as compared to that found when cells were only exposed to nLDL (Figure 4B, right panel). Expression of CX3CR1 was significantly higher in IMs and NCMs

than CMs (Figure 4C). Furthermore, nLDL induced a decrease in CX3CR1 expression that was even more evident in NCMs than CMs and IMs (Figure 4C, right panel). The exposure of cells to LPS, alone or in combination with nLDL, decreased the expression of CX3CR1 in all monocyte subpopulations (Figure 4C). Interestingly, the number of CX3CR1+ NCMs significantly decreased in response to nLDL (Figure 4D, right panel), while LPS together with nLDL had the same effect upon IMs and NCMs (Figure 4D, middle and right panels, respectively).

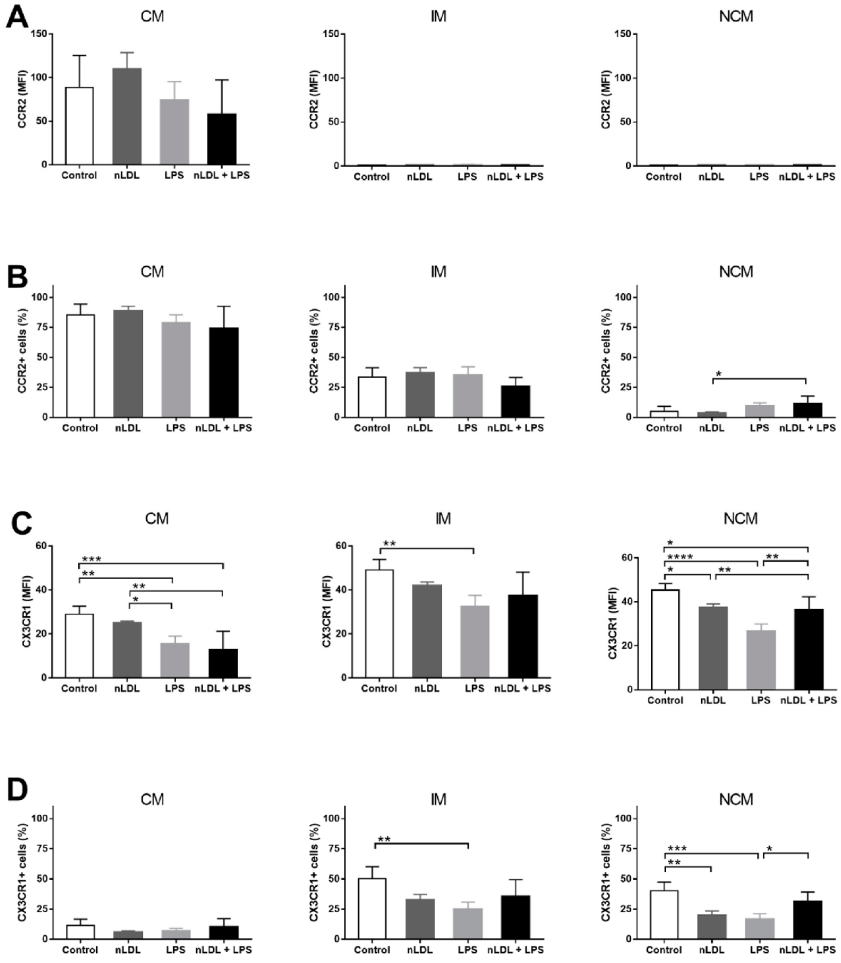


**Figure 4.** Effects of nLDL and LPS on CCR2 and CX3CR1 expression in human monocyte subpopulations. Although no significant differences were found, CCR2 expression was clearly higher in CMs than in IMs and NCMs (**A**, left, middle, and right panels, respectively). The number of CCR2+ cells increased in the CM subset as compared to IM and NCM subpopulations (**B**, left, middle, and right panels, respectively). In the NCM subset, LPS acted in synergy with nLDL to increase the amount of CCR2+ cells as compared to that found in cells only treated with nLDL (**B**, right panel). Expression

of CX3CR1 increased in IMs and NCMs as compared to CMs (**C**, left, middle, and right panels, respectively). In NCMs, nLDL significantly decreased CX3CR1 expression as compared to control cells (**C**, right panel). LPS, alone or in combination with nLDL, decreased CX3CR1 expression in CMs, IMs, and NCMs (**C**, left, middle, and right panels, respectively). In IMs, LPS decreased the percentage of CX3CR1+ cells as compared to control cells (**D**, middle panel). In NCMs, nLDL significantly decreased the amount of CX3CR1+ cells as compared to control cells (**D**, right panel). Cells were incubated in the presence or absence of 100 μg/mL nLDL and/or 10 ng/mL LPS for 9 h. Data are expressed as mean ± standard deviation. Data were compared using one-way ANOVA followed by the post-hoc Tukey test. Differences were considered significant when $p < 0.05$. * = $p < 0.05$; ** = $p < 0.01$; *** = $p < 0.001$; **** = $p < 0.0001$. CM, classical monocytes; IM, intermediate monocytes; NCM, non-classical monocytes; nLDL, native low-density lipoproteins; LPS, lipopolysaccharide; CCR2, C-C chemokine receptor type 2; CX3CR1, CX3C chemokine receptor 1; MFI, median fluorescence intensity.

In vitro, nLDL and LPS not only changed the balance of monocyte subsets but also the expression pattern of molecules that have been previously associated with the inflammatory response in atherogenesis. Thus, we decided to confirm these results by conducting similar experiments but now with an in vivo approach in patients with elevated LDL-C serum levels. Table 1 summarizes the differences in metabolic syndrome-related risk factors between subjects with normal and elevated LDL-C serum levels (76.53 ± 4.1 vs. 128.7 ± 3.6, respectively). There were no significant differences between subjects with LDL-C values below and above 100 mg/dL with respect to sex proportion, age, BMI, waist circumference, body fat percentage, triglycerides, HDL-C, fasting insulin and glucose, HOMA-IR, and CRP (Table 1). On the contrary, total cholesterol and Castelli's cardiovascular risk index II significantly increased in subjects with LDL-C greater than 100 mg/dL (Table 1).

**Table 1.** Anthropometric and biochemical parameters of the study subjects. The study participants were divided into two groups of LDL-C concentration, as follows: subjects with optimal concentration of LDL-C ≤ 100 mg/dL, and individuals with high concentration of LDL-C > 100 mg/dL. Total cholesterol and Castelli's atherogenic risk index significantly increased in patients with LDL-C greater than 100 mg/dL. Abbreviations: F, female; M, male; BMI, body mass index; LDL-C, low-density lipoproteins; HDL-C, high-density lipoproteins; HOMA-IR, homeostatic model assessment of insulin resistance; CRP, C-reactive protein; a.u., arbitrary units. Data are presented as mean ± standard deviation. Differences were considered significant when $p < 0.05$.

| | LDL-C | | |
|---|---|---|---|
| | **<100 mg/dL** | **>100 mg/dL** | ***p*-Value** |
| Sex (F/M) | 28/37 | 41/44 | 0.2650 |
| Age (years) | 47.2 ± 1.056 | 49.49 ± 1.031 | 0.1913 |
| BMI (kg/m$^2$) | 28.22 ± 1.172 | 28.05 ± 0.9035 | 0.9155 |
| Waist circumference (cm) | 91.58 ± 2.94 | 96.73 ± 2.002 | 0.1696 |
| Body fat (%) | 31.87 ± 1.696 | 31.91 ± 2.614 | 0.9909 |
| Cholesterol (mg/dL) | 166.7 ± 7.079 | 220.7 ± 4.723 | <0.0001 |
| Triglycerides (mg/dL) | 242.6 ± 41.08 | 186.4 ± 11.14 | 0.0769 |
| LDL-C (mg/dL) | 76.53 ± 4.156 | 128.7 ± 3.653 | <0.0001 |
| HDL-C (mg/dL) | 42.13 ± 3.44 | 47.06 ± 2.226 | 0.2332 |
| Insulin (μU/L) | 14.43 ± 1.057 | 13.52 ± 0.8046 | 0.5208 |
| Glucose (mmol/L) | 5.104 ± 0.2653 | 5.346 ± 0.2502 | 0.5675 |
| HOMA-IR (a.u.) | 3.299 ± 0.3261 | 3.126 ± 0.1866 | 0.6290 |
| CRP (mg/L) | 5.095 ± 0.4755 | 5.012 ± 0.6004 | 0.6328 |
| Castelli's risk index II | 1.966 ± 0.1827 | 2.892 ± 0.1294 | 0.0002 |

Confirming our in vitro results, the CM percentage significantly decreased in subjects with LDL-C > 100 mg/dL (Figure 5A). Although the IM percentage showed no differences (Figure 5B), the NCM percentage exhibited a significant 1.5-fold increase in individuals with LDL-C greater than 100 mg/dL (Figure 5C). The serum levels of IL-1 beta also significantly increased in subjects with LDL-C values above 100 mg/dL (Figure 5D). Moreover, LBP levels clearly raised in subjects with LDL-C > 100 mg/dL, suggesting the presence of abnormally high LPS serum values in these individuals (Figure 5E).

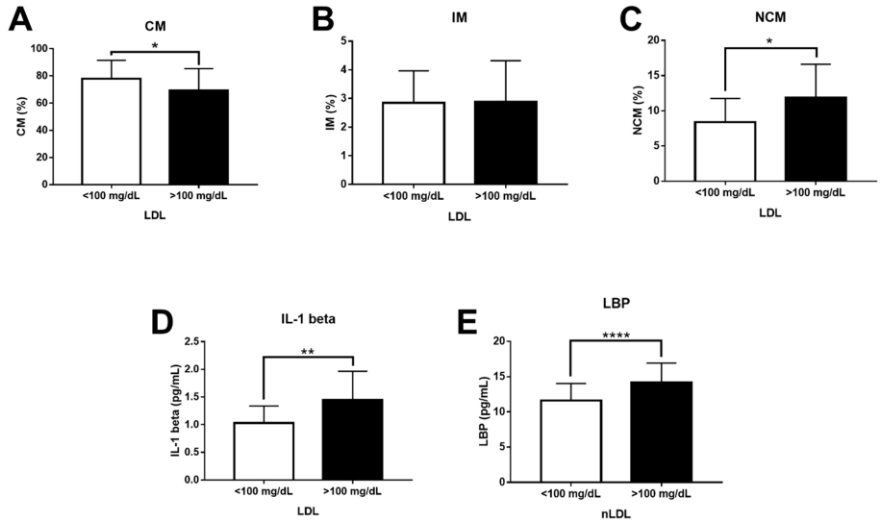


**Figure 5.** Levels of CMs, IMs, NCMs, IL-1 beta, and LBP in subjects with optimal and high serum levels of LDL-C. (**A**) The CM percentage significantly decreased in patients with serum LDL-C > 100 mg/dL (n = 85) as compared to controls (n = 65). (**B**) There were no significant changes between subjects with optimal and high LDL-C concentration for the IM percentage. (**C**) The NCM percentage significantly increased in patients with serum LDL-C > 100 mg/dL as compared to controls. (**D**) IL-1 beta serum levels significantly increased in patients with serum LDL-C > 100 mg/dL as compared to controls. (**E**) LBP serum levels significantly increased in patients with serum LDL-C > 100 mg/dL as compared to controls. Data are expressed as mean ± standard deviation. Data were compared using the unpaired Student's *t*-test. Differences were considered significant when $p < 0.05$. * = $p < 0.05$; ** = $p < 0.01$; **** = $p < 0.0001$. CM, classical monocytes; IM, intermediate monocytes; NCM, non-classical monocytes; IL-1 beta, interleukin 1 beta; LBP, LPS-binding protein; LDL-C, low-density lipoproteins.

## 4. Discussion

Macrophages and oxLDL are considered to be the main contributors to foam cell formation and inflammatory cell infiltration in atherosclerotic lesions [18]. However, the fact that monocytes and nLDL are able to interact in the blood stream has raised the question as to whether these precursors might also play a pivotal role in atherogenesis [19]. In this sense, intraperitoneal administration of triglyceride-rich lipoproteins decreases the number of non-classical Ly6C/Gr1low monocytes in mice [26]. Similarly, dyslipidemia with elevated levels of either LDL or very low-density lipoproteins (VLDL) increases both classical Ly6C/Gr1high and non-classical Ly6C/Gr1low monocyte subsets in mice fed a high-fat diet [19]. In line with this evidence, our results demonstrate that nLDL can alter the balance of human monocyte subpopulations by directly decreasing CMs and increasing NCMs in vitro and in vivo.

The mechanism through which nLDL induce imbalance of monocyte subsets remains unclear, and it probably involves CD14 and CD16 expression. As mentioned, CD14 and CD16 expression is the primary feature that defines monocyte subpopulations in humans [27]. CD14 is a transmembrane protein that forms the LPS receptor complex together with Toll-like receptor 4 (TLR4) and the myeloid differentiation factor 2 (MD-2) [28]. The trimeric CD14/TLR4/MD-2 complex triggers the nuclear factor kappa B (NFκB)-dependent signaling pathway in charge of regulating the expression of inflammatory cytokines such as IL-6, TNF-alpha, and IL-1 beta [29]. CD14 expression is regulated by specificity protein 1 (Sp1), a transcription factor that is activated via LDL receptor (LDLr)

promoter [30,31]. This body of evidence supports the idea that nLDL could decrease the CM proportion and increase the NCM percentage by regulating CD14 expression, probably via LDLr-Sp1. CD16 is an Fc-gamma receptor that recognizes IgG-coated microorganisms and immune complexes [32]. Recent evidence has demonstrated that CD16 expression is under the post-transcriptional control of microRNA (miR)-218 in human natural killer (NK) cells [33]. In vitro, oxLDL are able to decrease miR-218 expression in cardiac microvascular endothelial cells from rats. In vivo, miR-218 expression is inversely correlated with oxLDL levels in patients with coronary artery disease (CAD) [34]. In this sense, the increase in CD14+CD16+ non-classical monocytes and the decrease in CD14+CD16− classical monocytes that we found may be potentially related to the miR-218 suppression that in turn favors CD16 expression, promoting conversion of classical monocytes into non-classical monocytes in response to nLDL. Thus, circulating nLDL may induce imbalance of human monocyte subpopulations by mechanisms able to regulate CD14 and CD16 expression such as those orchestrated by LDLr, Sp1, and miR-218; however, this hypothesis remains to be elucidated in further studies.

A solid body of evidence has demonstrated that human monocyte subsets display important inflammatory actions by preferably expressing IL-1 beta in response to LPS [8,35]. LPS is a component of the outer membrane of Gram-negative bacteria that can translocate across the intestinal wall to the hepatic portal circulation, wherein it binds to LBP [36]. The LPS/LBP complex is considered a key inflammatory trigger for monocytes and macrophages and has been found to be increased in obese subjects with atherosclerotic heart disease, among whom nLDL is also increased [37,38]. Upon recognition, LPS induces the NFκB-dependent synthesis of pro-IL-1 beta, which in turn is proteolytically excised by the NOD-, LRR-, and pyrin domain-containing protein 3 (NLRP3) inflammasome to form mature IL-1 beta [39]. IL-1 beta has multiple functions in atherogenesis. In human microvascular endothelial cells, IL-1 beta stimulates the expression of the intracellular adhesion molecule-1 (ICAM-1) and the vascular cell adhesion molecule-1 (VCAM-1), which have the ability to recruit leukocytes into the inner layer of arteries [40]. In human aorta smooth muscle cells, IL-1 beta induces the expression of the monocyte chemoattractant protein-1 (MCP-1), which in turn contributes to mononuclear cell migration toward the vascular endothelium [41]. IL-1 beta also directly promotes atherosclerotic lesion formation by stimulating production of platelet-derived growth factor, a molecule with the ability to induce proliferation of vascular smooth muscle cells in the atheroma [42]. Interestingly, the exposure of endothelial cells and vascular smooth muscle cells to LPS increases release of IL-1 beta in atherosclerotic plaques of patients with suboptimally controlled hyperlipidemia LDL [43]. Our data expand on this body of evidence by demonstrating for the first time that LPS acts in synergy with nLDL to increase IL-1 beta synthesis in in vitro cultured human monocytes, especially CMs and IMs. In vivo, our results confirm this finding by revealing that subjects with elevated LDL-C serum levels also display higher LBP, IL-1 beta, and atherogenic index than those found in individuals with optimal LDL-C concentrations. However, it is worth mentioning that we still need to assess the potential effect of LDL particle number and size on the dynamics of human monocyte subpopulations and their ability to produce IL-1 beta, which may expand on the knowledge regarding the multiple actions of LDL in the inflammatory response associated with atherosclerosis.

nLDL and LPS not only displayed synergistic effects on the distribution of human monocyte subsets and their ability to produce IL-1 beta, but also affected the expression pattern of chemokine receptors such as CCR2 and CX3CR1. CCR2 is a C-C chemokine receptor mainly expressed in mononuclear cells that mediates migration of monocytes to inflamed tissues in response to MCP-1 [44]. CX3CR1 is the cell receptor for fractalkine, a chemokine with the ability to induce retention of monocytes in circulation, preferably those expressing CD16 such as IMs and NCMs [45]. In our study, the number of CCR2+ NCMs increased in response to nLDL and LPS, which may act in favor of promoting recruitment of these cells to the vascular endothelium. In line with these findings, a seminal work conducted by Han et al. informed that CCR2 expression increases in primary monocytes

from patients with elevated LDL-C serum values with respect to normocholesterolemic controls [46]. Additionally, exposure of THP-1 monocytes to nLDL induces a significant increase in both CCR2 expression and in vitro chemotactic response to MCP-1, suggesting that nLDL can directly enhance monocyte recruitment to the atherosclerotic lesion [46]. Concurring with the idea of increased cell recruitment, our data show that nLDL and LPS also decreased the amount of CX3CR1+ NCMs. In this sense, Nielsen et al. found altered expression of TNF-alpha and CX3CR1 in primary monocytes from patients with familial hypercholesterolemia as compared to subjects with normal LDL-C levels [47]. Interestingly, TNF-alpha and CX3CR1 expression positively correlated with increased intima-media thickness and hs-CRP, both of which are markers of atherosclerosis and cardiovascular risk [47]. In parallel, Geng et al. demonstrated that LPS administration to $ApoE^{-/-}$ mice enhances monocyte recruitment and macrophage accumulation in aortic atherosclerotic plaques, which concurs with increased lipid deposition in the atheroma [48]. Altogether, these findings support the idea that nLDL and LPS may directly contribute to atherogenesis by altering the expression pattern of inflammatory cytokines and chemokine receptors in monocytes, which may promote recruitment of these cells to atherosclerotic plaques. However, this notion should be still tested in in vivo experimental approaches focused on characterizing how nLDL and LPS affect the recruiting pattern of IL-1 beta-, CCR2-, and CX3CR1-producing monocytes to atherosclerotic lesions.

As we have outlined here, nLDL appear to have additional proinflammatory roles in atherogenesis that differed from those classically described for oxLDL [49]. Moreover, the effects of nLDL on the inflammatory ability of human monocyte subpopulations are enhanced by LPS, confirming previous evidence suggesting that nLDL and LBP form a negative loop that contributes to atherosclerosis [50–52].

## 5. Conclusions

In conclusion, using in vitro and in vivo complementary assays, this work demonstrates for the first time that nLDL act in synergy with LPS to alter the balance of human monocyte subsets and their ability to produce inflammatory cytokines and chemokine receptors with prominent roles in atherogenesis.

**Author Contributions:** Conceptualization, A.N.M.-R. and G.E.; methodology, A.N.M.-R., C.P.M.-R., J.A.A.-G., L.A.M.-G., M.E.-V., E.C.-T. and J.L.P.-C.; software data acquisition, J.L.P.-C. and A.N.M.-R.; formal analysis, A.N.M.-R., C.P.M.-R., S.L.-C., G.V.-A., J.M.F., O.P.-M. and G.E.; data curation, A.N.M.-R., S.L.-C., G.V.-A., O.P.-M., J.M.F. and G.E.; writing—original draft preparation, A.N.M.-R. and G.E.; writing—review and editing, S.L.-C., G.V.-A., J.M.F., O.P.-M. and G.E.; funding acquisition, G.E. All authors have read and agreed to the published version of the manuscript.

**Funding:** This work was supported by grant no. CB-2016-01-286209 from the Fondo Sectorial de Investigación para la Educación-CONACYT-México and grant no. SALUD-2017-02-290345 from the Fondo Sectorial de Investigación y Desarrollo en Salud y Seguridad Social SS/IMSS/ISSSTE/CONACYT-México to G.E.

**Institutional Review Board Statement:** The study was conducted in rigorous adherence to the principles described in the 1964 Declaration of Helsinki and its posterior amendment in 2013, and approved by the Ethics Committee of the General Hospital of Mexico with registration numbers of ethical approval code DI/20/501/03/17 and DIC/11/UME/05/029.

**Informed Consent Statement:** Informed consent was obtained from all subjects involved in the study.

**Data Availability Statement:** The data presented in this study are available upon request.

**Acknowledgments:** Aarón N. Manjarrez-Reyna is a doctoral student from the Programa de Doctorado en Ciencias Biomédicas, Universidad Nacional Autónoma de México (UNAM) and has received CONACyT fellowship 626423. The authors thank the Flow Cytometry core facility of "Coordinación de Investigación en Salud" at "Centro Médico Nacional Siglo XXI" of IMSS, Mexico for instrumentation and technical support.

**Conflicts of Interest:** The authors declare no conflict of interest regarding the publication of this article.

## References


1. Song, P.; Fang, Z.; Wang, H.; Cai, Y.; Rahimi, K.; Zhu, Y.; Fowkes, F.G.R.; Fowkes, F.J.I.; Rudan, I. Global and regional prevalence, burden, and risk factors for carotid atherosclerosis: A systematic review, meta-analysis, and modelling study. *Lancet Glob. Health* **2020**, *8*, e721–e729. [CrossRef]
2. Markin, A.; Sobenin, I.A.; Grechko, A.V.; Zhang, D.; Orekhov, A.N. Cellular Mechanisms of Human Atherogenesis: Focus on Chronification of Inflammation and Mitochondrial Mutations. *Front. Pharmacol.* **2020**, *11*, 642. [CrossRef] [PubMed]
3. Kloc, M.; Uosef, A.; Villagran, M.; Zdanowski, R.; Kubiak, J.; Wosik, J.; Ghobrial, R. RhoA- and Actin-Dependent Functions of Macrophages from the Rodent Cardiac Transplantation Model Perspective—Timing Is the Essence. *Biology* **2021**, *10*, 70. [CrossRef]
4. Ganesan, R.; Henkels, K.M.; Wrenshall, L.E.; Kanaho, Y.; Di Paolo, G.; Frohman, M.A.; Gomez-Cambronero, J. Oxidized LDL phagocytosis during foam cell formation in atherosclerotic plaques relies on a PLD2-CD36 functional interdependence. *J. Leukoc. Biol.* **2018**, *103*, 867–883. [CrossRef]
5. Chen, C.; Khismatullin, D.B. Oxidized Low-Density Lipoprotein Contributes to Atherogenesis via Co-activation of Macrophages and Mast Cells. *PLoS ONE* **2015**, *10*, e0123088. [CrossRef] [PubMed]
6. Marimuthu, R.; Francis, H.; Dervish, S.; Li, S.C.; Medbury, H.; Williams, H. Characterization of Human Monocyte Subsets by Whole Blood Flow Cytometry Analysis. *J. Vis. Exp.* **2018**, e57941. [CrossRef] [PubMed]
7. Appleby, L.J.; Nausch, N.; Midzi, N.; Mduluza, T.; Allen, J.; Mutapi, F. Sources of heterogeneity in human monocyte subsets. *Immunol. Lett.* **2013**, *152*, 32–41. [CrossRef]
8. Mukherjee, R.; Barman, P.K.; Thatoi, P.K.; Tripathy, R.; Das, B.K.; Ravindran, B. Non-Classical monocytes display inflammatory features: Validation in Sepsis and Systemic Lupus Erythematous. *Sci. Rep.* **2015**, *5*, 13886. [CrossRef] [PubMed]
9. Tacke, F.; Alvarez, D.; Kaplan, T.J.; Jakubzick, C.; Spanbroek, R.; Llodra, J.; Garin, A.; Liu, J.; Mack, M.; Van Rooijen, N.; et al. Monocyte subsets differentially employ CCR2, CCR5, and CX3CR1 to accumulate within atherosclerotic plaques. *J. Clin. Investig.* **2007**, *117*, 185–194. [CrossRef]
10. Idzkowska, E.; Eljaszewicz, A.; Miklasz, P.; Musial, W.J.; Tycinska, A.M.; Moniuszko, M. The Role of Different Monocyte Subsets in the Pathogenesis of Atherosclerosis and Acute Coronary Syndromes. *Scand. J. Immunol.* **2015**, *82*, 163–173. [CrossRef]
11. Dimitrov, S.; Shaikh, F.; Pruitt, C.; Green, M.; Wilson, K.; Beg, N.; Hong, S. Differential TNF production by monocyte subsets under physical stress: Blunted mobilization of proinflammatory monocytes in prehypertensive individuals. *Brain Behav. Immun.* **2013**, *27*, 101–108. [CrossRef]
12. Cockx, M.; Gouwy, M.; Ruytinx, P.; Lodewijckx, I.; Van Hout, A.; Knoops, S.; Pörtner, N.; Ronsse, I.; Vanbrabant, L.; Godding, V.; et al. Monocytes from patients with Primary Ciliary Dyskinesia show enhanced inflammatory properties and produce higher levels of pro-inflammatory cytokines. *Sci. Rep.* **2017**, *7*, 14657. [CrossRef] [PubMed]
13. González, Y.; Herrera, M.T.; Soldevila, G.; Garcia-Garcia, L.; Fabián, G.; Pérez-Armendariz, E.M.; Bobadilla, K.; Guzman-Beltran, S.; Sada, E.; Torres, M. High glucose concentrations induce TNF-α production through the down-regulation of CD33 in primary human monocytes. *BMC Immunol.* **2012**, *13*, 19. [CrossRef] [PubMed]
14. Dasu, M.R.; Jialal, I. Free fatty acids in the presence of high glucose amplify monocyte inflammation via Toll-like receptors. *Am. J. Physiol. Endocrinol. Metab.* **2011**, *300*, E145–E154. [CrossRef]
15. Grün, J.L.; Manjarrez-Reyna, A.N.; Gómez-Arauz, A.Y.; Leon-Cabrera, S.; Rückert, F.; Fragoso, J.M.; Bueno-Hernández, N.; Islas-Andrade, S.; Meléndez-Mier, G.; Escobedo, G. High-Density Lipoprotein Reduction Differentially Modulates to Classical and Nonclassical Monocyte Subpopulations in Metabolic Syndrome Patients and in LPS-Stimulated Primary Human Monocytes In Vitro. *J. Immunol. Res.* **2018**, *2018*, 2737040. [CrossRef]
16. Kopp, F.; Kupsch, S.; Schromm, A.B. Lipopolysaccharide-binding protein is bound and internalized by host cells and colocalizes with LPS in the cytoplasm: Implications for a role of LBP in intracellular LPS-signaling. *Biochim. Biophys. Acta Bioenerg.* **2016**, *1863*, 660–672. [CrossRef]
17. Aw, N.H.; Canetti, E.; Suzuki, K.; Goh, J. Monocyte Subsets in Atherosclerosis and Modification with Exercise in Humans. *Antioxidants* **2018**, *7*, 196. [CrossRef]
18. Orekhov, A.N.; Oishi, Y.; Nikiforov, N.G.; Zhelankin, A.V.; Dubrovsky, L.; Sobenin, I.A.; Kel, A.; Stelmashenko, D.; Makeev, V.J.; Foxx, K.; et al. Modified LDL Particles Activate Inflammatory Pathways in Monocyte-derived Macrophages: Transcriptome Analysis. *Curr. Pharm. Des.* **2018**, *24*, 3143–3151. [CrossRef] [PubMed]
19. Jackson, W.; Weinrich, T.W.; Woollard, K.J. Very-low and low-density lipoproteins induce neutral lipid accumulation and impair migration in monocyte subsets. *Sci. Rep.* **2016**, *6*, 20038. [CrossRef]
20. Combadiere, C.; Potteaux, S.; Rodero, M.; Simon, T.; Pezard, A.; Esposito, B.; Merval, R.; Proudfoot, A.; Tedgui, A.; Mallat, Z. Combined Inhibition of CCL2, CX3CR1, and CCR5 Abrogates Ly6C hi and Ly6C lo Monocytosis and Almost Abolishes Atherosclerosis in Hypercholesterolemic Mice. *Circulation* **2008**, *117*, 1649–1657. [CrossRef] [PubMed]
21. Wang, J.; Si, Y.; Wu, C.; Sun, L.; Ma, Y.; Ge, A.; Li, B. Lipopolysaccharide promotes lipid accumulation in human adventitial fibroblasts via TLR4-NF-κB pathway. *Lipids Health Dis.* **2012**, *11*, 139. [CrossRef] [PubMed]
22. Ahola, A.J.; Lassenius, M.I.; Forsblom, C.; Harjutsalo, V.; Lehto, M.; Groop, P.-H. Dietary patterns reflecting healthy food choices are associated with lower serum LPS activity. *Sci. Rep.* **2017**, *7*, 6511. [CrossRef] [PubMed]
23. Pendyala, S.; Walker, J.M.; Holt, P.R. A High-Fat Diet Is Associated With Endotoxemia That Originates From the Gut. *Gastroenterol.* **2012**, *142*, 1100–1101.e2. [CrossRef] [PubMed]

24. Zawada, A.M.; Fell, L.H.; Untersteller, K.; Seiler, S.; Rogacev, K.S.; Fliser, D.; Ziegler-Heitbrock, L.; Heine, G.H. Comparison of two different strategies for human monocyte subsets gating within the large-scale prospective CARE FOR HOMe Study. *Cytom. Part A* **2015**, *87*, 750–758. [CrossRef] [PubMed]
25. Expert Panel on Detection, Evaluation, and Treatment of High Blood Cholesterol in Adults. Executive Summary of the Third Report of the National Cholesterol Education Program (NCEP) Expert Panel on Detection, Evaluation, and Treatment of High Blood Cholesterol in Adults (Adult Treatment Panel III). *JAMA* **2001**, *285*, 2486–2497. [CrossRef] [PubMed]
26. Saja, M.F.; Baudino, L.; Jackson, W.; Cook, H.T.; Malik, T.H.; Fossati-Jimack, L.; Ruseva, M.; Pickering, M.C.; Woollard, K.J.; Botto, M. Triglyceride-Rich Lipoproteins Modulate the Distribution and Extravasation of Ly6C/Gr1low Monocytes. *Cell Rep.* **2015**, *12*, 1802–1815. [CrossRef] [PubMed]
27. Merah-Mourah, F.; Cohen, S.O.; Charron, D.; Mooney, N.; Haziot, A. Identification of Novel Human Monocyte Subsets and Evidence for Phenotypic Groups Defined by Interindividual Variations of Expression of Adhesion Molecules. *Sci. Rep.* **2020**, *10*, 4397. [CrossRef] [PubMed]
28. Calvano, J.E.; Agnese, D.; Um, J.Y.; Goshima, M.; Singhal, R.; Coyle, S.M.; Reddell, M.T.; Kumar, A.; Calvano, S.E.; Lowry, S.F. Modulation of the Lipopolysaccharide Receptor Complex (CD14, TLR4, MD-2) and Toll-Like Receptor 2 in Systemic Inflammatory Response Syndrome-Positive Patients With and Without Infection: Relationship to Tolerance. *Shock.* **2003**, *20*, 415–419. [CrossRef]
29. Ott, L.W.; Resing, K.A.; Sizemore, A.W.; Heyen, J.W.; Cocklin, R.R.; Pedrick, N.M.; Woods, H.C.; Chen, J.Y.; Goebl, M.G.; Witzmann, F.A.; et al. Tumor Necrosis Factor-alpha- and interleukin-1-induced cellular responses: Coupling proteomic and genomic information. *J. Proteome. Res.* **2007**, *6*, 2176–2185. [CrossRef]
30. E Zhang, D.; Hetherington, C.J.; Gonzalez, D.A.; Chen, H.M.; Tenen, D. Regulation of CD14 expression during monocytic differentiation induced with 1 alpha,25-dihydroxyvitamin D. *J. Immunol.* **1994**, *153*, 3276–3284.
31. Yieh, L.; Sanchez, H.B.; Osborne, T.F. Domains of transcription factor Sp1 required for synergistic activation with sterol regulatory element binding protein 1 of low density lipoprotein receptor promoter. *Proc. Natl. Acad. Sci. USA* **1995**, *92*, 6102–6106. [CrossRef]
32. Junker, F.; Gordon, J.; Qureshi, O. Fc Gamma Receptors and Their Role in Antigen Uptake, Presentation, and T Cell Activation. *Front. Immunol.* **2020**, *11*, 1393. [CrossRef] [PubMed]
33. Victor, A.R.; Weigel, C.; Scoville, S.D.; Chan, W.K.; Chatman, K.; Nemer, M.M.; Mao, C.; Young, K.A.; Zhang, J.; Yu, J.; et al. Epigenetic and Posttranscriptional Regulation of CD16 Expression during Human NK Cell Development. *J. Immunol.* **2017**, *200*, 565–572. [CrossRef] [PubMed]
34. Gao, W.; Cui, H.; Li, Q.; Zhong, H.; Yu, J.; Li, P.; He, X. Upregulation of microRNA-218 reduces cardiac microvascular endothelial cells injury induced by coronary artery disease through the inhibition of HMGB. *J. Cell. Physiol.* **2020**, *235*, 3079–3095. [CrossRef] [PubMed]
35. Devêvre, E.F.; Renovato-Martins, M.; Clément, K.; Sautes-Fridman, C.; Cremer, I.; Poitou, C. Profiling of the Three Circulating Monocyte Subpopulations in Human Obesity. *J. Immunol.* **2015**, *194*, 3917–3923. [CrossRef]
36. Guerville, M.; Boudry, G. Gastrointestinal and hepatic mechanisms limiting entry and dissemination of lipopolysaccharide into the systemic circulation. *Am. J. Physiol. Liver Physiol.* **2016**, *311*, G1–G15. [CrossRef]
37. Hersoug, L.; Møller, P.; Loft, S. Gut microbiota-derived lipopolysaccharide uptake and trafficking to adipose tissue: Implications for inflammation and obesity. *Obes. Rev.* **2016**, *17*, 297–312. [CrossRef]
38. Lepper, P.M.; Schumann, C.; Triantafilou, K.; Rasche, F.M.; Schuster, T.; Frank, H.; Schneider, E.M.; Triantafilou, M.; von Eynatten, M. Association of Lipopolysaccharide-Binding Protein and Coronary Artery Disease in Men. *J. Am. Coll. Cardiol.* **2007**, *50*, 25–31. [CrossRef]
39. Zasłona, Z.; Pålsson-McDermott, E.M.; Menon, D.; Haneklaus, M.; Flis, E.; Prendeville, H.; Corcoran, S.E.; Peters-Golden, M.; O'Neill, L.A.J. The Induction of Pro–IL-1β by Lipopolysaccharide Requires Endogenous Prostaglandin E2Production. *J. Immunol.* **2017**, *198*, 3558–3564. [CrossRef]
40. Haraldsen, G.; Kvale, D.; Lien, B.; Farstad, I.N.; Brandtzaeg, P. Cytokine-regulated expression of E-selectin, intercellular adhesion molecule-1 (ICAM-1), and vascular cell adhesion molecule-1 (VCAM-1) in human microvascular endothelial cells. *J. Immunol.* **1996**, *156*, 2558–2565. [PubMed]
41. Lim, J.H.; Um, H.J.; Park, J.-W.; Lee, I.-K.; Kwon, T.K. Interleukin-1β promotes the expression of monocyte chemoattractant protein-1 in human aorta smooth muscle cells via multiple signaling pathways. *Exp. Mol. Med.* **2009**, *41*, 757–764. [CrossRef]
42. Libby, P. Interleukin-1 Beta as a Target for Atherosclerosis Therapy. *J. Am. Coll. Cardiol.* **2017**, *70*, 2278–2289. [CrossRef] [PubMed]
43. Jiang, X.; Wang, F.; Wang, Y.; Gisterå, A.; Roy, J.; Paulsson-Berne, G.; Hedin, U.; Lerman, A.; Hansson, G.K.; Herrmann, J.; et al. Inflammasome-Driven Interleukin-1α and Interleukin-1β Production in Atherosclerotic Plaques Relates to Hyperlipidemia and Plaque Complexity. *JACC Basic Transl. Sci.* **2019**, *4*, 304–317. [CrossRef] [PubMed]
44. Teh, Y.C.; Ding, J.L.; Ng, L.G.; Chong, S.Z. Capturing the Fantastic Voyage of Monocytes Through Time and Space. *Front. Immunol.* **2019**, *10*, 834. [CrossRef] [PubMed]
45. Ancuta, P.; Rao, R.; Moses, A.; Mehle, A.; Shaw, S.K.; Luscinskas, F.W.; Gabuzda, D. Fractalkine Preferentially Mediates Arrest and Migration of CD16+ Monocytes. *J. Exp. Med.* **2003**, *197*, 1701–1707. [CrossRef]
46. Han, K.H.; Tangirala, R.K.; Green, S.R.; Quehenberger, O. Chemokine receptor CCR2 expression and monocyte chemoattractant protein-1-mediated chemotaxis in human monocytes. A regulatory role for plasma LDL. *Arterioscler. Thromb. Vasc. Biol.* **1998**, *18*, 1983–1991. [CrossRef] [PubMed]

47. Nielsen, M.H.; Irvine, H.; Vedel, S.; Raungaard, B.; Beck-Nielsen, H.; Handberg, A. Elevated Atherosclerosis-Related Gene Expression, Monocyte Activation and Microparticle-Release Are Related to Increased Lipoprotein-Associated Oxidative Stress in Familial Hypercholesterolemia. *PLoS ONE* **2015**, *10*, e0121516. [CrossRef]
48. Geng, S.; Chen, K.; Yuan, R.; Peng, L.; Maitra, U.; Diao, N.; Chen, C.; Zhang, Y.; Hu, Y.; Qi, C.-F.; et al. The persistence of low-grade inflammatory monocytes contributes to aggravated atherosclerosis. *Nat. Commun.* **2016**, *7*, 13436. [CrossRef]
49. Poznyak, A.V.; Nikiforov, N.G.; Markin, A.M.; Kashirskikh, D.A.; Myasoedova, V.A.; Gerasimova, E.V.; Orekhov, A.N. Overview of OxLDL and Its Impact on Cardiovascular Health: Focus on Atherosclerosis. *Front. Pharmacol.* **2021**, *11*, 613780. [CrossRef]
50. Bowman, J.D.; Surani, S.; Horseman, M. Endotoxin, Toll-like Receptor-4, and Atherosclerotic Heart Disease. *Curr. Cardiol. Rev.* **2017**, *13*, 86–93. [CrossRef]
51. Grin, P.; Dwivedi, D.J.; Chathely, K.M.; Trigatti, B.; Dino, L.; Prat, A.; Seidah, N.; Liaw, P.C.; Fox-Robichaud, A.E. Low-density lipoprotein (LDL)-dependent uptake of Gram-positive lipoteichoic acid and Gram-negative lipopolysaccharide occurs through LDL receptor. *Sci. Rep.* **2018**, *8*, 10496. [CrossRef] [PubMed]
52. Vreugdenhil, A.C.; Snoek, A.P.; van 't Veer, C.; Greve, J.W.; Buurman, W.A. LPS-binding protein circulates in association with apoB-containing lipoproteins and enhances endotoxin-LDL/VLDL interaction. *J. Clin. Investig.* **2001**, *107*, 225–234. [CrossRef] [PubMed]

*microorganisms*

MDPI

*Article*

# The Neutrophil-to-Monocyte Ratio and Lymphocyte-to-Neutrophil Ratio at Admission Predict In-Hospital Mortality in Mexican Patients with Severe SARS-CoV-2 Infection (Covid-19)

**Salma A. Rizo-Téllez [1,2,†], Lucia A. Méndez-García [1,†], Cruz Flores-Rebollo [1,3], Fernando Alba-Flores [1], Raúl Alcántara-Suárez [1], Aarón N. Manjarrez-Reyna [1], Neyla Baltazar-López [3], Verónica A. Hernández-Guzmán [3], José I. León-Pedroza [4], Rogelio Zapata-Arenas [5], Antonio González-Chávez [5], Joselín Hernández-Ruíz [6], José D. Carrillo-Ruíz [7], Raúl Serrano-Loyola [8], Guadalupe M. L. Guerrero-Avendaño [8] and Galileo Escobedo [1,*]**

1 Laboratory of Immunometabolism, Research Division, General Hospital of Mexico "Dr. Eduardo Liceaga", Mexico City 06720, Mexico; sart.17.04@gmail.com (S.A.R.-T.); angelica.mendez.86@hotmail.com (L.A.M.-G.); cruzifr3@gmail.com (C.F.-R.); feralflo.mcp@gmail.com (F.A.-F.); raul_as02@hotmail.com (R.A.-S.); aaron.manjarrez@gmail.com (A.N.M.-R.)
2 PECEM, Facultad de Medicina, Universidad Nacional Autónoma de México, Coyoacán, Mexico City 04510, Mexico
3 Research Coordination at Central Laboratories, General Hospital of Mexico "Dr. Eduardo Liceaga", Mexico City 06720, Mexico; neylabaltazar@yahoo.com.mx (N.B.-L.); veronicahgm@gmail.com (V.A.H.-G.)
4 Department of Intensive Medical Therapy, General Hospital of Mexico "Dr. Eduardo Liceaga", Mexico City 06720, Mexico; jisrael_leon@hotmail.com
5 Department of Internal Medicine, General Hospital of Mexico "Dr. Eduardo Liceaga", Mexico City 06720, Mexico; el_zarmx@hotmail.com (R.Z.-A.); antglez51@yahoo.com.mx (A.G.-C.)
6 Clinical Pharmacology Unit, General Hospital of Mexico "Dr. Eduardo Liceaga", Mexico City 06720, Mexico; hernandezjoselin@hotmail.com
7 Department of Neurology and Neurosurgery, General Hospital of Mexico "Dr. Eduardo Liceaga", Mexico City 06720, Mexico; josecarrilloruiz@yahoo.com
8 Department of Radiology and Imaging, General Hospital of Mexico "Dr. Eduardo Liceaga", Mexico City 06720, Mexico; serranoraul48@yahoo.com.mx (R.S.-L.); gpeguerrero@prodigy.net.mx (G.M.L.G.-A.)
* Correspondence: gescobedog@msn.com; Tel.: +52-(55)-2789-2000 (ext. 5646)
† These authors equally contributed to this work.

Received: 31 August 2020; Accepted: 7 October 2020; Published: 10 October 2020


**Abstract:** There is a deep need for mortality predictors that allow clinicians to quickly triage patients with severe coronavirus disease 2019 (Covid-19) into intensive care units at the time of hospital admission. Thus, we examined the efficacy of the lymphocyte-to-neutrophil ratio (LNR) and neutrophil-to-monocyte ratio (NMR) as predictors of in-hospital death at admission in patients with severe Covid-19. A total of 54 Mexican adult patients with Covid-19 that met hospitalization criteria were retrospectively enrolled, followed-up daily until hospital discharge or death, and then assigned to survival or non-survival groups. Clinical, demographic, and laboratory parameters were recorded at admission. A total of 20 patients with severe Covid-19 died, and 75% of them were men older than 62.90 ± 14.18 years on average. Type 2 diabetes, hypertension, and coronary heart disease were more prevalent in non-survivors. As compared to survivors, LNR was significantly fourfold decreased while NMR was twofold increased. LNR ≤ 0.088 predicted in-hospital mortality with a sensitivity of 85.00% and a specificity of 74.19%. NMR ≥ 17.75 was a better independent risk factor for mortality with a sensitivity of 89.47% and a specificity of 80.00%. This study demonstrates for the first time

that NMR and LNR are accurate predictors of in-hospital mortality at admission in patients with severe Covid-19.

**Keywords:** SARS-Cov-2; Covid-19; mortality predictor; in-hospital death risk; lymphocyte; monocyte; neutrophil; intensive care unit

## 1. Introduction

The outbreak of coronavirus disease 2019 (Covid-19) is an ongoing global pandemic caused by the novel severe acute respiratory syndrome coronavirus-2 (SARS-CoV-2) that has affected the lives of millions of people worldwide [1]. Although more than 85% of patients with Covid-19 show a self-limiting illness with symptoms such as mild fever, dry cough, and fatigue, some patients develop severe pneumonia that can progress to acute respiratory distress syndrome, multiple organ failure, and death [2]. Mortality rates directly attributed to severe Covid-19 ranges from 3% in countries like China to 10% in countries like Spain [3,4]. However, mortality rates above 10% have been alarmingly reported in other countries like Italy, UK, and Mexico [4–6]. In particular, a 145% excess mortality associated with severe Covid-19 has been recently estimated for some Mexico's cities, which is presumably associated with higher prevalence of comorbidities such as obesity, type 2 diabetes (T2D), and hypertension in our population [7]. Thus, it is of great importance to develop novel tools that help us to estimate the mortality risk at admission in patients with severe Covid-19 that need hospitalization, with the aim of quickly triaging them into intensive care units.

Clinical features of patients with Covid-19 have revealed a number of potential biochemical markers associated with in-hospital mortality. In particular, the blood levels of D-dimer, ferritin, C-reactive protein (CRP), troponin I, lactate dehydrogenase (LDH), and procalcitonin have been extensively studied due to their apparently good accuracy to discriminate patients with the most severe courses of the disease [8–13]. In parallel, numerous studies have also proposed the use of hematological markers such as lymphocyte, monocyte, and neutrophil counts that seem to associate with increased severity and mortality in patients with Covid-19 [14,15]. Actually, it has been consistently demonstrated that, in seriously ill patients with Covid-19, the blood count of lymphocyte and monocyte populations decreases whereas neutrophil counts increase [15]. However, total counts of these white blood cells (WBC) are merely associated with severity and mortality of Covid-19 but fails to predict death risk in clinical practice [14]. For this reason, a growing body of evidence has now proposed that ratios among lymphocytes, monocytes, and neutrophils are more accurate to predict mortality than cell count of lymphocytes, monocytes, and neutrophils by itself [16,17]. As a matter of fact, numerous reports have previously shown that the lymphocyte-to-neutrophil ratio (LNR) and the neutrophil-to-monocyte ratio (NMR) are markers associated with poorer survival in acute lung bacterial infection, sepsis, and many solid tumors including gastroesophageal, colorectal, pancreatic, prostate, and breast carcinoma [18–20]. Nevertheless, NLR and NMR have been scarcely explored as mortality predictors in patients with severe Covid-19, especially in countries with a disproportionate number of deaths related to this disease, such as Mexico.

For this reason, our main goal was to assess the efficacy of LNR and NMR as predictors of mortality at admission in adult patients with severe SARS-CoV-2 infection that met hospitalization criteria.

## 2. Material and Methods

### *2.1. Subjects*

A total of 54 Mexican patients of both sexes aged 18 years or older, with severe Covid-19, admitted to the Department of Intensive Medical Therapy of the General Hospital of Mexico, were retrospectively enrolled in the study from 23 March 2020 to 26 June 2020. The diagnosis

of Covid-19 was confirmed by specific detection of the SARS-CoV-2 in nasopharyngeal swabs using quantitative polymerase chain reaction (qPCR) according to the World Health Organization (WHO) technical guidance [21]. Patients seriously ill with Covid-19 that needed hospitalization were enrolled in the study if they met at least one of the following criteria: oxygen saturation level ($SpO_2$) < 93% on room air, respiratory distress > 30 breaths/min, and/or > 50% lung involvement on imaging. Patients were excluded from the study if they had previous diagnosis of cancer, end-stage kidney and/or liver failure, endocrine disorders, infectious diseases, and/or autoimmune disease. We also excluded from the study human immunodeficiency virus (HIV), hepatitis C virus (HCV), and hepatitis B virus (HBV)-seropositive individuals, patients under long-term immunomodulatory medication including non-steroidal anti-inflammatory drugs, unconscious patients that had lost ability to respond, and pregnant or lactating women. All participants provided written informed consent, previously approved by the institutional ethical committee of the General Hospital of Mexico (registration number of the ethical code approval: DI/20/501/03/17), which guaranteed that the study was conducted in rigorous adherence to the principles that were described in the 1964 Declaration of Helsinki and its posterior amendment in 2013.

### 2.2. Data Collection

Laboratory and clinical data were collected at hospital admission from all patients enrolled in the study using the digital version of the electronic health record of the General Hospital of Mexico. Demographic data and medical history including previous diagnosis of obesity (body mass index (BMI) > 30 kg/m$^2$), T2D (glycated hemoglobin (HbA1c) > 6.5% or medication to treat T2D), high blood pressure (>130/80 mm Hg or medication to treat hypertension), and coronary heart disease (CHD) were personally recorded at the Department of Intensive Medical Therapy. Furthermore, the need for invasive mechanical ventilation (IMV) with an oral endotracheal tube attached to a mechanical ventilator, time to extubation, inpatient days up to the main outcome, and drug regimen to treat Covid-19 were personally recorded at the Department of Intensive Medical Therapy. All patients were followed-up with daily, until hospital discharge or death, and then were assigned to survival or non-survival groups, respectively.

### 2.3. Laboratory Measures

Laboratory measures included biochemical parameters, liver function tests, and kidney function test as follows: blood glucose, triglycerides, total cholesterol, low-density lipoproteins (LDL), high-density lipoproteins (HDL), alanine aminotransferase (ALT), aspartate aminotransferase (AST), gamma glutamyl transferase (GGT), alkaline phosphatase (ALP), total bilirubin, direct bilirubin, indirect bilirubin, amylase, lipase, creatinine phosphokinase (CPK), creatinine kinase myocardial band (CK-MB), total protein, albumin, LDH, serum creatinine, uric acid, calcium, phosphorus, chloride, potassium, sodium, and magnesium. Additional measures also included hematological and immune parameters, and coagulation tests as follows: WBC count, red blood cell (RBC) count, lymphocytes, monocytes, eosinophils, basophils, band cells, neutrophils, hemoglobin, hematocrit, mean corpuscular volume (MCV), mean corpuscular hemoglobin (MCH), red blood cell distribution width (RDW), platelet count, mean platelet volume, CRP, troponin I, ferritin, procalcitonin, myoglobine, D-dimer, fibrinogen, prothrombin time (PT), international normalized ratio (INR), activated partial thromboplastin time (aPTT), and thrombin time (TT). LNR resulted of dividing the total lymphocyte count by the total neutrophil count. NMR resulted of dividing the total neutrophil count by the total monocyte count. All laboratory parameters were measured using the Beckman Coulter DxC 700 AU Chemistry Analyzer (Beckman Coulter Inc., Brea, CA, USA), the Coulter LH 780 Hematology Analyzer (Beckman Coulter Inc., Brea, CA, USA), and the BCS® XP System (Siemens Healthcare GmbH, Erlangen, Germany) following strict adherence to the standard operating procedures.

### 2.4. Statistics

All laboratory parameters were recorded at hospital admission and then analyzed retrospectively. Normality of data distribution was estimated by the Shapiro–Wilk test. The unpaired Student's T-test was used to compare age, BMI, blood glucose, triglycerides, total cholesterol, LDL, HDL, ALT, AST, GGT, alkaline phosphatase, total bilirubin, direct bilirubin, indirect bilirubin, total protein, albumin, LDH, serum creatinine, uric acid, calcium, phosphorus, chloride, potassium, sodium, magnesium, WBC count, RBC count, lymphocytes, monocytes, eosinophils, basophils, band cells, neutrophils, hemoglobin, hematocrit, mean corpuscular volume, mean corpuscular hemoglobin, mean corpuscular hemoglobin concentration, RDW, platelet count, mean platelet volume, CRP, troponin, ferritin, procalcitonin, D-dimer, fibrinogen, PT, INR, aPTT, TT, time to extubation, inpatient days, LNR, and NMR between survival and non-survival groups, and data are expressed as mean ± standard deviation. The chi-squared test was used to compare the prevalence of obesity, T2D, hypertension, coronary heart disease, the number of patients that required IMV, and the sex ratio in survival and non-survival groups, and data are expressed as absolute values or percentages. Receiver operating characteristic (ROC) curves were conducted to calculate area under the curve (AUC) and 95% confidence interval (95% CI) for LNR and NMR. ROC curves together with the Youden index was used to calculate optimal cut-off points, sensitivity, specificity, Relative Risk (RR), Odd Ratio (OR), and 95% CI for LNR and NMR. The sensitivity, specificity, and OR were also calculated for LNR and NMR together by means of the chi-squared test. Multiple regression analysis was performed to estimate the effect of potential confounding variables including obesity, T2D, hypertension, CHD, age, and gender on the accuracy of LNR and NMR as predictors of in-hospital death. Survival analyses were performed for LNR, NMR, and other potential mortality predictors by the Kaplan–Meier method. Differences were considered significant when $p < 0.05$. Statistical analyses were performed by means of the GraphPad Prism 6.01 software (GraphPad Software, La Jolla, CA 92037, USA), the MDCalc Software (New York, NY 10003, USA), the IBM SPSS Statistics version 26.0 (IBM, Armonk, NY, USA), and the R i386 3.5.2 terminal (Microsoft Corp., Boston, MA, USA).

## 3. Results

Figure 1 shows the selection process of patients enrolled in the study based on the inclusion and exclusion criteria.

After hospital admission, 63% ($n = 34$) seriously ill patients with Covid-19 survived, whereas nearly 37% ($n = 20$) patients with a severe course of this disease died (Table 1). Among non-survivors, 75% ($n = 15$) of patients were men ($p = 0.002$). Patients in the non-survival group were, on average, about 9 years older than individuals in the survival group (62.90 ± 14.18 versus 54.06 ± 12.43 years, respectively) (Table 1). In contrast, there were no significant differences between survivors and non-survivors for BMI (28.24 ± 4.60 versus 27.88 ± 4.05 kg/m$^2$, respectively). Furthermore, there were no significant differences between survivors and non-survivors with respect to the prevalence of obesity ($p = 0.277$). On the contrary, the prevalence of T2D ($p = 0.037$), hypertension ($p = 0.006$), and CHD ($p = 0.033$) was significantly increased in the non-survival group as compared to the survival group (Table 1). The need for intubation was significantly greater in the non-survival group than in the survival group (83.33 versus 30.43%, respectively) with no significant differences with respect to the time to extubation, number of days that patients spent in hospital, and the five-drug regimen used for treating patients that included aziythromycin, ceftriaxone, enoxaparin sodium, dexamethasone, and acetaminophen (Table 1).

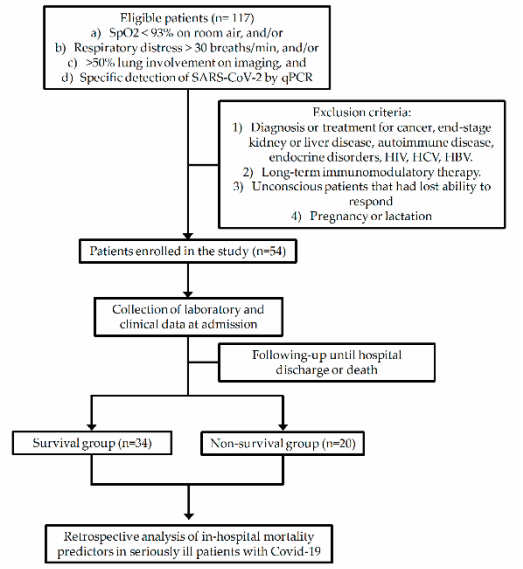


**Figure 1.** Schematic flow chart showing the selection process of patients enrolled in the study based on the inclusion and exclusion criteria. $SpO_2$, oxygen saturation level; SARS-CoV-2, novel severe acute respiratory syndrome coronavirus-2; qPCR, quantitative polymerase chain reaction; HIV, human immunodeficiency virus; HCV, hepatitis C virus; HBV, hepatitis B virus; Covid-19, coronavirus disease 2019.

**Table 1.** Demographic and clinical characteristics in hospitalized patients with severe Covid-19. Abbreviations: W, women; M, men; BMI, body mass index; T2D, type 2 diabetes; IMV, invasive mechanical ventilation. Normality of data distribution was estimated by the Shapiro–Wilk test. The unpaired Student's T-test was used to compare numerical variables and data are presented as mean ± standard deviation. The chi-squared test was used to compare categorical variables and data are expressed as absolute values or percentages. * Differences were considered significant when $p < 0.05$.

| Parameters | Survivors ($n = 34$) | Non-Survivors ($n = 20$) | $p$ Value |
|---|---|---|---|
| Gender (W/M) | 21/13 | 5/15 | 0.002 * |
| Age (years) | 54.06 ± 12.43 | 62.9 ± 14.18 | 0.020 * |
| BMI (kg/m$^2$) | 28.24 ± 4.60 | 27.88 ± 4.05 | 0.903 |
| Obesity prevalence (%) | 52.17 | 41.66 | 0.277 |
| T2D prevalence (%) | 43.47 | 75.00 | 0.037 * |
| Hypertension prevalence (%) | 17.39 | 58.33 | 0.006 * |
| Coronary heart disease (%) | 8.69 | 33.33 | 0.033 * |
| IMV (%) | 30.43 | 83.33 | 0.001 * |
| Time to extubation (days) | 2.43 ± 0.79 | 3.66 ± 0.82 | 0.167 |
| Inpatient days (days) | 15.65 ± 3.13 | 8.41 ± 1.66 | 0.060 |
| Drug regimen | Aziythromycin, ceftriaxone, enoxaparin sodium, dexamethasone, and acetaminophen | | - |

At hospital admission, there were no significant differences between survivors and non-survivors with respect to serum glucose, creatinine, uric acid, triglycerides, total bilirubin, indirect bilirubin, ALT, ALP, total protein, amylase, lipase, CPK, CK-MB, phosphorus, magnesium, sodium, potassium, chlorine, and calcium (Table 2). On the contrary, blood levels of urea ($p$ = 0.004), total cholesterol ($p$ = 0.010), HDL ($p$ = 0.015), LDL ($p$ = 0.012), direct bilirubin ($p$ = 0.012), AST ($p$ = 0.021), GGT ($p$ = 0.015), albumin ($p$ = 0.001), and LDH ($p$ = 0.001) showed statistically significant differences between survivors and non-survivors at hospital admission (Table 2).

**Table 2.** Biochemical parameters, kidney function tests, and liver function tests at admission in hospitalized patients with severe Covid-19. Abbreviations: HDL, high-density lipoproteins; LDL, low-density lipoproteins; ALT, alanine aminotransferase; AST, aspartate aminotransferase; ALP, alkaline phosphatase; GGT, gamma glutamyl transferase; LDH, lactate dehydrogenase; CPK, creatinine phosphokinase; CK-MB, creatinine kinase myocardial band. Normality of data distribution was estimated by the Shapiro–Wilk test. The unpaired Student's $t$-test was used to compare numerical variables and data are presented as mean ± standard deviation. * Differences were considered significant when $p < 0.05$.

| Parameters | Survivors ($n$ = 34) | Non-Survivors ($n$ = 20) | $p$ Value |
|---|---|---|---|
| Glucose (mg/dL) | 148.19 ± 92.13 | 148.16 ± 60.76 | 0.999 |
| Urea (mg/dL) | 42.05 ± 37.06 | 91.07 ± 77.16 | 0.004 * |
| Creatinine (mg/dL) | 0.995 ± 1.18 | 1.85 ± 2.79 | 0.133 |
| Uric Acid (mg/dL) | 5.65 ± 2.81 | 7.39 ± 4.09 | 0.097 |
| Total Cholesterol (mg/dL) | 151.77 ± 34.98 | 126.06 ± 20.85 | 0.010 * |
| Triglycerides (mg/dL) | 166.04 ± 67.93 | 169.75 ± 54.89 | 0.853 |
| HDL (mg/dL) | 34.30 ± 10.88 | 23.92 ± 12.09 | 0.015 * |
| LDL (mg/dL) | 95.30 ± 30.14 | 70.38 ± 18.69 | 0.012 * |
| Total bilirubin (mg/dL) | 0.684 ± 0.401 | 0.804 ± 0.315 | 0.349 |
| Direct bilirubin (mg/dL) | 0.185 ± 0.133 | 0.323 ± 0.215 | 0.012 * |
| Indirect bilirubin (mg/dL) | 0.492 ± 0.254 | 0.498 ± 0.153 | 0.939 |
| ALT (IU/L) | 35.42 ± 26.29 | 41.47 ± 28.92 | 0.465 |
| AST (IU/L) | 34.74 ± 22.86 | 59 ± 47.74 | 0.021 * |
| ALP (IU/L) | 91.00 ± 27.22 | 125.29 ± 120.86 | 0.134 |
| GGT (IU/L) | 69.54 ± 43.07 | 124.33 ± 101.26 | 0.015 * |
| Total Protein (mg/dL) | 6.59 ± 0.525 | 6.31 ± 0.627 | 0.099 |
| Albumin (mg/dL) | 3.59 ± 0.479 | 2.94 ± 0.409 | 0.001 * |
| LDH (IU/L) | 320.63 ± 132.11 | 475.63 ± 195.83 | 0.001 * |
| Amylase (IU/L) | 46.1 ± 35.39 | 56.83 ± 26.93 | 0.429 |
| Lipase (IU/L) | 116.00 ± 304.00 | 52.36 ± 52.27 | 0.502 |
| CPK (IU/L) | 101.52 ± 97.49 | 699.57 ± 1937.82 | 0.114 |
| CK-MB (IU/L) | 23.80 ± 11.90 | 44.43 ± 59.39 | 0.099 |
| Phosphorus (mg/dL) | 3.89 ± 2.01 | 4.25 ± 1.67 | 0.516 |
| Magnesium (mg/dL) | 2.74 ± 3.53 | 2.42 ± 0.629 | 0.698 |
| Sodium (mEq/L) | 136.00 ± 6.56 | 138.53 ± 6.31 | 0.182 |
| Potassium (mEq/L) | 5.56 ± 6.67 | 4.47 ± 0.719 | 0.484 |
| Chlorine (mEq/L) | 100.28 ± 7.19 | 101.84 ± 6.49 | 0.441 |
| Calcium (mg/dL) | 8.63 ± 0.686 | 8.14 ± 1.20 | 0.076 |

There were no significant differences between survivors and non-survivors for prothrombin time, INR, thrombin time, aPTT, fibrinogen, troponin I, and myoglobine (Table 3). On the other hand, non-survivors showed significantly higher values of D-dimer ($p$ = 0.017), ferritin ($p$ = 0.012), CRP ($p$ = 0.014), and procalcitonin ($p$ = 0.037) than survivors at the time of admission (Table 3).

**Table 3.** Coagulation and immune parameters at admission in hospitalized patients with severe Covid-19. Abbreviations: INR, international normalized ratio; aPTT, activated partial thromboplastin time; CRP, C-reactive protein. Normality of data distribution was estimated by the Shapiro–Wilk test. The unpaired Student's *t*-test was used to compare numerical variables and data are presented as mean ± standard deviation. * Differences were considered significant when $p < 0.05$.

| Parameters | Survivors ($n$ = 34) | Non-Survivors ($n$ = 20) | $p$ Value |
|---|---|---|---|
| Prothrombine time (s) | 11.97 ± 2.49 | 12.96 ± 1.55 | 0.237 |
| INR | 0.995 ± 0.246 | 1.10 ± 0.167 | 0.216 |
| Thrombin time (s) | 16.76 ± 1.61 | 17.78 ± 1.42 | 0.085 |
| aPTT (s) | 26.18 ± 6.99 | 26.36 ± 5.68 | 0.941 |
| Fibrinogen (mg/dL) | 637.23 ± 222.29 | 703.75 ± 206.92 | 0.400 |
| D-dimer (Ug/L) | 975.33 ± 477.81 | 8260.33 ± 13354.39 | 0.017 * |
| Ferritin (ng/mL) | 522.62 ± 451.93 | 937.00 ± 415.09 | 0.012 * |
| CRP (mg/L) | 129.43 ± 90.10 | 221.07 ± 108.32 | 0.014 * |
| Troponin I (ng/mL) | 37.68 ± 63.57 | 68.458 ± 112.73 | 0.338 |
| Myoglobine (ng/L) | 94.49 ± 107.76 | 254.38 ± 353.69 | 0.089 |
| Procalcitonin (ng/mL) | 0.220 ± 0.256 | 2.01 ± 4.07 | 0.037 * |

No significant differences between survivors and non-survivors were found for most of the hematological parameters including total cell counts of leukocytes, lymphocytes, monocytes, eosinophils, basophils, and RBC (Table 4). However, there were significant differences between survivors and non-survivors with respect to the percentage of neutrophils ($p = 0.041$), lymphocytes ($p = 0.001$) monocytes ($p = 0.001$), and eosinophils ($p = 0.007$), and the neutrophil count ($p = 0.003$) (Table 4).

**Table 4.** Hematological parameters at admission in hospitalized patients with severe Covid-19. Abbreviations: MCV, mean corpuscular volume; MHC, mean corpuscular hemoglobin; RDW, red blood cell distribution. Normality of data distribution was estimated by the Shapiro–Wilk test. The unpaired Student's *t*-test was used to compare numerical variables and data are presented as mean ± standard deviation. * Differences were considered significant when $p < 0.05$.

| Parameters | Survivors ($n$ = 34) | Non-Survivors ($n$ = 20) | $p$ Value |
|---|---|---|---|
| Leukocytes ($\times 10^3/\mu L$) | 13.48 ± 25.44 | 13.19 ± 6.34 | 0.960 |
| Neutrophil percentage (%) | 73.95 ± 17.19 | 84.72 ± 18.89 | 0.041 * |
| Lymphocyte percentage (%) | 16.79 ± 11.35 | 7.48 ± 5.65 | 0.001 * |
| Monocyte percentage (%) | 5.96 ± 2.54 | 3.35 ± 1.42 | 0.001 * |
| Band cells (%) | 0.000 ± 0.000 | 0.08 ± 0.358 | 0.217 |
| Eosinophil percentage (%) | 0.739 ± 0.974 | 0.110 ± 0.281 | 0.007 * |
| Basophil percentage (%) | 0.429 ± 1.23 | 0.085 ± 0.123 | 0.221 |
| Neutrophils ($\times 10^3/\mu L$) | 7.39 ± 4.44 | 11.93 ± 5.99 | 0.003 * |
| Lymphocytes ($\times 10^3/\mu L$) | 2.09 ± 4.40 | 0.750 ± 0.426 | 0.181 |
| Monocytes ($\times 10^3/\mu L$) | 0.519 ± 0.256 | 0.450 ± 0.276 | 0.364 |
| Eosinophils ($\times 10^3/\mu L$) | 0.096 ± 0.272 | 0.015 ± 0.049 | 0.193 |
| Basophils ($\times 10^3/\mu L$) | 0.339 ± 1.87 | 0.000 ± 0.000 | 0.423 |
| Erythrocyte ($\times 10^6/\mu L$) | 4.71 ± 0.893 | 4.75 ± 1.09 | 0.884 |
| Hemoglobin (g/dL) | 14.17 ± 2.56 | 14.42 ± 3.11 | 0.756 |
| Hematocrit (%) | 42.40 ± 7.58 | 42.82 ± 9.44 | 0.863 |
| MCV (fL) | 90.54 ± 5.88 | 91.35 ± 4.15 | 0.597 |
| MCH (pg) | 30.34 ± 2.73 | 30.42 ± 1.64 | 0.905 |
| RDW (%) | 15.07 ± 3.38 | 14.72 ± 2.07 | 0.685 |
| Platelets ($\times 10^3/\mu L$) | 266.61 ± 111.11 | 240.25 ± 113.83 | 0.416 |

On average, LNR showed a significant fourfold decrease in non-survivors as compared to survivors ($p = 0.003$) (Figure 2A). In parallel, NMR exhibited a significant twofold increase in non-survivors with respect to survivors ($p = 0.001$) (Figure 2B).

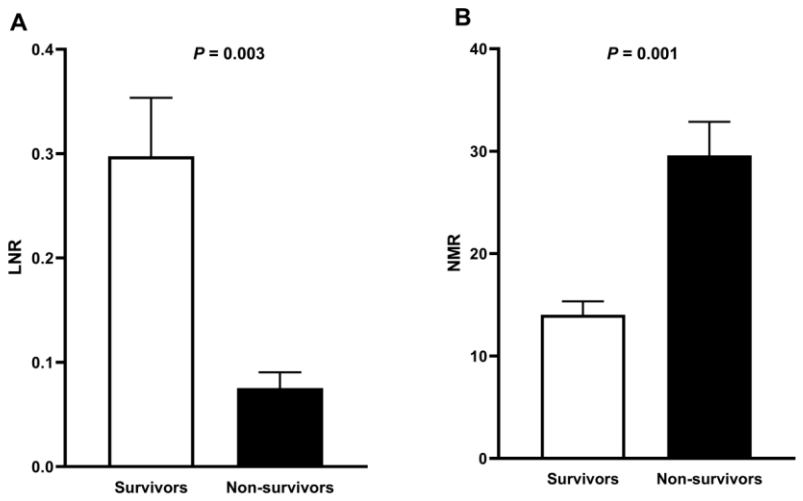


**Figure 2.** LNR and NMR at admission in hospitalized patients with severe Covid-19. (**A**) LNR showed a significant fourfold decrease in non-survivors as compared to survivors. LNR resulted of dividing the total lymphocyte count by the total neutrophil count. (**B**) NMR exhibited a significant twofold increase in non-survivors with respect to survivors. NMR resulted of dividing the total neutrophil count by the total monocyte count. Normality of data distribution was estimated by the Shapiro–Wilk test. The unpaired Student's *t*-test was used to compare LNR and MNR between survivors and non-survivors, and data are presented as mean ± standard deviation. Differences were considered significant when $p < 0.05$. LNR, Lymphocyte-to-neutrophil ratio; NMR, neutrophil-to-monocyte ratio.

The area under the ROC curve of LNR was 0.832 (95% CI, 0.701–0.922, $p < 0.001$) (Figure 3A). At hospital admission, the best cut-off point for LNR was ≤ 0.088 with a sensitivity of 85.00% and a specificity of 74.19% (Youden index = 0.5919, 95% CI 0.3380–0.7387). The RR and OR for LNR was 5.8933 (95% CI, 1.9661–17.6652) and 16.2917 (95% CI, 3.7550–70.6837), respectively (Figure 3A). LNR was less than 0.088 in 91% of patients with severe Covid-19 that died, whereas only 20% of patients with severe Covid-19 that survived showed LNR ≤ 0.088. Simultaneously, the area under the ROC curve of NMR was 0.890 (95% CI, 0.768–0.962, $p < 0.001$) (Figure 3B). The best cut-off value for NMR was ≥ 17.75 with a sensitivity of 89.47%, specificity of 80.00%, and Youden index of 0.6947 (95% CI, 0.4349–0.8333). The RR and OR for NMR was 8.8542 (95% CI, 2.2864–34.2878) and 27.9286 (95% CI, 5.1435–151.6497), respectively (Figure 3B). NMR was greater than 17.75 in 95% of patients with severe Covid-19 that died, whereas only 10% of patients with severe Covid-19 that survived had NMR ≥ 17.75. Additionally, LNR ≤ 0.088 together with NMR ≥ 17.75 predicted in-hospital mortality in seriously ill patients with Covid-19 with a sensitivity of 81.48%, specificity of 83.33%, and OR of 22.00 (95% CI, 4.556–106.238). The accuracy of LNR and MNR as independent risk factors for in-hospital death was not modified after adjusting by comorbidities, gender, or age in multiple regression analysis.

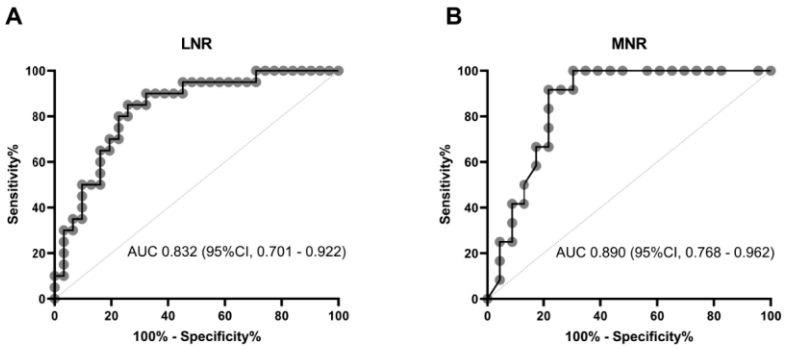


**Figure 3.** ROC curves for LNR and MNR to predict in-hospital mortality at admission in patients with severe Covid-19. (**A**) For LNR, the best cut-off point to predict in-hospital death was ≤ 0.088 with AUC of 0.832 (95% CI, 0.701–0.922), sensitivity of 85.00%, specificity of 74.19%, Youden index of 0.5919 (95% CI 0.3380–0.7387), RR of 5.8933 (95% CI, 1.9661–17.6652), and OR of 16.2917 (95% CI, 3.7550–70.6837). (**B**) For NMR, the best cut-off point to predict in-hospital death was ≥ 17.75 with AUC of 0.890 (95% CI, 0.768–0.962), sensitivity of 89.47%, specificity of 80.00%, Youden index of 0.6947 (95% CI, 0.4349–0.8333), RR of 8.8542 (95% CI, 2.2864–34.2878), and OR of 27.9286 (95% CI, 5.1435–151.6497). LNR resulted of dividing the total lymphocyte count by the total neutrophil count. NMR resulted of dividing the total neutrophil count by the total monocyte count. Statistical analyses were performed by means of the MDCalc Software (New York, NY 10003, USA) and the IBM SPSS Statistics version 26.0 (IBM, Armonk, NY, USA). Differences were considered significant when $p < 0.05$. LNR, Lymphocyte-to-neutrophil ratio; NMR, neutrophil-to-monocyte ratio; ROC, Receiver Operating Characteristic curves; AUC, area under the ROC curve; CI, confidence interval; RR, relative risk; OR, Odd ratio.

Table 5 confirmed that LNR and NMR are more accurate to predict mortality in Mexican patients with severe Covid-19 than WBC count by itself. In this sense, the area under the ROC curve of the total leukocyte count was 0.702 (95% CI, 0.557–0.822) (Table 5). The area under the ROC curves for neutrophil, lymphocyte, and monocyte counts were 0.746 (95% CI, 0.605–0.857), 0.735 (95% CI, 0.593–0.849), and 0.605 (95% CI, 0.458–0.739), respectively (Table 5). LNR and MNR were also better predictors for in-hospital mortality than the serum levels of several biochemical and immune parameters. As a matter of fact, the area under the ROC curves for D-dimer, ferritin, CRP, troponin I, LDH, and procalcitonin were 0.730, (95% CI, 0.548–0.869), 0.777 (95% CI, 0.601–0.901), 0.750 (95% CI, 0.569–0.884), 0.656 (95% CI, 0.464–0.816), 0.758 (95% CI, 0.618–0.867), and 0.826 (95% CI, 0.682–0.924), respectively (Table 5).

**Table 5.** Area under the ROC curves for hematological, biochemical, and immune parameters to predict in-hospital mortality at admission in patients with severe Covid-19. Statistical analyses were performed by means of the MDCalc Software (New York, NY 10003, USA) and the IBM SPSS Statistics version 26.0 (IBM, Armonk, NY, USA). Differences were considered significant when $p < 0.05$. Abbreviations: CRP, C-reactive protein; LDH, lactate dehydrogenase; ROC, Receiver Operating Characteristic curves; AUC, area under the ROC curve; CI, confidence interval.

| Parameters | AUC | CI 95% |
|---|---|---|
| Total leukocyte count | 0.702 | 0.557–0.822 |
| Neutrophil count | 0.746 | 0.605–0.857 |
| Lymphocyte count | 0.735 | 0.593–0.849 |
| Monocyte count | 0.605 | 0.458–0.739 |
| D-dimer | 0.730 | 0.548–0.869 |
| Ferritin | 0.777 | 0.601–0.901 |
| CRP | 0.750 | 0.569–0.884 |
| Troponin I | 0.656 | 0.464–0.816 |
| LDH | 0.758 | 0.618–0.867 |
| Procalcitonin | 0.826 | 0.682–0.924 |

Survival analysis revealed that patients seriously ill with Covid-19 showing NMR greater than 17.75 at admission have 50% survival probability after 9 days of hospitalization (Figure 4A). Patients with LNR less than 0.088 show 50% survival probability after 12 days of hospitalization (Figure 4B). When using the cut-off points for total leukocytes $> 11.4 \times 10^3/\mu L$, neutrophils $> 6.3 \times 10^3/\mu L$, lymphocytes $\leq 0.8 \times 10^3/\mu L$, and monocytes $\leq 0.3 \times 10^3/\mu L$ separately, the survival probability significantly decrease in patients with severe Covid-19 after 12–20 days of hospitalization (Figure 4C–F, respectively). Despite LDH values significantly differing between survivors and non-survivors ($320.63 \pm 132.11$ versus $475.63 \pm 195.83$, $p = 0.001$, respectively), patients with LDH > 362 IU/L show a significant decrease in the probability of survival up to 27 days after hospitalization (Figure 4G). In contrast, patients with severe Covid-19 and procalcitonin values greater than 0.1 ng/mL exhibit a 50% decrease in the survival probability after 12 days of hospitalization (Figure 4H).

Taking these results into account, we propose a new triage based on the use of NMR and LNR to assist clinicians to estimate in-hospital death risk in critically ill patients with Covid-19, with the aim of quickly admitting them into intensive care units and reducing the number of fatalities related to this disease (Figure 5).

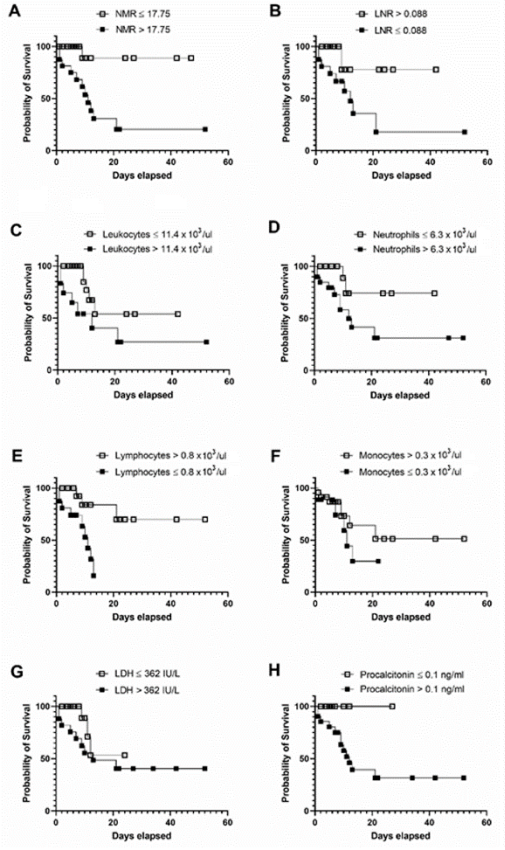


**Figure 4.** Kaplan–Meier curves for comparing the survival probability of different clinical predictors of in-hospital mortality at admission in patients seriously ill with Covid-19. (**A**) Patients with severe Covid-19 that show NMR > 17.75 at admission show 50% survival probability after 9 days of hospitalization. (**B**) Patients with LNR < 0.088 at admission show 50% survival probability after 12 days of hospitalization. (**C**) Patients with total leukocyte count > $11.4 \times 10^3/\mu L$ at admission exhibit a significant decrease in the survival probability up to 20 days after hospitalization. (**D**) Patients with total neutrophil count > $6.3 \times 10^3/\mu L$ at admission have 50% survival probability up to 13 days after hospitalization. (**E**) Patients with total lymphocyte count ≤ $0.8 \times 10^3/\mu L$ at admission show a significant decrease in the survival probability up to 14 days after hospitalization. (**F**) Patients with total monocyte count ≤ $0.3 \times 10^3/\mu L$ at admission exhibit a significant decrease in the survival probability up to 23 days after hospitalization. (**G**) Patients with LDH > 362 IU/L at admission show a significant decrease in the probability of survival up to 27 days after hospitalization. (**H**) Patients with procalcitonin values > 0.1 ng/mL at admission exhibit a 50% decrease in the survival probability after 12 days of hospitalization. Cut-off points for each marker are described at the top of the corresponding panel. Receiver operating characteristic (ROC) curves together with the Youden index was used to calculate optimal cut-off points for all markers. NMR resulted of dividing the total neutrophil count by the total monocyte count. LNR resulted of dividing the total lymphocyte count by the total neutrophil count. Survival analyses were performed by means of the Kaplan–Meier method using the GraphPad Prism 6.01 software. NMR, neutrophil-to-monocyte ratio; LNR, Lymphocyte-to-neutrophil ratio; LDH, lactate dehydrogenase.

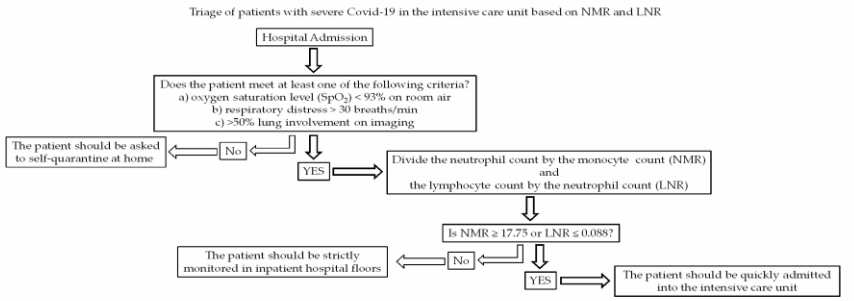


**Figure 5.** Proposal of triage based on NMR and LNR for patients seriously ill with Covid-19 that meet hospitalization criteria. At hospital admission, the neutrophil count should be divided by the monocyte count (NMR) and the lymphocyte count by the neutrophil count (LNR). If NMR ≥ 17.75 or LNR ≤ 0.088, the patient should be quickly admitted into the intensive care unit.

## 4. Discussion

The search for reliable, sensitive, and specific markers that can help us to discriminate patients with the most severe forms of Covid-19 at the time of hospital admission is still a matter of great urgency. In this sense, the analysis of routine laboratory results has revealed a strongly interdependent relationship among neutrophils, lymphocytes, and monocytes that is linked to the severity of Covid-19 [22].

To date, six retrospective clinical studies examining the potential use of NLR as a prognostic marker for severe Covid-19 have been published; none in Mexican patients until now [22–27]. All these clinical studies consistently conclude that NLR is an independent risk factor of mortality in critically ill patients with Covid-19. Concurring with this information, our results indicate that a LNR less than 0.088 at hospital admission is effective to early predict mortality of patients with severe Covid-19 (OR = 16.2917, 95% CI 3.7550–70.6837).

In parallel, we also wanted to explore if the apparent relationship between neutrophil and monocyte counts might be used to evaluate death risk in seriously ill patients with Covid-19. Unexpectedly, our data demonstrate that NMR is even more sensitive and specific than LNR to predict in-hospital mortality of Mexican patients with Covid-19. Indeed, our results demonstrate that having a NMR greater than 17.75 (OR = 27.9286, 95% CI 5.1435–151.6497) at the time of hospital admission is an independent risk factor for in-hospital mortality in patients with severe Covid-19, even after adjusting for comorbidities, gender, and age. Interestingly, the specificity of NMR slightly increases when using together with LNR, although the sensitivity significantly decreases and its possible clinical implementation should be made taking into account this information. Another important aspect that supports the possible implementation of NMR in clinical practice is the fact that this in-hospital mortality marker may assist in the early identification of patients with Covid-19 that will require a more aggressive clinical management. As a matter of fact, survival analyses revealed that using NMR > 17.75 at admission, clinicians might identify patients with severe Covid-19 at higher risk of experiencing 50% reduction in the probability of survival in 9 days. In contrast, identification of patients with poorer survival probability takes longer when using other markers such as lymphocyte count, LDH or procalcitonin. In other words, the use of NMR may help to clinicians to quickly identify patients at higher risk of in-hospital mortality with the aim of giving them priority into intensive care units.

As far as we know, this is the first study showing that NMR can be used as a cheap, fast, and reliable marker of in-hospital mortality in severe Covid-19. Hongmei Zhang and coworkers recently reported that NMR was significantly higher in patients with the most severe forms of Covid-19 as compared to those with mild and moderate courses of the disease [28]. However, these authors also found that NMR

failed to predict which patients had higher risk of developing a more severe form of Covid-19 [28]. This apparent controversy in the accuracy of NMR to discriminate patients at higher risk of death might be explained by understanding the impact of ethnicity on the development and clinical presentation of Covid-19. In this sense, several groups mostly from China have proposed that the serum levels of D-dimer, ferritin, CRP, troponin I, LDH, and procalcitonin are good predictors of mortality in patients with severe Covid-19 [8,9,13]. However, our study shows that in Mexican patients these biochemical and immune parameters exhibit poorer ability to predict mortality than that found for LNR and NMR. Again, these controversial findings may be related to differences in the genetic background and prevalence of comorbidities between Mexican-Mestizo subjects of the south-central region of Mexico and East Asian population. For all these reasons, we firmly believe that searching for markers associated with the most severe courses of Covid-19 should be conducted in a population-specific manner. In other words, LNR and NMR seem to be sensitive and specific markers of in-hospital mortality for severe Covid-19 in Mexican patients but no other populations such as Chinese people. Therefore, the clinical use of these ratios in patients with severe Covid-19 that require hospitalization should be carried out with caution in a population-specific manner.

The rationale behind using LNR and NMR to identify patients with severe Covid-19 at higher risk of death is probably given by the differential roles that lymphocytes, monocytes, and neutrophils play during immune response. In humans, neutrophils are the most abundant type of peripheral WBC with prominent functions in the acute inflammatory response by migrating toward injured tissues in response to chemoattractant signals such as interleukin (IL-) 8 [29]. Neutrophils are now considered one of the most important immune cells in defending the airway epithelium against the SARS-CoV-2 infection by locally stimulating the production of IL-1 beta, IL-6, tumor necrosis factor-alpha (TNF-alpha), and reactive oxygen species (ROS) [30]. Paradoxically, neutrophil hyperactivation and recruitment intensify the acute inflammatory response and worsen epithelial tissue damage thus leading to disease progression [30,31]. On the contrary, lymphocytes are very important leukocytes in charge of mediating immune tolerance to self-antigens, activation of pathogen-specific adaptive immunity, and, last but not less important, orchestration of immunomodulatory mechanisms [32,33]. Lymphocytes, including T and B cells, are able to orchestrate immunomodulatory mechanisms via IL-10 and transforming growth factor-beta 1 (TGF-beta 1) production, a couple of cytokines with key anti-inflammatory and wound-healing actions [34]. In parallel, monocytes are circulating leukocytes that in humans can be sorted into three subpopulations based on the cell surface expression of the cluster of differentiation (CD) 14 and CD16 [35]. The classical monocyte subpopulation expresses high CD14 levels with no CD16 expression. Intermediate monocytes show CD14 and CD16 expression; in contrast, non-classical monocytes express very low CD14 levels accompanied by CD16 expression [36]. Intermediate and non-classical monocytes have been shown to produce high levels of IL-1 beta in response to lipopolysaccharide and in patients with metabolic syndrome [37,38]. Interestingly, reduction in both intermediate and non-classical monocyte subpopulations has been recently associated with increased severity of the SARS-CoV-2 infection [39]. Additionally, monocytes can differentiate into alternatively activated macrophages and prevent inflammatory responses by promoting tissue repair via IL-10 and TGF-beta 1 production, which may also play a pivotal role in regulating hyperactivation of the inflammatory response described in patients with severe Covid-19 [40]. In other words, neutrophils and the cell populations of lymphocytes and monocytes seem to have typical antagonistic roles in multiple inflammatory scenarios including that provoked by the SARS-CoV-2 infection. Thus, it is feasible to assume that LNR and NMR might reflect an imbalance among these immune cells that in turn could be related to excessive inflammation and poorer survival in patients with severe Covid-19. For this reason, present results do not only offer novel mortality markers for severe Covid-19 but also reveal potential lines of treatment aimed to decrease neutrophil hyperactivation and increase lymphocyte and monocyte numbers by means of administering drugs as tofacitinib, reparixin, buspirone, and/or lanimostim. However, the possible efficacy of the aforementioned drugs in patients with severe Covid-19 should still be prospectively examined in randomized, placebo-controlled clinical trials.

Finally, concurring with previous literature [41], our study demonstrates that except for obesity, the prevalence of T2D, hypertension, and CHD was higher in the non-survival group than in patients with severe Covid-19 that survived. Likewise, patients in the non-survival group more frequently required IVM than surviving patients. In this way, our results confirm that the presence of previous non-communicable diseases such as T2D, hypertension, and CHD clearly aggravates disease severity and increases the number of fatalities related to Covid-19. So, the SARS-CoV-2 pandemic remarks again the urgency of more effective politics of public health aimed to control the incidence of noncommunicable diseases in countries like Mexico, which is facing a terrible disproportion in the number of deaths related to Covid-19.

This study has some limitations, including the sample size and exclusion of patients with previous diagnosis of other pathologies such as cancer, autoimmune disease, and/or other viral infections such as HIV and HCV. Improvement of these limitations may help to strengthen our findings and extend the use of LNR and NMR to predict in-hospital mortality in patients with high clinical heterogeneity.

## 5. Conclusions

This study demonstrates for the first time that an LNR less than 0.088 and an NMR greater than 17.75 at the time of admission can accurately predict in-hospital mortality of patients with severe Covid-19. Indeed, NMR is significantly more sensitive and specific than LNR to estimate the mortality risk in patients with Covid-19 that meet hospitalization criteria. In Mexican adult patients, both NMR and LNR are better predictors for in-hospital death related to severe Covid-19 than other markers such as D-dimer, ferritin, CRP, troponin I, LDH, and procalcitonin. Together with the presence of T2D, hypertension, CHD, male gender, and increased age (>63 years), NMR and LNR should be considered as independent risk factors for mortality in Mexican patients seriously ill with Covid-19. Simply by dividing the neutrophil count by the monocyte count, or the lymphocyte count by the neutrophil count, at the time of hospital admission, clinicians can have cheap, fast, and reliable predictors for in-hospital death in patients with Covid-19. In practical terms, we propose a new triage based on the use of NMR and LNR to assist clinicians to estimate in-hospital death risk in critically ill patients with Covid-19 with the aim of quickly admitting them into intensive care units and reducing the number of fatalities related to this disease (Figure 5). For this reason, we encourage other clinical research groups to assess the efficacy of these mortality predictors not only in Mexicans but also other Latin-American populations.

**Author Contributions:** Conceptualization, S.A.R.-T., L.A.M.-G. and G.E.; methodology, S.A.R.-T., L.A.M.-G., C.F.-R., F.A.-F., R.A.-S., A.N.M.-R., N.B.-L., V.A.H.-G., J.I.L.-P., R.Z.-A., A.G.-C., J.H.-R., J.D.C.-R., R.S.-L. and G.M.L.G.-A.; formal analysis, S.A.R.-T., L.A.M.-G., J.D.C.-R., R.S.-L., G.M.L.G.-A. and G.E.; data curation, S.A.R.-T., L.A.M.-G., J.D.C.-R., R.S.-L., G.M.L.G.-A. and G.E.; writing-original draft preparation, S.A.R.-T., L.A.M.-G. and G.E.; writing-review and editing, C.F.-R., F.A.-F., R.A.-S., A.N.M.-R., N.B.-L., V.A.H.-G., J.I.L.-P., R.Z.-A., A.G.-C., J.H.-R., J.D.C.-R., R.S.-L., G.M.L.G.-A. and G.E.; funding acquisition, G.E. All authors have read and agreed to the published version of the manuscript.

**Funding:** This work was supported by grant no. CB-2016-01-286209 from the Fondo Sectorial de Investigación para la Educación-CONACYT-México and grant no. SALUD-2017-02-290345 from the Fondo Sectorial de Investigación y Desarrollo en Salud y Seguridad Social SS/IMSS/ISSSTE/CONACYT-México to GE.

**Acknowledgments:** Salma Alejandra Rizo Téllez is a doctoral student from the Plan de Estudios Combinados en Medicina, Licenciatura y Doctorado (PECEM) of the Universidad Nacional Autónoma de México (UNAM) and has received CONACYT fellowship 762603.

**Conflicts of Interest:** The authors declare that there is no conflict of interest regarding the publication of this article.

## References


1. Lai, C.-C.; Shih, T.-P.; Ko, W.-C.; Tang, H.-J.; Hsueh, P.-R. Severe acute respiratory syndrome coronavirus 2 (SARS-CoV-2) and coronavirus disease-2019 (COVID-19): The epidemic and the challenges. *Int. J. Antimicrob. Agents* **2020**, *55*, 105924. [CrossRef] [PubMed]
2. Epidemiology Working Group for NCIP Epidemic Response, Chinese Center for Disease Control and Prevention. The epidemiological characteristics of an outbreak of 2019 novel coronavirus diseases (COVID-19) in China. *Zhonghua Liu Xing Bing Xue Za Zhi* **2020**, *41*, 145–151.
3. Yan, Y.; Shin, W.I.; Pang, Y.X.; Meng, Y.; Lai, J.; You, C.; Zhao, H.; Lester, E.; Wu, T.; Pang, C.H. The First 75 Days of Novel Coronavirus (SARS-CoV-2) Outbreak: Recent Advances, Prevention, and Treatment. *Int. J. Environ. Res. Public Health* **2020**, *17*, 2323. [CrossRef]
4. Ceylan, Z. Estimation of COVID-19 prevalence in Italy, Spain, and France. *Sci. Total. Environ.* **2020**, *729*, 138817. [CrossRef] [PubMed]
5. Vandoros, S. Excess mortality during the Covid-19 pandemic: Early evidence from England and Wales. *Soc. Sci. Med.* **2020**, *258*, 113101. [CrossRef]
6. Suárez, V.; Quezada, M.S.; Ruiz, S.O.; De Jesús, E.R. Epidemiology of COVID-19 in Mexico: From the 27th of February to the 30th of April 2020. *Rev. Clínica Española Engl. Ed.* **2020**. [CrossRef]
7. Friedman, J.; Calderón-Villarreal, A.; Bojorquez, I.; Hernández, C.V.; Schriger, D.L.; Hirashima, E.T. Excess Out-Of-Hospital Mortality and Declining Oxygen Saturation: The Sentinel Role of EMS Data in the COVID-19 Crisis in Tijuana, Mexico. *Ann. Emerg. Med.* **2020**. [CrossRef]
8. Zhang, L.; Yan, X.; Fan, Q.; Liu, H.; Liu, X.; Liu, Z.; Zhang, Z. D-dimer levels on admission to predict in-hospital mortality in patients with Covid-19. *J. Thromb. Haemost.* **2020**, *18*, 1324–1329. [CrossRef]
9. Lin, Z.; Long, F.; Yang, Y.; Chen, X.; Xu, L.; Yang, M. Serum ferritin as an independent risk factor for severity in COVID-19 patients. *J. Infect.* **2020**, *81*, 647–679. [CrossRef]
10. Sahu, B.R.; Kampa, R.K.; Padhi, A.; Panda, A.K. C-reactive protein: A promising biomarker for poor prognosis in COVID-19 infection. *Clin. Chim. Acta* **2020**, *509*, 91–94. [CrossRef]
11. Paul, P. Cardiac Troponin-I may be a predictor of complications and mortality in COVID-19 patients. *Curr. Med. Res. Pract.* **2020**, *10*, 130–131. [CrossRef] [PubMed]
12. Henry, B.M.; Aggarwal, G.; Wong, J.; Benoit, S.; Vikse, J.; Plebani, M.; Lippi, G. Lactate dehydrogenase levels predict coronavirus disease 2019 (COVID-19) severity and mortality: A pooled analysis. *Am. J. Emerg. Med.* **2020**, *38*, 1722–1726. [CrossRef] [PubMed]
13. Hu, R.; Han, C.; Pei, S.; Yin, M.; Chen, X. Procalcitonin levels in COVID-19 patients. *Int. J. Antimicrob. Agents* **2020**, *56*, 106051. [CrossRef] [PubMed]
14. Zhao, K.; Li, R.; Wu, X.; Zhao, Y.; Wang, T.; Zheng, Z.; Zeng, S.; Ding, X.; Nie, H. Clinical features in 52 patients with COVID-19 who have increased leukocyte count: A retrospective analysis. *Eur. J. Clin. Microbiol. Infect. Dis.* **2020**, 1–9. [CrossRef]
15. Zhao, Y.; Nie, H.-X.; Hu, K.; Wu, X.-J.; Zhang, Y.-T.; Wang, M.-M.; Wang, T.; Zheng, Z.-S.; Li, X.-C.; Zeng, S.-L. Abnormal immunity of non-survivors with COVID-19: Predictors for mortality. *Infect. Dis. Poverty* **2020**, *9*, 1–10. [CrossRef]
16. Liu, Y.; Du, X.; Chen, J.; Jin, Y.; Peng, L.; Wang, H.H.; Luo, M.; Chen, L.; Zhao, Y. Neutrophil-to-lymphocyte ratio as an independent risk factor for mortality in hospitalized patients with COVID-19. *J. Infect.* **2020**, *81*, e6–e12. [CrossRef]
17. Belice, T.; Demir, I.; Yüksel, A. Role of neutrophil-lymphocyte-ratio in the mortality of males diagnosed with COVID-19. *Iran. J. Microbiol.* **2020**, *12*, 194–197. [CrossRef]
18. Grenader, T.; Pavel, M.E.; Ruszniewski, P.B.; Ćwikła, J.B.; Phan, A.T.; Raderer, M.; Sedláčková, E.; Cadiot, G.; Wolin, E.M.; Capdevila, J.; et al. Prognostic value of the neutrophil/lymphocyte ratio in enteropancreatic neuroendocrine tumors. *Anti-Cancer Drugs* **2020**, *31*, 216–222. [CrossRef]
19. Ventriglia, J.; Petrillo, A.; Alváro, M.H.; Laterza, M.M.; Savastano, B.; Gambardella, V.; Tirino, G.; Pompella, L.; Diana, A.; Iovino, F.; et al. Neutrophil to Lymphocyte Ratio as a Predictor of Poor Prognosis in Metastatic Pancreatic Cancer Patients Treated with Nab-Paclitaxel plus Gemcitabine: A Propensity Score Analysis. *Gastroenterol. Res. Pract.* **2018**, *2018*, 2373868. [CrossRef] [PubMed]
20. Howard, R.; Kanetsky, P.A.; Egan, K.M. Exploring the prognostic value of the neutrophil-to-lymphocyte ratio in cancer. *Sci. Rep.* **2019**, *9*, 19670. [CrossRef] [PubMed]

21. Corman, V.M.; Landt, O.; Kaiser, M.; Molenkamp, R.; Meijer, A.; Chu, D.K.; Bleicker, T.; Brünink, S.; Schneider, J.; Schmidt, M.L.; et al. Detection of 2019 novel coronavirus (2019-nCoV) by real-time RT-PCR. *Eurosurveillance* **2020**, *25*, 2000045. [CrossRef] [PubMed]
22. Liu, J.; Li, S.; Liu, J.; Liang, B.; Wang, X.; Wang, H.; Li, W.; Tong, Q.; Yi, J.; Zhao, L.; et al. Longitudinal characteristics of lymphocyte responses and cytokine profiles in the peripheral blood of SARS-CoV-2 infected patients. *EBioMedicine* **2020**, *55*, 102763. [CrossRef] [PubMed]
23. Yan, X.; Li, F.; Wang, X.; Yan, J.; Zhu, F.; Tang, S.; Deng, Y.; Wang, H.; Chen, R.; Yu, Z.; et al. Neutrophil to lymphocyte ratio as prognostic and predictive factor in patients with coronavirus disease 2019: A retrospective cross-sectional study. *J. Med Virol.* **2020**. [CrossRef] [PubMed]
24. Basbus, L.; I Lapidus, M.; Martingano, I.; Puga, M.C.; Pollán, J. Neutrophil to lymphocyte ratio as a prognostic marker in COVID-19. *Medicina (B Aires)* **2020**, *80* (Suppl. 3), 31–36. [PubMed]
25. Tatum, D.; Taghavi, S.; Houghton, A.; Stover, J.; Toraih, E.; Duchesne, J. Neutrophil-to-Lymphocyte Ratio and Outcomes in Louisiana Covid-19 Patients. *Shock* **2020**. [CrossRef] [PubMed]
26. Zhang, J.-J.; Cao, Y.-Y.; Tan, G.; Dong, X.; Wang, B.-C.; Lin, J.; Yan, Y.-Q.; Liu, G.-H.; Akdis, M.; Akdis, C.A.; et al. Clinical, radiological and laboratory characteristics and risk factors for severity and mortality of 289 hospitalized COVID-19 patients. *Allergy* **2020**. [CrossRef]
27. Gormez, S.; Ekicibasi, E.; Degirmencioglu, A.; Paudel, A.; Erdim, R.; Gumusel, H.K.; Eroglu, E.; Tanboga, I.H.; Dagdelen, S.; Sariguzel, N.; et al. Association between renin–angiotensin–aldosterone system inhibitor treatment, neutrophil–lymphocyte ratio, D-Dimer and clinical severity of COVID-19 in hospitalized patients: A multicenter, observational study. *J. Hum. Hypertens.* **2020**. [CrossRef]
28. Zhang, H.; Cao, X.; Kong, M.; Mao, X.; Huang, L.; He, P.; Pan, S.; Li, J.; Lu, Z. Clinical and hematological characteristics of 88 patients with COVID-19. *Int. J. Lab. Hematol.* **2020**. [CrossRef]
29. Kolaczkowska, E.; Kubes, P. Neutrophil recruitment and function in health and inflammation. *Nat. Rev. Immunol.* **2013**, *13*, 159–175. [CrossRef]
30. Hemmat, N.; Derakhshani, A.; Baghi, H.B.; Silvestris, N.; Baradaran, B.; De Summa, S. Neutrophils, Crucial, or Harmful Immune Cells Involved in Coronavirus Infection: A Bioinformatics Study. *Front. Genet.* **2020**, *11*, 641. [CrossRef] [PubMed]
31. Feng, X.; Li, S.; Sun, Q.; Zhu, J.; Chen, B.; Xiong, M.; Cao, G. Immune-Inflammatory Parameters in COVID-19 Cases: A Systematic Review and Meta-Analysis. *Front. Med.* **2020**, *7*, 301. [CrossRef] [PubMed]
32. Chaplin, D.D. Overview of the immune response. *J. Allergy Clin. Immunol.* **2010**, *125*, S3–S23. [CrossRef] [PubMed]
33. Sakaguchi, S.; Yamaguchi, T.; Nomura, T.; Ono, M. Regulatory T cells and immune tolerance. *Cell* **2008**, *133*, 775–787. [CrossRef] [PubMed]
34. Taylor, A.; Verhagen, J.; Blaser, K.; Akdis, M.; Akdis, C.A. Mechanisms of immune suppression by interleukin-10 and transforming growth factor-beta: The role of T regulatory cells. *Immunology* **2006**, *117*, 433–442. [CrossRef] [PubMed]
35. Ziegler-Heitbrock, L.; Ancuta, P.; Crowe, S.; Dalod, M.; Grau, V.; Hart, D.N.; Leenen, P.J.M.; Liu, Y.-J.; MacPherson, G.; Randolph, G.J.; et al. Nomenclature of monocytes and dendritic cells in blood. *Blood* **2010**, *116*, e74–e80. [CrossRef]
36. Devêvre, E.F.; Renovato-Martins, M.; Clément, K.; Sautès-Fridman, C.; Cremer, I.; Poitou, C. Profiling of the Three Circulating Monocyte Subpopulations in Human Obesity. *J. Immunol.* **2015**, *194*, 3917–3923. [CrossRef]
37. Mukherjee, R.; Barman, P.K.; Thatoi, P.K.; Tripathy, R.; Das, B.K.; Ravindran, B. Non-Classical monocytes display inflammatory features: Validation in Sepsis and Systemic Lupus Erythematous. *Sci. Rep.* **2015**, *5*, 13886. [CrossRef]
38. Grün, J.L.; Manjarrez-Reyna, A.N.; Gómez-Arauz, A.Y.; León-Cabrera, S.; Rückert, F.; Fragoso, J.M.; Bueno-Hernández, N.; Islas-Andrade, S.; Melendez, G.; Escobedo, G. High-Density Lipoprotein Reduction Differentially Modulates to Classical and Nonclassical Monocyte Subpopulations in Metabolic Syndrome Patients and in LPS-Stimulated Primary Human Monocytes In Vitro. *J. Immunol. Res.* **2018**, *2018*, 2737040. [CrossRef]
39. Gatti, A.; Radrizzani, D.; Viganò, P.; Mazzone, A.; Brando, B. Decrease of non-classical and intermediate monocyte subsets in severe acute SARS-CoV -2 infection. *Cytom. Part A* **2020**, *97*, 887–890. [CrossRef]

40. Duque, G.A.; Descoteaux, A. Macrophage Cytokines: Involvement in Immunity and Infectious Diseases. *Front. Immunol.* **2014**, *5*, 491. [CrossRef]
41. Sanyaolu, A.; Okorie, C.; Marinkovic, A.; Patidar, R.; Younis, K.; Desai, P.; Hosein, Z.; Padda, I.; Mangat, J.; Altaf, M. Comorbidity and its Impact on Patients with COVID-19. *SN Compr. Clin. Med.* **2020**, *2*, 1069–1076. [CrossRef] [PubMed]

biomolecules

MDPI

Article

# Uric Acid Has Direct Proinflammatory Effects on Human Macrophages by Increasing Proinflammatory Mediators and Bacterial Phagocytosis Probably via URAT1

**Camilo P. Martínez-Reyes [1], Aarón N. Manjarrez-Reyna [1], Lucia A. Méndez-García [1], José A. Aguayo-Guerrero [1], Beatriz Aguirre-Sierra [1], Rafael Villalobos-Molina [2], Yolanda López-Vidal [3], Karen Bobadilla [4] and Galileo Escobedo [1,*]**

1 Laboratory for Proteomics and Metabolomics, Research Division, General Hospital of Mexico "Dr. Eduardo Liceaga", 06726 Mexico City, Mexico; nava111222@hotmail.com (C.P.M.-R.); aaron.manjarrez@gmail.com (A.N.M.-R.); angelica.mendez.86@hotmail.com (L.A.M.-G.); jose.aguayo01@iest.edu.mx (J.A.A.-G.); bety_agsi@hotmail.com (B.A.-S.)

2 Unidad de Biomedicina, Facultad de Estudios Superiores Iztacala, Universidad Nacional Autónoma de México, 54090 Mexico City, Mexico; villalobos@campus.iztacala.unam.mx

3 Programa de Inmunología Molecular Microbiana, Facultad de Medicina, Universidad Nacional Autónoma de México, 04510 Mexico City, Mexico; lvidal@unam.mx

4 Department of Immunology, Instituto Nacional de Enfermedades Respiratorias Ismael Cosío Villegas, 14080 Mexico City, Mexico; karenbolo@hushmail.com

* Correspondence: gescobedog@msn.com or gescobedo@unam.mx; Tel.: +52-(55)-2789-2000 (ext. 5646)

Received: 10 March 2020; Accepted: 5 April 2020; Published: 9 April 2020


**Abstract:** The relationship of uric acid with macrophages has not been fully elucidated. We investigated the effect of uric acid on the proinflammatory ability of human macrophages and then examined the possible molecular mechanism involved. Primary human monocytes were differentiated into macrophages for subsequent exposure to 0, 0.23, 0.45, or 0.9 mmol/L uric acid for 12 h, in the presence or absence of 1 mmol/L probenecid. Flow cytometry was used to measure proinflammatory marker production and phagocytic activity that was quantified as a percentage of GFP-labeled *Escherichia coli* positive macrophages. qPCR was used to measure the macrophage expression of the urate anion transporter 1 (URAT1). As compared to control cells, the production of tumor necrosis factor-alpha (TNF-alpha), toll-like receptor 4 (TLR4), and cluster of differentiation (CD) 11c was significantly increased by uric acid. In contrast, macrophages expressing CD206, CX3C-motif chemokine receptor 1 (CX3CR1), and C-C chemokine receptor type 2 (CCR2) were significantly reduced. Uric acid progressively increased macrophage phagocytic activity and downregulated URAT1 expression. Probenecid—a non-specific blocker of URAT1-dependent uric acid transport—inhibited both proinflammatory cytokine production and phagocytic activity in macrophages that were exposed to uric acid. These results suggest that uric acid has direct proinflammatory effects on macrophages possibly via URAT1.

**Keywords:** macrophage; uric acid; TNF-alpha; TLR4; phagocytosis; probenecid; URAT1

## 1. Introduction

In humans, monosodium urate—also referred to as uric acid—is the end-product of purine metabolism [1]. Uric acid is mainly excreted in urine and then reabsorbed in epithelial cells of the proximal convoluted tubule by urate transporters, such as the urate anion transporter 1 (URAT1), a transmembrane protein highly expressed in endothelial cells, adipocytes, and cartilage chondrocytes [2–5].

Normal blood levels of uric acid are 2.4–6.0 mg/dL for women and 3.4–7.0 mg/dL for men [6,7]. However, hyperuricemia is a pathological entity that is characterized by blood uric acid values beyond upper limits that has been largely associated with metabolic syndrome and increased cardiovascular risk [8–10]. In this sense, a recent study conducted in 22,983 Chinese adults demonstrated that subjects with hyperuricemia had higher prevalence of cardiovascular risk factors, such as dyslipidemia, hypertension, and type 2 diabetes (T2D), than individuals with normal uric acid values [11]. It is also worth mentioning that uric acid concentration associated directly with the number of cardiovascular risk factors; in other words, the cardiovascular risk increases as the uric acid elevates in blood.

The association of hyperuricemia with cardiovascular diseases is accompanied by a low-grade inflammation state that is characterized by increased proinflammatory activation of macrophages [11,12]. In this regard, the exposure of ApoE$^{-/-}$ mice to allopurinol (an inhibitor of uric acid production) does not only reduce atherosclerotic plaque size, but also macrophage infiltration and the expression of tumor necrosis factor-alpha (TNF-alpha) and interleukin (IL-) 1 beta, both typical proinflammatory cytokines [12]. Thus, such a seminal work proposed, for the first time, a relationship between uric acid and macrophages in the scenario of cardiovascular disease.

Macrophages are innate immune cells that differentiate from monocytes and play prominent roles in phagocytosis, inflammation, and wound healing [13]. Macrophages exhibit extremely high plasticity by exerting the ability of orchestrating either proinflammatory responses or anti-inflammatory actions, depending on the extracellular milieu [14]. In the presence of prototypical molecules, such as lipopolysaccharide (LPS) and/or interferon gamma (IFN-gamma), human macrophages show proinflammatory functions by producing TNF-alpha, IL-1 beta, CD11c, and toll-like receptor 4 (TLR4) [15,16]. On the contrary, the exposure of macrophages to dexamethasone or cytokines, such as interleukin IL-4 and IL-13, leads these cells to adopt an anti-inflammatory profile that is characterized by the production of IL-10 and/or CD206 [15]. Furthermore, the exposure of macrophages to pro- or anti-inflammatory stimuli also affects the expression of molecules that are involved in leukocyte trafficking, such as CX3C-motif chemokine receptor 1 (CX3CR1) and C-C chemokine receptor type 2 (CCR2) [17,18]. More importantly, the inflammatory activation enhances the ability of macrophages to ingest bacteria with respect to that described in macrophages with anti-inflammatory functions [19,20].

Although previous evidence suggests that high uric acid levels associate with increased proinflammatory activity of human macrophages, there is not yet conclusive data in this respect. For this reason, we investigated the effect of increasing uric acid concentrations on the proinflammatory or anti-inflammatory ability of primary human macrophages in vitro, and then examined the possible molecular mechanism involved.

## 2. Materials and Methods

### *2.1. Subjects*

Human monocytes were isolated from buffy coat suspensions of ten healthy male volunteers aged 18–35 years with no metabolic alterations, attending the Blood Bank of the General Hospital of Mexico. All of the participants provided written informed consent, being previously approved by the institutional ethical committee of the General Hospital of Mexico (registration number of the ethical code approval: DIC/11/UME/05/029), which guaranteed that the study was conducted in rigorous adherence to the principles that were described in the 1964 Declaration of Helsinki and its posterior amendment in 2013. Blood donors were excluded of the study if they had previous diagnosis of type 1 *Diabetes Mellitus* (T1D), T2D, cardiovascular disease, acute or chronic liver disease, acute or chronic renal disease, cancer, endocrine disorders, infectious diseases, and inflammatory or autoimmune disease. We also excluded of the study to HIV, HCV, and HBV-seropositive patients, and subjects with anti-inflammatory, antiplatelet drugs, anti-hypertensive, and immunomodulatory medication, including non-steroidal anti-inflammatory drugs.

### 2.2. Monocyte Isolation and Macrophage Culture

Buffy coat suspensions ($n = 10$) were separately diluted 1:2 with PBS1X (Sigma Aldrich, St. Louis, MO, USA) for the subsequent isolation of peripheral blood mononuclear cells (PBMCs) by density gradient centrifugation while using histopaque-1077 (Sigma Aldrich, St. Louis, MO, USA). The monocytes were then isolated from PBMCs by CD14-negative selection using magnetic columns (Miltenyi Biotec, Bergisch Gladbach, Germany). Purified monocytes were placed in RPMI-1640 medium (Sigma Aldrich, St. Louis, MO, USA) containing 10% fetal bovine serum (FBS) (Gibco™, Grand Island, NY, USA), 2 mM L-glutamine, 50 µg/mL gentamicin, and 10 ng/mL macrophage-colony stimulating factor (M-CSF) (Gibco™, Grand Island, NY, USA) in six-well cell-culture plates (Costar, Kennebunk, ME, USA), at a density of $3 \times 10^6$ monocytes per well. Culture media and M-CSF were replaced every other day for seven days. Upon differentiation, the monocyte-derived macrophages (MDM) were cultured in RPMI-1640 medium supplemented, as mentioned above and exposed to 0.23, 0.45, or 0.9 mmol/L uric acid (Sigma Aldrich, St. Louis, MO, USA) for 12 h. After performing several time-response curves at 1, 3, 6, and 12 h, and one, three, six, and nine days, we found that MDM exhibited the most significant proinflammatory activity at 12 h of in vitro culture in the presence of uric acid, and we decided to perform all experiments at this time. Prior uric acid exposure, 1 mmol/L probenecid—a non-specific blocker of URAT1-dependent uric acid transport (St. Louis, MO, USA)—was added and replaced after 6 h by culture media that contained different uric acid concentrations. Control MDM were placed in supplemented RPMI-1640 medium in the absence of uric acid for the same time. Immediately after, MDM were collected while using sterile cell scrapers (Corning, Reynosa, Tamaulipas, Mexico) and equally divided into 1 mL PBS1X (Sigma Aldrich, St. Louis, MO, USA) for flow cytometry analysis or 300 µL TRIzol Reagent (Life Technologies, Carlsbad, CA, USA) for quantitative polymerase chain reaction (qPCR) assays.

### 2.3. Flow Cytometry Assays

After collecting the cells, $1 \times 10^6$ MDM were resuspended in 50 µL Cell Staining Buffer (BioLegend, Inc., San Diego, CA, USA). Subsequently, the cells were incubated with anti-CD14 PE/Cy7, anti-CD206 APC/Cy7, anti-TLR4 PE, anti-CX3CR1 BV510, anti-CCR2 AF647 (BioLegend, Inc., San Diego, CA, USA), and 5 µL True-Stain Monocyte Blocker™ (BioLegend, Inc., San Diego, CA, USA) for 20 min. in darkness at 4 °C. After being rinsed with Cell Staining Buffer (BioLegend, Inc., San Diego, CA, USA), MDM were incubated with 7-AAD (BD Pharmingen™, San Jose, CA, USA) for 10 min. for subsequent analysis on a FACSCanto II flow cytometer (BD Biosciences, San Jose, CA, USA) by means of BD FACSDiva™ software 6.0, acquiring 20,000 events per test in triplicate. The compensation controls were performed using UltraComp eBeads™ (Invitrogen, Carlsbad, CA, USA) for each fluorochrome. Flow cytometry data were analyzed using the FlowJo 10.0.7 software (TreeStar, Inc, Ashland, OR, USA). For intracellular cytokine stain, MDM were treated with 1:1000 Brefeldin A (BioLegend, Inc., San Diego, CA, USA) for the last 2 h of in vitro culture. After collecting cells, $1 \times 10^6$ MDM were resuspended in 50 µL Cell Staining Buffer (BioLegend, Inc., San Diego, CA, USA). Immediately after, the MDM were simultaneously incubated with anti-CD14 PE/Cy7, anti-CD11c PE/Cy5, Zombie UV Fixable Viability Kit, and 5 µL True-Stain Monocyte Blocker™ (BioLegend, Inc., San Diego, CA, USA) for 20 min. in darkness at 4 °C. Afterwards, MDM were incubated with 100 µL Fixation Medium A (FIX & PERM™ Cell Permeabilization Kit) (Invitrogen™, Carlsbad, CA, USA) for 15 min. at room temperature. Afterwards, MDM were rinsed with Cell Staining Buffer (BioLegend, Inc., San Diego, CA, USA) for subsequent incubation with 100 µL Permeabilization Medium B (FIX & PERM™ Cell Permeabilization Kit) (Invitrogen™, Carlsbad, CA, USA), and anti-TNF-alpha AF488 and anti-IL-1 beta Pacific Blue for 20 min. in darkness at room temperature. Immediately after, the MDM were rinsed with Cell Staining Buffer (BioLegend, Inc., San Diego, CA, USA) and then acquired on a BD Influx flow cytometer (BD Biosciences, San Jose, CA, USA) by means of BD Sortware™ software 1.2, acquiring 20,000 events per test in triplicate. Compensation controls were performed using UltraComp eBeads™

(Invitrogen™, Carlsbad, CA, USA) for each fluorochrome. Flow cytometry data were analyzed while using the FlowJo 10.0.7 software (TreeStar, Inc, Ashland, OR, USA).

### *2.4. Macrophage Phagocytic Activity*

*Escherichia coli* of the strain DH5a were transformed while using the green fluorescent protein (GFP)-mut2 encoding plasmid pCD353 (*E. coli*-GFP+) that is regulated by a lactac promoter. GFP was induced using 1mM isopropyl-b-D-1-thiogalactopyranoside (Sigma Aldrich, St. Louis, MO, USA), as previously described [21]. *E. coli*-GFP+ were in vitro cultured with macrophages in a ratio of bacteria:cells = 30:1 for 1 h. Afterwards, cell suspensions were centrifuged at 2500 rpm/15 min. to remove remnant bacteria and then resuspended in 50 µL of sterile PBS 1X for posterior analysis on a FACSCanto II flow cytometer (BD Biosciences, San Jose, CA, USA) by means of BD FACSDiva™ software 6.0, acquiring 20,000 events per test in triplicate.

### *2.5. URAT1 Gene Expression by qPCR*

After collecting cells, $1 \times 10^6$ MDM were resuspended in TRIzol Reagent (Life Technologies, Life Technologies, Carlsbad, CA, USA) at 4 °C. Immediately after, the total RNA was isolated by the phenol/chloroform/guanidine isothiocyanate method according to the manufacturer's instructions. Total RNA samples were quantified and subjected to reverse transcription using the M-MLV Retrotranscriptase system in the presence of dT primer (Invitrogen, Carlsbad, CA, USA). After being incubated at 37 °C for 60 min., cDNA samples were obtained and used for amplification while using the real-time polymerase chain reaction (qPCR) in the presence of SYBR Green Master Mix and AmpliTaq® Fast DNA Polymerase (Applied biosystems, Foster City, CA, USA), according to the manufacturer's instructions. Human-specific primers for URAT1 were designed using the Primer-BLAST software from the National Center for Biotechnology Information (NCBI), U.S. National Library of Medicine, as follows: forward primer 5′-CGGACCTGTATCTCCACGTT-3′, reverse primer 5′-TGCCTTCTTTACTGCCTGGT-3′, denaturation at 94 °C for 30 s, annealing at 60 °C for 45 s, elongation at 72 °C for 45 s, and 28 thermal cycles for a 570 base pair (bp) product length. The 18S-ribosomal RNA sequence was used as house-keeping gene control as follows: forward primer 5′-CGCGGTTCTATTTTGTTGGT-3′, reverse primer 5′-AGTCGGCATCGTTTATGGTC-3′, denaturation at 94 °C for 30 s, annealing at 60 °C for 30 s, elongation at 72 °C for 30 s, and 40 thermal cycles for a 570 bp product length. URAT1 mRNA expression was normalized using the house-keeping gene control and reported as 2^(ΔΔCt). The qPCR experiments are reported according to the Minimum Information for Publication of Quantitative Real-Time PCR Experiments (MIQE) guidelines to guarantee reproducibility.

### *2.6. Statistics*

The Shapiro–Wilk test estimated the normality of data distribution. One-way ANOVA, followed by a post-hoc Tukey test, was used to compare the expression of CD11c, CD206, TNF-alpha, IL-1 beta, TLR4, CX3CR1, CCR2, and URAT1, as well as the intracellular amount of *E. coli*-GFP+ in monocyte-derived macrophages that were exposed to 0, 0.23, 0.45, or 0.9 mmol/L uric acid. All of the statistical analyses were performed using the GraphPad Prism 7 software. Differences were considered to be significant when $p < 0.05$.

## 3. Results

Upon differentiation in the presence of M-CSF for seven days, human monocyte-derived macrophages (MDM) showed significantly higher cell size than monocytes (Figure 1A,B). Furthermore, while monocytes exhibited a typical appearance that consisted of round cells, differentiated MDM appeared as fusiform-shaped cells with numerous pseudopodia that increased their cell complexity with respect to monocytes (Figure 1A,B). Additionally, macrophage differentiation was also confirmed by means of CD14 cell surface expression. In this sense, MDM showed a significant 20% reduction in CD14 expression when compared to that found in monocytes (Figure 1C). Once gated for singlets

on a forward scatter height/forward scatter area density plot (Figure 1D), the living cells were gated while using the 7-AAD staining for dead cells. The living monocytes were then gated on a forward scatter area/side scatter area plot to assess CD14 positive expression together with TNF-alpha, IL-1 beta, CD11c, CD206, and CX3CR1, and CCR2 (Figure 1D).

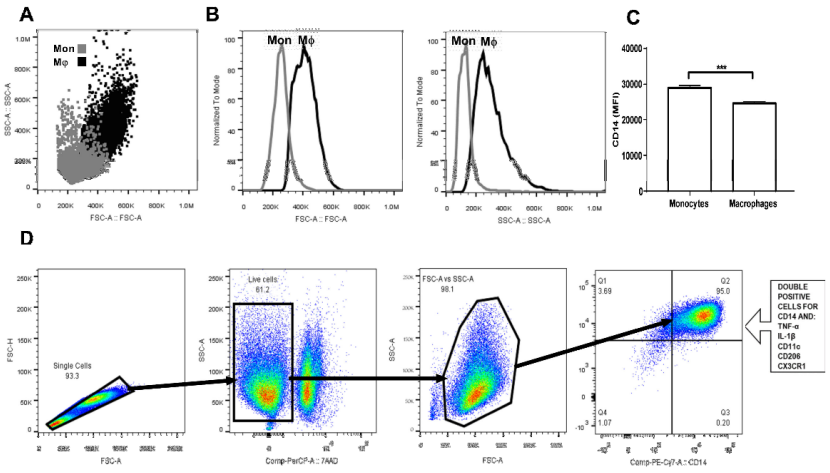


**Figure 1.** Gating strategy for primary human monocyte-derived macrophage characterization. Primary human monocytes were isolated from buffy coat suspensions ($n$ = 10) and differentiated into macrophages in the presence of M-CSF for seven days. (**A**) Dot plot showing a comparison between monocytes (grey dots) and macrophages (black dots) in terms of cell size and complexity. (**B**) Macrophages are considerably larger and more complex than monocytes. (**C**) As previously reported, macrophages exhibit significantly decreased CD14 cell surface expression as compared to that found in monocytes. (**D**) Monocyte-derived macrophages (MDM) were gated for singlets on a forward scatter height/forward scatter area density plot. Resulting cells were gated again for detection of living macrophages by means of the 7AAD or Zombie UV stains. Macrophages were then gated on a side scatter area/forward scatter area density plot for detection of CD14+ cells that simultaneously expressed tumor necrosis factor-alpha (TNF-alpha), interleukin (IL-1) beta, CD11c, CD206, CX3CR1, and CCR2. Mon, monocyte population; Mϕ, macrophage population; MFI, mean fluorescence intensity; FSC-H, forward scatter height density plot; FSC-A, forward scatter area density plot; SSC-A, side scatter area density plot; TNF-a, tumor necrosis factor alpha; IL-1b, interleukin 1 beta; CD11c, cluster of differentiation 11c; CD206, cluster of differentiation 206 or mannose receptor; CX3CR1, CX3C-motif chemokine receptor 1; CCR2, C-C chemokine receptor type 2; M-CSF, macrophage-colony stimulating factor.

Regarding the production of proinflammatory cytokines, the exposure of MDM to increasing uric acid concentrations tended to raise the number of TNF-alpha+ cells, although no significant changes were reached (Figure 2A). However, MDM in vitro cultured in the presence of 0.23 mmol/L uric acid showed a significant 25% increase in TNF-alpha production with respect to that found in the control cells (Figure 2B). No significant differences were found when compared MDM exposed to 0.45 or 0.9 mmol/L uric acid with control cells, thus suggesting that uric acid exerts its effects on TNF-alpha production in a dose-dependent fashion (Figure 2B). Despite exposure of MDM to increasing uric acid levels tended to diminish either the number of IL-1 beta+ cells or IL-1 beta production, no significant differences were found (Figure 2C,D, respectively).

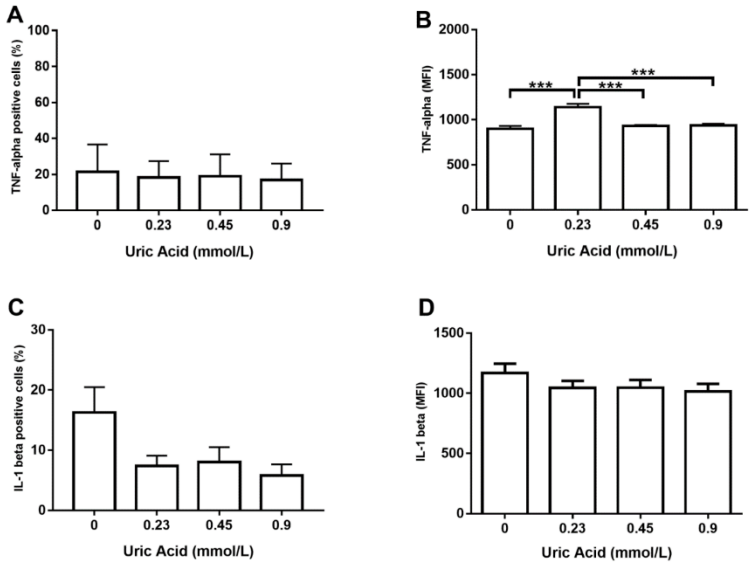


**Figure 2.** Intracellular production of TNF-alpha and IL-1 beta in primary human monocyte-derived macrophages in vitro exposed to uric acid. In vitro exposure to increasing concentrations of uric acid did not alter the percentage of primary human monocyte-derived macrophages expressing TNF-alpha (**A**). In vitro exposure to 0.23 mmol/L uric acid significantly increased TNF-alpha production in primary human monocyte-derived macrophages as compared to control cells (0 mmol/L uric acid) (**B**). In vitro exposure to increasing concentrations of uric acid tended to decrease the percentage of primary human monocyte-derived macrophages expressing IL-1 beta, although no significant differences were found (**C**). In vitro exposure to increasing concentrations of uric acid did not alter IL-1 beta production in primary human monocyte-derived macrophages (**D**). Data were analyzed using one-way ANOVA followed by the post-hoc Tukey test to estimate significant differences. Data are expressed as mean ± standard deviation. Differences were considered significant when $p < 0.05$ and are marked with asterisks as follows: *** = $p < 0.0001$. TNF-alpha, tumor necrosis factor alpha; IL-1 beta, interleukin 1 beta; MFI, mean fluorescence intensity.

We decided to measure TLR4 production as a key regulator of TNF-alpha synthesis since exposure of MDM to uric acid increased the expression of TNF-alpha, but not IL-1 beta. In this sense, uric acid induced TLR4 expression on MDM in a dose-dependent fashion, even though no significant differences were reached in terms of the number of TLR4+ cells (Figure 3A). However, exposure of MDM to 0.23 mmol/L uric acid promoted a significant 30% increase in TLR4 production in a very similar way than that observed for the case of TNF-alpha (Figure 3B). TNF-alpha positive macrophages have been also shown to produce CD11c, an integrin that is highly expressed in proinflammatory monocytes recruited toward atherosclerotic plaques. Uric acid did not affect the number of MDM expressing CD11c (Figure 3C); however, uric acid increased CD11c expression on MDM in a dose-dependent fashion, reaching the highest production of this integrin at 0.23 and 0.45 mmol/L uric acid (Figure 3D).

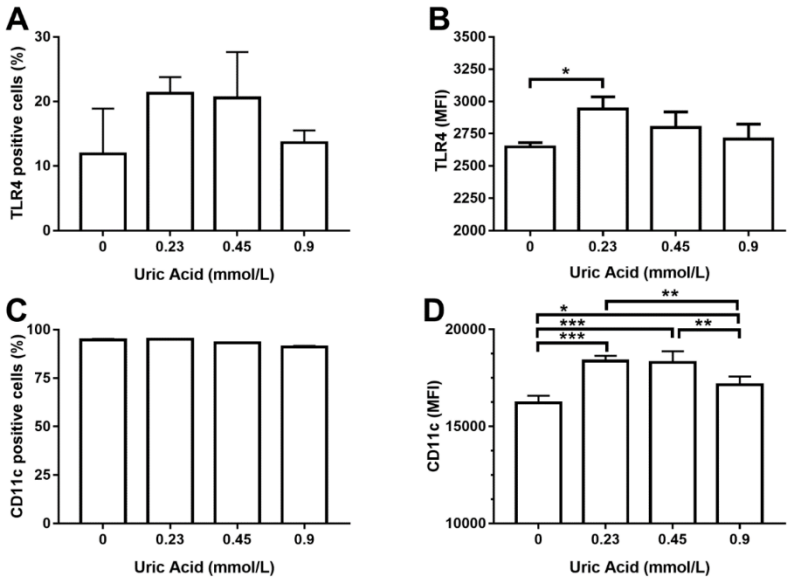


**Figure 3.** Cell surface expression of TLR4 and CD11c in primary human monocyte-derived macrophages in vitro exposed to uric acid. In vitro exposure to increasing concentrations of uric acid did not alter the percentage of primary human monocyte-derived macrophages expressing TLR4 (**A**). In vitro exposure to 0.23 mmol/L uric acid significantly increased TLR4 production in primary human monocyte-derived macrophages as compared to control cells (0 mmol/L uric acid) (**B**). In vitro exposure to increasing concentrations of uric acid did not alter the percentage of primary human monocyte-derived macrophages expressing CD11c (**C**). In vitro exposure to 0.23, 0.45, and 0.9 mmol/L uric acid significantly altered CD11c production in primary human monocyte-derived macrophages in a dose-response manner as compared to control cells (0 mmol/L uric acid) (**D**). Data were analyzed using one-way ANOVA, followed by the post-hoc Tukey test to estimate significant differences. Data are expressed as mean ± standard deviation. Differences were considered to be significant when $p < 0.05$ and are marked with asterisks as follows: * = $p < 0.01$; ** = $p < 0.001$; *** = $p < 0.0001$. TLR4, toll-like receptor 4; CD11c, cluster of differentiation 11c; MFI, mean fluorescence intensity.

It is well known that macrophages gain proinflammatory ability while losing the anti-inflammatory capacity. For this reason, we wanted to measure CD206 production, a typical anti-inflammatory marker of human and murine macrophages. As expected, the exposure of MDM to increasing levels of uric acid progressively reduced the number of cells expressing CD206 with respect to control cells (Figure 4A). Overall, uric acid did not affect CD206 expression in MDM, except for 0.45 mmol/L uric acid that induced a slight increase in the expression of this anti-inflammatory marker (Figure 4B).

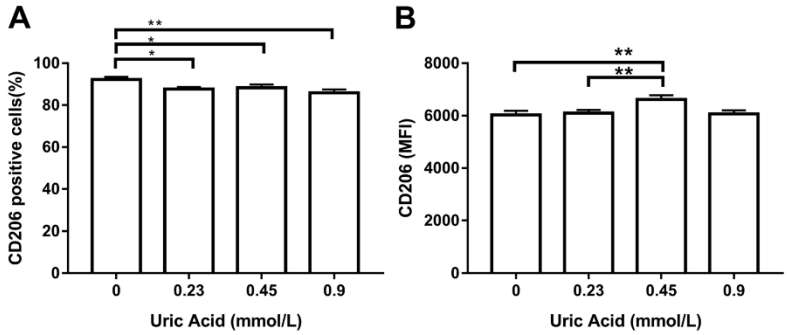


**Figure 4.** Cell surface expression of CD206 in primary human monocyte-derived macrophages in vitro exposed to uric acid. In vitro exposure to 0.23, 0.45, and 0.9 mmol/L uric acid significantly decreased the percentage of primary human monocyte-derived macrophages expressing CD206 as compared to control cells (0 mmol/L uric acid) (**A**). In vitro exposure to 0.45 mmol/L uric acid significantly increased CD206 production in primary human monocyte-derived macrophages as compared to control cells (0 mmol/L uric acid) (**B**). Data were analyzed using one-way ANOVA followed by the post-hoc Tukey test to estimate significant differences. Data are expressed as mean ± standard deviation. Differences were considered significant when $p < 0.05$ and are marked with asterisks as follows: * = $p < 0.01$; ** = $p < 0.001$. CD206, cluster of differentiation 206 or mannose receptor; MFI, mean fluorescence intensity.

We decided to examine the effect of this metabolite on the expression of CX3CR1 and CCR2, two chemokine receptors that decreases in proinflammatory macrophages. The exposure of MDM to uric acid progressively diminished the number of CX3CR1+ macrophages, reaching the maximum response when cells were incubated in the presence of 0.9 mmol/L uric acid (Figure 5A). Likewise, uric acid gradually reduced CX3CR1 expression in MDM as compared to that found in the control cells (Figure 5B). In parallel, the exposure of MDM to uric acid gradually decreased the number of cells expressing CCR2, reaching the lowest level of this chemokine receptor when using 0.9 mmol/L uric acid (Figure 5C). As expected, uric acid also diminished CCR2 expression in MDM at 0.45 and 0.9 mmol/L and provided solid experimental evidence that CX3CR1 and CCR2 production behaves similarly in macrophages that were exposed either to LPS or uric acid.

Proinflammatory activation of human macrophages is also associated with an increased ability to phagocytose bacteria. Thus, we evaluated the effect of increasing uric acid concentrations on the phagocytic activity of MDM while using *E. coli*-GFP+. In the absence of uric acid, MDM were able to ingest around 15% of *E. coli*-GFP+ (Figure 6). Notably, the exposure of MDM to 0.23 mmol/L uric acid induced a significant 26% increase in the intracellular number of *E. coli*-GFP+ as compared to control cells (Figure 6). Accordingly, MDM exposed to 0.45 and 0.9 mmol/L uric acid showed significant 40 and 120% increases, respectively, in the intracellular amount of *E. coli*-GFP+ as compared to control cells (Figure 6), which confirmed that uric acid acts as a proinflammatory stimulus for in vitro cultured human macrophages.

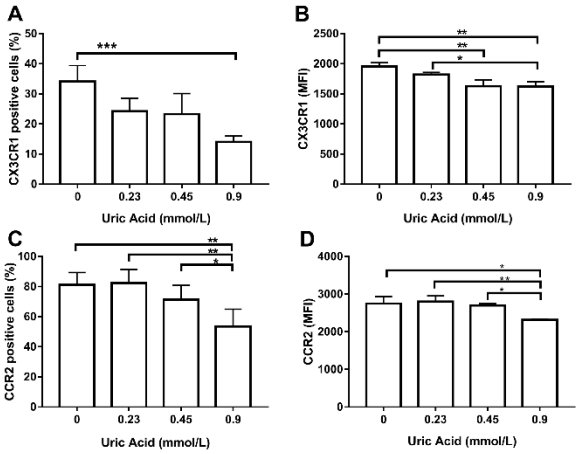


**Figure 5.** Cell surface expression of CX3CR1 and CCR2 in primary human monocyte-derived macrophages in vitro exposed to uric acid. In vitro exposure to 0.9 mmol/L uric acid significantly decreased the percentage of primary human monocyte-derived macrophages expressing CX3CR1 as compared to control cells (0 mmol/L uric acid) (**A**). In vitro exposure to 0.45 and 0.9 mmol/L uric acid significantly decreased CX3CR1 production in primary human monocyte-derived macrophages as compared to control cells (0 mmol/L uric acid) (**B**). In vitro exposure to 0.9 mmol/L uric acid significantly decreased the percentage of primary human monocyte-derived macrophages expressing CCR2 as compared to control cells (0 mmol/L uric acid (**C**). In vitro exposure to 0.9 mmol/L uric acid significantly decreased CCR2 production in primary human monocyte-derived macrophages as compared to control cells (0 mmol/L uric acid) (**D**). Data were analyzed using one-way ANOVA followed by the post-hoc Tukey test to estimate significant differences. Data are expressed as mean ± standard deviation. Differences were considered to be significant when $p < 0.05$ and are marked with asterisks as follows: * = $p < 0.01$; ** = $p < 0.001$; *** = $p < 0.0001$. CX3CR1, CX3C-motif chemokine receptor 1; CCR2, C-C chemokine receptor type 2; MFI, mean fluorescence intensity.

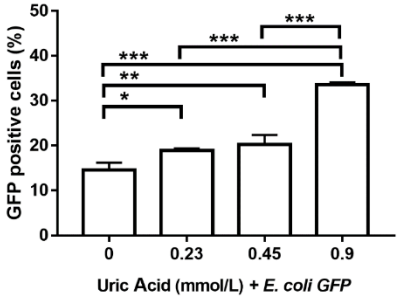


**Figure 6.** Bacterial phagocytic activity of primary human monocyte-derived macrophages in vitro exposed to uric acid. In vitro exposure to 0.23, 0.45, and 0.9 mmol/L uric acid significantly enhanced the phagocytic activity of primary human monocyte-derived macrophages by progressively increasing the percentage of *Escherichia coli*-green fluorescent protein (GFP) positive cells as compared to controls (0 mmol/L uric acid). Data were analyzed using one-way ANOVA followed by the post-hoc Tukey test to estimate significant differences. Data are expressed as mean ± standard deviation. Differences were considered significant when $p < 0.05$ and are marked with asterisks as follows: * = $p < 0.01$; ** = $p < 0.001$; *** = $p < 0.0001$. GFP, green fluorescent protein; *E. coli*, *Escherichia coli*.

An additional goal of this work was to explore the possible molecular mechanism by which uric acid exerts its effects on human monocyte-derived macrophages. For this reason, we decided to evaluate URAT1 expression, a key mediator of uric acid transport inside the cell. Notably, the exposure of MDM to 0.23 mmol/L uric acid induced a significant 90% reduction in URAT1 expression when compared to that found in control cells cultured in the absence of this metabolite (Figure 7). Similarly, MDM exposed to 0.45 mmol/L uric acid showed a significant 95% decrease in the mRNA levels of URAT1 with respect to that found in control cells (Figure 7). It is worth mentioning that exposure of MDM to 0.9 mmol/L uric acid totally abolished URAT1 expression (Figure 7), thus suggesting that URAT1 is sensitive to uric acid concentrations and it may take part in mediating the effects of this metabolite on macrophages.

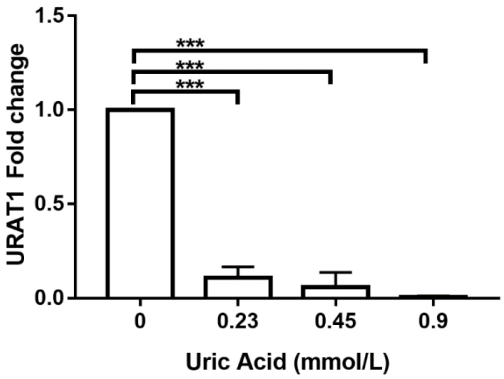


**Figure 7.** URAT1 expression in primary human monocyte-derived macrophages in vitro exposed to uric acid. In vitro exposure to 0.23, 0.45, and 0.9 mmol/L uric acid progressively abolished URAT1 expression in primary human monocyte-derived macrophages as compared to controls (0 mmol/L uric acid). URAT1 expression was normalized using the 18S-ribosomal RNA gene as house-keeping control gene and reported as 2^(ΔΔCt)-fold change by real-time polymerase chain reaction (qPCR) using SYBR Green Master Mix and AmpliTaq® Fast DNA Polymerase. Data were analyzed using one-way ANOVA followed by the post-hoc Tukey test to estimate significant differences. Data are expressed as mean ± standard deviation. Differences were considered significant when $p < 0.05$ and are marked with asterisks as follows: *** = $p < 0.0001$. URAT1, urate anion transporter 1.

We decided to use probenecid that is able to inhibit URAT1-dependent uric acid transport also examining its effect on TNF-alpha production and phagocytic activity to confirm the apparent involvement of URAT1 in macrophages. As expected, the use of probenecid totally abolished TNF-alpha production in macrophages that were also exposed to different concentrations of uric acid (Figure 8A). Likewise, probenecid also induced an 11% decrease in the intracellular number of *E. coli*-GFP+ macrophages that were treated with 0.23 mmol/L uric acid (Figure 8B). Furthermore, MDM treated with probenecid showed significant 78 and 61% reductions in the percentage of *E. coli*-GFP+, even in the presence of 0.45 and 0.9 mmol/L uric acid, respectively (Figure 8B). These results functionally suggest that uric acid might be transported inside the macrophage via URAT1 that, in turn, could mediate its proinflammatory effects on these immune cells.

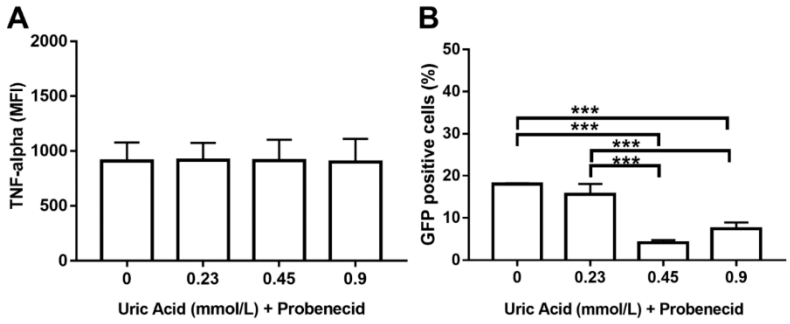


**Figure 8.** Probenecid seems to abolish URAT1-dependent proinflammatory effects of uric acid on primary human monocyte-derived macrophages. In vitro exposure to 1 mmol/L probenecid abolished the stimulatory effect of uric acid on TNF-alpha production in primary human monocyte-derived macrophages as compared to cells exposed to uric acid in the absence of probenecid (**A**). In vitro exposure to 1 mmol/L probenecid significantly decreased the stimulatory effect of uric acid on the phagocytic activity of primary human monocyte-derived macrophages by decreasing the percentage of Escherichia coli-GFP positive cells as compared to macrophages exposed to uric acid in the absence of probenecid (**B**). Data were analyzed using one-way ANOVA followed by the post-hoc Tukey test to estimate significant differences. Data are expressed as mean ± standard deviation. Differences were considered significant when $p < 0.05$ and are marked with asterisks, as follows: *** = $p < 0.0001$. TNF-a, tumor necrosis factor alpha; MFI, mean fluorescence intensity; GFP, green fluorescent protein.

## 4. Discussion

The association of hyperuricemia with the risk of developing metabolic abnormalities and cardiovascular diseases has been linked to an increased proinflammatory activity of macrophages [22,23]. However, it remains unknown whether hyperuricemia merely concurs with changes in macrophage activity or if uric acid is able to directly induce proinflammatory activation of human macrophages. For this reason, we decided to test the in vitro effect of increasing the uric acid concentrations on the proinflammatory profile of primary human macrophages differentiated from circulating monocytes.

We found that uric acid stimulates TNF-alpha production, but not IL-1 beta, in a dose-dependent fashion after confirming that human monocytes were properly differentiated into macrophages using a strategy that combined cell size and complexity as well CD14 expression. TNF-alpha and IL-1 beta are proinflammatory cytokines that play key roles in fever, cachexia, tumorigenesis inhibition, pyroptosis-related cell death, and immune cell recruitment [24–26]. However, TNF-alpha, but not IL-1 beta, has been consistently associated with increased serum levels of uric acid in several pathologic scenarios. For instance, the serum uric acid levels rise as TNF-alpha-producing monocytes also increase in women with preeclampsia [27]. Similarly, uric acid has been shown to stimulate TNF-alpha expression in vascular smooth muscle cells of Sprague–Dawley rats [28]. On the other hand, plasma IL-1 beta showed very poor association with increasing serum levels of uric acid in 1684 women and men, whereas TNF-alpha serum values rose in the same proportion than plasma uric acid [10]. Together with previous information, our results provide strong experimental evidence that uric acid might favor a proinflammatory state by predominantly stimulating TNF-alpha production in human macrophages. It is well known that TNF-alpha synthesis depends on the TLR4-dependent signaling pathway, whereas IL-1 beta production depends on the activity of the NLRP3 (NOD-LRR-and pyrin domain-containing protein 3) inflammasome [29–31]. For this reason, we decided to assess TLR4 in the same in vitro differentiated macrophages.

TLR4 is a transmembrane protein that is able to recognize numerous damage-associated molecular patterns (DAMP) and pathogen-associated molecular patterns (PAMPs), including free-fatty acids and

LPS [32,33]. Upon activation, TLR4 is capable of inducing downstream nuclear factor-kappa B (NF-kB) activation, finally leading to TNF-alpha production [34]. Concurring with this information, our results demonstrate that TLR4 is produced in response to uric acid in the same way that TNF-alpha does in human macrophages. In this regard, a previous work reported that the risk of gout—a pathology known by deposition of monosodium urate crystals in joints—is directly associated with the polymorphism rs2149356 related to high TLR4 production [35]. Likewise, a very recent study demonstrated that uric acid promotes the mRNA expression of TLR4 in rat adipocytes in vitro [36]. Thus, we speculate that uric acid is able to induce TNF-alpha production via TLR4 activation, a phenomenon that provides proinflammatory features to human macrophages. However, the idea that uric acid can activate TLR4 should be taken with caution, since we only evaluated TLR4 at the protein level without assessing its ability as a cell signal transducer.

Until here, our results appeared to indicate that uric acid exerts the ability to polarize human macrophages towards a proinflammatory state. Thus, we decided to confirm the apparently proinflammatory capacity of macrophages by analyzing CD11c and CD206. CD11c is a beta-2 integrin that is highly expressed in monocytes and macrophages with prominent proinflammatory functions, whereas CD206—also referred to as the mannose receptor—is a C-type lectin that is predominantly expressed in murine and human macrophages exerting anti-inflammatory actions [37–39]. Interestingly, we found that uric acid is able to increase CD11c production at the same time, which reduces the number of macrophages expressing CD206. In this sense, it has been previously reported that blockage of uric acid synthesis by uricase treatment decreases the number of CD11c+ monocytes in mice [40], which suggested, for the first time, a relationship between uric acid and CD11c production. In parallel, a previous report showed that macrophages from synovial fluid of patients with gout tend to show reduced CD206 expression as compared to that found in the macrophages of patients with rheumatoid arthritis [41]. Altogether, this information concurs with the idea that macrophages adopt proinflammatory functions while losing anti-inflammatory capacities in the presence of elevated levels of uric acid.

The idea that uric acid might act as a direct proinflammatory stimulus for human macrophages is also supported by two additional facts: (a) the expression pattern of CX3CR1 and CCR2 and (b) the phagocytic activity of macrophages. CX3CR1 and CCR2 are both involved in mediating monocyte recruitment to the inflammation sites, where these cells will differentiate into macrophages and orchestrate inflammatory responses or tissue repair [42,43]. Interestingly, numerous studies have consistently reported the downregulation of CX3CR1 and CCR2 in the presence of prototypical inflammatory stimuli, such as LPS. In this sense, a seminal work reported that circulating monocytes either of septic patients or incubated with LPS show dramatically decreased CX3CR1 expression [44]. Similarly, in vitro and in vivo exposure of murine peripheral blood cells to LPS can downregulate CCR2 expression with direct consequences for macrophage migratory ability [45,46]. Therefore, CX3CR1 and CCR2 expression appears to behave similarly in macrophages that are exposed either to LPS or uric acid, which provides solid experimental evidence regarding the possible inflammatory role of this metabolite in macrophages. Additionally, it is well known that macrophages with proinflammatory functions show greater ability to phagocytose bacteria than that described in anti-inflammatory macrophages [19,20]. Interestingly, the exposure of macrophages to increasing uric acid concentrations progressively improved their phagocytic activity, which once again supports the notion that uric acid acts as a direct proinflammatory stimulus for these immune cells.

Besides studying the apparently proinflammatory effect of uric acid on macrophages, we also wanted to explore the molecular mechanism that is potentially involved. In our study, the production of TNF-alpha, TLR4, and CD11c in response to uric acid exhibited a typical dose-response relationship, where a maximum effect is found and, beyond this point, a plateau can be seen, which indicates saturation and the abolishment of the observed effect [47]. The dose-response relationship has been attributed to the interaction between ligand and its receptor [47,48], which suggested to us the possible involvement of a molecule able to transport uric acid inside the macrophage, as is the case of URAT1.

In this way, we describe for, the first time, that human macrophages express URAT1, a transmembrane protein that had been only reported in endothelial cells, adipocytes, and cartilage chondrocytes [5]. Notably, we found that URAT1 expression in macrophages decreased as uric acid concentration increased, which might partially explain the fact that TNF-alpha, TLR4, and CD11c expression reached a saturation point, which in turn led to a decrease their protein levels. Taking into consideration that uric acid can increase NF-kB transcriptional activity in the pancreatic beta cell line Min6 [49], we thus speculate that TNF-alpha production in macrophages might depend on the interaction among uric acid, URAT1, and possibly NF-kB.

We performed functional assays aimed to pharmacologically block this urate transporter using probenecid to confirm the possible involvement of URAT1 in mediating the effects of uric acid on macrophages. Probenecid acts as a competitive inhibitor of URAT1 thus preventing reuptake and transport of uric acid by cells of the renal proximal tube [50]. Interestingly, the blockage of URAT1 abolished TNF-alpha production and phagocytic activity previously seen with uric acid, which suggests that the proinflammatory effect of uric acid entirely depends on its entry to macrophages. In this regard, it has been previously proposed that the entry of monosodium urate to THP-1 cells can induce IkB phosphorylation via Src family tyrosine kinases, thus leading to NF-kB activation and, finally, proinflammatory cytokine production [51]. In this way, our results confirm that (1) the entry of uric acid to macrophages has proinflammatry effects by a mechanism that is still unknown, and (2) entry of uric acid to macrophages seems to involve URAT1, whose expression is, in turn, sensitive to different concentrations of uric acid. However, URAT1 is not the only urate transporter and probenecid is not a URAT1 specific inhibitor, so measuring in macrophages other urate transporters, including organic anion transporter (OAT) 1, OAT3, and ATP-binding cassette subfamily G member 2 (ABCG2), and testing other urate uptake inhibitors, such as benzbromarone, dotinurad, and losartan, remains to be done.

## 5. Conclusions

Uric acid acts as a proinflammatory stimulus for in vitro cultured primary human macrophages through (a) increasing the production of TNF-alpha, TLR4, and CD11c, (b) improving the macrophage phagocytic activity, and (c) decreasing CD206, CX3CR1, and CCR2 expression. The possible mechanism by which uric acid exerts its proinflammatory effects on human macrophages appears to involve URAT1 in a dose-response fashion. URAT1 might, in turn, enhance NF-kB activation and lead to the production of proinflammatory cytokines by ways that remain to be elucidated. The use of probenecid functionally demonstrated that the entry of uric acid to the macrophage (d) has proinflammatory actions and (e) partially depends on URAT1. These results provide solid experimental evidence supporting the idea that elevated levels of uric acid can directly promote the macrophage-mediated systemic inflammatory state that is, in turn, associated with high cardiovascular risk in patients with chronic diseases. The idea that uric acid might act as a metabolic ligand with proinflammatory effects on human macrophages should be further examined.

**Author Contributions:** Conceptualization, C.P.M.-R. and G.E.; methodology, C.P.M.-R., A.N.M.-R., J.A.A.-G., L.A.M.-G. and B.A.-S.; formal analysis, C.P.M.-R., A.N.M.-R., K.B. and G.E.; data curation, C.P.M.-R., A.N.M.-R., R.V.-M., Y.L.-V., K.B. and G.E.; writing—original draft preparation, C.P.M.-R. and G.E.; writing—review and editing, R.V.-M., Y.L.-V., K.B. and G.E.; funding acquisition, G.E. All authors have read and agreed to the published version of the manuscript.

**Funding:** This work was supported by grant no. CB-2016-01-286209 from the Fondo Sectorial de Investigación para la Educación-CONACYT-México and grant no. SALUD-2017-02-290345 from the Fondo Sectorial de Investigación y Desarrollo en Salud y Seguridad Social SS/IMSS/ISSSTE/CONACYT-México to GE.

**Acknowledgments:** Camilo Pablo Martinez Reyes is a doctoral student from the Programa de Doctorado en Ciencias Biomédicas, Universidad Nacional Autónoma de México (UNAM) and has received CONACyT fellowship 582451. Authors thank to the Flow Cytometry core facility of "Coordinación de Investigación en Salud" at "Centro Médico Nacional Siglo XXI" of IMSS, Mexico for instrumentation and technical support, especially to Jessica L. Prieto-Chávez.

**Conflicts of Interest:** The authors declare that there is no conflict of interest regarding the publication of this article.

## References


1. Enomoto, A.; Kimura, H.; Chairoungdua, A.; Shigeta, Y.; Jutabha, P.; Cha, S.H.; Hosoyamada, M.; Takeda, M.; Sekine, T.; Igarashi, T.; et al. Molecular identification of a renal urate anion exchanger that regulates blood urate levels. *Nature* **2002**, *417*, 447–452. [CrossRef] [PubMed]
2. Price, K.L.; Sautin, Y.Y.; Long, D.A.; Zhang, L.; Miyazaki, H.; Mu, W.; Endou, H.; Johnson, R.J. Human vascular smooth muscle cells express a urate transporter. *J. Am. Soc. Nephrol.* **2006**, *17*, 1791–1795. [CrossRef] [PubMed]
3. Sautin, Y.Y.; Nakagawa, T.; Zharikov, S.; Johnson, R.J. Adverse effects of the classic antioxidant uric acid in adipocytes: NADPH oxidase-mediated oxidative/nitrosative stress. *Am. J. Physiol. Cell Physiol.* **2007**, *293*, C584–C596. [CrossRef] [PubMed]
4. Sugihara, S.; Hisatome, I.; Kuwabara, M.; Niwa, K.; Maharani, N.; Kato, M.; Ogino, K.; Hamada, T.; Ninomiya, H.; Higashi, Y.; et al. Depletion of Uric Acid Due to SLC22A12 (URAT1) Loss-of-Function Mutation Causes Endothelial Dysfunction in Hypouricemia. *Circ. J.* **2015**, *79*, 1125–1132. [CrossRef]
5. Zhang, B.; Duan, M.; Long, B.; Zhang, B.; Wang, D.; Zhang, Y.; Chen, J.; Huang, X.; Jiao, Y.; Zhu, L.; et al. Urate transport capacity of glucose transporter 9 and urate transporter 1 in cartilage chondrocytes. *Mol. Med. Rep.* **2019**, *20*, 1645–1654. [CrossRef]
6. Bardin, T.; Richette, P. Definition of hyperuricemia and gouty conditions. *Curr. Opin. Rheumatol.* **2014**, *26*, 186–191. [CrossRef]
7. Chen-Xu, M.; Yokose, C.; Rai, S.K.; Pillinger, M.H.; Choi, H.K. Contemporary Prevalence of Gout and Hyperuricemia in the United States and Decadal Trends: The National Health and Nutrition Examination Survey, 2007–2016. *Arthritis Rheumatol.* **2019**, *71*, 991–999. [CrossRef]
8. Liu, Z.; Que, S.; Zhou, L.; Zheng, S. Dose-response Relationship of Serum Uric Acid with Metabolic Syndrome and Non-alcoholic Fatty Liver Disease Incidence: A Meta-analysis of Prospective Studies. *Sci. Rep.* **2015**, *5*, 14325. [CrossRef]
9. Yu, T.Y.; Jee, J.H.; Bae, J.C.; Jin, S.M.; Baek, J.H.; Lee, M.K.; Kim, J.H. Serum uric acid: A strong and independent predictor of metabolic syndrome after adjusting for body composition. *Metabolism* **2016**, *65*, 432–440. [CrossRef]
10. Lyngdoh, T.; Marques-Vidal, P.; Paccaud, F.; Preisig, M.; Waeber, G.; Bochud, M.; Vollenweider, P. Elevated serum uric acid is associated with high circulating inflammatory cytokines in the population-based Colaus study. *PLoS ONE* **2011**, *6*, e19901. [CrossRef]
11. Wu, J.; Qiu, L.; Cheng, X.Q.; Xu, T.; Wu, W.; Zeng, X.J.; Ye, Y.C.; Guo, X.Z.; Cheng, Q.; Liu, Q.; et al. Hyperuricemia and clustering of cardiovascular risk factors in the Chinese adult population. *Sci. Rep.* **2017**, *7*, 5456. [CrossRef] [PubMed]
12. Kushiyama, A.; Okubo, H.; Sakoda, H.; Kikuchi, T.; Fujishiro, M.; Sato, H.; Kushiyama, S.; Iwashita, M.; Nishimura, F.; Fukushima, T.; et al. Xanthine oxidoreductase is involved in macrophage foam cell formation and atherosclerosis development. *Arterioscler. Thromb. Vasc. Biol.* **2012**, *32*, 291–298. [CrossRef] [PubMed]
13. Wynn, T.A.; Chawla, A.; Pollard, J.W. Macrophage biology in development, homeostasis and disease. *Nature* **2013**, *496*, 445–455. [CrossRef]
14. Murray, P.J. Macrophage Polarization. *Annu. Rev. Physiol* **2017**, *79*, 541–566. [CrossRef]
15. Martinez, F.O.; Gordon, S.; Locati, M.; Mantovani, A. Transcriptional profiling of the human monocyte-to-macrophage differentiation and polarization: New molecules and patterns of gene expression. *J. Immunol.* **2006**, *177*, 7303–7311. [CrossRef]
16. Li, G.; Qiao, W.; Zhang, W.; Li, F.; Shi, J.; Dong, N. The shift of macrophages toward M1 phenotype promotes aortic valvular calcification. *J. Thorac. Cardiovasc. Surg.* **2017**, *153*, 1318–1327.e1. [CrossRef]
17. Amsellem, V.; Abid, S.; Poupel, L.; Parpaleix, A.; Rodero, M.; Gary-Bobo, G.; Latiri, M.; Dubois-Rande, J.L.; Lipskaia, L.; Combadiere, C.; et al. Roles for the CX3CL1/CX3CR1 and CCL2/CCR2 Chemokine Systems in Hypoxic Pulmonary Hypertension. *Am. J. Respir. Cell. Mol. Biol.* **2017**, *56*, 597–608. [CrossRef]
18. Deci, M.B.; Ferguson, S.W.; Scatigno, S.L.; Nguyen, J. Modulating Macrophage Polarization through CCR2 Inhibition and Multivalent Engagement. *Mol. Pharm.* **2018**, *15*, 2721–2731. [CrossRef]

19. Zhang, M.; Hutter, G.; Kahn, S.A.; Azad, T.D.; Gholamin, S.; Xu, C.Y.; Liu, J.; Achrol, A.S.; Richard, C.; Sommerkamp, P.; et al. Anti-CD47 Treatment Stimulates Phagocytosis of Glioblastoma by M1 and M2 Polarized Macrophages and Promotes M1 Polarized Macrophages In Vivo. *PLoS ONE* **2016**, *11*, e0153550. [CrossRef]
20. Lam, R.S.; O'Brien-Simpson, N.M.; Holden, J.A.; Lenzo, J.C.; Fong, S.B.; Reynolds, E.C. Unprimed, M1 and M2 Macrophages Differentially Interact with Porphyromonas gingivalis. *PLoS ONE* **2016**, *11*, e0158629. [CrossRef]
21. Gille, C.; Spring, B.; Tewes, L.; Poets, C.F.; Orlikowsky, T. A new method to quantify phagocytosis and intracellular degradation using green fluorescent protein-labeled Escherichia coli: Comparison of cord blood macrophages and peripheral blood macrophages of healthy adults. *Cytom. A* **2006**, *69*, 152–154. [CrossRef] [PubMed]
22. Haryono, A.; Nugrahaningsih, D.A.A.; Sari, D.C.R.; Romi, M.M.; Arfian, N. Reduction of Serum Uric Acid Associated with Attenuation of Renal Injury, Inflammation and Macrophages M1/M2 Ratio in Hyperuricemic Mice Model. *Kobe. J. Med. Sci.* **2018**, *64*, E107–E114. [PubMed]
23. Lu, W.; Xu, Y.; Shao, X.; Gao, F.; Li, Y.; Hu, J.; Zuo, Z.; Shao, X.; Zhou, L.; Zhao, Y.; et al. Uric Acid Produces an Inflammatory Response through Activation of NF-kappaB in the Hypothalamus: Implications for the Pathogenesis of Metabolic Disorders. *Sci. Rep.* **2015**, *5*, 12144. [CrossRef] [PubMed]
24. McGeough, M.D.; Wree, A.; Inzaugarat, M.E.; Haimovich, A.; Johnson, C.D.; Pena, C.A.; Goldbach-Mansky, R.; Broderick, L.; Feldstein, A.E.; Hoffman, H.M. TNF regulates transcription of NLRP3 inflammasome components and inflammatory molecules in cryopyrinopathies. *J. Clin. Investig.* **2017**, *127*, 4488–4497. [CrossRef]
25. Patel, H.J.; Patel, B.M. TNF-alpha and cancer cachexia: Molecular insights and clinical implications. *Life Sci.* **2017**, *170*, 56–63. [CrossRef]
26. Kaplanov, I.; Carmi, Y.; Kornetsky, R.; Shemesh, A.; Shurin, G.V.; Shurin, M.R.; Dinarello, C.A.; Voronov, E.; Apte, R.N. Blocking IL-1beta reverses the immunosuppression in mouse breast cancer and synergizes with anti-PD-1 for tumor abrogation. *Proc. Natl. Acad. Sci. USA* **2019**, *116*, 1361–1369. [CrossRef]
27. Peracoli, M.T.; Bannwart, C.F.; Cristofalo, R.; Borges, V.T.; Costa, R.A.; Witkin, S.S.; Peracoli, J.C. Increased reactive oxygen species and tumor necrosis factor-alpha production by monocytes are associated with elevated levels of uric acid in pre-eclamptic women. *Am. J. Reprod. Immunol.* **2011**, *66*, 460–467. [CrossRef]
28. Tang, L.; Xu, Y.; Wei, Y.; He, X. Uric acid induces the expression of TNFalpha via the ROSMAPKNFkappaB signaling pathway in rat vascular smooth muscle cells. *Mol. Med. Rep.* **2017**, *16*, 6928–6933. [CrossRef]
29. Lin, X.; Kong, J.; Wu, Q.; Yang, Y.; Ji, P. Effect of TLR4/MyD88 signaling pathway on expression of IL-1beta and TNF-alpha in synovial fibroblasts from temporomandibular joint exposed to lipopolysaccharide. *Mediat. Inflamm.* **2015**, *2015*, 329405. [CrossRef]
30. Grebe, A.; Hoss, F.; Latz, E. NLRP3 Inflammasome and the IL-1 Pathway in Atherosclerosis. *Circ. Res.* **2018**, *122*, 1722–1740. [CrossRef]
31. He, Y.; Franchi, L.; Nunez, G. TLR agonists stimulate Nlrp3-dependent IL-1beta production independently of the purinergic P2X7 receptor in dendritic cells and in vivo. *J. Immunol.* **2013**, *190*, 334–339. [CrossRef] [PubMed]
32. Rocha, D.M.; Caldas, A.P.; Oliveira, L.L.; Bressan, J.; Hermsdorff, H.H. Saturated fatty acids trigger TLR4-mediated inflammatory response. *Atherosclerosis* **2016**, *244*, 211–215. [CrossRef] [PubMed]
33. Park, B.S.; Lee, J.O. Recognition of lipopolysaccharide pattern by TLR4 complexes. *Exp. Mol. Med.* **2013**, *45*, e66. [CrossRef] [PubMed]
34. Harada, K.; Ohira, S.; Isse, K.; Ozaki, S.; Zen, Y.; Sato, Y.; Nakanuma, Y. Lipopolysaccharide activates nuclear factor-kappaB through toll-like receptors and related molecules in cultured biliary epithelial cells. *Lab. Investig.* **2003**, *83*, 1657–1667. [CrossRef]
35. Rasheed, H.; McKinney, C.; Stamp, L.K.; Dalbeth, N.; Topless, R.K.; Day, R.; Kannangara, D.; Williams, K.; Smith, M.; Janssen, M.; et al. The Toll-Like Receptor 4 (TLR4) Variant rs2149356 and Risk of Gout in European and Polynesian Sample Sets. *PLoS ONE* **2016**, *11*, e0147939. [CrossRef]
36. Zhang, J.; Diao, B.; Lin, X.; Xu, J.; Tang, F. TLR2 and TLR4 mediate an activation of adipose tissue renin-angiotensin system induced by uric acid. *Biochimie* **2019**, *162*, 125–133. [CrossRef]

37. Arnold, I.C.; Mathisen, S.; Schulthess, J.; Danne, C.; Hegazy, A.N.; Powrie, F. CD11c(+) monocyte/macrophages promote chronic Helicobacter hepaticus-induced intestinal inflammation through the production of IL-23. *Mucosal Immunol.* **2016**, *9*, 352–363. [CrossRef]
38. Torres-Castro, I.; Arroyo-Camarena, U.D.; Martinez-Reyes, C.P.; Gomez-Arauz, A.Y.; Duenas-Andrade, Y.; Hernandez-Ruiz, J.; Bejar, Y.L.; Zaga-Clavellina, V.; Morales-Montor, J.; Terrazas, L.I.; et al. Human monocytes and macrophages undergo M1-type inflammatory polarization in response to high levels of glucose. *Immunol. Lett.* **2016**, *176*, 81–89. [CrossRef]
39. Nawaz, A.; Aminuddin, A.; Kado, T.; Takikawa, A.; Yamamoto, S.; Tsuneyama, K.; Igarashi, Y.; Ikutani, M.; Nishida, Y.; Nagai, Y.; et al. CD206(+) M2-like macrophages regulate systemic glucose metabolism by inhibiting proliferation of adipocyte progenitors. *Nat. Commun.* **2017**, *8*, 286. [CrossRef]
40. Kool, M.; Soullie, T.; van Nimwegen, M.; Willart, M.A.; Muskens, F.; Jung, S.; Hoogsteden, H.C.; Hammad, H.; Lambrecht, B.N. Alum adjuvant boosts adaptive immunity by inducing uric acid and activating inflammatory dendritic cells. *J. Exp. Med.* **2008**, *205*, 869–882. [CrossRef]
41. Jeong, J.H.; Jung, J.H.; Lee, J.S.; Oh, J.S.; Kim, Y.G.; Lee, C.K.; Yoo, B.; Hong, S. Prominent Inflammatory Features of Monocytes/Macrophages in Acute Calcium Pyrophosphate Crystal Arthritis: A Comparison with Acute Gouty Arthritis. *Immune Netw.* **2019**, *19*, e21. [CrossRef] [PubMed]
42. Bjorkander, S.; Heidari-Hamedani, G.; Bremme, K.; Gunnarsson, I.; Holmlund, U. Peripheral monocyte expression of the chemokine receptors CCR2, CCR5 and CXCR3 is altered at parturition in healthy women and in women with systemic lupus erythematosus. *Scand. J. Immunol.* **2013**, *77*, 200–212. [CrossRef]
43. Lee, M.; Lee, Y.; Song, J.; Lee, J.; Chang, S.Y. Tissue-specific Role of CX3CR1 Expressing Immune Cells and Their Relationships with Human Disease. *Immune Netw.* **2018**, *18*, e5. [CrossRef]
44. Pachot, A.; Cazalis, M.A.; Venet, F.; Turrel, F.; Faudot, C.; Voirin, N.; Diasparra, J.; Bourgoin, N.; Poitevin, F.; Mougin, B.; et al. Decreased expression of the fractalkine receptor CX3CR1 on circulating monocytes as new feature of sepsis-induced immunosuppression. *J. Immunol.* **2008**, *180*, 6421–6429. [CrossRef] [PubMed]
45. Zhou, Y.; Yang, Y.; Warr, G.; Bravo, R. LPS down-regulates the expression of chemokine receptor CCR2 in mice and abolishes macrophage infiltration in acute inflammation. *J. Leukoc. Biol.* **1999**, *65*, 265–269. [CrossRef] [PubMed]
46. Heesen, M.; Renckens, R.; de Vos, A.F.; Kunz, D.; van der Poll, T. Human endotoxemia induces down-regulation of monocyte CC chemokine receptor 2. *Clin. Vaccine. Immunol.* **2006**, *13*, 156–159. [CrossRef]
47. Salahudeen, M.S.; Nishtala, P.S. An overview of pharmacodynamic modelling, ligand-binding approach and its application in clinical practice. *Saudi. Pharm. J.* **2017**, *25*, 165–175. [CrossRef]
48. Auerbach, A. Dose-Response Analysis When There Is a Correlation between Affinity and Efficacy. *Mol. Pharmacol.* **2016**, *89*, 297–302. [CrossRef]
49. Jia, L.; Xing, J.; Ding, Y.; Shen, Y.; Shi, X.; Ren, W.; Wan, M.; Guo, J.; Zheng, S.; Liu, Y.; et al. Hyperuricemia causes pancreatic beta-cell death and dysfunction through NF-kappaB signaling pathway. *PLoS ONE* **2013**, *8*, e78284. [CrossRef]
50. Tan, P.K.; Ostertag, T.M.; Miner, J.N. Mechanism of high affinity inhibition of the human urate transporter URAT1. *Sci. Rep.* **2016**, *6*, 34995. [CrossRef]
51. Liu-Bryan, R.; Lioté, F. Monosodium urate and calcium pyrophosphate dihydrate (CPPD) crystals, inflammation, and cellular signaling. *Jt. Bone Spine* **2005**, *72*, 295–302. [CrossRef]


Hindawi
Journal of Immunology Research
Volume 2019, Article ID 6105059, 10 pages
https://doi.org/10.1155/2019/6105059

*Clinical Study*

# A Single 48 mg Sucralose Sip Unbalances Monocyte Subpopulations and Stimulates Insulin Secretion in Healthy Young Adults

**Angélica Y. Gómez-Arauz,[1] Nallely Bueno-Hernández,[1] Leon F. Palomera,[1] Raúl Alcántara-Suárez,[1] Karen L. De León,[1] Lucía A. Méndez-García,[1] Miguel Carrero-Aguirre,[1] Aaron N. Manjarrez-Reyna,[1] Camilo P. Martínez-Reyes,[1] Marcela Esquivel-Velázquez,[1] Alejandra Ruiz-Barranco,[2] Neyla Baltazar-López,[3] Sergio Islas-Andrade,[1] Galileo Escobedo,[1] and Guillermo Meléndez[1]**

[1]*Laboratory for Proteomics and Metabolomics, Research Division, General Hospital of Mexico "Dr. Eduardo Liceaga", 06720 Mexico City, Mexico*
[2]*Clinical Nutrition Division, General Hospital of Mexico "Dr. Eduardo Liceaga", 06720 Mexico City, Mexico*
[3]*Research Coordination at Central Laboratories, General Hospital of Mexico "Dr. Eduardo Liceaga", 06720 Mexico City, Mexico*

Correspondence should be addressed to Galileo Escobedo; gescobedog@msn.com
and Guillermo Meléndez; melendez651@gmail.com

Received 12 December 2018; Revised 25 February 2019; Accepted 14 March 2019; Published 28 April 2019

Guest Editor: Daniel Ortuño-Sahagún



Sucralose is a noncaloric artificial sweetener that is widely consumed worldwide and has been associated with alteration in glucose and insulin homeostasis. Unbalance in monocyte subpopulations expressing CD11c and CD206 hallmarks metabolic dysfunction but has not yet been studied in response to sucralose. Our goal was to examine the effect of a single sucralose sip on serum insulin and blood glucose and the percentages of classical, intermediate, and nonclassical monocytes in healthy young adults subjected to an oral glucose tolerance test (OGTT). This study was a randomized, placebo-controlled clinical trial. Volunteers randomly received 60 mL water as placebo ($n = 20$) or 48 mg sucralose dissolved in 60 mL water ($n = 25$), fifteen minutes prior to an OGTT. Blood samples were individually drawn every 15 minutes for 180 minutes for quantifying glucose and insulin concentrations. Monocyte subsets expressing CD11c and CD206 were measured at -15 and 180 minutes by flow cytometry. As compared to controls, volunteers receiving sucralose exhibited significant increases in serum insulin at 30, 45, and 180 minutes, whereas blood glucose values showed no significant differences. Sucralose consumption caused a significant 7% increase in classical monocytes and 63% decrease in nonclassical monocytes with respect to placebo controls. Pearson's correlation models revealed a strong association of insulin with sucralose-induced monocyte subpopulation unbalance whereas glucose values did not show significant correlations. Sucralose ingestion decreased CD11c expression in all monocyte subsets and reduced CD206 expression in nonclassical monocytes suggesting that sucralose does not only unbalance monocyte subpopulations but also alter their expression pattern of cell surface molecules. This work demonstrates for the first time that a 48 mg sucralose sip increases serum insulin and unbalances monocyte subpopulations expressing CD11c and CD206 in noninsulin-resistant healthy young adults subjected to an OGTT. The apparently innocuous consumption of sucralose should be reexamined in light of these results.

## 1. Introduction

Noncaloric artificial sweeteners, including aspartame, acesulfame k, and sucralose, are food additives that preserve the taste of sweetness without increasing the calories of food and beverages [1]. For this reason, consumption of noncaloric artificial sweeteners is now widely spread among people from all ages and socioeconomic status worldwide [2, 3].

Nevertheless, a growing number of clinical and experimental studies have now suggested that noncaloric artificial sweeteners are linked to the development of metabolic abnormalities including insulin resistance and glucose intolerance, especially sucralose [4–8]. A seminal study demonstrated that ingestion of 48 mg sucralose significantly increases the serum values of glucose and insulin in morbidly obese subjects of both sexes subjected to a 75 g oral glucose tolerance test (OGTT) [9]. Similarly, overweight subjects that consumed sucralose prior to an OGTT exhibited a 1.2-fold elevation in the insulin peak as compared to placebo controls [10]. Therefore, the apparently innocuous effect of sucralose and others noncaloric artificial sweeteners on glucose and insulin homeostasis should be reexamined in light of this evidence.

It is now well accepted that low-grade systemic inflammation is a central player in obesity and contributes to the pathogenesis of metabolic disease, especially alteration of glucose and insulin homeostasis [11–13]. Besides being characterized by abnormally high levels of cytokines such as tumor necrosis factor alpha (TNF-alpha) and interleukin-1 beta (IL-1beta), low-grade systemic inflammation is accompanied by alteration in monocyte subpopulations [14]. In humans, circulating monocytes are sorted in three different subpopulations according to the cell surface expression of CD14 and CD16 [15]. Classical monocytes exhibit high CD14 levels and show no expression of CD16 ($CD14^{++}$ $CD16^{-}$). The intermediate monocyte subpopulation shows high CD14 expression and also exhibit CD16 expression ($CD14^{++}CD16^{+}$) whereas nonclassical monocytes produce low CD14 levels and show expression of CD16 ($CD14^{+}$ $CD16^{+}$) [15, 16]. Interestingly, the percentage of nonclassical monocytes has been shown to elevate in obese subjects that exhibit increased insulin resistance and metabolic syndrome [17, 18]. In the same sense, the classical monocyte subpopulation has been shown to increase in obese individuals and correlates with higher proportion of $CD11c^{+}$ macrophages in the visceral adipose tissue (VAT) [19]. CD11c is a beta-2 integrin with prominent functions in cell adherence of monocytes and macrophages to vascular endothelial tissue and VAT [19, 20]. Furthermore, monocytes have been shown to express CD206 [21], a cell surface marker highly expressed in anti-inflammatory macrophages that is also associated with improved insulin sensitivity in both humans and mice [22, 23]. In this way, modulation of CD11c and CD206 expression in monocyte-macrophage lineage cells is crucial not only in typical immune functions such as cell migration and inflammation but also in obesity and insulin resistance [24]. Thus, imbalance in monocyte subpopulations expressing CD11c and CD206 hallmarks metabolic dysfunction but has not yet been studied in response to noncaloric artificial sweetener consumption such as sucralose.

The main goal of this study was to examine the effect of a single sucralose sip on the percentages of classical, intermediate, and nonclassical monocytes expressing CD11c and CD206 in healthy young adults subjected to an OGTT, while also exploring the possible relationship of monocyte subpopulations with changes in glucose and insulin homeostasis.

## 2. Materials and Methods

*2.1. Subjects and Study Design.* Forty-five healthy adult volunteers of both sexes with homeostasis model assessment (HOMA) values ≤3.8, aging between 18 and 35 years, who attended to the Department of Internal Medicine and the Laboratory for Proteomics and Metabolomics of the General Hospital of Mexico from September 2016 to April 2018 were included in the randomized, parallel-group, placebo-controlled clinical trial. All of the study participants provided written informed consent, previously approved by the Institutional Ethical Committee of the General Hospital of Mexico, which guaranteed that the study was conducted in rigorous adherence to the principles described in the 1964 Declaration of Helsinki and its posterior amendment in 2013. Subjects were excluded of the study if they had previous diagnosis of type 1 diabetes mellitus (T1D), type 2 diabetes mellitus (T2D), cardiovascular disease, acute or chronic liver disease, acute or chronic renal disease, cancer, endocrine disorders, infectious diseases, and inflammatory or autoimmune disease. We also excluded of the study to HIV-, HCV-, and HBV-seropositive patients, pregnant or lactating women, and individuals with anti-inflammatory, antiaggregant, antihypertensive, and immunomodulatory medication including nonsteroidal anti-inflammatory drugs. All participants included in the study had 8-10 hr overnight fasting before being subjected to the OGTT.

*2.2. Oral Glucose Tolerance Test.* The present study was a randomized, parallel-group, placebo-controlled clinical trial, where volunteers randomly drank 60 mL water as placebo ($n = 20$) or 48 mg sucralose dissolved in 60 mL water ($n = 25$), fifteen minutes prior to an OGTT. A regular "light" beverage available in the market approximately contains 48 mg sucralose. For this reason, we decided to use 48 mg sucralose dissolved in 60 mL water, as previously reported [9]. Each participant had up to three minutes to finish the sip of water or sucralose. Starting with oral glucose load at min zero, venous blood samples were drawn from all study subjects every 15 min for 180 min for quantifying the blood levels of glucose and insulin. Additional blood samples were also collected at -15 and 180 min for white blood cell isolation and characterization of monocyte subpopulations by flow cytometry.

*2.3. Anthropometric and Biochemical Measurements.* Body mass index (BMI), waist circumference, and blood pressure were measured in all study volunteers. Serum levels of insulin were measured in triplicate by the enzyme-linked immunosorbent assay (ELISA) following the manufacturer's instructions (Abnova Corporation, Taiwan). Serum levels of glucose were measured in triplicate by the glucose oxidase assay, following the manufacturer's instructions (Megazyme International, Ireland). The HOMA index was individually calculated by multiplying glucose concentration (mmol/L) by insulin concentration (mU/L) and then divided by 22.5. The cut-off point for HOMA index was established according to studies previously validated in a Mexican population [25]. Total cholesterol, low-density lipoproteins (LDL), high-

density lipoproteins (HDL), and triglyceride levels were measured in triplicate by enzymatic assays following the manufacturer's instructions (Roche Diagnostics, Mannheim, Germany). Glycated hemoglobin (HbA1c), blood urea nitrogen (BUN), serum creatinine, and hematic biometry were determined by standard laboratory assays.

*2.4. Flow Cytometry.* Isolation of white blood cells was performed by centrifuging blood samples previously collected in tubes containing EDTA (Vacutainer™, BD Diagnostics, NJ, USA) at 1800 g for 10 min. Then, white blood cells were placed in 1.6 mL pyrogen-free Eppendorf tubes containing 1 mL ACK Lysing Buffer (Life Technologies, USA) and incubated at 4°C for 5 min. Afterward, cell suspension was centrifuged at 1800 g/4°C for 10 min and cell pellets washed twice with PBS 1x (Sigma-Aldrich, Mexico). After an additional centrifugation step and removal of the supernatant, cell pellets were resuspended in 50 $\mu$L PBS 1x (Sigma-Aldrich, Mexico). Immediately after, 3 $\mu$L Human TruStrain Reagent (BioLegend Inc., USA) was added to $2 \times 10^5$ white blood cells and then incubated for 10 min at 4°C. Then, each cell suspension was incubated with anti-CD14 PE/Cy7, anti-CD16 FITC, anti-CD11c APC, and anti-CD206 PE (BioLegend Inc., USA) for 30 min at 4°C. Flow cytometry analysis was performed on a FACSCanto II flow cytometer by using the BD FACSDiva™ software 6.0 (BD Biosciences, Mexico), acquiring $1 \times 10^5$ monocyte events per test in duplicate.

*2.5. Gating Strategy for Flow Cytometry.* White blood cells were gated for singlets on a forward scatter height/forward scatter area density plot. Afterward, areas corresponding to lymphocyte, polymorphonuclear leukocyte, and monocyte cell populations were clearly revealed and gated on a FSC-A/side scatter area plot. The monocyte gate was then selected for detection of living monocytes by using the Live/Dead Aqua Stain (Thermo Fisher Scientific Inc., USA) and posterior measurement of CD14, CD16, CD11c, and CD206 exclusively on this immune cell population. In this way, we deliberately excluded any other CD14-CD16-CD11c-CD206 signal coming from a different cellular source than monocytes. Monocyte subpopulations were then characterized according to the cell surface expression of CD14 and CD16 as follows: $CD14^{++}CD16^{-}$, classical monocytes; $CD14^{++}CD16^{+}$, intermediate monocytes; and $CD14^{+}CD16^{+}$, nonclassical monocytes.

*2.6. Statistics.* Normality of data distribution was estimated by the Shapiro-Wilk test. The Student $T$-test was used to compare the placebo and sucralose groups regarding age, BMI, waist circumference, systolic and diastolic blood pressure, blood glucose, glycated hemoglobin percentage, serum insulin, HOMA-IR, total cholesterol, LDL, HDL, triglycerides, blood urea nitrogen, serum creatinine, and hematic biometry, and data were expressed as mean ± standard deviation. The mean fluorescence intensity (MFI) of CD11c and CD206 as well as the percentages of classical, intermediate, and nonclassical monocytes at -15 and 180 min of the OGTT were analyzed using two-tailed 2-way ANOVA with correction for multiple comparisons by means of the Bonferroni multiple comparison test, and data were expressed as media ± standard deviation. Differences in the mean values of glucose and insulin at -15, 0, 15, 30, 45, 60, 75, 90, 105, 120, and 180 min of the OGTT, between volunteers enrolled in placebo or sucralose groups, were estimated by means of two-tailed 2-way ANOVA with correction for multiple comparisons using the Bonferroni multiple comparison test. Furthermore, the women/men proportion in placebo and sucralose groups was analyzed by means of the chi-squared test and data expressed as absolute values. Pearson's correlation coefficients were estimated for examining the statistical correlation of classical, intermediate, and nonclassical monocytes with glucose and insulin and expressed as coefficients ($r$) and $P$ values. Differences were considered significant when $P < 0.05$. Statistical analyses were performed by means of the GraphPad Prism 6.01 software (GraphPad Software, La Jolla, CA 92037 USA).

## 3. Results

There were no differences between subjects receiving placebo ($n = 20$) or sucralose ($n = 25$) in terms of demographic, metabolic, and hematic characteristics, including gender, age, BMI, HOMA-IR, lipid profile, renal function, and monocytes per microliter of blood (Table 1).

Blood glucose values showed no significant differences in subjects receiving placebo or sucralose all along the oral glucose tolerance test (Figure 1(a)). On the contrary, volunteers that received 48 mg sucralose prior glucose load showed a significant 1.3-fold increase in the serum levels of insulin at 30 min as compared to subjects drinking water as placebo ($P = 0.041$) (Figure 1(b)). At 45 min, subjects receiving sucralose exhibited a significant 1.4-fold elevation in serum insulin with respect to placebo controls ($P = 0.046$) (Figure 1(b)). At 180 min, subjects that received sucralose showed a significant 2-fold increase in the serum levels of insulin as compared to placebo controls ($P = 0.048$) (Figure 1(b)).

Representative dot plots illustrating monocyte subpopulations in subjects that received placebo or sucralose are shown in Figure 2. At the beginning of the oral glucose tolerance test (-15 min), no differences were seen in the percentages of classical, intermediate, and nonclassical monocytes in subjects receiving placebo or sucralose (Figure 2(a) versus 2c, respectively). At the end of the experiment (180 min), the percentage of classical monocytes increased in subjects that received 48 mg sucralose as compared to placebo controls (Figure 2(d) versus 2b, respectively). In contrast, the nonclassical monocyte percentage was reduced in subjects exposed to sucralose with respect to placebo controls (Figure 2(d) versus 2b, respectively). Quantification of monocyte subpopulation percentages confirmed a significant 7% increase in the number of classical monocytes from subjects that received sucralose in comparison to controls receiving placebo ($P = 0.0028$) (Figure 2(e)). On the other side, the nonclassical monocyte percentage exhibited a significant 63% reduction in subjects exposed to sucralose with respect to placebo controls ($P < 0.0001$) (Figure 2(e)). No significant differences were found in the percentage of intermediate monocytes in subjects that received placebo or sucralose.

Table 1: Demographic, metabolic, and hematic characteristics of the study population.

| Parameters | Placebo | Sucralose | $P$ value |
|---|---|---|---|
| Gender (W/M) | 8/12 | 8/17 | 0.288 |
| Age (years) | 21.55 ± 2.18 | 22.36 ± 2.99 | 0.158 |
| BMI (kg/m$^2$) | 24.58 ± 3.63 | 23.67 ± 2.88 | 0.177 |
| Waist circumference (cm) | 82.27 ± 8.44 | 78.57 ± 8.37 | 0.074 |
| SBP (mmHg) | 111.10 ± 8.16 | 113.70 ± 13.91 | 0.225 |
| DBP (mmHg) | 70.75 ± 5.77 | 71.16 ± 7.33 | 0.419 |
| Blood glucose (mg/dL) | 88.20 ± 6.65 | 89.96 ± 5.68 | 0.172 |
| HbA1c (%) | 5.26 ± 0.24 | 5.23 ± 0.19 | 0.497 |
| Serum insulin ($\mu$U/L) | 7.94 ± 2.91 | 8.31 ± 2.82 | 0.335 |
| HOMA-IR (a.u.) | 1.75 ± 0.70 | 1.85 ± 0.65 | 0.298 |
| Total cholesterol (mg/dL) | 166.70 ± 31.21 | 168.60 ± 32.53 | 0.418 |
| LDL (mg/dL) | 102.10 ± 28.92 | 99.80 ± 26.60 | 0.393 |
| HDL (mg/dL) | 43.05 ± 10.60 | 44.40 ± 12.20 | 0.349 |
| Triglycerides (mg/dL) | 111.20 ± 58.10 | 118.20 ± 102.70 | 0.392 |
| BUN (mg/dL) | 22.40 ± 6.98 | 23.71 ± 5.95 | 0.249 |
| Serum creatinine (mg/dL) | 0.82 ± 0.13 | 0.78 ± 0.13 | 0.165 |
| Hematocrit (%) | 45.63 ± 3.53 | 44.04 ± 4.37 | 0.097 |
| Total leukocytes ($10^3/\mu$L) | 6.38 ± 1.49 | 6.05 ± 0.96 | 0.187 |
| Monocytes ($10^3/\mu$L) | 0.43 ± 0.11 | 0.39 ± 0.10 | 0.109 |
| Monocytes (%) | 6.94 ± 1.77 | 6.42 ± 1.33 | 0.134 |

Data are expressed as media ± standard deviation. The Shapiro-Wilk test was used to estimate normality in data distribution. Significant differences were estimated by means of performing the Student $T$-test with the exception of women/men proportion that was estimated by means of the chi-squared test. Differences were considered significant when $P < 0.05$. Abbreviations: W: women; M: men; BMI: body mass index; SBP: systolic blood pressure; DBP: diastolic blood pressure; HbA1c: glycated hemoglobin; HOMA-IR: homeostatic model assessment of insulin resistance; LDL: low-density lipoprotein; HDL: high-density lipoprotein; BUN: blood urea nitrogen; a.u.: arbitrary units.

Analysis of Pearson's correlation coefficients showed no significant associations of monocyte subpopulations with blood glucose (Table 2). On the contrary, serum insulin showed a positive relationship with classical monocytes ($r = 0.41$, $P = 0.02$), whereas it also exhibited a strong inverse association with nonclassical monocytes ($r = -0.42$, $P = 0.01$) (Table 2).

At the beginning of the OGTT, CD11c expression in classical, intermediate, and nonclassical monocytes showed no significant differences in subjects receiving placebo or sucralose (Figure 3(a)). At 180 min, CD11c expression was significantly reduced in intermediate and nonclassical monocytes of subjects receiving sucralose as compared to placebo controls ($P = 0.0012$ and $P = 0.0064$, respectively) (Figure 3(a)). CD11c expression also exhibited a significant reduction in intermediate and nonclassical monocytes of subjects exposed to sucralose at the beginning (-15 min) and at the end (180 min) of the OGTT ($P = 0.0004$ and $P = 0.0001$, respectively) (Figure 3(a)). In classical monocytes, CD11c expression significantly diminished in the sucralose group at the beginning (-15 min) and at the end (180 min) of the OGTT ($P = 0.0008$) (Figure 3(a)).

At the beginning of the OGTT, CD206 expression in classical, intermediate, and nonclassical monocytes showed no significant differences in subjects that received placebo or sucralose (Figure 3(b)). At 180 min, CD206 expression was significantly reduced in nonclassical monocytes of volunteers that received sucralose as compared to placebo controls ($P = 0.0098$) (Figure 3(b)).

## 4. Discussion

Noncaloric artificial sweeteners are now consumed by millions of people from all ages, gender, and socioeconomic status around the globe [26]. However, sucralose and other noncaloric artificial sweeteners have been now linked to disturbances in glucose and insulin homeostasis in both animal models and humans [5–9]. For this reason, it is still of great relevance to keep characterizing the possible deleterious effects of sucralose on human metabolism in randomized, parallel-group, placebo-controlled clinical trials.

In this study, we found that one single 48 mg sip of sucralose, a sucralose amount that is contained in numerous "light" beverages available in the market, increases serum insulin but not glucose in age- and sex-matched healthy young adults subjected to an OGTT. These data appear contrary to previous information showing that a similar amount of sucralose is able to elevate both insulin and glucose in morbidly obese individuals receiving a glucose load [9]. Nevertheless, this apparently contradictory evidence should

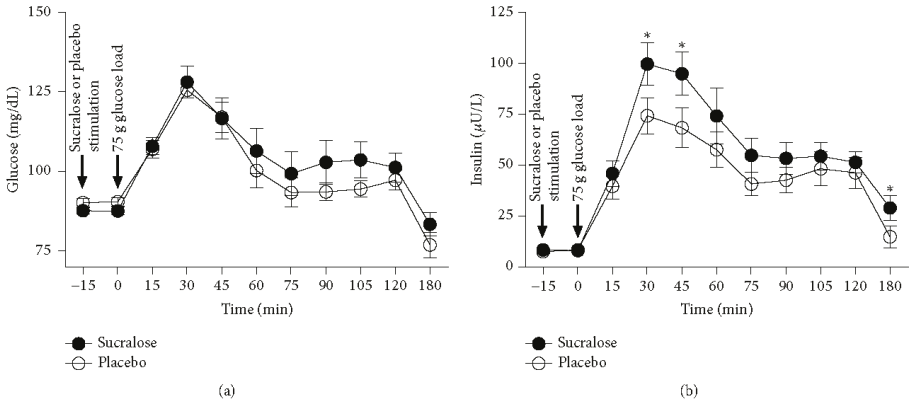


Figure 1: Blood levels of glucose and insulin in healthy young adults that received sucralose or placebo during an oral glucose tolerance test. Volunteers randomly received 60 mL water as placebo ($n = 20$) or 48 mg sucralose dissolved in 60 mL water ($n = 25$) 15 min prior to a 75 g oral glucose tolerance test (OGTT). Starting with glucose load at minute zero, venous blood samples were drawn from all study subjects every 15 min for 180 min for quantifying the blood levels of glucose and insulin. (a) Blood glucose did not show significant changes in subjects receiving placebo or sucralose all along the OGTT. (b) Serum insulin significantly increased at 30, 45, and 180 min in volunteers that received sucralose as compared to placebo controls. Timing of stimulation with sucralose, placebo, or glucose is shown on the graphic by black arrows. The placebo group is shown in open circles, whereas the sucralose group can be seen in closed circles. Data are expressed as media ± standard error. Significant differences between subjects receiving placebo or sucralose were estimated on each point of the OGTT by performing two-tailed 2-way ANOVA with correction for multiple comparisons by means of the Bonferroni multiple comparisons test. Significant differences are indicated by asterisks. Differences were considered significant when $P < 0.05$.

be examined in light of previous information showing that healthy young adults with no insulin resistance have the ability to increase insulin secretion and thus effectively decrease the excess of blood glucose [27, 28]. In contrast, numerous studies have consistently shown that nondiabetic morbidly obese subjects exposed to a glucose load can clearly increase insulin secretion without achieving blood glucose clearance due to a marked insulin resistance [29–32]. In this scenario, it is feasible to suppose that sucralose consumption may have differential effects on healthy young adults and morbidly obese subjects due to the presence of insulin resistance. In other words, sucralose ingestion may stimulate insulin secretion and, in this way, reduce glucose levels in healthy young adults but not morbidly obese subjects that show higher levels of insulin resistance and thus glucose intolerance. The fact that sucralose is able to stimulate directly insulin secretion has been previously reported in pancreatic beta cell lines and mouse islets [33], but remains elusive in humans. However, present results support the role of sucralose in promoting pancreatic insulin secretion in healthy young women and men that show normal insulin sensitivity, a probable phenomenon that needs to be confirmed in other human populations with different genetic background.

As mentioned before, low-grade activation of monocytes and macrophages has been shown to associate with the development of hyperinsulinemia, glucose intolerance, and insulin resistance [17–19, 34]. In this sense, it is well known that nutritive sweeteners such as sucrose or glucose exert the ability to increase TNF-alpha and IL-1beta expression and downregulate interleukin-10 (IL-10) production in human monocyte-derived macrophages *in vitro* [35, 36]. However, the effect of noncaloric artificial sweeteners on immune cells remains elusive. A previous study showed that exposure of human whole blood leukocytes to sucralose is able to suppress interleukin-6 (IL-6) and IL-10 secretion *in vitro*, even in the presence of phytohemagglutinin (PHA) or lipopolysaccharide (LPS) [37]. Likewise, the $CD3^+$ T cell percentage has been shown to increase in Peyer's patches and lamina propria of mice receiving sucralose in drinking water [5]. Moreover, $CD3^+$ T cells in Peyer's patches also showed elevation in TNF-alpha and interferon-gamma (IFN-gamma) production, accompanied by reduced expression of IL-10, which supports the role of sucralose in modulating immune cell activation [5]. Concurring with previous information, our findings show for the first time that a single sip of sucralose significantly increases the percentage of classical monocytes and reduces the nonclassical monocyte subpopulation in healthy young adults receiving a 75 g glucose load.

Another phenomenon captured in our study involves the possible mechanism by which sucralose exerts its effects on classical and nonclassical monocytes in healthy young adults. Sweet taste of sucralose and other caloric and noncaloric sweeteners is mediated by G protein-coupled receptors (GPCR) T1R1, T1R2, and T1R3 [38]. Sweet taste receptors were firstly described in the gut [39], enteroendocrine cells, and pancreas [40]. Nevertheless, T1R3 has been also indentified in mouse peritoneal macrophages [41]. Notably, *in vitro* exposure of T1R3 to trehalose (a disaccharide consisting of two molecules of glucose) has been shown to associate with suppression of TNF-alpha and IL-1beta

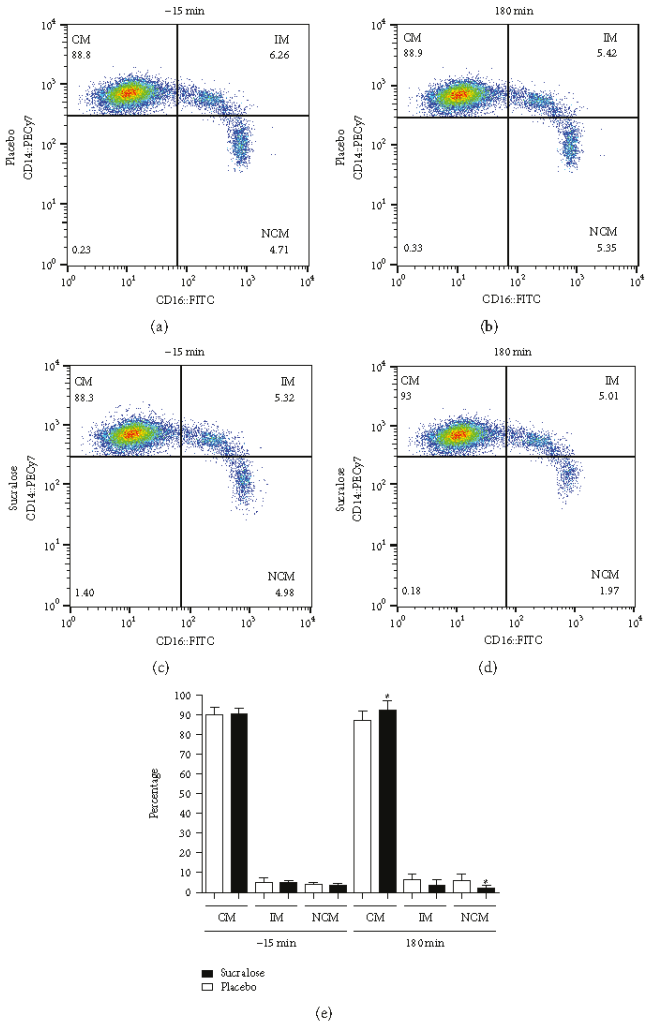


Figure 2: Percentages of classical, intermediate, and nonclassical monocytes in healthy young adults that received sucralose or placebo at the beginning and at the end of an oral glucose tolerance test. Representative flow cytometry dot plots showing the percentages of classical (CM), intermediate (IM), and nonclassical monocytes (NCM) in the placebo group at the beginning (a) and at the end (b) of the oral glucose tolerance test (OGTT). Representative dot plots showing the percentages of CM, IM, and NCM in the sucralose group at the beginning and at the end of the OGTT can be seen in (c) and (d), respectively. (e) As expected, quantification of monocyte subpopulation percentages showed no differences between placebo and sucralose groups at the beginning of the OGTT (-15 min). At 180 min, the CM percentage significantly increased whereas the NCM percentage decreased in volunteers that received 48 mg sucralose as compared to subjects that received water as placebo. No significant differences were seen in the IM percentage. The placebo group is shown in open bars, whereas the sucralose group can be seen in closed bars. Monocytes were gated on a $CD14^+CD16^+$ dot plot to identify monocyte subpopulations as follows: $CD14^{++}CD16^-$, classical monocytes; $CD14^{++}CD16^+$, intermediate monocytes; and $CD14^+CD16^+$, nonclassical monocytes. Data are expressed as media ± standard deviation. Significant differences between placebo and sucralose groups were estimated by performing two-tailed, 2-way ANOVA followed by the Bonferroni multiple comparisons test. Significant differences are indicated by asterisks. Differences were considered significant when $P < 0.05$.

Table 2: Statistical correlations of monocyte subpopulations with blood levels of glucose and insulin in placebo and sucralose groups.

| | Placebo | | | | Sucralose | | | | |
|---|---|---|---|---|---|---|---|---|---|
| | -15 | | 180 | | -15 | | 180 | | |
| | *r* | *P* | *r* | *P* | *r* | *P* | *r* | *P* | |
| Classical monocyte (%) | 0.24 | 0.12 | 0.35 | 0.06 | 0.19 | 0.18 | 0.14 | 0.25 | |
| Intermediate monocyte (%) | -0.15 | 0.28 | -0.25 | 0.13 | -0.20 | 0.16 | 0.06 | 0.38 | Glucose |
| Nonclassical monocyte (%) | -0.20 | 0.18 | -0.24 | 0.14 | -0.37 | 0.06 | 0.12 | 0.27 | |
| Classical monocyte (%) | 0.01 | 0.46 | 0.10 | 0.33 | 0.06 | 0.37 | *0.41* | *0.02* | |
| Intermediate monocyte (%) | 0.31 | 0.08 | -0.21 | 0.17 | 0.24 | 0.12 | -0.27 | 0.09 | Insulin |
| Nonclassical monocyte (%) | -0.36 | 0.06 | 0.04 | 0.42 | -0.29 | 0.07 | *-0.42* | *0.01* | |

Coefficients ($r$) and $P$ values were calculated by the Pearson correlation model. The correlation level was considered significant when $P < 0.05$. Significant associations are marked in italic.

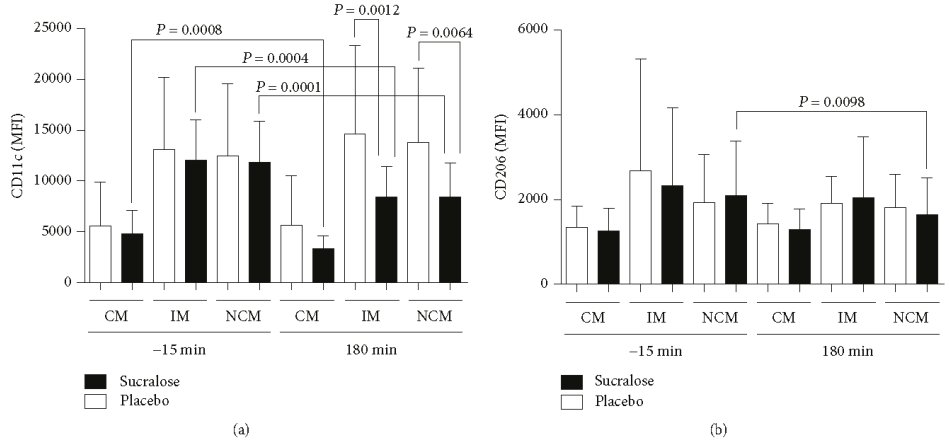


Figure 3: Cell surface expression of CD11c and CD206 in classical, intermediate, and nonclassical monocytes of healthy young adults that received sucralose or placebo at the beginning and at the end of an oral glucose tolerance test. (a) As expected, CD11c expression showed no differences between placebo and sucralose groups at the beginning (-15 min) of the oral glucose tolerance test (OGTT). At 180 min, CD11c expression significantly decreased in intermediate monocytes (IM) and nonclassical monocytes (NCM) of subjects that received 48 mg sucralose as compared to placebo controls. When comparing -15 and 180 min, classical monocytes (CM), IM, and NCM showed decreased CD11c expression in volunteers receiving sucralose. (b) CD206 expression showed no differences in subjects receiving placebo or sucralose at the beginning of the OGTT (-15 min). At 180 min, CD206 expression significantly decreased in the NCM subpopulation of subjects that received sucralose as compared to placebo controls. The placebo group is shown in open bars, whereas the sucralose group can be seen in closed bars. Monocytes were gated on a $CD14^+CD16^+$ dot plot to identify $CD14^{++}CD16^-$ classical monocytes, $CD14^{++}CD16^+$ intermediate monocytes, and $CD14^+CD16^+$ nonclassical monocytes and then measure the mean fluorescence intensity (MFI) of CD11c and CD206 on each monocyte subset. Data are expressed as media ± standard deviation. Significant differences between subjects receiving placebo or sucralose were estimated by performing two-tailed, 2-way ANOVA followed by the Bonferroni multiple comparisons test. Significant differences are indicated by asterisks. Differences were considered significant when $P < 0.05$.

expression in murine macrophages [41]. It is then feasible to speculate that sucralose may alter CD14 and CD16 expression via T1R3, which would lead to unbalance in the percentages of classical and nonclassical monocytes. However, we still need to measure sweet taste receptor expression on human monocyte subpopulations to draw major conclusions regarding this point.

Another possible mechanism by which sucralose may orchestrate dynamic changes in classical and nonclassical monocyte subsets involves the probable role of serum insulin. In our study, increase in serum insulin was importantly correlated with elevation of classical monocytes and reduction of nonclassical monocytes only in volunteers that drank sucralose but not placebo. Devevre and coworkers previously demonstrated that serum insulin is significantly associated with classical, intermediate, and nonclassical monocyte subpopulations of morbidly obese patients with insulin resistance [18]. Moreover, another study showed that insulin is able to

induce protein kinase B (AKT) phosphorylation in both human classical and nonclassical monocyte subsets in a dose-dependent fashion *in vitro* [42]. Furthermore, Bunn and coworkers also reported that insulin boosts the palmitate-induced TNF-alpha and IL-6 expression in human monocytes *in vitro* [43]. Taking into account that (1) sucralose can directly stimulate pancreatic insulin secretion via T1R2 and T1R3 [33] and (2) insulin is able to regulate human monocyte activity [42, 43], it is then reasonable to suppose that serum insulin may directly modify the percentages of classical and nonclassical monocytes in subjects receiving sucralose but not placebo. Although plausible, it is a speculative scenario and further experimental studies should be performed with the aim of determining the exact mechanism by which sucralose affects human monocyte subpopulations *in vivo*.

In humans, monocyte subpopulations have been shown to exert different immune roles that are associated with expression patterns of cell surface molecules [16]. In this sense, classical and intermediate monocytes have been described to express CCR2 and CD11c and thus play pivotal roles in cell adhesion and migration [19, 44]. On the other hand, nonclassical monocytes have been shown to exert inflammatory actions within the circulation and progressive loss of CD206 expression on these immune cells is associated with enhanced proinflammatory capacity [21]. In this sense, our results show that sucralose consumption associates with low CD11c expression in all monocyte subsets and suggest alteration of the migratory capacity of these cells. However, such a hypothesis needs to be experimentally tested before drawing major conclusions regarding the effect of sucralose on the monocyte migratory capacity. To this respect, it has been previously reported that trehalose ingestion reduces CD11c expression in the colonic mucosa of mice treated with 2,4,6-trinitrobenzenesulfonic acid (TNBS), which in turn was associated with less infiltration of immune cells and improvement of intestinal inflammation [45]. However, to the best of our knowledge this is the first study reporting that sucralose consumption is able to decrease CD11c expression in human monocytes, a notion that may open new avenues to investigate the effect of sucralose on immune cells. In parallel, our findings also show that sucralose consumption associates with low expression levels of CD206 in nonclassical monocytes. Since CD206 is a cell surface marker related to the anti-inflammatory ability of mononuclear cells, it is thus feasible to speculate that sucralose ingestion may associate with increased proinflammatory capacity of human monocytes. As mentioned above, Rosales-Gomez and collaborators recently demonstrated that sucralose consumption exerts proinflammatory effects on mouse $CD3^+$ T cells by rising TNF-alpha and IFN-gamma expression and reducing the expression of IL-10 [5]. Similarly, Bian and coworkers found increased expression of the proinflammatory markers TNF-alpha and nitric-oxide synthase 2 (NOS2) in the liver of mice receiving sucralose in the drinking water [46]. Present evidence concurs with our findings and supports the idea that sucralose may exert proinflammatory actions on nonclassical monocytes by decreasing CD206 expression. Nevertheless, we want to state that we still did not conduct any experimental *in vitro* study that firmly supports a direct role of sucralose on the anti-inflammatory activity of monocyte subsets and we are unable to draw solid conclusions regarding this topic at this time. Therefore, further *in vitro* studies are needed to characterize the possible effect of sucralose as a nonprototypic proinflammatory signal able to decrease CD206 expression in human monocytes.

It is worth mentioning that this study has some limitations including a possible participation of the sucralose sweet taste that may modify insulin secretion via the central nervous system as well the limited number of participants in each group. The amendment of these limitations (i.e., by using capsules containing sucralose) will bring more solid data to study the effect of sucralose on human metabolism and immunology.

## 5. Conclusions

This work demonstrates that a single sip of 48 mg sucralose increases the serum levels of insulin in age- and sex-matched non-insulin-resistant young adults subjected to an OGTT. Sucralose consumption was not only related to elevated levels of insulin but also increased proportion of classical monocytes and reduced percentage of nonclassical monocytes that in turn showed low expression levels of CD11c and CD206. Present results expand on the body of work that links sucralose consumption with unbalance of immune cell populations and alteration of insulin homeostasis. This work is relevant since the amount of sucralose studied here is contained in numerous "light" beverages available in the market and encourages further research focused on exploring the potential long-term impact of noncaloric artificial sweeteners on insulin metabolism and immune response in humans.

## Data Availability

The data used to support the findings of this study are available from the corresponding author upon request.

## Conflicts of Interest

The authors declare that there is no conflict of interest regarding the publication of this article.

## Authors' Contributions

Angélica Y. Gómez-Arauz, and Nallely Bueno-Hernández equally contributed to this work.

## Acknowledgments

This work was supported by grant no. 261575 from the Fondo Sectorial de Investigación y Desarrollo en Salud y Seguridad Social SS/IMSS/ISSSTE/CONACYT-México to G Meléndez and grant no. 286209 from the Fondo Sectorial de Investigación para la Educación-CONACYT-México to G Escobedo, and is a component of the M.Sc. requirements of A-Y Gómez-Arauz in the Posgrado en Ciencias Médicas, Odontológicas y de la Salud de la Universidad Nacional

Autónoma de México. Dr. Blair Brown from the Medical School of the University of Minnesota corrected the English version of the manuscript. Authors thank the Flow Cytometry core facility from "Coordinación de Investigación en Salud" at "Centro Médico Nacional, Siglo XXI" of IMSS for instrumentation.

## References

[1] E. Palkowska-Gozdzik, A. Bigos, and D. Rosolowska-Huszcz, "Type of sweet flavour carrier affects thyroid axis activity in male rats," *European Journal of Nutrition*, vol. 57, no. 2, pp. 773–782, 2018.

[2] P. J. Rogers, P. S. Hogenkamp, C. de Graaf et al., "Does low-energy sweetener consumption affect energy intake and body weight? A systematic review, including meta-analyses, of the evidence from human and animal studies," *International Journal of Obesity*, vol. 40, no. 3, pp. 381–394, 2016.

[3] S. E. Swithers, "Artificial sweeteners are not the answer to childhood obesity," *Appetite*, vol. 93, pp. 85–90, 2015.

[4] T. Feehley and C. R. Nagler, "Health: the weighty costs of non-caloric sweeteners," *Nature*, vol. 514, no. 7521, pp. 176-177, 2014.

[5] C. A. Rosales-Gomez, B. E. Martinez-Carrillo, A. A. Resendiz-Albor et al., "Chronic consumption of sweeteners and its effect on glycaemia, cytokines, hormones, and lymphocytes of GALT in CD1 mice," *BioMed Research International*, vol. 2018, Article ID 1345282, 15 pages, 2018.

[6] A. Lertrit, S. Srimachai, S. Saetung et al., "Effects of sucralose on insulin and glucagon-like peptide-1 secretion in healthy subjects: a randomized, double-blind, placebo-controlled trial," *Nutrition*, vol. 55-56, pp. 125–130, 2018.

[7] J. Suez, T. Korem, D. Zeevi et al., "Artificial sweeteners induce glucose intolerance by altering the gut microbiota," *Nature*, vol. 514, no. 7521, pp. 181–186, 2014.

[8] K. I. Rother, E. M. Conway, and A. C. Sylvetsky, "How non-nutritive sweeteners influence hormones and health," *Trends in Endocrinology & Metabolism*, vol. 29, no. 7, pp. 455–467, 2018.

[9] M. Y. Pepino, C. D. Tiemann, B. W. Patterson, B. M. Wice, and S. Klein, "Sucralose affects glycemic and hormonal responses to an oral glucose load," *Diabetes Care*, vol. 36, no. 9, pp. 2530–2535, 2013.

[10] A. C. Sylvetsky, R. J. Brown, J. E. Blau, M. Walter, and K. I. Rother, "Hormonal responses to non-nutritive sweeteners in water and diet soda," *Nutrition & Metabolism*, vol. 13, no. 1, p. 71, 2016.

[11] P. Gonzalez-Muniesa, M. A. Martinez-Gonzalez, F. B. Hu et al., "Obesity," *Nature Reviews Disease Primers*, vol. 3, article 17034, 2017.

[12] C. Herder, S. Schneitler, W. Rathmann et al., "Low-grade inflammation, obesity, and insulin resistance in adolescents," *The Journal of Clinical Endocrinology & Metabolism*, vol. 92, no. 12, pp. 4569–4574, 2007.

[13] C. N. Lumeng and A. R. Saltiel, "Inflammatory links between obesity and metabolic disease," *The Journal of Clinical Investigation*, vol. 121, no. 6, pp. 2111–2117, 2011.

[14] R. V. Considine, "Activated monocytes: yet another link between systemic inflammation and obesity," *The Journal of Clinical Endocrinology & Metabolism*, vol. 99, no. 7, pp. 2347–2349, 2014.

[15] R. Mukherjee, P. Kanti Barman, P. Kumar Thatoi, R. Tripathy, B. Kumar Das, and B. Ravindran, "Non-classical monocytes display inflammatory features: validation in sepsis and systemic lupus erythematous," *Scientific Reports*, vol. 5, no. 1, article 13886, 2015.

[16] L. Ziegler-Heitbrock, "Blood monocytes and their subsets: established features and open questions," *Frontiers in Immunology*, vol. 6, p. 423, 2015.

[17] J. L. Grun, A. N. Manjarrez-Reyna, A. Y. Gomez-Arauz et al., "High-density lipoprotein reduction differentially modulates to classical and nonclassical monocyte subpopulations in metabolic syndrome patients and in LPS-stimulated primary human monocytes in vitro," *Journal of Immunology Research*, vol. 2018, Article ID 2737040, 12 pages, 2018.

[18] E. F. Devevre, M. Renovato-Martins, K. Clement, C. Sautes-Fridman, I. Cremer, and C. Poitou, "Profiling of the three circulating monocyte subpopulations in human obesity," *The Journal of Immunology*, vol. 194, no. 8, pp. 3917–3923, 2015.

[19] K. Wouters, K. Gaens, M. Bijnen et al., "Circulating classical monocytes are associated with $CD11c^+$ macrophages in human visceral adipose tissue," *Scientific Reports*, vol. 7, no. 1, article 42665, 2017.

[20] H. Wu, X. D. Perrard, Q. Wang et al., "CD11c expression in adipose tissue and blood and its role in diet-induced obesity," *Arteriosclerosis, Thrombosis, and Vascular Biology*, vol. 30, no. 2, pp. 186–192, 2010.

[21] W. D. Cornwell, V. Kim, X. Fan et al., "Activation and polarization of circulating monocytes in severe chronic obstructive pulmonary disease," *BMC Pulmonary Medicine*, vol. 18, no. 1, p. 101, 2018.

[22] M. D. Kristensen, M. T. Lund, M. Hansen et al., "Macrophage area content and phenotype in hepatic and adipose tissue in patients with obesity undergoing roux-en-Y gastric bypass," *Obesity*, vol. 25, no. 11, pp. 1921–1931, 2017.

[23] D. Liu, F. E. Morales, H. B. IglayReger et al., "Expression of macrophage genes within skeletal muscle correlates inversely with adiposity and insulin resistance in humans," *Applied Physiology, Nutrition, and Metabolism*, vol. 43, no. 2, pp. 187–193, 2018.

[24] J. M. Wentworth, G. Naselli, W. A. Brown et al., "Pro-inflammatory $CD11c^+CD206^+$ adipose tissue macrophages are associated with insulin resistance in human obesity," *Diabetes*, vol. 59, no. 7, pp. 1648–1656, 2010.

[25] H. Q. Qu, Q. Li, A. R. Rentfro, S. P. Fisher-Hoch, and J. B. McCormick, "The definition of insulin resistance using HOMA-IR for Americans of Mexican descent using machine learning," *PLoS One*, vol. 6, no. 6, article e21041, 2011.

[26] V. Purohit and S. Mishra, "The truth about artificial sweeteners – are they good for diabetics?," *Indian Heart Journal*, vol. 70, no. 1, pp. 197–199, 2018.

[27] K. Takahashi, H. Nakamura, H. Sato, H. Matsuda, K. Takada, and T. Tsuji, "Four plasma glucose and insulin responses to a 75 g OGTT in healthy young Japanese women," *Journal Diabetes Research*, vol. 2018, article 5742497, 7 pages, 2018.

[28] D. Young-Hyman, D. G. Schlundt, L. Herman, F. De Luca, and D. Counts, "Evaluation of the insulin resistance syndrome in 5- to 10-year-old overweight/obese African-American children," *Diabetes Care*, vol. 24, no. 8, pp. 1359–1364, 2001.

[29] A. Algoblan, M. Alalfi, and M. Khan, "Mechanism linking diabetes mellitus and obesity," *Diabetes, Metabolic Syndrome and Obesity: Targets and Therapy*, vol. 7, pp. 587–591, 2014.

[30] A. C. Meyer-Gerspach, L. Cajacob, D. Riva et al., "Mechanisms regulating insulin response to intragastric glucose in lean and non-diabetic obese subjects: a randomized, double-blind, parallel-group trial," *PLoS One*, vol. 11, no. 3, article e0150803, 2016.

[31] M. E. Røder, D. Porte Jr., R. S. Schwartz, and S. E. Kahn, "Disproportionately elevated proinsulin levels reflect the degree of impaired B cell secretory capacity in patients with noninsulin-dependent diabetes mellitus," *The Journal of Clinical Endocrinology & Metabolism*, vol. 83, no. 2, pp. 604–608, 1998.

[32] P. A. Velasquez-Mieyer, P. A. Cowan, K. L. Arheart et al., "Suppression of insulin secretion is associated with weight loss and altered macronutrient intake and preference in a subset of obese adults," *International Journal of Obesity*, vol. 27, no. 2, pp. 219–226, 2003.

[33] Y. Nakagawa, M. Nagasawa, S. Yamada et al., "Sweet taste receptor expressed in pancreatic $\beta$-cells activates the calcium and cyclic AMP signaling systems and stimulates insulin secretion," *PLoS One*, vol. 4, no. 4, article e5106, 2009.

[34] J. F. Ferguson, R. Y. Shah, R. Shah, N. N. Mehta, M. R. Rickels, and M. P. Reilly, "Activation of innate immunity modulates insulin sensitivity, glucose effectiveness and pancreatic $\beta$-cell function in both African ancestry and European ancestry healthy humans," *Metabolism*, vol. 64, no. 4, pp. 513–520, 2015.

[35] K. Moganti, F. Li, C. Schmuttermaier et al., "Hyperglycemia induces mixed M1/M2 cytokine profile in primary human monocyte-derived macrophages," *Immunobiology*, vol. 222, no. 10, pp. 952–959, 2017.

[36] I. Torres-Castro, U. D. Arroyo-Camarena, C. P. Martinez-Reyes et al., "Human monocytes and macrophages undergo M1-type inflammatory polarization in response to high levels of glucose," *Immunology Letters*, vol. 176, pp. 81–89, 2016.

[37] F. Rahiman and E. J. Pool, "The in vitro effects of artificial and natural sweeteners on the immune system using whole blood culture assays," *Journal of Immunoassay and Immunochemistry*, vol. 35, no. 1, pp. 26–36, 2014.

[38] M. O. Welcome, N. E. Mastorakis, and V. A. Pereverzev, "Sweet taste receptor signaling network: possible implication for cognitive functioning," *Neurology Research International*, vol. 2015, Article ID 606479, 13 pages, 2015.

[39] D. Hofer, B. Puschel, and D. Drenckhahn, "Taste receptor-like cells in the rat gut identified by expression of alpha-gustducin," *Proceedings of the National Academy of Sciences of the United States of America*, vol. 93, no. 13, pp. 6631–6634, 1996.

[40] I. Kojima and Y. Nakagawa, "The role of the sweet taste receptor in enteroendocrine cells and pancreatic $\beta$-cells," *Diabetes & Metabolism Journal*, vol. 35, no. 5, pp. 451–457, 2011.

[41] K. Taya, K. Hirose, and S. Hamada, "Trehalose inhibits inflammatory cytokine production by protecting I$\kappa$B-$\alpha$ reduction in mouse peritoneal macrophages," *Archives of Oral Biology*, vol. 54, no. 8, pp. 749–756, 2009.

[42] M. M. Thewissen, J. van de Gaar, A. T. den Boer, M. J. Munsters, E. E. Blaak, and A. Duijvestijn, "Monocytes, but not T cells, respond to insulin with Akt(S473) phosphorylation independent of the donor glucometabolic state," *Diabetes/Metabolism Research and Reviews*, vol. 30, no. 4, pp. 323–332, 2014.

[43] R. C. Bunn, G. E. Cockrell, Y. Ou, K. M. Thrailkill, C. K. Lumpkin, and J. L. Fowlkes, "Palmitate and insulin synergistically induce IL-6 expression in human monocytes," *Cardiovascular Diabetology*, vol. 9, no. 1, p. 73, 2010.

[44] C. Shi and E. G. Pamer, "Monocyte recruitment during infection and inflammation," *Nature Reviews Immunology*, vol. 11, no. 11, pp. 762–774, 2011.

[45] D. C. Macias-Ceja, J. Cosin-Roger, D. Ortiz-Masia et al., "Stimulation of autophagy prevents intestinal mucosal inflammation and ameliorates murine colitis," *British Journal of Pharmacology*, vol. 174, no. 15, pp. 2501–2511, 2017.

[46] X. Bian, L. Chi, B. Gao, P. Tu, H. Ru, and K. Lu, "Gut microbiome response to sucralose and its potential role in inducing liver inflammation in mice," *Frontiers in Physiology*, vol. 8, p. 487, 2017.

Received: 12 June 2018 | Revised: 27 August 2018 | Accepted: 2 September 2018

DOI: 10.1111/sji.12716

EXPERIMENTAL IMMUNOLOGY

WILEY Scandinavian Journal of Immunology

# Infliximab ameliorates tumor necrosis factor-alpha-induced insulin resistance by attenuating PTP1B activation in 3T3L1 adipocytes in vitro

**Lucia A. Méndez-García**[1] | **Fernanda Trejo-Millán**[1] | **Camilo P. Martínez-Reyes**[1] | **Aarón N. Manjarrez-Reyna**[1] | **Marcela Esquivel-Velázquez**[1] | **Guillermo Melendez-Mier**[1] | **Sergio Islas-Andrade**[1] | **Araceli Rojas-Bernabé**[2] | **Julia Kzhyshkowska**[3] | **Galileo Escobedo**[1]

[1]Laboratory for Proteomics and Metabolomics, Research Division, General Hospital of Mexico "Dr. Eduardo Liceaga", Mexico City, Mexico

[2]Research Unit for Experimental Medicine, School of Medicine, National Autonomous University of Mexico, Mexico City, Mexico

[3]Department of Innate Immunity and Tolerance, Institute of Transfusion Medicine and Immunology, Medical Faculty Mannheim, Heidelberg University, Mannheim, Germany

**Correspondence**
Galileo Escobedo, Laboratory for Proteomics and Metabolomics, Research Division, General Hospital of Mexico "Dr. Eduardo Liceaga", Mexico City, Mexico.
Email: gescobedo@unam.mx; gescobedog@msn.com.

**Funding information**
Marie Curie International Research Staff Exchange Scheme, Grant/Award Number: 295185-EULAMDIMA; Fondo Sectorial de Investigación para la Educación SEP-CONACYT-México, Grant/Award Number: 286209

**Abstract**

Insulin resistance is the inability to respond to insulin and is considered a key pathophysiological factor in the development of type 2 diabetes. Tumor necrosis factor-alpha (TNF-alpha) can directly contribute to insulin resistance by disrupting the insulin signalling pathway via protein-tyrosine phosphatase 1B (PTP1B) activation, especially in adipocytes. Infliximab (Remicade®) is a TNF-alpha-neutralizing antibody that has not been fully studied in insulin resistance. We investigated the effect of infliximab on TNF-alpha-induced insulin resistance in 3T3L1 adipocytes in vitro, and examined the possible molecular mechanisms involved. Once differentiated, adipocytes were cultured with 5 mmol $L^{-1}$ 2-deoxy-D-glucose-$^{3}$H and stimulated twice with 2 μmol $L^{-1}$ insulin, in the presence or absence of 5 ng/mL TNF-alpha and/or 10 ng/mL infliximab. Glucose uptake was measured every 20 minutes for 2 hour, and phosphorylated forms of insulin receptor (IR), insulin receptor substrate-2 (IRS-2), protein kinase B (AKT) and PTP1B were determined by Western blotting. TNF-alpha-treated adipocytes showed a significant 64% decrease in insulin-stimulated glucose uptake as compared with control cells, whereas infliximab reversed TNF-alpha actions by significantly improving glucose incorporation. Although IR phosphorylation remained unaltered, TNF-alpha was able to increase PTP1B activation and decrease phosphorylation of IRS-2 and AKT. Notably, infliximab restored phosphorylation of IRS-2 and AKT by attenuating PTP1B activation. This work demonstrates for the first time that infliximab ameliorates TNF-alpha-induced insulin resistance in 3T3L1 adipocytes in vitro by restoring the insulin signalling pathway via PTP1B inhibition. Further clinical research is needed to determine the potential benefit of using infliximab for treating insulin resistance in patients.

## 1 | INTRODUCTION

Insulin resistance is the inability of skeletal muscle, liver and adipose tissue to respond to normal levels of insulin that results in alteration of glucose homeostasis.[1] In normal conditions, insulin binds to IR and orchestrates phosphorylation of the IRS protein family.[2] Downstream, IRS activation leads to phosphorylation of PI3-kinase (PI3K) that in turn triggers phosphorylation of AKT.[2] Upon activation, AKT orchestrates translocation of cytoplasmic vesicles

  

containing glucose transporter proteins (GLUT) into the plasma membrane that facilitates transport of glucose for cell metabolism.[1,2] Glucose uptake via activation of the IRS-PI3K-AKT pathway is able to reduce glucose levels in the extracellular milieu, which in turn contributes to decrease hyperglycaemia.[3] In insulin resistance, activation of the insulin signalling pathway is progressively abrogated resulting in glucose intolerance, hyperglycaemia and hyperinsulinemia.[4] For this reason, insulin resistance is considered a key pathophysiological factor in the development of type 2 diabetes (T2D),[4,5] a chronic disease with increasing morbidity and mortality rates around the globe.[6]

TNF-alpha is a cytokine with prominent actions in cell differentiation and apoptosis, inflammation, autoimmunity and recruitment of other immune cell types toward peripheral tissues.[7-9] TNF-alpha has been also shown to play a pivotal role in glucose homeostasis by promoting insulin resistance in mice and humans, especially in adipose tissue.[10,11] In this sense, mRNA and protein levels of TNF-alpha have been previously reported to elevate in visceral adipose tissue of high-fat diet (HFD)-fed mice and obese subjects that show increased insulin resistance.[12] Moreover, TNF-alpha-deficient mice are protected against insulin resistance development,[13] while also TNF-alpha directly induces insulin resistance in 3T3L1 adipocytes in vitro.[14]

TNF-alpha favours insulin resistance by abrogating phosphorylation of IRS-1 and AKT in a variety of insulin-dependent cells including adipocytes.[15] Besides reducing IRS-1 and AKT activation, TNF-alpha can also attenuate GLUT4 expression in adipocytes,[11,16] which demonstrates that this proinflammatory cytokine is able to disrupt the insulin signalling pathway in adipose tissue. Thus, blockage of TNF-alpha actions is now considered a matter of urgency to improve insulin action in adipose tissue of patients with insulin resistance such as T2D patients.

Infliximab (Remicade®) is a chimeric monoclonal IgG1 antibody that specifically binds to TNF-alpha and prevents the interaction of TNF-alpha with TNF-alpha receptor (TNFR) 1 and TNFR2.[17] For this reason, infliximab has been used to treat a variety of autoimmune and chronic inflammatory diseases such as rheumatoid arthritis, Crohn's disease, ulcerative colitis, psoriatic arthritis and ankylosing spondylitis.[18-23] Interestingly, besides exerting anti-inflammatory actions, infliximab has been also shown to improve insulin resistance. In this sense, rheumatoid arthritis patients receiving infliximab show decreased values of the homeostatic model assessment of insulin resistance (HOMA-IR) as well as increase in the quantitative insulin sensitivity check index (QUICKI).[24] Similarly, non-diabetic patients with ankylosing spondylitis also exhibit reduced HOMA-IR and increased QUICKI after 2 hour of receiving an intravenous infliximab infusion.[25] However, despite the clinical evidence, there are no studies exploring the effect of infliximab on TNF-alpha-induced insulin resistance in target organs of insulin such as adipose tissue. Here, we investigated the effect of infliximab on TNF-alpha-induced insulin resistance in 3T3L1 adipocytes in vitro and examined the possible molecular mechanisms involved.

## 2 | MATERIAL AND METHODS

### 2.1 | 3T3L1 cell line differentiation

The murine 3T3L1 cell line (ATCC®, USA) was propagated in Dulbecco's Modified Eagle Medium (DMEM)-High Glucose (Thermo Fisher-Scientific, USA) containing 10% foetal bovine serum (FBS) and 50 μg/mL gentamicin (Sigma-Aldrich, USA) for 4 days at 37°C in humidified 5% $CO_2$ atmosphere, using 6-well cell-culture plates (Costar, USA) at a density of $50 \times 10^3$ cells per well. Once fibroblasts reached about 80% confluence, they were differentiated into adipocytes using DMEM supplemented with 10% FBS, 50 μg/mL gentamicin, 1 μmol $L^{-1}$ dexamethasone, 0.5 mmol $L^{-1}$ IBMX and 1 μmol $L^{-1}$ insulin (Sigma-Aldrich, USA). Culture media were replaced every other day for 6 days. Mature adipocytes were seen after 10 days on the in vitro culture conditions described above.

### 2.2 | Glucose uptake assay

For glucose uptake assay, 3T3L1 mature adipocytes were in vitro cultured in DMEM containing 10% FBS, 50 μg/mL gentamicin and 5 mmol $L^{-1}$ 2-deoxy-D-glucose-$^3$H (Sigma-Aldrich, USA) for 2 hour at 37°C in humidified 5% $CO_2$ atmosphere, using 6-well cell-culture plates at a density of $30 \times 10^4$ cells per well. Adipocytes were stimulated twice at zero and 60 minutes with 2 μmol $L^{-1}$ insulin. In the infliximab-treated group, adipocytes were stimulated with 10 ng/mL infliximab (Remicade®, Janssen Biotech, USA) at the beginning of the 2-hour in vitro assay. In the TNF-alpha-treated group, adipocytes were stimulated with 5 ng/mL murine TNF-alpha (Peprotech,Mexico) at the beginning of the 2-hour in vitro assay. In the infliximab+TNF-alpha-treated adipocyte group, 10 ng/mL infliximab was added at the beginning of the 2-hour in vitro assay, whereas 5 ng/mL murine TNF-alpha was added five minutes later. Control cells received neither infliximab nor TNF-alpha stimulation. All cultured 3T3L1 adipocytes were collected every 20 minutes for 2 hour for measuring glucose uptake in counts per minute (cpm), using a liquid scintillation counter (Beckman-Coulter, USA).

### 2.3 | Western blot for pIR, pIRS-2, pAKT and pPTP1B

Two hours after having been incubated with or without TNF-alpha and/or infliximab, 3T3L1 adipocytes were collected

and disrupted in protein extraction buffer containing 500 mmol $L^{-1}$ Tris-HCl (1 mL/50 × $10^4$ cells) and protease inhibitor cocktail (Calbiochem, Germany). After 15 minutes of centrifugation at 20 800 g/4°C, the supernatant was recovered for total protein quantification by measuring absorbance at 595 nm using the Bradford Protein Assay (Bio-Rad, USA). Then, 30 mg of total protein extract was boiled in Laemmli sample buffer and separated by SDS-PAGE (10% acrylamide) to transfer into PVDF membranes. Membranes were blocked overnight in PBS 1× buffer (0.2% Tween 20) containing 1% BSA. Immediately after, PVDF membranes were washed five times in PBS 1X-Tween 20 and separately incubated for up to 60 minutes at room temperature with 1:250 rabbit anti-mouse phosphorylated insulin receptor (pIR, 90 KDa), 1:500 rabbit anti-mouse phosphorylated pan-AKT (pAKT, 56 KDa), 1:650 rabbit anti-mouse phosphorylated protein-tyrosine phosphatase 1B (pPTP1B, 50 KDa), 1:1000 goat anti-mouse beta-Actin (42 KDa) (Abcam, USA) or 1:250 rabbit anti-human phosphorylated insulin receptor substrate-2 (pIRS-2, 160 KDa) (Merck-Millipore, Germany). Protein bands for pIR, pIRS-2, pAKT and pPTP1B were visualized using the peroxidase-diaminobenzidine reaction (Sigma-Aldrich, Mexico) and quantified by optical density (OD) analysis using beta-Actin as control.

### 2.4 | Statistical analysis

The Shapiro-Wilk test was performed to estimate normality in data distribution and then proceed to perform one-way ANOVA followed by a post-hoc Tukey test. Data represent at least five independent experiments and are expressed as media ± SD. Statistical analysis was performed using the GraphPad Prism 6.01 software. Areas under the curve (AUC) were calculated using R statistics and expressed as arbitrary units (a.u). Differences were considered significant when $P < 0.05$.

## 3 | RESULTS

After 40 minutes of having been in vitro stimulated with insulin, TNF-alpha-treated 3T3L1 adipocytes started to show a significant decrease in glucose uptake with respect to control untreated cells (Figure 1A). Infliximab exhibited no deleterious effects on glucose incorporation when added alone but clearly blocked TNF-alpha actions by improving glucose uptake in 3T3L1 cells in vitro (Figure 1A). At the end of the in vitro culture, 3T3L1 adipocytes treated with TNF-alpha showed a significant 2.6-fold reduction in glucose incorporation as compared to control cells ($P < 0.0001$). In contrast, adipose cells stimulated with infliximab and TNF-alpha exhibited a 2-fold increase in glucose uptake with respect to adipocytes only treated with TNF-alpha ($P < 0.0001$),

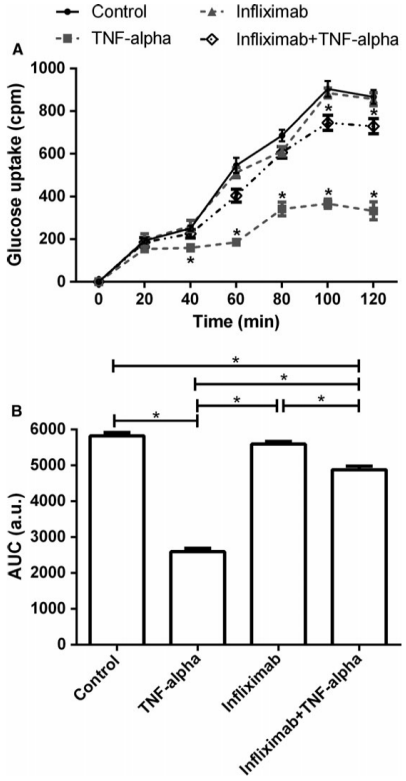


**FIGURE 1** Infliximab restores insulin-dependent glucose uptake in TNF-alpha-treated 3T3L1 adipocytes. 3T3L1 adipocytes were in vitro stimulated twice with 2 μmol $L^{-1}$ insulin at zero and 60 minutes in the presence of 2-deoxy-D-glucose-$^3$H as well as infliximab and/or TNF-alpha for 2 hours. Control adipocytes received neither infliximab nor TNF-alpha stimulation. (A) After 40 minutes, TNF-alpha (dotted grey line with solid squares) significantly decreased glucose uptake in 3T3L1 adipocytes as compared to control (black line with solid circles) and infliximab-treated adipocytes (dotted grey line with solid triangles). In contrast, infliximab restored cellular glucose incorporation by inhibiting TNF-alpha (dotted black line with hollow rhombus). Asterisks (*) indicate significant differences with respect to control untreated cells. (B) Glucose uptake kinetics in all groups was quantified as area under the curve (AUC). Overall, TNF-alpha induced 64% decrease in the AUC of glucose uptake as compared with control and infliximab-treated adipocytes. On the contrary, infliximab partially blocked TNF-alpha actions by increasing 50% the AUC of glucose uptake in 3T3L1 adipocytes. Asterisks (*) indicate significant differences among groups. Data are expressed as media ± SD. Significant differences were estimated by means of performing one-way ANOVA followed by a *post-hoc* Tukey test. Differences were considered significant when $P < 0.05$ and can be seen as asterisks (*) on the figure. TNF-alpha, tumor necrosis factor-alpha; cpm, counts per minute; a.u., arbitrary units

although glucose incorporation values were 0.15-fold lower than those found in control cells ($P = 0.0002$) (Figure 1A). Glucose uptake kinetics in 3T3L1 adipocytes was also analyzed as area under the curve (AUC) and can be seen in Figure 1B. Overall, TNF-alpha-treated 3T3L1 adipocytes showed a significant 64% decrease in the AUC of glucose uptake as compared with control cells ($P < 0.0001$) (Figure 1B). On the contrary, infliximab did not alter the AUC of glucose incorporation when added alone but partially reverted TNF-alpha actions by increasing 50% the AUC of glucose uptake in these adipose cells ($P < 0.0001$) (Figure 1B). Although use of infliximab significantly reversed the effect of TNF-alpha on 3T3L1 adipocytes in vitro, the AUC of glucose incorporation was 15% lower than that found in control cells ($P < 0.001$) (Figure 1B).

Neither TNF-alpha nor infliximab, alone or combined, altered the phosphorylation pattern of pIR in 3T3L1 adipocytes when compared to untreated cells (Figure 2A, B). On the contrary, pIRS-2 was significantly decreased by 3.25-fold in 3T3L1 adipocytes treated with TNF-alpha as compared to untreated cells ($P < 0.0001$) (Figure 2A, C). Infliximab showed no effect on pIRS-2 when added alone but significantly reverted TNF-alpha actions by restoring phosphorylation of pIRS-2 at similar levels than those found in control cells ($P < 0.0001$) (Figure 2A, C). When in vitro treated with TNF-alpha, 3T3L1 adipocytes showed a significant 2-fold decrease in pAKT as compared to untreated cells ($P < 0.0001$) (Figure 2A, D). On the other hand, infliximab had no effect on pAKT when added alone but partially reestablished phosphorylation of this protein in TNF-alpha-treated 3T3L1 adipocytes ($P = 0.0021$); however, AKT phosphorylation levels remained nether in comparison to control cells (Figure 2A and D) ($P = 0.0034$).

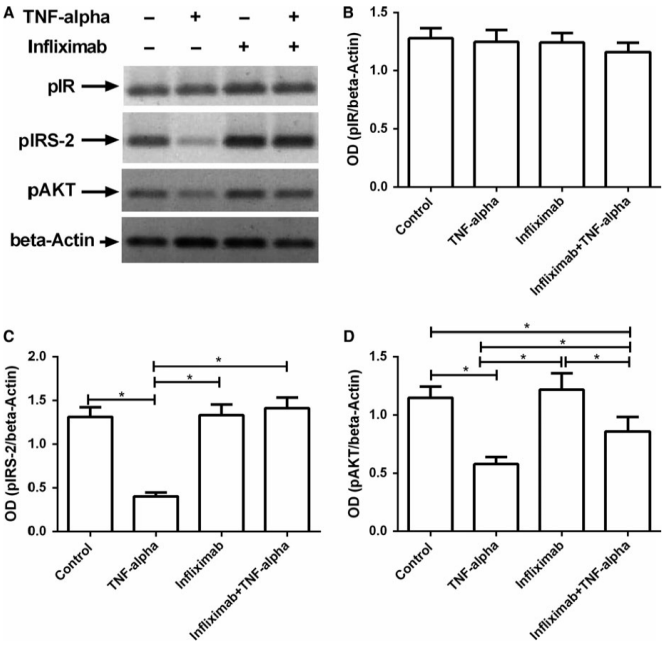


**FIGURE 2** Infliximab restores phosphorylation of the insulin signaling pathway in TNF-alpha-treated 3T3L1 adipocytes. (A) Representative Western blot showing phosphorylated forms of IR, IRS-2 and AKT in 3T3L1 adipocytes with and without TNF-alpha or infliximab treatment. The beta-Actin was used as control for optical density (OD) analysis. (B) According to OD analysis, neither TNF-alpha nor infliximab, alone or combined, altered pIR in 3T3L1 adipocytes. (C) TNF-alpha induced 65% decrease in pIRS-2 as compared with control and infliximab-treated adipocytes. On the contrary, infliximab blocked TNF-alpha actions by restoring phosphorylation of IRS-2 in 3T3L1 adipocytes. (D) TNF-alpha induced 50% decrease in pAKT as compared with control and infliximab-treated adipocytes. On the other hand, infliximab blocked TNF-alpha actions by partially restoring phosphorylation of AKT in 3T3L1 adipocytes. Asterisks (*) indicate significant differences among groups. Data are expressed as media ± SD. Significant differences were estimated by means of performing one-way ANOVA followed by a post-hoc Tukey test. Differences were considered significant when $P < 0.05$. TNF-alpha, tumor necrosis factor-alpha; pIR, phosphorylated form of insulin receptor; pIRS-2, phosphorylated form of insulin receptor substrate-2; pAKT, phosphorylated form of protein kinase B; OD, optical density

The effects of TNF-alpha and infliximab on pPTP1B can be seen in the representative Western blotting shown in Figure 3A. TNF-alpha-treated 3T3L1 adipocytes exhibited a significant 4-fold increase in pPTP1B as compared to untreated cells ($P = 0.0055$) (Figure 1B). On the contrary, infliximab showed no effect on pPTP1B when added alone but revoked TNF-alpha actions by partially reducing phosphorylation of PTP1B in 3T3L1 adipocytes ($P = 0.0372$) (Figure 3B).

## 4 | DISCUSSION

TNF-alpha has been consistently shown to play a causal role in the development of insulin resistance in adipose tissue of HFD-fed mice and humans with obesity. For instance, T2D patients carrying the TNF-alpha 308 G/A polymorphism that has been associated with increased TNF-alpha levels, show higher values of the homeostatic model assessment of insulin resistance (HOMA-IR) than patients with the G/G wild genotype.[26] For this reason, numerous studies are now focused on finding novel therapeutic agents with the ability to abrogate the effects of TNF-alpha on insulin sensitivity, although results are still controversial. In this regard, Sprague-Dawley rats treated with goat anti-murine TNF-alpha IgG antibody showed improvement in insulin-mediated glucose transport in skeletal muscle.[27] In contrast, blockage of TNF-alpha using the recombinant-engineered human TNF-alpha-neutralizing antibody CDP571 did not show improvement in insulin sensitivity of patients with T2D.[28] Our study shows that neutralization of TNF-alpha improves glucose uptake by reversing insulin resistance and provides solid evidence regarding the use of therapeutic agents against TNF-alpha for improving insulin sensitivity in adipose cells. However, these results should be considered with caution as they reflect only the behaviour of an adipocyte cell line on in vitro culture conditions.

Infliximab is a medication used to treat patients with autoimmune and chronic inflammatory diseases.[18-22] Notably, besides improving joint pain, swelling and inflammation, infliximab also reduces the levels of serum insulin, fasting glucose and insulin resistance in patients with ankylosing spondylitis and rheumatoid arthritis.[29,30] It has been also reported that obese people show improvement in insulin resistance when treated with 5 mg/kg infliximab every 2 months, including a T2D patient who did not longer require insulin administration about 5 months after infliximab therapy.[31] Concurring with previous evidence, our data reveal that infliximab directly reverses insulin resistance and restores glucose homeostasis in adipose cells, even under proinflammatory conditions such as those promoted by TNF-alpha.

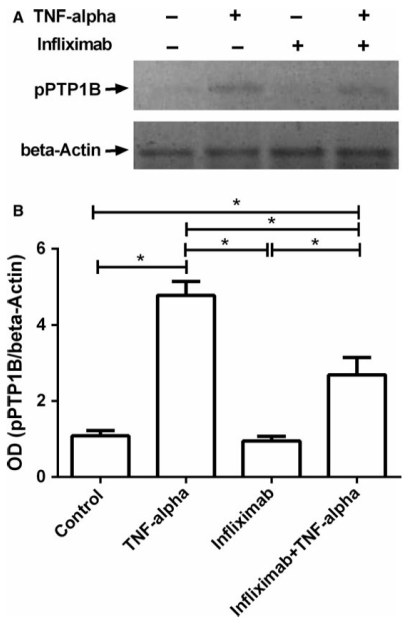


**FIGURE 3** Infliximab attenuates TNF-alpha-induced PTP1B activation in 3T3L1 adipocytes. (A) Representative Western blot showing phosphorylated form of PTP1B in 3T3L1 adipocytes with and without TNF-alpha or infliximab treatment. beta-Actin was used as control for optical density (OD) analysis. (B) According to OD analysis, TNF-alpha induced a 4-fold increase in phosphorylation of PTP1B as compared to control and infliximab-treated adipocytes. However, infliximab blocked TNF-alpha actions by decreasing PTP1B activation in 3T3L1 adipocytes. Asterisks (*) indicate significant differences among groups. Data are expressed as media ± standard deviation. Significant differences were estimated by means of performing one-way ANOVA followed by a *post-hoc* Tukey test. Differences were considered significant when $P < 0.05$. TNF-alpha, tumor necrosis factor-alpha; pPTP1B, phosphorylated form of protein-tyrosine phosphatase 1B; OD, optical density

Another phenomenon captured in our study involves the possible molecular mechanism by which infliximab exerts its beneficial effects on TNF-alpha-induced insulin resistance in 3T3L1 adipocytes in vitro. Our data show that TNF-alpha is not able to impair insulin-mediated IR phosphorylation, a finding that has been previously reported in mice and rats.[14,32,33] Thus, it is reasonable to consider that TNF-alpha may promote adipocyte insulin resistance by inducing downstream activation of PTP1B. PTP1B is a negative regulator of the insulin signalling pathway with the ability to dephosphorylate tyrosine residues in numerous activated tyrosine kinase proteins including the IRS protein family.[33,34] A previous work reported that mice

lacking PTP1B expression ($PTP1B^{-/-}$) show enhanced insulin sensitivity and normal body weight, even after having been fed a HFD.[35] Notably, re-expression of PTP1B in the liver of $PTP1B^{-/-}$ mice attenuated whole-body insulin sensitivity and IRS-2 activation in hepatocytes.[35] A similar study showed that PTP1B activity abrogates phosphorylation of IRS-1 in skeletal muscle cells that results in decreased insulin sensitivity and altered glucose homeostasis.[36] Our data expand on this body of work by revealing for the first time that TNF-alpha-induced PTP1B activation can directly decrease phosphorylation of IRS-2 in adipose cells, which in turn might lead to AKT inhibition and increased insulin resistance. Furthermore, our results also demonstrate that infliximab is able to reverse PTP1B activation, which (a) confirms the causative role of TNF-alpha in insulin resistance and (b) might explain the improvement of IRS-2 phosphorylation and glucose uptake in adipocytes exposed to a proinflammatory milieu (Figure 4).

PTP1B has now emerged as a key molecule in mediating TNF-alpha-induced insulin resistance in insulin-dependent cells as is the case of skeletal muscle cells and adipocytes. For this reason, a growing number of studies have examined the effect of PTP1B inhibitors on insulin resistance. In this sense, Yi-ming Ma and coworkers previously showed that CCF06240, a PTP1B inhibitor, restores insulin sensitivity in HFD-fed mice and promotes phosphorylation of IRS-1 in HepG2 cells in vitro.[37] Similarly, a recent study reported a decrease in blood glucose and insulin resistance in ob/ob mice receiving Fudan-Yueyang-Ganoderma-lucidum (FYGL), a proteoglycan with the ability to inhibit PTP1B.[38] Interestingly, FYGL was also shown to improve insulin-stimulated glucose uptake and activation of IRS-1, PI3K and AKT by blocking PTP1B activation in rat myoblast L6 cells.[38] Consistent with previous evidence, we found that infliximab also acts as PTP1B inhibitor by exerting the ability to improve insulin signalling pathway and consequently glucose homeostasis in 3T3L1 adipocytes exposed to TNF-alpha in vitro.

Little is known yet about the activity of PTP1B in other tissues different from adipose tissue. In this sense,

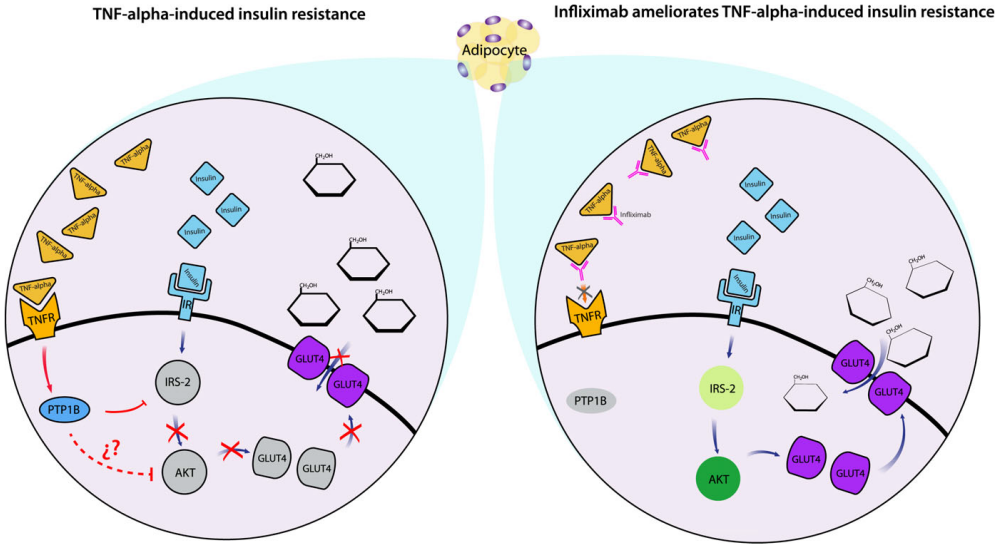


**FIGURE 4** Possible molecular mechanism involved in mediating the effect of infliximab on TNF-alpha-induced insulin resistance in adipocytes in vitro. In TNF-alpha-induced insulin resistance (left panel), TNF-alpha binds to TNFR found on the cell surface of adipocytes, which in turn triggers PTP1B activation. Downstream, PTP1B is able to dephosphorylate IRS-2 that in turn leads to AKT arrest, even though insulin is continually binding to IR. Alternatively, AKT phosphorylation may be directly inhibited by PTP1B; however, there are not yet solid evidence supporting this notion. As a consequence of IRS-2 and AKT attenuation, GLUT4 translocation into the plasma membrane is arrested that in turn impedes the intracellular transport of glucose and leads to hyperglycaemia. On the contrary (right panel), infliximab specifically binds to TNF-alpha and neutralizes the interaction of TNF-alpha with TNFR that results in PTP1B attenuation. In consequence, IRS-2 and AKT are normally phosphorylated in response to insulin, which facilitates membrane translocation of GLUT4 and promotes glucose homeostasis, even when TNF-alpha levels are elevated. TNF-alpha, tumor necrosis factor-alpha; TNFR, tumor necrosis factor-alpha receptor; PTP1B, protein-tyrosine phosphatase 1B; IR, insulin receptor; IRS-2, insulin receptor substrate-2; AKT, protein kinase B; GLUT4, glucose transporter protein 4

liver-specific PTP1B$^{-/-}$ mice show improved glucose homeostasis and lipid metabolism, accompanied by reduction in HFD-induced endoplasmic reticulum stress.[39] Interestingly, aging has been shown to increase PTP1B expression and insulin resistance in liver of rats, a phenomenon that can be reversed by workout.[40] It has been also shown that PTP1B contributes to hypothalamic inflammation and leptin resistance in rodents fed a HFD.[41] As a matter of fact, PTP1B$^{-/-}$ mice exhibit decreased TNF-alpha expression, accompanied by increased interleukin-10 mRNA levels in the hypothalamus, even under HFD-feeding.[42] Notably, TNF-alpha has been shown to increase PTP1B expression in hypothalamic organotypic cultures in a dose and time-dependent fashion.[43] Nevertheless, despite PTP1B has been consistently shown to mediate insulin and leptin resistance in response to proinflammatory signals including endoplasmic reticulum stress, aging and TNF-alpha, there is still scant evidence regarding the benefit of using PTP1B and TNF-alpha-specific inhibitors. In this sense, this work brings to light the potential impact of using infliximab as a PTP1B inhibitor for ameliorating TNF-alpha-induced insulin resistance in adipose tissue. For this reason, we encourage exploring the possible effect of infliximab on other signaling cascades stimulated by TNF-alpha that may also disrupt insulin-dependent glucose uptake in adipocytes *in vitro* and in vivo, such as those depending on ceramides and extracellular-signal-regulated kinases (ERK). The implications for understanding the mechanisms through which infliximab improves TNF-alpha-induced insulin resistance are profound, and the idea that further knowledge of these pathways might allow prediction of susceptibility to type 2 diabetes adds a compelling degree of urgency to further study.

In conclusion, this work demonstrates for the first time that infliximab ameliorates TNF-alpha-induced insulin resistance in 3T3L1 adipocytes in vitro by restoring phosphorylation of key mediators of the insulin signaling pathway such as IRS-2 and AKT via PTP1B inhibition that in consequence improves insulin-dependent glucose uptake in these adipose cells (Figure 4).

## ACKNOWLEDGMENT

This work was supported by grant no. 286209 from the Fondo Sectorial de Investigación para la Educación SEP-CONACYT-México to GE. The authors thank Ing. Omar Agni García Hernández for his valuable technical assistance with electronic artwork. This project has received funding from the Marie Curie International Research Staff Exchange Scheme with the 7$^{th}$ European Community Framework Program under grant agreement No. 295185-EULAMDIMA.

## CONFLICT OF INTEREST

The authors declare that there is no conflict of interests regarding the publication of this manuscript.

## ORCID

*Galileo Escobedo* http://orcid.org/0000-0002-9224-7400

## REFERENCES

1. DeFronzo RA, Tripathy D. Skeletal muscle insulin resistance is the primary defect in type 2 diabetes. *Diabetes Care*. 2009;32 (Suppl 2):S157-S163.
2. Boucher J, Kleinridders A, Kahn CR. Insulin receptor signaling in normal and insulin-resistant states. *Cold Spring Harb Perspect Biol*. 2014;6:a009191.
3. Stanford KI, Goodyear LJ. Exercise and type 2 diabetes: molecular mechanisms regulating glucose uptake in skeletal muscle. *Adv Physiol Educ*. 2014;38:308-314.
4. Shanik MH, Xu Y, Skrha J, Dankner R, Zick Y, Roth J. Insulin resistance and hyperinsulinemia: is hyperinsulinemia the cart or the horse? *Diabetes Care*. 2008;31(Suppl 2):S262-S268.
5. Taylor R. Insulin resistance and type 2 diabetes. *Diabetes*. 2012;61:778-779.
6. Zheng Y, Ley SH, Hu FB. Global aetiology and epidemiology of type 2 diabetes mellitus and its complications. *Nat Rev Endocrinol*. 2018;14:88-98.
7. Baregamian N, Song J, Bailey CE, Papaconstantinou J, Evers BM, Chung DH. Tumor necrosis factor-alpha and apoptosis signal-regulating kinase 1 control reactive oxygen species release, mitochondrial autophagy, and c-Jun N-terminal kinase/p38 phosphorylation during necrotizing enterocolitis. *Oxid Med Cell Longev*. 2009;2:297-306.
8. Sade-Feldman M, Kanterman J, Ish-Shalom E, Elnekave M, Horwitz E, Baniyash M. Tumor necrosis factor-alpha blocks differentiation and enhances suppressive activity of immature myeloid cells during chronic inflammation. *Immunity*. 2013;38:541-554.
9. Chyuan IT, Tsai HF, Liao HJ, Wu CS, Hsu PN. An apoptosis-independent role of TRAIL in suppressing joint inflammation and inhibiting T-cell activation in inflammatory arthritis. *Cell Mol Immunol*. 2017; https://doi.org/10.1038/cmi.2017.2.
10. Tse MCL, Herlea-Pana O, Brobst D, et al. Tumor necrosis factor-alpha promotes phosphoinositide 3-kinase enhancer A and AMP-activated protein kinase interaction to suppress lipid oxidation in skeletal muscle. *Diabetes*. 2017;66:1858-1870.
11. Akash MSH, Rehman K, Liaqat A. Tumor necrosis factor-alpha: role in development of insulin resistance and pathogenesis of type 2 diabetes mellitus. *J Cell Biochem*. 2018;119:105-110.
12. Hotamisligil GS. The role of TNFalpha and TNF receptors in obesity and insulin resistance. *J Intern Med*. 1999;245:621-625.
13. Hotamisligil GS. Inflammatory pathways and insulin action. *Int J Obes Relat Metab Disord*. 2003;27(Suppl 3):S53-S55.
14. Stephens JM, Lee J, Pilch PF. Tumor necrosis factor-alpha-induced insulin resistance in 3T3-L1 adipocytes is accompanied by a loss of insulin receptor substrate-1 and GLUT4 expression without a loss of insulin receptor-mediated signal transduction. *J Biol Chem*. 1997;272:971-976.

15. Hotamisligil GS, Peraldi P, Budavari A, Ellis R, White MF, Spiegelman BM. IRS-1-mediated inhibition of insulin receptor tyrosine kinase activity in TNF-alpha- and obesity-induced insulin resistance. *Science*. 1996;271:665-668.
16. Guilherme A, Virbasius JV, Puri V, Czech MP. Adipocyte dysfunctions linking obesity to insulin resistance and type 2 diabetes. *Nat Rev Mol Cell Biol*. 2008;9:367-377.
17. Lis K, Kuzawinska O, Balkowiec-Iskra E. Tumor necrosis factor inhibitors - state of knowledge. *Arch Med Sci*. 2014;10:1175-1185.
18. Alten R, van den Bosch F. Dose optimization of infliximab in patients with rheumatoid arthritis. *Int J Rheum Dis*. 2014;17:5-18.
19. Colombel JF, Loftus EV Jr, Tremaine WJ, et al. The safety profile of infliximab in patients with Crohn's disease: the Mayo clinic experience in 500 patients. *Gastroenterology*. 2004;126:19-31.
20. Fiorino G, Cortes PN, Ellul P, et al. Discontinuation of infliximab in patients with ulcerative colitis is associated with increased risk of relapse: a multinational retrospective cohort study. *Clin Gastroenterol Hepatol*. 2016;14:1426-1432 e1.
21. Antoni C, Krueger GG, de Vlam K, et al. Infliximab improves signs and symptoms of psoriatic arthritis: results of the IMPACT 2 trial. *Ann Rheum Dis*. 2005;64:1150-1157.
22. Braun J, Deodhar A, Dijkmans B, et al. Efficacy and safety of infliximab in patients with ankylosing spondylitis over a two-year period. *Arthritis Rheum*. 2008;59:1270-1278.
23. Dahlen R, Strid H, Lundgren A, et al. Infliximab inhibits activation and effector functions of peripheral blood T cells in vitro from patients with clinically active ulcerative colitis. *Scand J Immunol*. 2013;78:275-284.
24. Burska AN, Sakthiswary R, Sattar N. Effects of tumour necrosis factor antagonists on insulin sensitivity/resistance in rheumatoid arthritis: a systematic review and meta-analysis. *PLoS ONE*. 2015;10:e0128889.
25. Miranda-Filloy JA, Llorca J, Carnero-Lopez B, Gonzalez-Juanatey C, Blanco R, Gonzalez-Gay MA. TNF-alpha antagonist therapy improves insulin sensitivity in non-diabetic ankylosing spondylitis patients. *Clin Exp Rheumatol*. 2012;30:850-855.
26. Golshani H, Haghani K, Dousti M, Bakhtiyari S. Association of TNF-alpha 308 G/A polymorphism with type 2 diabetes: a case-control study in the Iranian Kurdish Ethnic Group. *Osong Public Health Res Perspect*. 2015;6:94-99.
27. Borst SE, Lee Y, Conover CF, Shek EW, Bagby GJ. Neutralization of tumor necrosis factor-alpha reverses insulin resistance in skeletal muscle but not adipose tissue. *Am J Physiol Endocrinol Metab*. 2004;287:E934-E938.
28. Ofei F, Hurel S, Newkirk J, Sopwith M, Taylor R. Effects of an engineered human anti-TNF-alpha antibody (CDP571) on insulin sensitivity and glycemic control in patients with NIDDM. *Diabetes*. 1996;45:881-885.
29. Kiortsis DN, Mavridis AK, Vasakos S, Nikas SN, Drosos AA. Effects of infliximab treatment on insulin resistance in patients with rheumatoid arthritis and ankylosing spondylitis. *Ann Rheum Dis*. 2005;64:765-766.
30. Stagakis I, Bertsias G, Karvounaris S, et al. Anti-tumor necrosis factor therapy improves insulin resistance, beta cell function and insulin signaling in active rheumatoid arthritis patients with high insulin resistance. *Arthritis Res Ther*. 2012;14:R141.
31. Yazdani-Biuki B, Stelzl H, Brezinschek HP, et al. Improvement of insulin sensitivity in insulin resistant subjects during prolonged treatment with the anti-TNF-alpha antibody infliximab. *Eur J Clin Invest*. 2004;34:641-642.
32. Zinker BA, Rondinone CM, Trevillyan JM, et al. PTP1B antisense oligonucleotide lowers PTP1B protein, normalizes blood glucose, and improves insulin sensitivity in diabetic mice. *Proc Natl Acad Sci USA*. 2002;99:11357-11362.
33. Picardi PK, Caricilli AM, de Abreu LL, Carvalheira JB, Velloso LA, Saad MJ. Modulation of hypothalamic PTP1B in the TNF-alpha-induced insulin and leptin resistance. *FEBS Lett*. 2010;584:3179-3184.
34. Nieto-Vazquez I, Fernandez-Veledo S, Kramer DK, Vila-Bedmar R, Garcia-Guerra L, Lorenzo M. Insulin resistance associated to obesity: the link TNF-alpha. *Arch Physiol Biochem*. 2008;114:183-194.
35. Haj FG, Zabolotny JM, Kim YB, Kahn BB, Neel BG. Liver-specific protein-tyrosine phosphatase 1B (PTP1B) re-expression alters glucose homeostasis of PTP1B-/-mice. *J Biol Chem*. 2005;280:15038-15046.
36. Tiganis T. PTP1B and TCPTP–nonredundant phosphatases in insulin signaling and glucose homeostasis. *FEBS J*. 2013;280:445-458.
37. Ma YM, Tao RY, Liu Q, et al. PTP1B inhibitor improves both insulin resistance and lipid abnormalities in vivo and in vitro. *Mol Cell Biochem*. 2011;357:65-72.
38. Yang Z, Wu F, He Y, et al. A novel PTP1B inhibitor extracted from Ganoderma lucidum ameliorates insulin resistance by regulating IRS1-GLUT4 cascades in the insulin signaling pathway. *Food Funct*. 2018;9:397-406.
39. Delibegovic M, Zimmer D, Kauffman C, et al. Liver-specific deletion of protein-tyrosine phosphatase 1B (PTP1B) improves metabolic syndrome and attenuates diet-induced endoplasmic reticulum stress. *Diabetes*. 2009;58:590-599.
40. de Moura LP, Souza Pauli LS, Cintra DE, et al. Acute exercise decreases PTP-1B protein level and improves insulin signaling in the liver of old rats. *Immun Ageing*. 2013;10:8.
41. White CL, Whittington A, Barnes MJ, Wang Z, Bray GA, Morrison CD. HF diets increase hypothalamic PTP1B and induce leptin resistance through both leptin-dependent and -independent mechanisms. *Am J Physiol Endocrinol Metab*. 2009;296:E291-E299.
42. Tsunekawa T, Banno R, Mizoguchi A, et al. Deficiency of PTP1B attenuates hypothalamic inflammation via activation of the JAK2-STAT3 pathway in microglia. *EBioMedicine*. 2017;16:172-183.
43. Ito Y, Banno R, Hagimoto S, Ozawa Y, Arima H, Oiso Y. TNFalpha increases hypothalamic PTP1B activity via the NFkappaB pathway in rat hypothalamic organotypic cultures. *Regul Pept*. 2012;174:58-64.

**How to cite this article:** Méndez-García LA, Trejo-Millán F, Martínez-Reyes CP, et al. Infliximab ameliorates tumor necrosis factor-alpha-induced insulin resistance by attenuating PTP1B activation in 3T3L1 adipocytes in vitro. *Scand J Immunol*. 2018;88:e12716. https://doi.org/10.1111/sji.12716

Hindawi
Journal of Immunology Research
Volume 2018, Article ID 2737040, 12 pages
https://doi.org/10.1155/2018/2737040

*Research Article*

# High-Density Lipoprotein Reduction Differentially Modulates to Classical and Nonclassical Monocyte Subpopulations in Metabolic Syndrome Patients and in LPS-Stimulated Primary Human Monocytes *In Vitro*

**Johanna L. Grün,[1,2,3] Aaron N. Manjarrez-Reyna,[3,4] Angélica Y. Gómez-Arauz,[3,4] Sonia Leon-Cabrera,[5] Felix Rückert,[2] José M. Fragoso,[6] Nallely Bueno-Hernández,[4] Sergio Islas-Andrade,[4] Guillermo Meléndez-Mier,[4] and Galileo Escobedo[3,4]**

[1]*Department of Innate Immunity and Tolerance, Institute of Transfusion Medicine and Immunology, Medical Faculty Mannheim, Heidelberg University, 68167 Mannheim, Germany*
[2]*Department of Surgery, University Medical Centre Mannheim, Medical Faculty Mannheim, Heidelberg University, 68167 Mannheim, Germany*
[3]*Laboratory for Liver, Pancreas and Motility, Unit of Experimental Medicine, School of Medicine, National University of Mexico, General Hospital of Mexico "Dr. Eduardo Liceaga", 06726 Mexico City, Mexico*
[4]*Laboratory for Proteomics and Metabolomics, Research Division, General Hospital of Mexico "Dr. Eduardo Liceaga", 06726 Mexico City, Mexico*
[5]*Carrera de Médico Cirujano, Unidad de Biomedicina, Facultad de Estudios Superiores-Iztacala, Universidad Nacional Autónoma de México, Avenida de los Barrios 1, 54090 Los Reyes Iztacala, MEX, Mexico*
[6]*Departamento de Biología Molecular, Instituto Nacional de Cardiología "Ignacio Chávez", Ciudad de México, Mexico*

Correspondence should be addressed to Guillermo Meléndez-Mier; melendez651@hgm.mx
and Galileo Escobedo; gescobedog@msn.com

Received 2 October 2017; Revised 20 January 2018; Accepted 6 February 2018; Published 3 April 2018

Academic Editor: Abdallah Elkhal



The effect of metabolic syndrome on human monocyte subpopulations has not yet been studied. Our main goal was to examine monocyte subpopulations in metabolic syndrome patients, while also identifying the risk factors that could directly influence these cells. Eighty-six subjects were divided into metabolic syndrome patients and controls. Monocyte subpopulations were quantified by flow cytometry, and interleukin- (IL-) 1$\beta$ secretion levels were measured by ELISA. Primary human monocytes were cultured in low or elevated concentrations of high-density lipoprotein (HDL) and stimulated with lipopolysaccharide (LPS). The nonclassical monocyte (NCM) percentage was significantly increased in metabolic syndrome patients as compared to controls, whereas classical monocytes (CM) were reduced. Among all metabolic syndrome risk factors, HDL reduction exhibited the most important correlation with monocyte subpopulations and then was studied *in vitro*. Low HDL concentration reduced the CM percentage, whereas it increased the NCM percentage and IL-1$\beta$ secretion in LPS-treated monocytes. The LPS effect was abolished when monocytes were cultured in elevated HDL concentrations. Concurring with *in vitro* results, IL-1$\beta$ serum values significantly increased in metabolic syndrome patients with low HDL levels as compared to metabolic syndrome patients without HDL reduction. Our data demonstrate that HDL directly modulates monocyte subpopulations in metabolic syndrome.

## 1. Introduction

In humans, circulating monocytes have been sorted into three different subpopulations according to the cell surface expression of CD14 and CD16 [1, 2]. The vast majority of circulating monocytes show high expression of CD14 and no expression of CD16 ($CD14^{high}CD16^{-}$) and constitute the fraction of classical monocytes (CM). Monocytes producing CD16 are divided into two subgroups: intermediate monocytes (IM) that show high expression of CD14 and also show CD16 expression ($CD14^{high}CD16^{+}$) and nonclassical monocytes (NCM) that exhibit low CD14 levels accompanied by CD16 expression ($CD14^{low}CD16^{+}$) [1]. Monocyte subpopulations also show different immunological functions. The NCM subset has been shown to produce high amounts of interleukin- (IL-) 1$\beta$ under basal conditions or in response to lipopolysaccharide (LPS) stimulation, which has led to a postulation that NCM exerts the most important inflammatory functions in circulation [3–5]. On the contrary, CM and IM subpopulations have been demonstrated to participate in endothelial adhesion and cell migration by preferably expressing chemokines and chemokine receptors without showing prominent inflammatory roles [1, 5, 6]. Thus, IL-1$\beta$ production is considered to be a marker of inflammatory activity in human nonclassical monocytes.

Monocyte subsets are typically modulated by immune factors including tumor necrosis factor alpha (TNF-$\alpha$) and Toll-like receptor (TLR) 2, TLR4, and TLR8 ligands [4, 7]. However, recent data show that dynamic changes in monocyte subpopulations can be influenced not only by immune agents but also by different pathophysiological conditions such as obesity [3, 4]. Indeed, a previous work of Devevre et al. has shown that an increase in body mass index (BMI) is capable of decreasing the CM percentage while also increasing the number of NCM, when comparing normal-weight controls with morbidly obese patients [3]. Interestingly, this study did not only show a direct relationship between body weight gain and increased NCM percentage but also revealed that this immune cell subpopulation seems to be the main monocytic source of IL-1$\beta$ in obese individuals. Additional studies have consistently reported an increased percentage of NCM in subjects with BMI > 30 $kg/m^2$ as compared to normal-weight individuals, which has brought to light the association between monocyte subpopulations and obesity [8]. However, it is a well-known fact that obesity is strongly linked to the development of metabolic abnormalities that are encompassed in metabolic syndrome [9]. Metabolic syndrome is a clustering of factors including abdominal obesity, hyperglycemia, high levels of blood pressure and triglycerides, and low concentration of high-density lipoproteins (HDL) that significantly increase the risk of having a cardiovascular event [10–12]. Therefore, it is reasonable to assume that metabolic syndrome may also have major effects upon monocyte subpopulations by mechanisms with the ability to alter the fragile balance among classical, intermediate, and nonclassical monocytes. Thereby, our main goal was to examine the percentages of classical, intermediate, and nonclassical monocytes in subjects with metabolic syndrome while also identifying the risk factors that could directly contribute to alter the monocyte subpopulation balance by performing *in vitro* cultures using primary human monocytes.

## 2. Materials and Methods

*2.1. Subjects.* Eighty-six women and men between 20 and 60 years old attending to the Blood Bank of the General Hospital of Mexico "Dr. Eduardo Liceaga" were included in the study. All participants provided written informed consent, previously approved by the institutional ethical committee of the General Hospital of Mexico, which guaranteed that the study was conducted in accordance with the principles described in the Helsinki Declaration. Subjects were excluded if they had previous diagnosis of diabetes mellitus, cardiovascular diseases, acute or chronic hepatic disease, acute or chronic renal disease, inflammatory or autoimmune disorders, acute or chronic infectious diseases, cancer, and endocrine disorders. We also excluded HIV-, HCV-, and HBV-seropositive patients, pregnant or lactating women, and subjects under any kind of anti-inflammatory, antiaggregant, and antihypertensive medication. All of the individuals enrolled in the study received full medical evaluation, including clinical history and physical examination by a physician.

*2.2. Anthropometric and Metabolic Measurements.* In all participants, BMI, waist circumference, and body fat percentage were recorded. The BMI is a result of dividing weight by height squared ($kg/m^2$). Waist circumference was obtained from each study subject by measuring at the midpoint between the lower rib margin and the iliac crest using a conventional tape in centimeters (cm). Body fat percentage was individually recorded by means of using a body composition analyzer (TANITA® Body Composition Analyzer, Model TBF-300A, Tokyo, Japan). Systolic blood pressure was individually measured using a digital automatic blood pressure monitor (OMRON Healthcare, Germany). Blood samples were individually obtained from each subject after an 8 h overnight fasting and collected into pyrogen-free tubes (Vacutainer, BD Diagnostics, NJ, USA) at room temperature. Collection tubes were then centrifuged at 1800$g$ for 10 min, and serum samples were obtained and stored at −80°C in numerous aliquots until use. Serum glucose levels were measured in triplicate by the glucose oxidase assay, following the manufacturer's instructions (Megazyme International, Ireland). Serum insulin levels were measured in triplicate by enzyme-linked immunosorbent assay (ELISA), following the manufacturer's instructions (Abnova Corporation, Taiwan). The estimate of insulin resistance was individually calculated by means of the homeostasis model assessment of insulin resistance (HOMA-IR). Total cholesterol, triglyceride, low-density lipoproteins (LDL), and high-density lipoproteins (HDL) levels were individually measured in triplicate by enzymatic assays according to the manufacturer's instructions (Roche Diagnostics, Mannheim, Germany). IL-1$\beta$ was measured in serum samples and culture supernatants in triplicate by Sandwich ELISA (PeproTech, Mexico) using serum samples diluted 1 : 250 in PBS 1x (Sigma-Aldrich, Mexico) and culture supernatants

without any dilution. All of the biochemical measurements were performed at the same time in order to avoid procedural variations.

*2.3. Diagnosis of Metabolic Syndrome.* Diagnosis of metabolic syndrome was performed according to the criteria of the National Cholesterol Education Program's Adult Treatment Panel III report (ATP III) [13], when three of five of the following factors were present: central obesity denoted by a waist circumference greater than 80 cm in women and 90 cm in men (cut-off points recommended for the Hispano-American population [14]), hypertriglyceridemia (circulating triglyceride levels > 150 mg/dL), decreased serum values of HDL-cholesterol (serum HDL < 40 mg/dL in men and 50 mg/dL in women), blood pressure higher than 120/80 mmHg, and hyperglycemia (fasting blood glucose > 100 mg/dL). According to the presence or absence of metabolic syndrome, participants were divided into metabolic syndrome and control groups.

*2.4. White Blood Cell Isolation and Characterization of Monocyte Subpopulations by Flow Cytometry.* Six milliliters of venous blood was obtained from each participant and collected into tubes containing EDTA (Vacutainer™, BD Diagnostics, NJ, USA). Collection tubes were then centrifuged at 1800$g$ for 10 minutes and white blood cells (WBCs) separated using a micropipette. Total WBCs were separately placed into 1.6 mL pyrogen-free Eppendorf tubes containing 1 mL of ACK Lysing Buffer (Life Technologies, USA) and incubated at 4°C for 8 minutes. Immediately after, each sample was centrifuged at 1800g/4°C for 4 minutes and cell pellets washed twice with PBS 1x (Sigma-Aldrich, Mexico). After an additional centrifugation step and removal of the supernatant, each cell pellet was resuspended in 50 L of PBS 1x (Sigma-Aldrich, Mexico). On each test, 3 $\mu$L of Human TruStrain Reagent (BioLegend Inc., USA) was added to $2 \times 10^5$ WBCs and then incubated for 10 minutes on ice. Immediately after, WBCs were incubated with anti-CD14 PE/Cy7 and anti-CD16 FITC (BioLegend Inc., USA) for 30 minutes on ice for posterior analysis on a FACSCanto II flow cytometer (BD Biosciences, Mexico) by means of BD FACSDiva™ software 6.0, acquiring $1 \times 10^5$ monocyte events per test in duplicate. PE/Cy7 mouse IgG2 and FITC mouse IgG1 were used as isotype control antibodies for cell surface staining of CD14 and CD16, respectively. For gating strategy, white blood cells were firstly gated for singlets on a forward scatter height (FSC-H)/forward scatter area (FSC-A) density plot. Then, lymphocyte, granulocyte, and monocyte populations were gated on a FSC-A/side scatter area (SSC-A) plot. On the monocyte gate, living cells were further gated using the Live/Dead Aqua stain (Thermo Fisher Scientific Inc., USA). Living monocytes were then gated to determine CD14- and CD16-positive expression. Assessment of monocyte subpopulations was performed according to the cell surface expression of CD14 and CD16, as follows: $CD14^{high}CD16^{-}$, classical monocytes; $CD14^{high}CD16^{+}$, intermediate monocytes; and $CD14^{low}CD16^{+}$, nonclassical monocytes.

*2.5. HDL Removal for In Vitro Cultures.* Blood samples were collected into pyrogen-free tubes (Vacutainer, BD Diagnostics, NJ, USA) from nine volunteers with diagnosis of metabolic syndrome that specifically included central obesity, fasting hyperglycemia, increased triglyceride levels, and low HDL concentration. Collection tubes were then centrifuged at 1800$g$ for 10 min and serum samples obtained. Serum fractions were treated with HDL precipitation buffer (Abcam, Cambridge, MA) for HDL removal, as previously reported [15]. HDL removal was verified by Western blot using an anti-HDL polyclonal antibody that specifically recognizes a 31 kDa protein, according to the manufacturer's instructions (Abcam, Cambridge, MA). Resulting serum samples were supplemented using the same amount of RPMI 1640 medium containing 2 mM L-glutamine and 50 $\mu$g/mL gentamicin (Sigma-Aldrich, Mexico), and then 0.77 mmol/L or 1.55 mmol/L purified HDL (Sigma-Aldrich, Mexico) was added. HDL-enriched culture media were differentially used to simulate the low (0.77 mmol/L = 30 mg/dL) and high (1.55 mmol/L = 60 mg/dL) HDL levels found in metabolic syndrome patients and healthy subjects, respectively. A negative control with total absence of HDL was included in all different *in vitro* culture conditions.

*2.6. In Vitro Cultures of Primary Human Monocytes and LPS Stimulation.* For *in vitro* studies, blood samples were collected into tubes containing EDTA (Vacutainer, BD Diagnostics, NJ, USA) from the same nine donors with diagnosis of metabolic syndrome mentioned above. Blood samples were separately diluted 1 : 2 with phosphate saline buffer 1x (PBS 1x, Sigma-Aldrich, Mexico) for posterior isolation of WBCs by density gradient centrifugation (Sigma-Aldrich, Mexico). Monocytes were then isolated from WBCs by CD14-positive selection using magnetic columns (Miltenyi Biotec, Germany). Purified monocytes were placed in 0.77 mmol/L or 1.55 mmol/L HDL-enriched culture media in 12-well cell-culture plates (CoStar, USA), at a density of $1 \times 10^6$ monocytes per well. Each culture well was incubated with or without gram-negative bacteria-derived LPS (Sigma-Aldrich, Mexico) at 1 $\mu$g/mL for six hours at 37°C in humidified 5% $CO_2$ atmosphere. After 6 h incubation, LPS-stimulated and untreated monocytes were obtained and resuspended in 50 $\mu$L of PBS 1x for being incubated with anti-CD14 PE/Cy7 and anti-CD16 FITC (BioLegend Inc., USA) antibodies as described above. For gating strategy, untreated and LPS-treated cells were firstly gated for singlets on a FSC-H/FSC-A density plot. On the monocyte gate, living untreated and LPS-treated cells were further gated using the Live/Dead Aqua stain. Living monocytes were then gated to determine CD14- and CD16-positive expression and identify monocyte subpopulations as follows: $CD14^{high}CD16^{-}$, classical monocytes; $CD14^{high}CD16^{+}$, intermediate monocytes; and $CD14^{low}CD16^{+}$, nonclassical monocytes. The cell viability rate was determined based on the Live/Dead Aqua stain and ranged from 91 to 96% for all acquired cell samples, without showing significant differences between untreated and LPS-treated monocytes. FACS analysis was performed in a FACSCanto II flow cytometer (BD Biosciences, Mexico) by means of BD FACSDiva software 6.0, acquiring $1 \times 10^5$

Table 1: Demographical and metabolic parameters of the study population.

| Parameters | Control | Metabolic syndrome | $P$ value |
|---|---|---|---|
| Gender (W/M) | 17/25 | 16/28 | 0.313 |
| Age (years) | 49.25 ± 5.88 | 48.38 ± 5.47 | 0.296 |
| BMI (kg/m$^2$) | 26.12 ± 4.09 | 29.92 ± 5.26 | 0.006 |
| Waist circumference (cm) | 90.18 ± 9.22 | 100.41 ± 10.71 | 0.004 |
| Body fat (%) | 27.38 ± 7.63 | 33.35 ± 10.13 | 0.012 |
| SBP (mmHg) | 124.0 ± 2.47 | 126.0 ± 5.61 | 0.306 |
| FBG (mg/dL) | 82.37 ± 18.74 | 106.50 ± 23.48 | 0.001 |
| Insulin (mU/L) | 13.67 ± 5.30 | 13.90 ± 3.82 | 0.428 |
| HOMA-IR | 2.77 ± 1.21 | 3.63 ± 1.26 | 0.005 |
| Total cholesterol (mg/dL) | 209.04 ± 41.49 | 200.26 ± 32.87 | 0.204 |
| Triglycerides (mg/dL) | 165.04 ± 95.12 | 235.53 ± 95.26 | 0.006 |
| HDL (mg/dL) | 53.20 ± 13.34 | 38.53 ± 8.62 | 0.001 |
| LDL (mg/dL) | 116.95 ± 33.45 | 109.50 ± 29.46 | 0.203 |

Data are expressed as mean ± standard deviation. The Shapiro-Wilk test was used to estimate normality in data distribution. Significant differences were estimated by means of performing Student's $t$-test with the exception of women/men proportion in each group, which was estimated by means of the chi-squared test. Differences were considered significant when $P < 0.05$. W: women; M: men; BMI: body mass index; SBP: systolic blood pressure; FBG: fasting blood glucose; HOMA-IR: homeostatic model assessment of insulin resistance; HDL: high-density lipoprotein; LDL: low-density lipoprotein. Diagnosis of metabolic syndrome was performed according to the ATP III criteria, when three of five of the following factors were present: central obesity denoted by a waist circumference greater than 80 cm in women and 90 cm in men, circulating triglyceride levels > 150 mg/dL, serum HDL < 40 mg/dL in men and 50 mg/dL in women, blood pressure higher than 120/80 mmHg, fasting blood glucose > 100 mg/dL.

monocyte events per test in duplicate. Assessment of monocyte subpopulations was performed as described above and supernatants collected for posterior IL-1$\beta$ measuring by ELISA as mentioned before.

*2.7. Statistical Analysis.* The Shapiro-Wilk test was performed to estimate normality in data distribution and then proceed to perform Student's $t$-test to compare metabolic syndrome patients and healthy subjects in terms of BMI, waist circumference, body fat percentage, fasting glucose, fasting insulin, HOMA-IR, systolic blood pressure, total cholesterol, triglycerides, LDL, HDL, IL-1$\beta$, CM, IM, and NCM. Significant differences in women/men proportion were estimated by means of the chi-squared test. One-way ANOVA, followed by a post hoc Tukey test, was used to compare the serum levels of IL-1$\beta$ in subjects with different numbers of metabolic syndrome risk factors. Data were expressed as median ± standard deviation. Pearson's correlation coefficients were calculated for examining the association of CM, IM, and NCM with anthropometric, biochemical, and immunological parameters in the study population. Pearson's correlation results were expressed as coefficients ($r$) and $P$ values. Differences were considered significant when $P < 0.05$. All statistical analyses were performed using the GraphPad Prism 6.01 software.

## 3. Results

Eighty-six participants were included in the study, and no significant differences were seen between controls and subjects with metabolic syndrome in age, women/men proportion, systolic blood pressure, plasma insulin, total cholesterol, and LDL levels (Table 1). On the contrary, metabolic syndrome subjects had higher BMI than control individuals (29.92 ± 5.26 versus 26.12 ± 4.09, resp.), while waist circumference was also significantly elevated in this study group (100.41 ± 10.71 versus 90.18 ± 9.22, resp.). Furthermore, body fat percentage exhibited a significant 21% increase in metabolic syndrome subjects with respect to control individuals (33.35 ± 10.13 versus 27.38 ± 7.63 percent, resp.) (Table 1). Similarly, fasting blood glucose concentration was 30% increased in patients with metabolic syndrome as compared to controls (106.50 ± 23.48 versus 82.37 ± 18.74, resp.), while HOMA-IR value was raised by 31% (3.63 ± 1.26 versus 2.77 ± 1.21, resp.). In the same sense, triglycerides were 42% augmented in the metabolic syndrome group as compared to controls (235.53 ± 95.26 versus 165.04 ± 95.12, resp.), whereas HDL levels showed a clear 27% reduction in the scenario of metabolic syndrome with respect to normal conditions (38.53 ± 8.62 versus 53.20 ± 13.34, resp.) (Table 1). According to the ATP III criteria, the prevalence of metabolic syndrome in our study population was 58%, which suggests that half of the apparently normal subjects enrolled into the study had higher cardiovascular risk. In the metabolic syndrome group, the most frequently seen risk factor was central obesity (89%, which means that 9 in 10 metabolic syndrome patients were abdominally obese), followed by HDL reduction (78%), hypertriglyceridemia (52%), hyperglycemia (18%), and high blood pressure (13%).

Monocyte subpopulations were analyzed according to CD14 and CD16 cell surface expression by flow cytometry (Figure 1). Representative dot plots showing CD14 and CD16 expression in classical (CM), intermediate (IM), and nonclassical (NCM) monocyte subsets from control individuals and subjects with metabolic syndrome can be seen in Figures 1(a) and 1(b), respectively. The percentage of CM ($CD14^{high}CD16^{-}$) showed a significant 15% decrease in subjects with metabolic syndrome as compared to controls

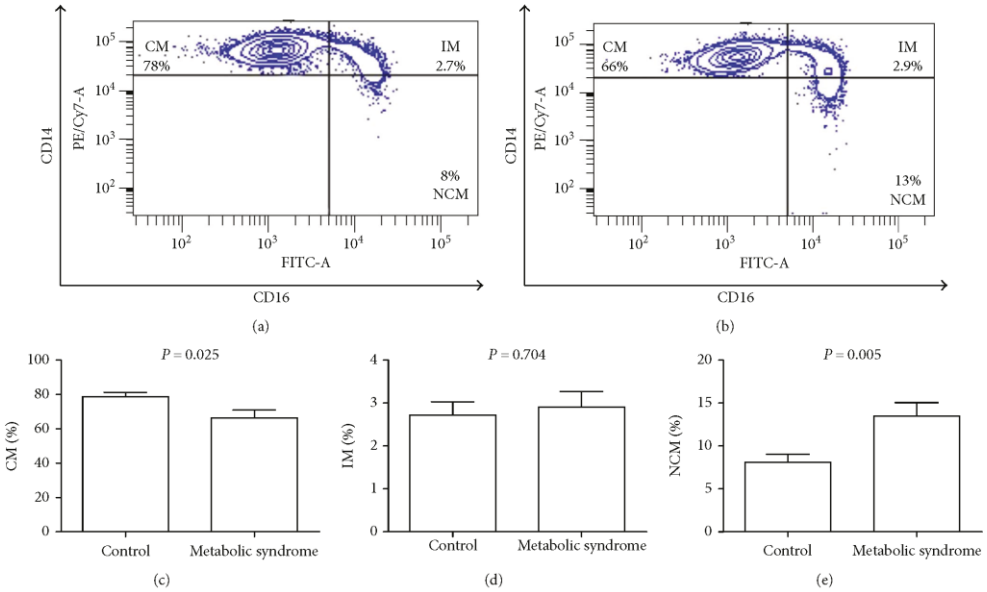


FIGURE 1: Percentage of classical, intermediate, and nonclassical monocytes in metabolic syndrome patients and control subjects. Representative flow cytometry dot plots showing the percentage of classical (CM), intermediate (IM), and nonclassical monocytes (NCM) in control subjects (a) and patients with metabolic syndrome (b). The CM percentage is significantly decreased in metabolic syndrome patients as compared to controls (c). The IM percentage showed no significant differences between metabolic syndrome patients and controls (d). The NCM percentage is significantly increased in metabolic syndrome patients as compared to controls (e). For gating strategy, white blood cells were firstly gated for singlets on a FSC-H/FSC-A density plot. Then, lymphocyte, granulocyte, and monocyte populations were gated on a FSC-A/SSC-A plot. On the monocyte gate, living cells were further gated using the Live/Dead Aqua stain. Living monocytes were then gated to determine CD14- and CD16-positive expression and identify monocyte subpopulations as follows: $CD14^{high}CD16^{-}$, classical monocytes; $CD14^{high}CD16^{+}$, intermediate monocytes; and $CD14^{low}CD16^{+}$, nonclassical monocytes. In panels (c)–(e), data are expressed as mean ± standard deviation. Significant differences were estimated by means of performing Student's *t*-test. Differences were considered significant when $P < 0.05$. Diagnosis of metabolic syndrome was performed according to the ATP III criteria, when three of five of the following factors were present: central obesity denoted by a waist circumference greater than 80 cm in women and 90 cm in men, hypertriglyceridemia (circulating triglyceride levels > 150 mg/dL), decreased serum values of HDL-cholesterol (serum HDL < 40 mg/dL in men and 50 mg/dL in women), blood pressure higher than 120/80 mmHg, and hyperglycemia (fasting blood glucose > 100 mg/dL).

(66.46 ± 4.5 versus 78.62 ± 2.68, resp.) (Figure 1(c)). The IM subpopulation ($CD14^{high}CD16^{+}$) did not show any significant difference between controls and metabolic syndrome subjects (2.72 ± 0.30 versus 2.90 ± 0.36, resp.) (Figure 1(d)). In contrast, the percentage of NCM expressing CD16 and low CD14 levels exhibited a significant 65% increase in the metabolic syndrome group as compared to controls (13.47 ± 1.59 versus 8.12 ± 0.89, resp.) (Figure 1(e)).

After evaluating the percentage of classical, intermediate, and nonclassical monocyte subsets in subjects with metabolic syndrome and controls, we attempted to identify what anthropometric and metabolic variables had a significant correlation level with these innate immune cells (Table 2). In control individuals without metabolic syndrome, we saw that anthropometric parameters such as BMI, waist circumference, and body fat percentage had the strongest correlation with monocyte subpopulations (Table 2). In contrast, anthropometric parameters were shown to lose statistical correlations with monocyte subpopulations in the scenario of metabolic syndrome. However, we found a remarkable emerging association between HDL and classical and nonclassical monocytes in subjects with metabolic syndrome. In fact, a moderate relationship between increasing percentage of CM and elevated HDL levels was seen in metabolic syndrome patients ($r = 0.531$, $P = 0.013$) (Table 2). On the opposite, the NCM subpopulation showed a strong inverse association with increased concentrations of HDL ($r = -0.621$, $P = 0.009$) (Table 2). Interestingly, the inverse relationship between CM and NCM was significantly stronger when studied in patients with metabolic syndrome than in control individuals ($r = -0.727$, $P < 0.001$, and $r = -0.585$, $P = 0.001$, resp.) (Table 2).

By means of performing statistical analyses, HDL was identified as the molecule exerting the most important

Table 2: Correlation coefficients of monocyte subpopulations with anthropometric, metabolic, and cellular parameters in patients with metabolic syndrome and controls.

| Parameters | Control | | | | | | Metabolic syndrome | | | | | |
|---|---|---|---|---|---|---|---|---|---|---|---|---|
| | CM | | IM | | NCM | | CM | | IM | | NCM | |
| | *r* | *P* | *r* | *P* | *r* | *P* | *r* | *P* | *r* | *P* | *r* | *P* |
| Age | 0.242 | 0.126 | 0.046 | 0.414 | −0.217 | 0.153 | 0.078 | 0.351 | 0.203 | 0.159 | −0.028 | 0.446 |
| BMI | *−0.523* | *0.004* | 0.140 | 0.256 | *0.592* | *0.001* | 0.037 | 0.427 | −0.077 | 0.354 | 0.034 | 0.433 |
| WC | −0.323 | 0.065 | 0.220 | 0.155 | *0.353* | *0.049* | 0.103 | 0.307 | 0.011 | 0.477 | −0.011 | 0.477 |
| Body fat | *−0.363* | *0.043* | 0.236 | 0.139 | *0.438* | *0.018* | 0.240 | 0.118 | −0.005 | 0.488 | −0.051 | 0.402 |
| SBP | 0.024 | 0.548 | 0.017 | 0.471 | 0.057 | 0.210 | 0.051 | 0.412 | 0.072 | 0.347 | 0.054 | 0.207 |
| FBG | −0.237 | 0.132 | −0.342 | 0.059 | 0.326 | 0.081 | 0.139 | 0.249 | 0.150 | 0.231 | −0.082 | 0.344 |
| Insulin | −0.012 | 0.476 | −0.006 | 0.487 | −0.052 | 0.403 | −0.066 | 0.373 | 0.103 | 0.306 | 0.025 | 0.451 |
| HOMA-IR | −0.042 | 0.421 | −0.161 | 0.224 | 0.098 | 0.323 | 0.017 | 0.465 | 0.172 | 0.199 | −0.005 | 0.489 |
| Cholesterol | −0.204 | 0.169 | 0.171 | 0.212 | −0.093 | 0.332 | 0.010 | 0.478 | 0.008 | 0.484 | −0.175 | 0.196 |
| Triglycerides | −0.111 | 0.306 | −0.018 | 0.466 | −0.187 | 0.196 | −0.009 | 0.481 | 0.185 | 0.181 | −0.154 | 0.226 |
| HDL | −0.032 | 0.440 | −0.180 | 0.198 | 0.086 | 0.343 | *0.531* | *0.013* | 0.209 | 0.152 | *−0.621* | *0.009* |
| LDL | −0.214 | 0.156 | 0.249 | 0.120 | −0.046 | 0.414 | −0.144 | 0.240 | −0.158 | 0.220 | 0.026 | 0.449 |
| CM | — | — | 0.325 | 0.060 | *−0.585* | *0.001* | — | — | 0.237 | 0.121 | *−0.727* | *<0.001* |
| IM | 0.319 | 0.064 | — | — | 0.084 | 0.695 | 0.237 | 0.121 | — | — | −0.166 | 0.207 |
| NCM | *−0.585* | *0.001* | 0.084 | 0.347 | — | — | *−0.727* | *<0.001* | −0.166 | 0.207 | — | — |

Coefficients ($r$) and $P$ values were calculated by Pearson's correlation model. The correlation level was considered significant when $P < 0.05$. Significant associations are marked in italics. CM: classical monocytes; IM: intermediate monocytes; NCM: nonclassical monocytes; BMI: body mass index; WC: waist circumference; SBP: systolic blood pressure; FBG: fasting blood glucose; HOMA-IR: homeostatic model assessment of insulin resistance; HDL: high-density lipoprotein; LDL: low-density lipoprotein. Diagnosis of metabolic syndrome was performed according to the ATP III criteria, when three of five of the following factors were present: central obesity denoted by a waist circumference greater than 80 cm in women and 90 cm in men, hypertriglyceridemia (circulating triglyceride levels > 150 mg/dL), decreased serum values of HDL-cholesterol (serum HDL < 40 mg/dL in men and 50 mg/dL in women), blood pressure higher than 120/80 mmHg, and hyperglycemia (fasting blood glucose > 100 mg/dL).

association with classical and nonclassical monocytes in metabolic syndrome. For this reason, our next step was to study the effect of HDL on the monocyte subpopulation dynamic by conducting *in vitro* cell culture experiments (Figure 2). Figure 2(a) illustrates a representative polyacrylamide gel showing a metabolic syndrome patient's serum sample in which HDL was totally removed (left) and then reconstituted with 0.77 mmol/L (middle) or 1.55 mmol/L HDL (right) (Figure 2(a)). In culture conditions using low HDL levels (30 mg/dL), LPS stimulation induced a 17% reduction in the CM percentage as compared to untreated cells (Figure 2(b), middle panel). In contrast, the effect of LPS on this monocyte subset was abolished when using HDL concentrations that resembled those found in healthy subjects without metabolic syndrome (60 mg/dL) (Figure 2(b), right panel). The IM percentage tended to decrease when treated with LPS either in low HDL level or in normal HDL concentration without showing significant differences (Figure 2(c)). On the contrary, in culture conditions mimicking the HDL reduction that is observed in metabolic syndrome patients, LPS stimulation promoted a 40% increase in the NCM percentage with respect to untreated cells (Figure 2(d), middle panel). Interestingly, the LPS-stimulated NCM increase was revoked when monocytes were cultured in the presence of high HDL levels mimicking those found in healthy individuals without metabolic syndrome (Figure 2(d), right panel). Interestingly, classical and nonclassical monocytes cultured in the absence of HDL showed a similar response pattern than that found in 30 mg/dL HDL (left panels at Figures 2(b) and 2(d), resp.). As previously mentioned, IL-1$\beta$ is a key cytokine that is mainly produced by NCM in response to LPS. In parallel to the NCM increase, LPS stimulation also enhanced IL-1$\beta$ secretion by 216% in monocytes cultured in zero and 30 mg/dL HDL (Figure 2(e), left and middle panels, resp.). However, the effect of LPS on IL-1$\beta$ production was 1.5-fold decreased when tested in 60 mg/dL HDL (Figure 2(e), right panel).

Since not only monocyte subpopulations were modified by HDL but also their ability to produce IL-1$\beta$, we decided to measure IL-1$\beta$ serum levels in the metabolic syndrome population (Figure 3). Abdominally obese patients with metabolic syndrome showed similar IL-1$\beta$ serum levels than those found in metabolic syndrome patients without central obesity (Figure 3(a)). No significant differences in the IL-1$\beta$ serum levels were also seen in metabolic syndrome patients with and without high blood pressure or hyperglycemia (Figures 3(b) and 3(c), resp.). Metabolic syndrome patients with hypertriglyceridemia exhibited a nonsignificant increase in serum IL-1$\beta$ as compared to metabolic syndrome patients without abnormally high triglyceride values (Figure 3(d)). On the opposite, the serum levels of IL-1$\beta$ showed a significant 1.5-fold increase when studied in metabolic syndrome patients with low HDL levels as compared to metabolic syndrome patients without showing HDL reduction (Figure 3(e)).

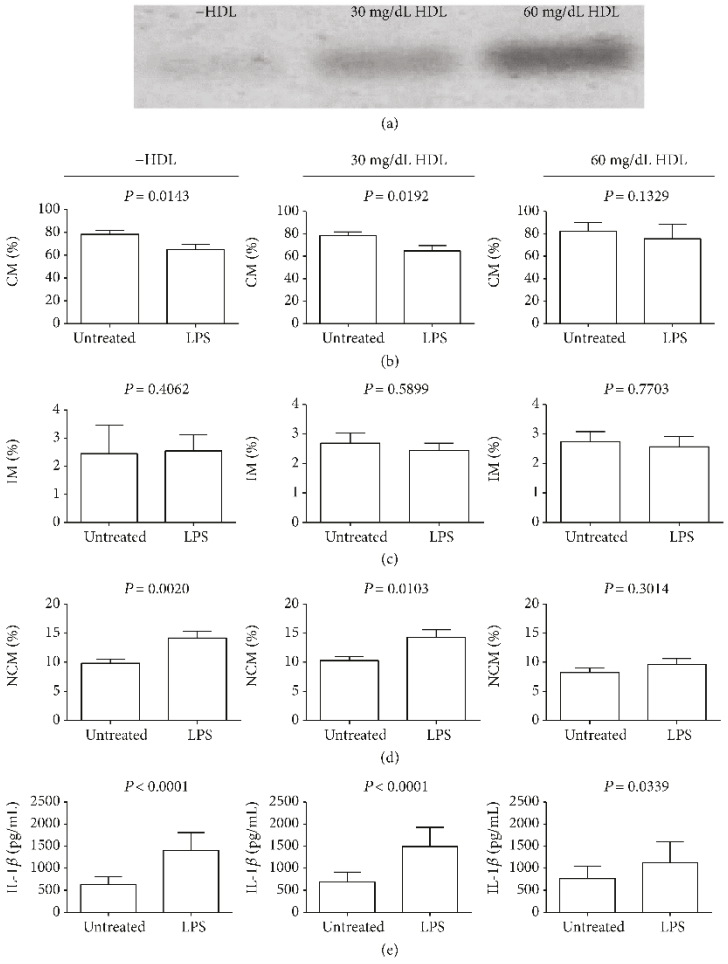


FIGURE 2: Effect of HDL on LPS-stimulated primary human monocytes *in vitro*. Representative polyacrylamide gel showing a metabolic syndrome patient's serum sample in which HDL was totally removed (−HDL) and then reconstituted with 0.77 mmol/L (30 mg/dL) or 1.55 mmol/L (60 mg/dL) HDL (a). As compared to untreated cells, LPS stimulation induced reduction in the CM percentage in low HDL levels (zero and 30 mg/dL) (b, left and middle panels, resp.). In contrast, the effect of LPS on the CM percentage was abolished in 60 mg/dL HDL that resembled a high HDL concentration (b, right panel). LPS stimulation did not significantly modify the IM percentage neither in low nor in high HDL concentrations (c, left, middle and right panels, resp.). As compared to untreated cells, LPS stimulation increased the NCM percentage in zero and 30 mg/dL HDL (d, left and middle panels, resp.). On the contrary, the effect of LPS on the NCM percentage was abolished in high HDL concentrations (d, right panel). As compared to untreated cells, LPS stimulation increased IL-1$\beta$ production in primary human monocytes cultured in low HDL concentrations (e, left and middle panels, resp.). In contrast, the effect of LPS on IL-1$\beta$ production was 1.5-fold reduced in 60 mg/dL HDL (e, right panel). Monocytes were isolated from white blood cells by CD14-positive selection using magnetic columns and placed in 0.77 mmol/L (30 mg/dL) or 1.55 mmol/L (60 mg/dL) HDL-enriched culture media ($1 \times 10^6$ monocytes per well), in the presence or absence of gram-negative bacteria-derived LPS at 1 $\mu$g/mL for six hours at 37°C. After this time, monocytes were incubated with anti-CD14 PE/Cy7 and anti-CD16 FITC as described. For the gating strategy, untreated and LPS-treated cells were firstly gated for singlets on a FSC-H/FSC-A density plot. On the monocyte gate, living untreated and LPS-treated cells were further gated using the Live/Dead Aqua stain. Living monocytes were then gated to determine CD14- and CD16-positive expression and identify monocyte subpopulations as follows: $CD14^{high}CD16^{-}$, classical monocytes; $CD14^{high}CD16^{+}$, intermediate monocytes; and $CD14^{low}CD16^{+}$, nonclassical monocytes. In (b–e), data are expressed as mean ± standard deviation. Significant differences were considered when $P < 0.05$.

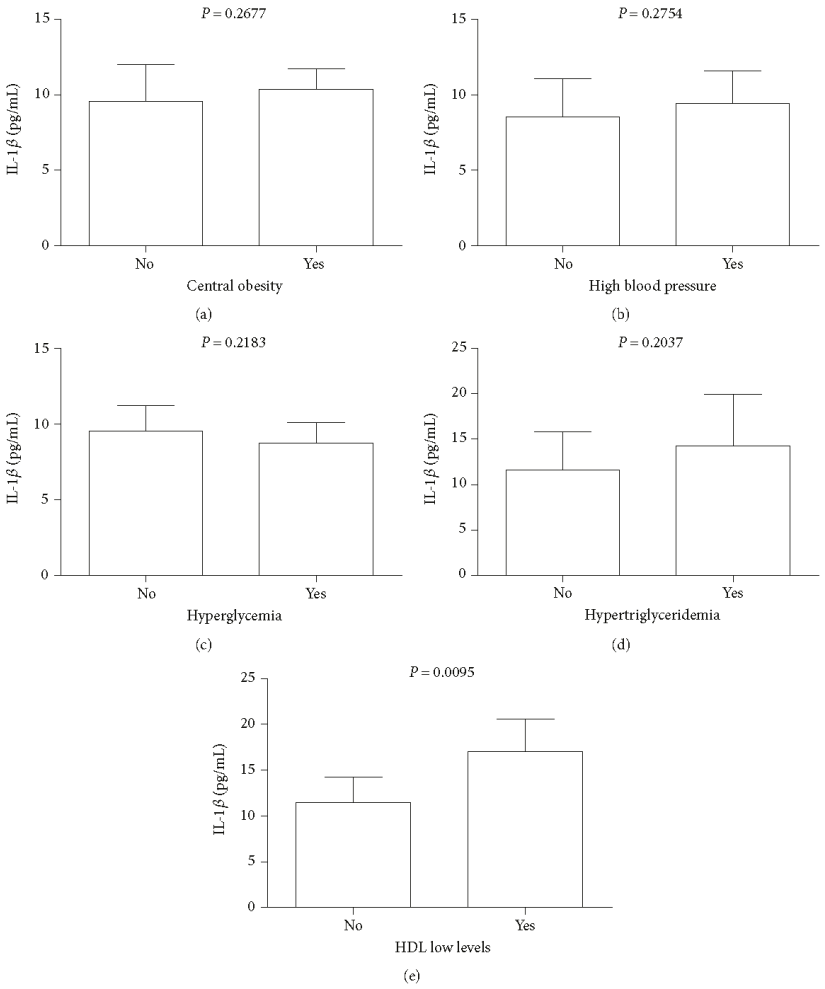


Figure 3: Serum levels of IL-1$\beta$ in the study patients according to different metabolic syndrome risk factors. (a) Metabolic syndrome patients displaying central obesity ($n = 39$) showed similar IL-1$\beta$ serum levels than did metabolic syndrome patients that had a normal waist circumference ($n = 5$). (b) The serum levels of IL-1$\beta$ did not show significant differences in metabolic syndrome patients with elevated blood pressure ($n = 6$) as compared to metabolic syndrome patients with normal blood pressure ($n = 38$). (c) Metabolic syndrome patients showing fasting hyperglycemia ($n = 8$) exhibited similar IL-1$\beta$ circulating levels than did metabolic syndrome patients with normal glycemic values ($n = 36$). (d) The serum levels of IL-1$\beta$ tended to increase in metabolic syndrome patients with hypertriglyceridemia ($n = 23$) but did not show significant differences with respect to metabolic syndrome patients showing normal triglyceride values ($n = 21$). (e) In contrast, IL-1$\beta$ was significantly increased in metabolic syndrome patients with HDL low levels ($n = 34$) as compared to metabolic syndrome patients exhibiting normal HDL values ($n = 10$). Data are expressed as mean ± standard deviation. Significant differences were estimated by means of performing the Mann–Whitney test. Differences were considered significant when $P < 0.05$. Central obesity was diagnosed when women and men had a waist circumference greater than 80 cm and 90 cm, respectively. High blood pressure was diagnosed in women and men with blood pressure values higher than 120/80 mmHg. Hyperglycemia was diagnosed in women and men with fasting blood glucose greater than 100 mg/dL. Hypertriglyceridemia was diagnosed in women and men with triglyceride values higher than 150 mg/dL. Decreased serum values of HDL were established in women and men with HDL serum values lower than 50 mg/dL and 40 mg/dL, respectively.

## 4. Discussion

Previous studies have demonstrated a monocyte subset imbalance in morbidly obese patients that is mainly characterized by increased percentages of nonclassical monocytes [3]. Nevertheless, obesity is frequently accompanied by cardiovascular risk factors that are encompassed in the metabolic syndrome [10–12]. For this reason, we attempted to examine the monocyte subpopulation percentages when considering the presence of metabolic syndrome.

As expected, our data show that BMI, waist circumference, and body fat percentage are directly related to increased NCM percentage and decreased CM amount, which concurs with previous works reporting that obesity is associated with imbalance in monocyte subsets [3]. However, this association was only seen in overweight and obese subjects that did not meet the rest of criteria for being diagnosed with metabolic syndrome. Beyond obesity, in the scenario of metabolic syndrome, we found decreasing percentages of classical monocytes and prominent elevations in the nonclassical monocyte subpopulation that were related to HDL levels and showed no association with obesity-related anthropometric parameters. In this context, it is reasonable to consider the fact that the monocyte subpopulation dynamic is not only modified by obesity but is also due to other factors such as those encompassed in the metabolic syndrome, especially the serum levels of HDL.

HDL is a protein of blood plasma that is capable of binding to lipid molecules such as triglycerides and cholesterol and participates in the cholesterol clearance—the main reason why HDL is also called the "good cholesterol" [16, 17]. High serum levels of HDL have been related to low cardiovascular risk, whereas a reduction in this lipoprotein accompanied by increased levels of LDL is considered to increase the risk of having metabolic syndrome, heart disease, or stroke [16, 18]. In our study, HDL showed a positive correlation with classical monocytes but a negative relationship with nonclassical monocytes. In other words, the present results suggest that elevated HDL levels may restrict the proportion of the inflammatory nonclassical monocytes but also favor expanding the classical monocyte subset that has no prominent inflammatory actions. However, the idea that HDL seems to be associated with imbalance between classical and nonclassical monocyte subsets was conceived after performing a merely statistical approach. In view of the fact that statistical correlation models do not allow us to find a causative role for HDL in modulating monocyte subsets, we decided to culture blood-isolated monocytes in the presence of high and low HDL levels *in vitro*. To simulate the microenvironment found in metabolic syndrome, we used serum samples from subjects having HDL reduction, central obesity, hyperglycemia, and hypertriglyceridemia, in which we specifically removed HDL. Then, we deliberately supplemented each serum sample with 0.77 mmol/L (30 mg/dL) or 1.55 mmol/L (60 mg/dL) purified HDL for having monocyte culture conditions with low and high HDL levels, respectively. In this form, we were able to corroborate our *in vivo* findings by studying the effect of HDL on LPS-stimulated monocytes *in vitro*. As expected, in culture conditions simulating the microenvironment found in metabolic syndrome with low HDL levels, LPS stimulation was able to induce decreased CM percentage and at the same time increased the NCM subset, which concurs with Mukherjee et al. who reported the same result [5]. In contrast, when the HDL concentration was deliberately increased until the levels found in healthy subjects without metabolic syndrome were reached, the effect of LPS on classical and nonclassical monocytes was abolished. As mentioned, numerous studies have suggested that HDL is positively associated with classical monocytes but at the same time negatively related to nonclassical monocytes. In this sense, previous studies have demonstrated that nonclassical monocyte percentages increase as HDL plasma levels decrease in adults and children with familial hypercholesterolemia [19, 20]. Concomitantly, a positive correlation between HDL plasma levels and classical monocytes was also reported by Christensen et al. [20]. Additional studies have also confirmed that HDL levels negatively correlate with increasing percentage of NCM [21–23], which concurs with present results. Interestingly, our findings also demonstrate that absence of HDL has similar *in vitro* effects on monocyte subpopulations than those found when using 30 mg/dL HDL, which suggest that HDL may prevent raising nonclassical monocytes in concentrations above 60 mg/dL. To the best of our knowledge, this is the first report to not only suggest an association between HDL levels and monocyte subpopulations but also demonstrate that low HDL levels directly contribute to a decrease in CM and an increase in NCM in response to prototypical stimuli such as LPS. This finding brings to light the importance of studying the probable role of HDL in the regulation of the CD14 and CD16 expression in human monocytes, which is the primary feature defining classical, intermediate, and nonclassical monocyte subpopulations.

CD14 is a surface protein that preferably expresses on human monocytes and macrophages [24]. CD14 forms the trimeric LPS receptor complex together with TLR4 and MD-2, aimed at recognizing bacterial endotoxins and consequently triggering the NF$\kappa$B-dependent inflammatory cytokine expression such as TNF-$\alpha$, IL-6, and IL-1$\beta$ [24–26]. Notably, it has been reported that infusion with reconstituted HDL is able to reduce CD14 expression in peripheral monocytes of healthy volunteers while also decreasing the serum concentrations of TNF-$\alpha$ and IL-6 [27]. It is worth mentioning that monocytes isolated from reconstituted HDL-treated healthy volunteers still showed decreased expression of CD14 even upon *in vitro* stimulation with LPS [27]. Similarly, Galbois et al. demonstrated that CD14 expression is diminished in circulating monocytes of cirrhotic patients and healthy controls after having been cultured in the presence of HDL [28]. In the specific case of CD16 (an Fc$\gamma$ receptor that binds to Fc fragments of immunoglobulin G in the cell surface of innate immune cells [1]), HDL levels have an apparent association with CD16 expression in monocytes of patients with stable coronary artery disease [21–23]. However, to the best of our knowledge, there are no experimental works studying the possible mechanisms by which HDL is linked to CD16 expression in human monocytes. Altogether, this information suggests that HDL may exert its effects on monocyte

subpopulations by modulating the expression of CD14, and probably CD16, via TLR4 and NFκB activation. Nevertheless, it is important to note there are not yet concluding studies aimed at characterizing the possible mechanism by which HDL is able to impact monocyte subpopulations, and the discussion of these results makes no attempt to conjecture beyond that. On the other hand, the idea that HDL exerts its effects by activating prominent inflammatory pathways could not only involve the dynamic changes found in monocyte subsets but also the ability of monocytes to produce key proinflammatory cytokines such as IL-1$\beta$.

IL-1$\beta$ is a cytokine predominantly produced by nonclassical monocytes and activated macrophages with prominent roles in the regulation of the inflammatory response as well as cell differentiation and apoptosis [3, 5]. Our results show that LPS-stimulated IL-1$\beta$ production in cultured primary human monocytes is favored when HDL is totally absent or in low levels. In other words, culture conditions mimicking the levels of HDL that are found in metabolic syndrome do not only increase the NCM percentage but also enhance production of IL-1$\beta$. Concurring with this notion, restoration of the HDL concentration until reaching the levels found in healthy subjects without metabolic syndrome was able to diminish the LPS-stimulated IL-1$\beta$ production in cultured primary human monocytes *in vitro*. These findings are consistent with prior studies suggesting that high HDL values, as those seen in metabollicaly healthy individuals, seem to exert anti-inflammatory actions, whereas low HDL levels may predispose the organism to more robust proinflammatory responses [17–19, 27]. However, it is important to proceed with caution in trying to transfer our *in vitro* results that support an effect of HDL on monocyte subpopulations toward a much more complicated clinical scenario such as metabolic syndrome, in which monocytes subsets are not only in contact with HDL but also in the presence of many other risk factors. For this reason, it is still of enormous importance to clarify whether high HDL levels have prominent anti-inflammatory actions in transversal and prospective clinical trials aimed at understanding the role of HDL in metabolic syndrome and its comorbidities.

IL-1$\beta$ has been shown to be primarily produced by nonclassical monocytes either under basal conditions or in response to LPS [3, 5]. On the contrary, classical monocytes are mainly involved in cell migration functions by predominantly expressing chemokine receptors without showing significant IL-1$\beta$ production [5, 29–31]. Therefore, we want to speculate that nonclassical monocytes were the main cellular source of IL-1$\beta$ in our *in vitro* experiments, a notion that concurs with the fact that while this monocyte subpopulation increased the IL-1$\beta$ production also augmented and both of them were downregulated by HDL. These *in vitro* findings agree with our *in vivo* results showing that serum values of IL-1$\beta$ significantly increased in metabolic syndrome patients with low HDL levels as compared to metabolic syndrome patients without HDL reduction. Thus, present data suggest a direct relationship among increased percentage of nonclassical monocytes, elevated concentrations of IL-1$\beta$, and low HDL levels in patients with metabolic syndrome. In this sense, a previous work reported an association between IL-1$\beta$ gene polymorphisms and metabolic syndrome in patients with coronary heart disease [32]. Furthermore, Al-Shorman et al. recently showed that IL-1$\beta$ serum levels are significantly elevated in obese adolescents with metabolic syndrome as compared to normal-weight controls without metabolic alterations [33]. Altogether, this information concurs with our data that demonstrate elevation in the serum levels of IL-1$\beta$ in patients with metabolic syndrome. However, to the best of our knowledge this is the first report suggesting that nonclassical monocytes could be a main cellular source of IL-1$\beta$ in subjects with metabolic syndrome that show low HDL levels. The idea that both nonclassical monocytes and IL-1$\beta$ may exert their prominent inflammatory actions in metabolic syndrome patients is congruent with numerous works showing that systemic inflammation is linked to the pathogenesis of metabolic dysfunction [7, 18, 34, 35]. However, IL-1$\beta$ was only measured in serum samples and direct evidence regarding the role of nonclassical monocytes in IL-1$\beta$ production in metabolic syndrome patients remains to be further elucidated; therefore, discussion of these results makes no attempt to conjecture beyond that.

A final phenomenon captured in our study is that both classical and nonclassical monocytes show a strong interdependent relationship, most of all in the setting of metabolic syndrome. It has been previously demonstrated that M1 macrophages can be shifted toward M2 macrophages, and vice versa, in response to the cell microenvironment [36–38]. However, there is scant information supporting a possible shift between monocytes with no prominent inflammatory actions and monocytes primed to inflammatory activities. In this sense, our results suggest that classical monocytes may be converted into nonclassical monocytes in response to metabolic syndrome risk factors such as HDL, thus supporting the notion that monocytes and macrophages may be primed toward proinflammatory activation profiles in the early stages of metabolic dysfunction. The possibility that monocyte subsets can be influenced by metabolic syndrome risk factors should be taken into consideration when designing molecular therapeutic interventions aimed at switching nonclassical monocytes into classical monocytes in patients at higher cardiovascular risk such as individuals with metabolic syndrome.

## 5. Conclusions

Our data demonstrate for the first time that HDL reduction directly contributes to an increase in the nonclassical monocyte subpopulation and concomitantly a decrease in the classical monocyte percentage in patients with metabolic syndrome and in LPS-stimulated primary human monocytes *in vitro*. In this work, HDL reduction was also shown to induce higher IL-1$\beta$ production in LPS-stimulated primary human monocytes and associate with increased IL-1$\beta$ serum levels in patients with metabolic syndrome. Altogether, these findings support the notion that metabolic dysfunction has a pivotal component in the systemic inflammatory response that is mediated by dynamic changes in monocyte subpopulations. The exact molecular mechanisms by which HDL is able to modulate monocyte subpopulations and IL-

1$\beta$ production remain to be elucidated. The potential impact of understanding the role of metabolic signals in immune cell activation adds a compelling degree of urgency to further studies.

## Conflicts of Interest

The authors declare that there is no conflict of interest regarding the publication of this article.

## Acknowledgments

This work was supported by Grant no. 261575 from the Fondo Sectorial de Investigación y Desarrollo en Salud y Seguridad Social SS/IMSS/ISSSTE/CONACYT-México and is a component of the PhD requirements of Johanna L. Grün in the MD/PhD program of the University of Heidelberg. This project has received funding from the Marie Curie International Research Staff Exchange Scheme with the 7th European Community Framework Program under Grant Agreement no. 295185-EULAMDIMA.

## References

[1] L. Ziegler-Heitbrock, P. Ancuta, S. Crowe et al., "Nomenclature of monocytes and dendritic cells in blood," *Blood*, vol. 116, no. 16, pp. e74–e80, 2010.

[2] X. Ren, W. Mou, C. Su et al., "Increase in peripheral blood intermediate monocytes is associated with the development of recent-onset type 1 diabetes mellitus in children," *International Journal of Biological Sciences*, vol. 13, no. 2, pp. 209–218, 2017.

[3] E. F. Devevre, M. Renovato-Martins, K. Clement, C. Sautes-Fridman, I. Cremer, and C. Poitou, "Profiling of the three circulating monocyte subpopulations in human obesity," *The Journal of Immunology*, vol. 194, no. 8, pp. 3917–3923, 2015.

[4] H. Ghanim, A. Aljada, D. Hofmeyer, T. Syed, P. Mohanty, and P. Dandona, "Circulating mononuclear cells in the obese are in a proinflammatory state," *Circulation*, vol. 110, no. 12, pp. 1564–1571, 2004.

[5] R. Mukherjee, P. Kanti Barman, P. Kumar Thatoi, R. Tripathy, B. Kumar Das, and B. Ravindran, "Non-classical monocytes display inflammatory features: validation in sepsis and systemic lupus erythematous," *Scientific Reports*, vol. 5, no. 1, article 13886, 2015.

[6] C. Shi and E. G. Pamer, "Monocyte recruitment during infection and inflammation," *Nature Reviews Immunology*, vol. 11, no. 11, pp. 762–774, 2011.

[7] M. Fresno, R. Alvarez, and N. Cuesta, "Toll-like receptors, inflammation, metabolism and obesity," *Archives of Physiology and Biochemistry*, vol. 117, no. 3, pp. 151–164, 2011.

[8] M. A. de Matos, T. C. Duarte, V. d. O. Ottone et al., "The effect of insulin resistance and exercise on the percentage of $CD16^+$ monocyte subset in obese individuals," *Cell Biochemistry and Function*, vol. 34, no. 4, pp. 209–216, 2016.

[9] T. S. Han and M. E. Lean, "A clinical perspective of obesity, metabolic syndrome and cardiovascular disease," *JRSM Cardiovascular Disease*, vol. 5, 2016.

[10] S. A. Ritchie and J. M. C. Connell, "The link between abdominal obesity, metabolic syndrome and cardiovascular disease," *Nutrition, Metabolism and Cardiovascular Diseases*, vol. 17, no. 4, pp. 319–326, 2007.

[11] C. N. Lumeng and A. R. Saltiel, "Inflammatory links between obesity and metabolic disease," *The Journal of Clinical Investigation*, vol. 121, no. 6, pp. 2111–2117, 2011.

[12] S. A. Reina, M. M. Llabre, D. C. Vidot et al., "Metabolic syndrome in Hispanic youth: results from the Hispanic Community Children's Health Study/Study of Latino Youth," *Metabolic Syndrome and Related Disorders*, vol. 15, no. 8, pp. 400–406, 2017.

[13] S. M. Grundy, Brewer HBJr., J. I. Cleeman et al., "Definition of metabolic syndrome: report of the National Heart, Lung, and Blood Institute/American Heart Association conference on scientific issues related to definition," *Circulation*, vol. 109, no. 3, pp. 433–438, 2004.

[14] K. G. M. M. Alberti, P. Zimmet, and J. Shaw, "The metabolic syndrome—a new worldwide definition," *The Lancet*, vol. 366, no. 9491, pp. 1059–1062, 2005.

[15] C. Liu, R. Desikan, Z. Ying et al., "Effects of a novel pharmacologic inhibitor of myeloperoxidase in a mouse atherosclerosis model," *PLoS One*, vol. 7, no. 12, article e50767, 2012.

[16] S. Arora, S. K. Patra, and R. Saini, "HDL—a molecule with a multi-faceted role in coronary artery disease," *Clinica Chimica Acta*, vol. 452, pp. 66–81, 2016.

[17] E. A. Podrez, "Anti-oxidant properties of high-density lipoprotein and atherosclerosis," *Clinical and Experimental Pharmacology and Physiology*, vol. 37, no. 7, pp. 719–725, 2010.

[18] P. Holvoet, "Relations between metabolic syndrome, oxidative stress and inflammation and cardiovascular disease," *Verhandelingen - Koninklijke Academie voor Geneeskunde van Belgie*, vol. 70, no. 3, pp. 193–219, 2008.

[19] G. P. Fadini, F. Simoni, R. Cappellari et al., "Pro-inflammatory monocyte-macrophage polarization imbalance in human hypercholesterolemia and atherosclerosis," *Atherosclerosis*, vol. 237, no. 2, pp. 805–808, 2014.

[20] J. J. Christensen, L. T. Osnes, B. Halvorsen et al., "Altered leukocyte distribution under hypercholesterolemia: a cross-sectional study in children with familial hypercholesterolemia," *Atherosclerosis*, vol. 256, pp. 67–74, 2017.

[21] R. H. Yang, Y. F. Liu, X. J. Wang, J. G. Liang, and J. C. Liu, "Correlation between high density lipoprotein and monocyte subpopulations among stable coronary atherosclerotic heart disease patients," *International Journal of Clinical and Experimental Medicine*, vol. 8, no. 9, pp. 16969–16977, 2015.

[22] S. Jiang, D. Li, J. Li, and Y. An, "Correlation between high-density lipoprotein and monocyte subsets in patients with stable coronary heart disease," *Medical Science Monitor*, vol. 21, pp. 3129–3135, 2015.

[23] K. A. Krychtiuk, S. P. Kastl, S. Pfaffenberger et al., "Small high-density lipoprotein is associated with monocyte subsets in stable coronary artery disease," *Atherosclerosis*, vol. 237, no. 2, pp. 589–596, 2014.

[24] H. W. L. Ziegler-Heitbrock and R. J. Ulevitch, "CD14: cell surface receptor and differentiation marker," *Immunology Today*, vol. 14, no. 3, pp. 121–125, 1993.

[25] H. W. Löms Ziegler-Heitbrock, M. Frankenberger, and A. Wedel, "Tolerance to lipopolysaccharide in human blood monocytes," *Immunobiology*, vol. 193, no. 2-4, pp. 217–223, 1995.

[26] E. T. Rietschel, T. Kirikae, F. U. Schade et al., "Bacterial endotoxin: molecular relationships of structure to activity and function," *The FASEB Journal*, vol. 8, no. 2, pp. 217–225, 1994.

[27] D. Pajkrt, J. E. Doran, F. Koster et al., "Antiinflammatory effects of reconstituted high-density lipoprotein during human endotoxemia," *Journal of Experimental Medicine*, vol. 184, no. 5, pp. 1601–1608, 1996.

[28] A. Galbois, D. Thabut, K. A. Tazi et al., "*Ex vivo* effects of high-density lipoprotein exposure on the lipopolysaccharide-induced inflammatory response in patients with severe cirrhosis," *Hepatology*, vol. 49, no. 1, pp. 175–184, 2009.

[29] G. Thomas, R. Tacke, C. C. Hedrick, and R. N. Hanna, "Nonclassical patrolling monocyte function in the vasculature," *Arteriosclerosis, Thrombosis, and Vascular Biology*, vol. 35, no. 6, pp. 1306–1316, 2015.

[30] E. Idzkowska, A. Eljaszewicz, P. Miklasz, W. J. Musial, A. M. Tycinska, and M. Moniuszko, "The role of different monocyte subsets in the pathogenesis of atherosclerosis and acute coronary syndromes," *Scandinavian Journal of Immunology*, vol. 82, no. 3, pp. 163–173, 2015.

[31] J. Yang, L. Zhang, C. Yu, X. F. Yang, and H. Wang, "Monocyte and macrophage differentiation: circulation inflammatory monocyte as biomarker for inflammatory diseases," *Biomarker Research*, vol. 2, no. 1, p. 1, 2014.

[32] K. W. Carter, J. Hung, B. L. Powell et al., "Association of interleukin-1 gene polymorphisms with central obesity and metabolic syndrome in a coronary heart disease population," *Human Genetics*, vol. 124, no. 3, pp. 199–206, 2008.

[33] A. Al-Shorman, H. Al-Domi, and A. Faqih, "Markers of subclinical atherosclerosis in schoolchildren with obesity and metabolic syndrome," *Swiss Medical Weekly*, vol. 147, no. 2122, 2017.

[34] R. Cancello and K. Clement, "Is obesity an inflammatory illness? Role of low-grade inflammation and macrophage infiltration in human white adipose tissue," *BJOG: An International Journal of Obstetrics & Gynaecology*, vol. 113, no. 10, pp. 1141–1147, 2006.

[35] C. Bing, "Is interleukin-1$\beta$ a culprit in macrophage-adipocyte crosstalk in obesity?," *Adipocytes*, vol. 4, no. 2, pp. 149–152, 2015.

[36] F. O. Martinez, A. Sica, A. Mantovani, and M. Locati, "Macrophage activation and polarization," *Frontiers in Bioscience*, vol. 13, no. 13, pp. 453–461, 2008.

[37] D. L. Morris, K. Singer, and C. N. Lumeng, "Adipose tissue macrophages: phenotypic plasticity and diversity in lean and obese states," *Current Opinion in Clinical Nutrition and Metabolic Care*, vol. 14, no. 4, pp. 341–346, 2011.

[38] Y. C. Liu, X. B. Zou, Y. F. Chai, and Y. M. Yao, "Macrophage polarization in inflammatory diseases," *International Journal of Biological Sciences*, vol. 10, no. 5, pp. 520–529, 2014.

Hindawi
Journal of Diabetes Research
Volume 2018, Article ID 7209872, 11 pages
https://doi.org/10.1155/2018/7209872

*Clinical Study*

# Serum Levels of Interleukin-13 Increase in Subjects with Insulin Resistance but Do Not Correlate with Markers of Low-Grade Systemic Inflammation

**Camilo P. Martínez-Reyes,[1] Angélica Y. Gómez-Arauz,[1] Israel Torres-Castro,[1] Aarón N. Manjarrez-Reyna,[1] León F. Palomera,[1] Alfonso Olivos-García,[2] Edith Mendoza-Tenorio,[2] Gabriela A. Sánchez-Medina,[3] Sergio Islas-Andrade,[3] Guillermo Melendez-Mier,[3] and Galileo Escobedo[1]**

[1]*Unit of Experimental Medicine, School of Medicine, National University of Mexico, General Hospital of Mexico "Dr. Eduardo Liceaga", 06726 Mexico City, Mexico*
[2]*Departamento de Medicina Experimental, Facultad de Medicina, Universidad Nacional Autónoma de México, 04510 México, DF, Mexico*
[3]*Research Division, General Hospital of Mexico "Dr. Eduardo Liceaga", 06726 Mexico City, Mexico*

Correspondence should be addressed to Galileo Escobedo; gescobedog@msn.com

Received 1 September 2017; Revised 7 December 2017; Accepted 18 December 2017; Published 21 February 2018

Academic Editor: Bernard Portha



Experimental evidence in mice suggests a role for interleukin- (IL-) 13 in insulin resistance and low-grade systemic inflammation. However, IL-13 serum levels have not been assessed in subjects with insulin resistance, and associations of IL-13 with parameters of low-grade systemic inflammation are still unknown. Our main goal was to examine the systemic levels of IL-13 in patients with insulin resistance, while also studying the relationship of IL-13 with anthropometric, metabolic, and low-grade systemic inflammatory markers. Ninety-two participants were included in the study and divided into insulin-resistant patients and noninsulin-resistant controls. Blood levels of IL-13, glucose, insulin, triglycerides, cholesterol, tumor necrosis factor-alpha (TNF-$\alpha$), IL-10, proinflammatory (Mon-CD11c$^+$CD206$^-$), and anti-inflammatory (Mon-CD11c$^-$CD206$^+$) monocytes, as well as anthropometric parameters, were measured in all volunteers. Insulin-resistant patients showed 2.5-fold higher serum levels of IL-13 than controls ($P < 0.0001$) and significantly increased values of TNF-$\alpha$ and Mon-CD11c$^+$CD206$^-$, with concomitant reductions in IL-10 and Mon-CD11c$^-$CD206$^+$. Increased IL-13 was extraordinarily well associated with hyperglycemia ($r = 0.7362$) and hypertriglyceridemia ($r = 0.7632$) but unexpectedly exhibited no significant correlations with TNF-$\alpha$ ($r = 0.2907$), IL-10 ($r = -0.3882$), Mon-CD11c$^+$CD206$^-$ ($r = 0.2745$) or Mon-CD11c$^-$CD206$^+$ ($r = -0.3237$). This study demonstrates that IL-13 serum levels are elevated in patients with insulin resistance without showing correlation with parameters of low-grade systemic inflammation.

## 1. Introduction

Insulin resistance is a key pathophysiological event in the development of type 2 diabetes (T2D), a serious public health problem of global proportions, with alarmingly high morbidity and mortality rates in several countries including USA and Mexico [1, 2]. A growing body of clinical and experimental evidence has consistently shown that insulin resistance is linked to obesity and low-grade systemic inflammation [3, 4]. Specifically, increased body mass index (BMI) and visceral fat accumulation have been shown to augment the risk to develop dyslipidemia, hyperglycemia, and insulin resistance [5]. Low-grade systemic inflammation is characterized by abnormally high serum levels of proinflammatory cytokines (i.e., tumor necrosis factor alpha [TNF-$\alpha$]) and increased percentage of proinflammatory monocytes such

as monocytes that exhibit high expression of CD11c and no expression of CD206 (Mon-CD11c$^+$CD206$^-$) [6, 7]. Low-grade systemic inflammation is also associated with decreased serum concentrations of anti-inflammatory cytokines such as interleukin- (IL-) 10 and low percentages of monocytes exerting anti-inflammatory abilities as is the case of monocytes that show high expression of CD206 and no expression of CD11c (Mon-CD11c$^-$CD206$^+$) [7, 8]. High amounts of TNF-$\alpha$ have been reported to concur with increased adiposity [9], hypertriglyceridemia [8], and impaired insulin sensitivity in adipose and hepatic tissue [10]. Moreover, Saghizadeh and coworkers have previously demonstrated that TNF-$\alpha$ is actively expressed in skeletal muscle tissue of insulin-resistant patients as compared to subjects with normal insulin sensitivity [11]. In the same sense, TNF-$\alpha$ infusion in healthy individuals is able to induce muscle insulin resistance by increasing phosphorylation of p70 S6 kinase, extracellular signal-regulated kinase −1/2 (ERK-1/2), and c-Jun NH2 terminal kinase (JNK) [12]. Interestingly, phosphorylation of p70 S6 kinase, ERK-1/2, and JNK is associated with decreased activation of the insulin receptor substrate-1 (IRS-1) and Akt substrate 160 [12], which supports the notion that TNF-$\alpha$ is a major contributor of insulin resistance in skeletal muscle. On the other side, decreased IL-10 has been related to elevated serum concentrations of TNF-$\alpha$, increased proportion of Mon-CD11c$^+$CD206$^-$ over the Mon-CD11c$^-$CD206$^+$ subpopulation, hyperglycemia, and higher levels of insulin resistance in obese subjects [7, 13]. Therefore, low-grade systemic inflammation has now gained increasing attention since it appears to play a causative role in the development of insulin resistance in liver, adipose tissue, and skeletal muscle of obese patients [14].

IL-13 is a cytokine belonging to the alpha-helix protein family that is mainly produced by activated Th2 cells, mast cells, and basophils and has been widely studied in the scenario of helminth parasite infections and allergic asthma [15, 16]. Nevertheless, recent experimental evidence in mice has now found that IL-13 may also participate in low-grade systemic inflammation and insulin resistance [17, 18]. In this sense, it has been reported that exogenous administration of IL-13 improves insulin sensitivity while also decreasing TNF-$\alpha$ expression and macrophage infiltration in epididymal adipose tissue of C57BL/6J mice fed a high-fat diet (HFD) [17]. Likewise, a further study demonstrated that IL-13 gene transfer plays a protective role during experimental obesity by diminishing adipocyte hypertrophy, glucose intolerance, insulin resistance, and macrophage infiltration into adipose tissue of HFD-fed C57BL/6J mice [18]. Interestingly, IL-13 has been also associated with improved insulin secretion. In this sense, Darkhal and colleagues previously showed that IL-13 gene overexpression concurs with increased insulin serum levels in mice [18]. Additionally, a recent study demonstrated that IL-13 *in vitro* increases insulin secretion in beta-cells of humans and rats [19], supporting the fact that IL-13 also has an impact on insulin production and release. In parallel, IL-13 has been also shown to play a role in the development of insulin resistance in human beings. In this regard, a previous study demonstrated that IL-13 serum levels are reduced in T2D patients that exhibit increased insulin resistance [20]. However, the role of IL-13 in the pathogenesis of insulin resistance in humans is still unclear, and potential associations of this cytokine with parameters of low-grade systemic inflammation and metabolic dysfunction remain obscure.

The main goal of this work was to examine the systemic levels of IL-13 in patients with insulin resistance, while also studying the relationship of IL-13 with parameters of low-grade systemic inflammation such as TNF-$\alpha$, IL-10, Mon-CD11c$^+$CD206$^-$ percentage, and Mon-CD11c$^-$CD206$^+$ percentage, and other insulin resistance-related metabolic markers including fasting blood glucose and insulin, BMI, central obesity, body fat percentage, waist-to-hip ratio, triglycerides, and cholesterol.

## 2. Materials and Methods

*2.1. Subjects.* Ninety-two Mexican adult women and men from the south-central region of Mexico were included in the study. All of the volunteers provided written informed consent, previously approved by the institutional review board of the General Hospital of Mexico, which guaranteed that the study was conducted in accordance with the principles described at the Helsinki Declaration. Volunteers were excluded from the study if they had previous or recent diagnosis of *Diabetes Mellitus*, cardiovascular diseases, chronic renal disease, chronic or acute hepatic disease, blood pressure higher than 135/85 mm Hg, inflammatory or autoimmune disorders, acute or chronic infectious diseases, cancer, and endocrine disorders including hypothyroidism. We also excluded pregnant or lactating women, patients with cardiovascular drug therapy including anti-inflammatory, antiaggregant, and antihypertensive drugs, and subjects without having an overnight fasting of 8–10 hours. All participants enrolled into the study received full medical evaluation, including achievement of clinical history and physical examination by expert physicians.

*2.2. Insulin Resistance Assessment.* The insulin resistance level was estimated by means of calculating the homeostatic model assessment of insulin resistance (HOMA-IR) in each participant. The HOMA-IR value resulted from multiplying fasting insulin concentration (mU/l) by fasting glucose concentration (mmol/l) and then divided by 22.5. Cut-off points for insulin resistance were given according to previous studies validated in the Mexican population [21], as follows: subjects showing HOMA-IR $< 3.8$ were considered as the control group by having a normal level of insulin resistance. On the contrary, subjects showing HOMA-IR $\geq 3.8$ were considered as the insulin-resistant group by having a significant level of insulin resistance.

*2.3. Anthropometric Measurements.* BMI resulted from dividing corporal weight (kg) by height squared ($m^2$) and was recorded in all participants, as follows: BMI 18.5–24.9 kg/$m^2$, normal weight subjects; BMI 25–29.9 kg/$m^2$, overweight subjects; and BMI $\geq 30$ kg/$m^2$, obese subjects. Central obesity was estimated in each participant by measuring the midpoint

between the lower rib margin and iliac crest with a conventional tape in centimeters (cm). Cut-off point values for central obesity were given as follows: women showing 80 cm waist circumference or higher were considered to have central obesity, while men showing 90 cm waist circumference or higher were considered to have central obesity. Body fat percentage was individually estimated by means of using a body composition analyzer (TANITA®, Body Composition Analyzer, Model TBF-300A, Tokyo, Japan).

*2.4. Metabolic Measurements.* Blood samples were collected after overnight fasting and placed into pyrogen-free tubes (Vacutainer™, BD Diagnostics, NJ, USA) at room temperature. Afterwards, collection tubes were centrifuged at 1000$g$/4°C for 25 min and serum samples obtained and stored at −80°C until use. Serum levels of insulin were individually measured in triplicate by means of the Enzyme-Linked ImmunoSorbent Assay (ELISA), following the manufacturer's instructions (Abnova Corporation, Taiwan). Serum levels of glucose were individually measured in triplicate by the glucose oxidase assay, following the manufacturer's instructions (Megazyme International, Ireland). Total cholesterol and triglyceride levels were individually measured in triplicate by enzymatic assays according to the manufacturer's instructions (Roche Diagnostics, Mannheim, Germany). All biochemical parameters were measured at the same time to avoid procedural variations.

*2.5. Assessment of the Serum Levels of IL-13, TNF-α, and IL-10 by ELISA.* Blood samples were collected after overnight fasting and placed into pyrogen-free tubes (Vacutainer, BD Diagnostics, NJ, USA) at room temperature. Afterwards, collection tubes were centrifuged at 1000$g$/4°C for 25 min and serum samples obtained and stored at −80°C until use. Serum levels of IL-13, TNF-α, and IL-10 were determined in triplicate by ELISA, following the manufacturer's instructions (Peprotech, Mexico). All cytokines were measured at the same time to avoid procedural variations.

*2.6. Characterization of Monocyte Surface Markers by Flow Cytometry.* Blood samples were collected after overnight fasting and placed into pyrogen-free tubes containing EDTA (Vacutainer, BD Diagnostics, NJ, USA). Afterwards, collection tubes were centrifuged at 1800$g$/8°C for 10 min and white blood cells (WBCs) separated using a micropipette. WBCs were separately placed into 1.6 ml pyrogen-free eppendorf tubes containing 1 ml of ACK Lysing Buffer (Life Technologies, USA) and incubated at 4°C for 5 min. Immediately after, cell suspensions were centrifuged at 1800$g$/8°C for 5 minutes and resulting cell pellets washed twice using PBS 1X (Sigma-Aldrich, Mexico). After an extra centrifugation step, supernatants were discarded and resulting cell pellets resuspended in 50 $\mu$l of PBS 1X (Sigma-Aldrich, Mexico) for posterior cell counting using trypan blue staining with Neubauer chamber. In each case, 3 $\mu$l of Human TruStrain Reagent (BioLegend Inc., USA) was added to $1 \times 10^6$ WBCs and then incubated for 7 minutes on ice. Afterwards, each WBC sample was simultaneously incubated with human anti-CD14 PE/Cy7, anti-CD11c PE/Cy5, and anti-CD206/Cy7 APC at 8°C for 20 min in the absence of light. Analysis of the cell surface markers CD11c and CD206 was exclusively performed on CD14-positive cells that correspond to monocytes, using a FACSCanto II flow cytometer (BD Biosciences, Mexico) by means of BD FACSDiva™ software 6.0, acquiring 50,000 events per test in triplicate. PE/Cy7 mouse IgG2, APC/Cy7 mouse IgG1, and PE/Cy5 mouse IgG1 (BioLegend Inc., USA) were used as isotype control antibodies.

*2.7. Statistical Analysis.* Student's $t$-test was used to compare noninsulin-resistant (NIR) and insulin-resistant (IR) subjects in terms of age, HOMA-IR, BMI, waist circumference, body fat percentage, waist-to-hip ratio, fasting blood glucose, serum insulin, systolic blood pressure, total cholesterol, triglycerides, TNF-α, IL-10, Mon-CD11c$^+$CD206$^-$ percentage, and Mon-CD11c$^-$CD206$^+$ percentage. Student's $t$-test results are expressed as mean ± standard deviation. Pearson's correlation coefficient was calculated for examining the association of IL-13 with anthropometric, metabolic, and systemic inflammation parameters. Pearson's correlation coefficient results are expressed as coefficients ($r$) and $P$ values. Differences were considered significant when $P < 0.05$. All statistical analyses were performed using the GraphPad Prism 6.01 software.

## 3. Results

Ninety-two participants of both sexes were included in the study (47 noninsulin-resistant and 45 insulin-resistant subjects). No significant differences were found in age (for noninsulin-resistant controls mean age 31.02 ± 10.41 years, whereas for insulin-resistant subjects mean age 36.75 ± 11.18 years), woman/man proportion (23 women and 24 men in the noninsulin-resistant group, whereas 22 women and 23 men in the insulin-resistant group), and systolic blood pressure (SBP) (for noninsulin-resistant controls mean systolic pressure 128.40 ± 3.57 mmHg, whereas for insulin-resistant subjects mean systolic pressure 127.9 ± 4.28 mmHg) (Table 1). On the other hand, BMI, waist circumference, and body fat percentage exhibited a significant increase in insulin-resistant subjects as compared to noninsulin-resistant controls (Table 1). Similarly, fasting blood glucose, serum insulin, and HOMA-IR were also higher in the insulin-resistant group than in the noninsulin-resistant group (Table 1). When dyslipidemia was evaluated, triglyceride values showed a clear elevation in insulin-resistant subjects with respect to noninsulin-resistant controls; however, cholesterol levels did not significantly differ between groups (Table 1). In terms of systemic inflammatory parameters, serum levels of TNF-α were significantly increased in the insulin-resistant group as compared to noninsulin-resistant individuals, whereas IL-10 was clearly reduced in insulin-resistant subjects with respect to controls (Table 1). At the same time, insulin-resistant subjects showed a significant increase in the proinflammatory monocyte percentage (Mon-CD11c$^+$CD206$^-$) accompanied by decreasing numbers of monocytes with anti-inflammatory profile (Mon-CD11c$^-$CD206$^+$) as compared to controls. Figure 1 shows representative flow cytometry dot plots illustrating the

Table 1: Demographic, anthropometric, metabolic, and immunological characteristics of the study subjects.

| Parameters | NIR | IR | $P$ |
|---|---|---|---|
| Gender (W/M) | 23/24 | 22/23 | n.s. |
| Age (years) | 31.02 ± 10.41 | 36.75 ± 11.18 | n.s. |
| BMI (kg/m$^2$) | 26.82 ± 4.89 | 32.92 ± 2.34 | <0.001 |
| Waist circumference (cm) | 86.87 ± 13.00 | 105.00 ± 6.21 | <0.001 |
| Body fat (%) | 26.61 ± 8.15 | 36.99 ± 7.42 | <0.001 |
| Waist-to-hip ratio | 0.92 ± 0.12 | 0.97 ± 0.04 | n.s. |
| SBP (mmHg) | 128.4 ± 3.57 | 127.9 ± 4.28 | n.s. |
| Blood glucose (mg/dl) | 84.17 ± 9.79 | 104.9 ± 5.58 | <0.0001 |
| Serum insulin (mU/l) | 11.16 ± 2.38 | 21.56 ± 1.89 | <0.0001 |
| HOMA-IR | 2.28 ± 0.39 | 5.59 ± 0.64 | <0.0001 |
| Total cholesterol (mg/dl) | 193.7 ± 10.28 | 198.0 ± 10.18 | n.s. |
| Triglycerides (mg/dl) | 159.40 ± 37.93 | 256.6 ± 13.19 | <0.0001 |
| TNF-$\alpha$ (pg/ml) | 8.26 ± 3.45 | 30.29 ± 3.93 | <0.0001 |
| IL-10 (pg/ml) | 100.8 ± 26.41 | 37.04 ± 10.36 | <0.0001 |
| Mon-CD11c$^+$CD206$^-$ (%) | 28.30 ± 17.18 | 60.93 ± 20.68 | <0.001 |
| Mon-CD11c$^-$CD206$^+$ (%) | 24.23 ± 9.46 | 6.05 ± 5.71 | <0.0001 |

Data are expressed as mean ± standard deviation. Significant differences were estimated by means of performing two-way Student's $t$-test. Differences were considered significant when $P < 0.05$. W: women; M: men; BMI: body mass index; SBP: systolic blood pressure; HOMA-IR: homeostatic model assessment of insulin resistance; TNF-$\alpha$: tumor necrosis factor alpha; IL: interleukin; Mon CD11c$^+$CD206$^-$: proinflammatory monocytes; Mon CD11c$^-$CD206$^+$: anti-inflammatory monocytes; n.s.: nonsignificant differences.

amount of Mon-CD11c$^+$CD206$^-$ in (A) noninsulin-resistant controls and (B) patients with insulin resistance, as well as the amount of Mon-CD11c$^-$CD206$^+$ in (C) noninsulin-resistant controls and (D) patients with insulin resistance.

When IL-13 was examined, we found a significant 2.5-fold increase in the serum levels of IL-13 in insulin-resistant subjects as compared to noninsulin-resistant controls (37.69 ± 17.82 versus 15.88 ± 6.71 pg/ml, resp.) (Figure 2).

IL-13 was significantly elevated in the insulin-resistant group. Therefore, our next step was to identify anthropometric, metabolic, and inflammatory parameters that were clearly related to the elevation in the serum concentrations of this cytokine. IL-13 exhibited a strong positive correlation with BMI ($r = 0.6727$, $P < 0.0001$) and waist circumference ($r = 0.6394$, $P < 0.0001$) (Figures 3(a) and 3(b), resp.). Moreover, serum levels of IL-13 were moderately associated with body fat percentage ($r = 0.4310$, $P < 0.001$) and waist-to-hip ratio ($r = 0.2410$, $P = 0.026$) (Figures 3(c) and 3(d), resp.).

In the specific case of metabolic parameters, serum IL-13 showed a strong positive relationship with fasting blood glucose ($r = 0.7362$, $P < 0.0001$) and HOMA-IR ($r = 0.6673$, $P < 0.0001$) (Figures 4(a) and 4(c), resp.). Despite being significant, statistical correlation between IL-13 and serum insulin was positive but tended to be moderate ($r = 0.5468$, $P < 0.0001$) (Figure 4(b)). Furthermore, IL-13 was strongly related to the amount of triglycerides ($r = 0.7632$, $P < 0.0001$) but showed no significant correlation with total cholesterol ($r = 0.2104$, $P = 0.055$) (Figures 5(a) and 5(b), resp.).

In terms of systemic inflammatory markers, circulating levels of IL-13 exhibited no significant correlations with serum TNF-$\alpha$ ($r = 0.2907$, $P = 0.066$) or Mon-CD11c$^{+-}$ CD206$^-$ monocyte percentage ($r = 0.2745$, $P = 0.062$), both of them typical proinflammatory parameters (Figures 6(a) and 6(b), resp.). On the contrary, IL-13 was barely correlated with IL-10 serum levels ($r = -0.3882$, $P = 0.0471$) but showed no significant association with Mon-CD11c$^-$CD206$^+$ monocyte percentage ($r = -0.3237$, $P = 0.0544$), which have been shown to exert anti-inflammatory actions (Figures 6(c) and 6(d), resp.).

## 4. Discussion

IL-13 is a cytokine that belongs to the alpha-helix protein family and is mainly produced by Th2-activated T lymphocytes, mast cells, and basophils [22]. Besides having been shown to play a critical role in helminth parasite infections and allergic asthma [13, 14], IL-13 has been now suggested to exert additional functions in the development of metabolic alterations such as insulin resistance and hyperglycemia [17, 18]. However, clinical findings in humans regarding the role of IL-13 in metabolic disease are still controversial.

In this sense, it has been previously shown that serum levels of IL-13 are significantly reduced in type 2 diabetic patients with coronary artery disease as compared to healthy controls [23]. Similarly, a recent study demonstrated that type 2 diabetic patients show decreased serum levels of IL-13 with respect to normal-glucose tolerant individuals [20]. On the contrary, it has been also reported that morbidly obese patients with insulin resistance exhibit higher values of serum IL-13 than normal weight controls, and bariatric surgery was able to reduce IL-13 serum concentrations after 1-year of the surgical procedure [24]. Likewise, expression of interleukin-13 receptor subunit alpha-2 (IL-13RA2) has been demonstrated to increase in peripheral blood mononuclear cells (PBMC) of obese children with abnormal insulin sensitivity as compared to normal weight boys [25]. This apparent contradiction could be attributed to the possible role of IL-13 in the insulin resistance pathogenesis that involves the liver, adipose tissue, skeletal muscle, and pancreatic beta-cells. In this regard, a previous study in mice showed that IL-13 gene deficiency concurs with reduced phosphorylation of IRS-1 and AKT in liver, adipose tissue, and skeletal muscle, which was directly related to decreased insulin sensitivity in the aforementioned tissues [26]. Interestingly, IRS-1 and AKT phosphorylation was found to depend on the activation of the signal transducer and activator of transcription (STAT) 3 and STAT6 [26], a well-known family of transcription factors with the ability to elicit anti-inflammatory signaling pathways in response to IL-13. Also, IL-13 has been shown to promote insulin secretion in pancreatic beta-cells [19], which is associated with compensatory hyperinsulinemia aimed to counteract hyperglycemia and insulin resistance. Then, it is reasonable to speculate that IL-13 plays a protective role in insulin resistance by promoting IRS-1 and AKT phosphorylation in insulin-dependent tissues via STAT3 and STAT6 activation as well as improvement of the beta-cell function. However, together with other

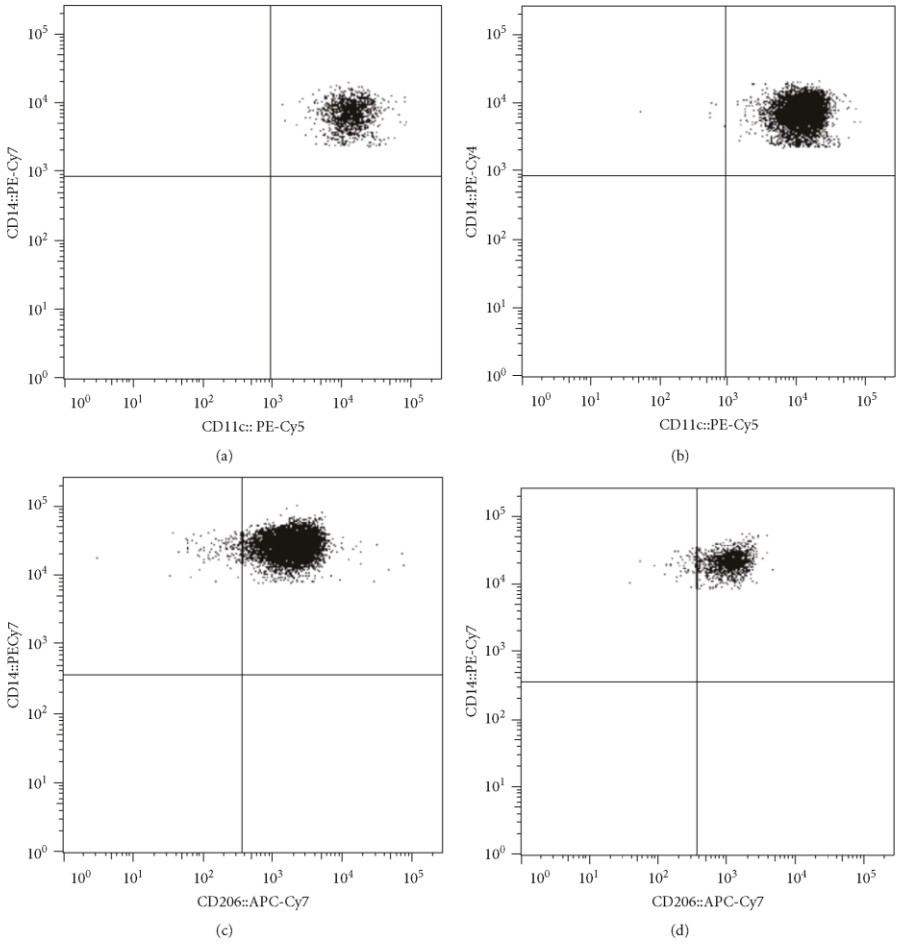


FIGURE 1: Representative dot plots showing percentages of proinflammatory and anti-inflammatory monocytes in patients with insulin resistance and noninsulin-resistant controls. (a) and (b) illustrate representative flow cytometry dot plots showing percentages of proinflammatory monocytes that express CD11c but do not express CD206 (Mon-CD11c$^+$CD206$^-$) in controls and insulin-resistant patients, respectively. (c) and (d) illustrate representative dot plots showing percentages of anti-inflammatory monocytes that express CD206 but do not express CD11c (Mon-CD11c$^-$CD206$^+$) in controls and insulin-resistant patients, respectively. Dot plot quantification can be seen in Table 1.

studies [17, 24, 25], our work shows a significant increase in the serum levels of IL-13 in insulin-resistant patients, which appears to disagree with previous evidence. In this sense, a previous work showed that IL-13 serum levels significantly increase as the severity of T2D-related chronic heart failure also increases [27]. Similarly, a very recent study demonstrated that IL-13 gene expression tended to increase in the left ventricular free wall of T2D patients with heart failure as compared to healthy donors [28]. Interestingly, despite IL-13 gene tended to be upregulated, the IL-13 receptor subunit alpha 1 (IL-13R$\alpha$1) production was significantly decreased in the same cardiac muscle specimens of T2D patients with heart failure, who are by definition insulin-resistant [28]. In some extent, this information is consistent with our findings and suggests a progressive loss of the cellular capacity to respond to IL-13 in the scenario of insulin resistance. Such a state of "IL-13 action resistance" may partially explain the increment of the IL-13 serum levels in

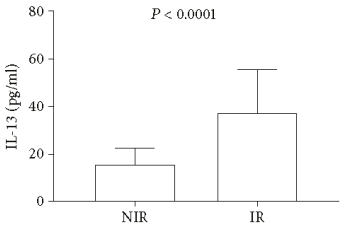


FIGURE 2: Serum levels of IL-13 in patients with insulin resistance and controls. Systemic levels of IL-13 showed a 2.5-fold significant increase in patients with insulin resistance as compared to noninsulin resistance controls. NIR: noninsulin resistance controls; IR: patients with insulin resistance. A 3.8 cut-off point was used for defining insulin resistance in the study population. Data are expressed as mean ± standard deviation. Differences were considered significant when $P < 0.05$ and calculated using Student's $t$-test.

several cohorts of patients with insulin resistance, including our own study population. To the best of our knowledge, this is one of the first studies suggesting a state of IL-13 action resistance, characterized by high levels of IL-13, reduced activation of the IL-13-dependent signaling pathway in insulin-dependent tissue, and consequently increased insulin resistance. Nevertheless, we have drawn a speculative hypothesis to explain the apparently contradictory results regarding the role of IL-13 in the development of insulin resistance, and the discussion of this information makes no attempt to conjecture beyond that. For this reason, it is still of enormous importance to study the role of IL-13 in the pathogenesis of insulin resistance, also evaluating the possible existence of a state of IL-13 action resistance in patients with altered insulin sensitivity.

In our study, serum concentrations of IL-13 exhibited a strong correlation with obesity-related anthropometrical parameters including BMI and central obesity. As it has been previously reported, increased BMI and central obesity are key contributing factors to the development of insulin resistance, metabolic syndrome, and type 2 diabetes [29]. Central obesity directly results from the expansion of white adipose cells that accumulate around the viscera of the abdominal cavity [30]. Interestingly, it has been recently shown that increased central obesity and body weight are associated with elevation in the circulating levels of IL-13 [31]. Furthermore, Kwon and coworkers demonstrated that IL-13 is overproduced in the white adipose tissue of HFD-fed mice and obese humans while also reported that adipocytes were the main cellular source of this cytokine [17]. These findings may explain the extremely strong association observed in our study between serum IL-13 levels and obesity-related anthropometrical parameters such as central obesity and, in some extent, BMI. In other words, our data confirm a direct link between fat mass expansion and IL-13 overproduction, which could be supported by the fact that hypertrophic and hyperplasic adipocytes increase their ability to synthesize IL-13. However, we only studied the relationship of obesity-related anthropometrical parameters with IL-13 serum concentrations by means of statistical correlation models and the discussion of these results makes no attempt to conjecture beyond that. Further research is needed to draw conclusions regarding the capacity of white adipose cells to release IL-13 into the bloodstream and the potential role of this cytokine in the development of insulin resistance in obese patients.

Another phenomenon captured in our study is that IL-13 serum levels appear to be extraordinarily correlated with elevated blood values of glucose in the study population, and especially in subjects with insulin resistance. Consistent with our results, Nehete and coworkers previously demonstrated that obese chimpanzees show increased serum levels of IL-13, glucose, and glucagon, a peptide hormone in charge of raising glucose concentration in the bloodstream [32]. This finding suggests a direct link among IL-13, glucagon, and elevated glucose levels. In this sense, glucagon-like peptide-1 (GLP-1) is a peptide hormone able to reduce glucose levels by restricting the secretion of glucagon [33]. Recently, GLP-1 has been also shown to decrease IL-13 production in LPS-treated human eosinophils [34], which supports the idea that increased serum IL-13 could be directly associated with elevated blood glucose levels via glucagon-dependent mechanisms. Nevertheless, it is important to note that IL-13 has been also demonstrated to downregulate the hepatic production of glucose in mice [26] and increase glucose uptake in skeletal muscle cells *in vitro* [20], which seems to disagree with our results. We want to speculate that such a discrepancy could be explained by the fact that protective effects of IL-13 depend on reaching a critical concentration, in which high IL-13 levels are able to counteract the elevation of blood glucose and insulin resistance. In this hypothetical scenario, it is expected to find a positive correlation between IL-13 and insulin, a hormone widely known to counteract the effects of glucagon and decrease glucose levels. Interestingly, our results show a positive correlation between increased IL-13 and elevated values of serum insulin. Consistent with this hypothesis, it has been recently demonstrated that IL-13 promotes beta-cell survival and insulin secretion in human pancreatic beta-cell *in vitro* cultures [19]. However, it is still of great importance to examine the possible effect of IL-13 in regulating glucagon, GLP-1, insulin, and blood glucose levels with the aim of merging apparently controversial data regarding the role of this cytokine in glucose metabolism.

Numerous studies have suggested a direct relationship between IL-13 and lipid metabolism, especially in the scenario of metabolic dysfunction. For instance, a recent work demonstrated that PBMC show increased IL-13 expression in type 2 diabetic nephropathy patients that also exhibit hypertriglyceridemia [35]. Similarly, overweight and obese pregnant women with gestational hypertension show increased IL-13 concentration, which in turn is associated with elevated triglyceride levels [36]. Moreover, metabolic syndrome subjects exhibit increased serum IL-13 that is also correlated with rising concentration of blood sugar and triglycerides [37]. Our data expand on this body of work by revealing that circulating levels of IL-13 are strongly correlated with triglyceride values in insulin-resistant individuals.

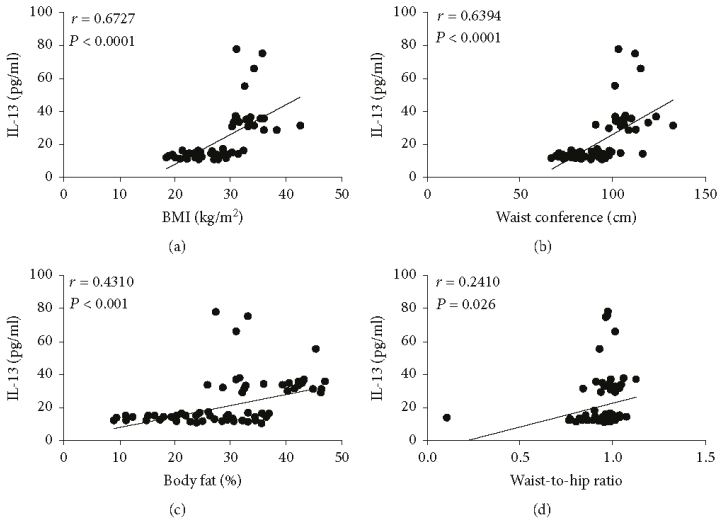


Figure 3: Correlation analysis between IL-13 serum levels and anthropometric parameters in the study population. (a) Correlation analysis between IL-13 serum levels and BMI. (b) Correlation analysis between IL-13 serum levels and waist circumference. (c) Correlation analysis between IL-13 serum levels and body fat percentage. (d) Correlation analysis between IL-13 serum levels and waist-to-hip ratio. Serum levels of IL-13 were moderately associated with BMI and waist circumference and showed to be barely related to body fat percentage and waist-to-hip ratio. BMI: body mass index. Coefficients ($r$) and $P$ values were calculated by Pearson's correlation model. The correlation level was considered significant when $P < 0.05$.

Interestingly, Tsao and coworkers previously demonstrated that IL-4, another Th2 cytokine with a similar structure and function to IL-13, is able to induce lipolysis in 3T3L1 adipocytes, thus increasing glycerol release and secretion into the culture supernatant [38]. This work concurs with our findings and reveals a novel function of Th2 cytokines in the regulation of triglyceride metabolism; however, there is no evidence yet exploring whether IL-13 may have a similar effect to IL-4. Further research is needed to evaluate the possible role of IL-13 in lipid metabolism and identify novel molecular targets with the aim of reducing triglyceride levels and cardiovascular risk in patients with insulin resistance.

Besides examining its association with insulin resistance-related metabolic markers, IL-13 was also studied in terms of low-grade systemic inflammation. As described above, low-grade systemic inflammation is hallmarked by increased levels of proinflammatory cells and cytokines whereby immune cells and cytokines with anti-inflammatory actions are decreased [39]. Consistent with this notion, we saw a clear elevation in the circulating levels of TNF-$\alpha$ and proinflammatory monocytes Mon-CD11c$^+$CD206$^-$ in insulin-resistant patients with respect to noninsulin-resistant controls. Simultaneously, circulating levels of IL-10 and anti-inflammatory monocytes Mon-CD11c$^-$CD206$^+$ were also significantly diminished in patients with insulin resistance. However, this state of low-grade systemic inflammation did not relate to serum IL-13, although several reports suggest an association of IL-13 with proinflammatory and anti-inflammatory immune responses [17, 18, 40, 41]. In this sense, it has been previously reported that IL-13 does not always correlate with low-grade systemic inflammation parameters. In fact, a recent study conducted in morbidly obese men with metabolic syndrome showed a significant increase in the serum levels of IL-6 and IL-12, both cytokines with proinflammatory actions, without reporting any difference in IL-13 [42]. Similarly, TNF-$\alpha$ soluble receptor levels were shown to raise in plasma of burn-induced systemic inflammatory response syndrome children whereas IL-13 serum levels remained unchanged [43]. Furthermore, Matia-García and coworkers recently reported that young obese subjects with hypertriglyceridemia exhibit low-grade systemic inflammation characterized by increasing levels of C-reactive protein (CRP) and IL-6, accompanied by reduced IL-10 serum concentration [44]. Interestingly, IL-13 showed neither statistical changes between obese and normal weight subjects nor significant correlation coefficients with CRP, IL-6, and IL-10 [44]. Therefore, our results reveal that serum levels of IL-13 elevate in insulin resistance without showing correlation with markers of low-grade systemic inflammation in humans.

Finally, it is important to note that serum IL-13 levels appear to be grouped in two main clusters, characterized by high and low production of this cytokine. Notably, ninety-five percent of low-IL-13 producers showed a HOMA-IR value below 3, whereas an inverse tendency was seen in high-IL-13 producers that exhibited increasing levels of

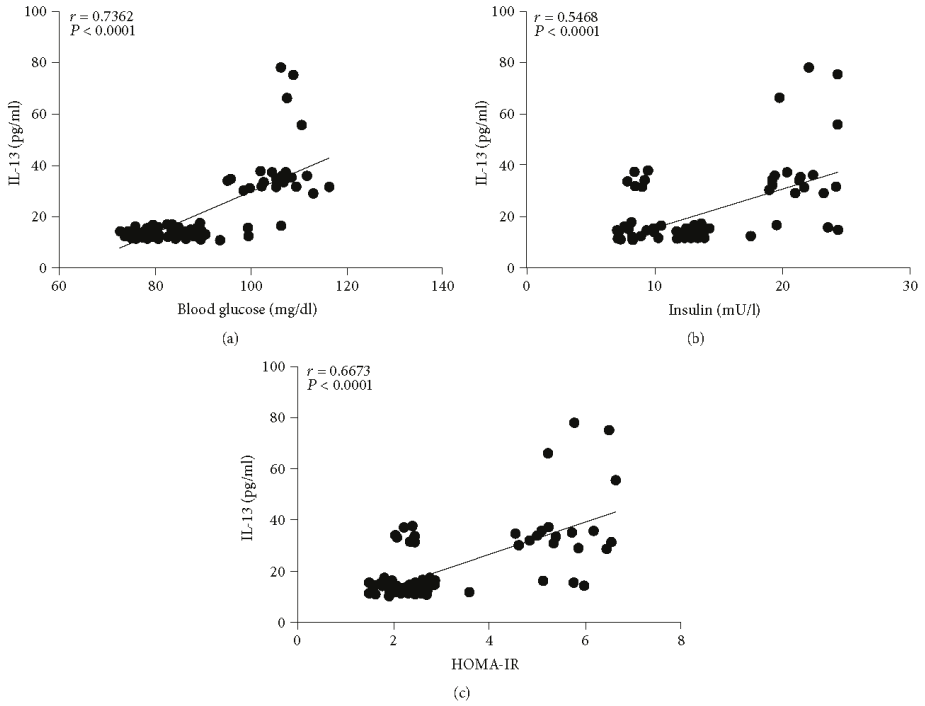


Figure 4: Correlation analysis between IL-13 serum levels and parameters of glucose metabolism in the study population. (a) Correlation analysis between IL-13 serum levels and blood glucose. (b) Correlation analysis between IL-13 serum levels and insulin. (c) Correlation analysis between IL-13 serum levels and HOMA-IR value. Serum levels of IL-13 were strongly associated with blood glucose and showed to be moderately related to insulin and HOMA-IR value. HOMA-IR, homeostatic model assessment of insulin resistance. Coefficients ($r$) and $P$ values were calculated by Pearson's correlation model. The correlation level was considered significant when $P < 0.05$.

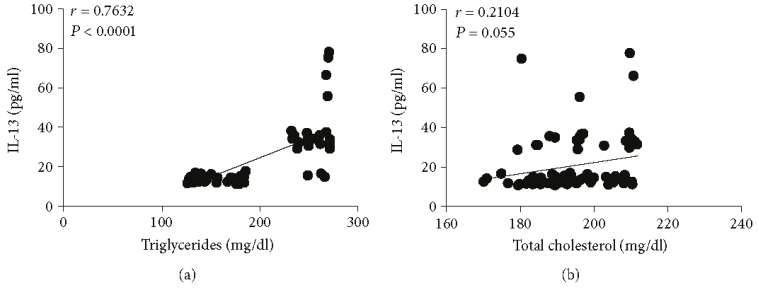


Figure 5: Correlation analysis between IL-13 serum levels and parameters of lipid metabolism in the study population. (a) Correlation analysis between IL-13 serum levels and triglycerides. (b) Correlation analysis between IL-13 serum levels and total cholesterol. Serum levels of IL-13 were strongly associated with blood triglycerides but showed no significant correlation with cholesterol. Coefficients ($r$) and $P$ values were calculated by Pearson's correlation model. The correlation level was considered significant when $P < 0.05$.

insulin resistance (HOMA-IR > 4.5). Moreover, ninety percent of high-IL-13 producers had central obesity and hyperglycemia, while a similar amount also showed triglyceride levels higher than 200 mg/dl (data not shown), which suggests that increased IL-13 could concur with the development of metabolic syndrome. However, we did not categorize the

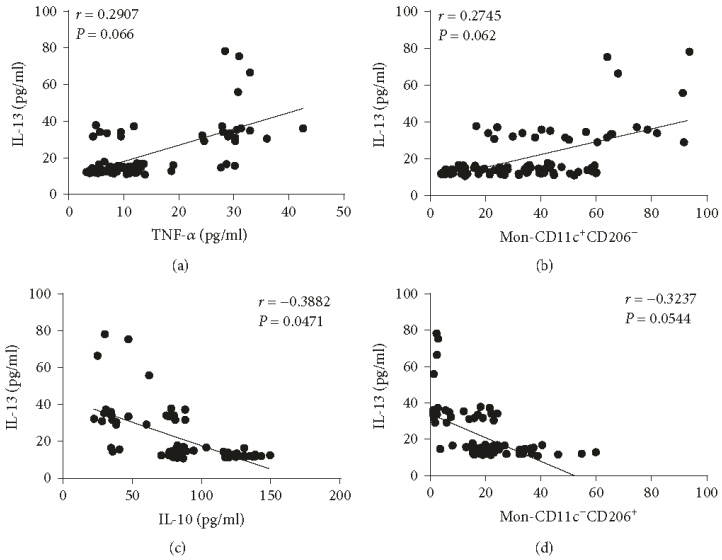


Figure 6: Correlation analysis between IL-13 serum levels and parameters of low-grade systemic inflammation in the study population. (a) Correlation analysis between IL-13 serum levels and circulating concentration of TNF-$\alpha$. (b) Correlation analysis between IL-13 serum levels and the percentage of proinflammatory monocytes Mon-CD11c$^+$CD206$^-$. (c) Correlation analysis between IL-13 serum levels and circulating concentration of IL-10. (d) Correlation analysis between IL-13 serum levels and the percentage of anti-inflammatory monocytes Mon-CD11c$^-$CD206$^+$. Serum levels of IL-13 were barely associated with IL-10 but showed no significant correlations with TNF-$\alpha$, Mon-CD11c$^+$CD206$^-$, and Mon-CD11c$^-$CD206$^+$. Mon-CD11c$^+$CD206$^-$, proinflammatory monocytes that express CD11c but do not express CD206; Mon-CD11c$^-$CD206$^+$, anti-inflammatory monocytes that express CD206 but do not express CD11c. Coefficients ($r$) and $P$ values were calculated by Pearson's correlation model. The correlation level was considered significant when $P < 0.05$.

study subjects according to the number of metabolic syndrome risk factors and the discussion of these results makes no attempt to conjecture beyond that. Further clinical research is needed to understand whether low and high-IL-13 producers have different risks for developing metabolic syndrome and its cardiovascular comorbidities.

## 5. Conclusions

This study demonstrates that serum levels of IL-13 are significantly elevated in insulin-resistant patients without showing correlation with parameters of low-grade systemic inflammation such as TNF-$\alpha$, IL-10, and monocytes that show expression of CD11c and CD206. Hyperglycemia and hypertriglyceridemia appear to be strongly linked to the increase in IL-13, which suggest a novel role of this cytokine in the regulation of glucagon-dependent pathways and lipolysis that should be addressed in patients at higher cardiovascular risk such as the vast majority of individuals living with insulin resistance, metabolic syndrome, and T2D. Current results also allow us to speculate regarding the existence of a state of IL-13 action resistance that could be associated with increased serum IL-13 levels in insulin-resistant patients, a notion that needs to be elucidated in basic and clinical research studies. The study of IL-13 in the development of insulin resistance may provide novel insights regarding the role of cytokines in the pathogenesis of metabolic disease and immune hyperactivation. We also remark the urgency of performing clinical studies evaluating whether IL-13 may represent a novel risk marker of insulin resistance in human beings.

## Conflicts of Interest

The authors declare that there is no conflict of interest regarding the publication of this article.

## Acknowledgments

This work was supported by Grants (no. 261575) from the Fondo Sectorial de Investigación y Desarrollo en Salud y Seguridad Social SS/IMSS/ISSSTE/CONACYT-México and CONACYT 247430 and is a component of the Ph.D. requirements of Camilo P. Martínez-Reyes in the Programa de Doctorado en Ciencias Biomédicas de la Universidad Nacional Autónoma de México. Camilo P. Martínez-Reyes thanks financial support from CONACYT by granting the Scholarship no. 414033.

## References


[1] R. Meza, T. Barrientos-Gutierrez, R. Rojas-Martinez et al., "Burden of type 2 diabetes in Mexico: past, current and future prevalence and incidence rates," *Preventive Medicine*, vol. 81, pp. 445–450, 2015.

[2] E. K. Spanakis and S. H. Golden, "Race/ethnic difference in diabetes and diabetic complications," *Current Diabetes Reports*, vol. 13, no. 6, pp. 814–823, 2013.

[3] N. Esser, S. Legrand-Poels, J. Piette, A. J. Scheen, and N. Paquot, "Inflammation as a link between obesity, metabolic syndrome and type 2 diabetes," *Diabetes Research and Clinical Practice*, vol. 105, no. 2, pp. 141–150, 2014.

[4] N. Mahalle, M. V. Kulkarni, S. S. Naik, and M. K. Garg, "Association of dietary factors with insulin resistance and inflammatory markers in subjects with diabetes mellitus and coronary artery disease in Indian population," *Journal of Diabetes and its Complications*, vol. 28, no. 4, pp. 536–541, 2014.

[5] R. V. Shah, V. L. Murthy, S. A. Abbasi et al., "Visceral adiposity and the risk of metabolic syndrome across body mass index: the MESA study," *JACC: Cardiovascular Imaging*, vol. 7, no. 12, pp. 1221–1235, 2014.

[6] S. U. Amano, J. L. Cohen, P. Vangala et al., "Local proliferation of macrophages contributes to obesity-associated adipose tissue inflammation," *Cell Metabolism*, vol. 19, no. 1, pp. 162–171, 2014.

[7] I. Torres-Castro, U. D. Arroyo-Camarena, C. P. Martinez-Reyes et al., "Human monocytes and macrophages undergo M1-type inflammatory polarization in response to high levels of glucose," *Immunology Letters*, vol. 176, pp. 81–89, 2016.

[8] S. Leon-Cabrera, Y. Arana-Lechuga, E. Esqueda-Leon et al., "Reduced systemic levels of IL-10 are associated with the severity of obstructive sleep apnea and insulin resistance in morbidly obese humans," *Mediators of Inflammation*, vol. 2015, Article ID 493409, 9 pages, 2015.

[9] T. Tzanavari, P. Giannogonas, and K. P. Karalis, "TNF-$\alpha$ and obesity," *Current Directions in Autoimmunity*, vol. 11, pp. 145–156, 2010.

[10] H. Kwon and J. E. Pessin, "Adipokines mediate inflammation and insulin resistance," *Frontiers in Endocrinology*, vol. 4, p. 71, 2013.

[11] M. Saghizadeh, J. M. Ong, W. T. Garvey, R. R. Henry, and P. A. Kern, "The expression of TNF alpha by human muscle. Relationship to insulin resistance," *The Journal of Clinical Investigation*, vol. 97, no. 4, pp. 1111–1116, 1996.

[12] P. Plomgaard, K. Bouzakri, R. Krogh-Madsen, B. Mittendorfer, J. R. Zierath, and B. K. Pedersen, "Tumor necrosis factor-$\alpha$ induces skeletal muscle insulin resistance in healthy human subjects via inhibition of Akt substrate 160 phosphorylation," *Diabetes*, vol. 54, no. 10, pp. 2939–2945, 2005.

[13] C. N. Lumeng, J. L. Bodzin, and A. R. Saltiel, "Obesity induces a phenotypic switch in adipose tissue macrophage polarization," *The Journal of Clinical Investigation*, vol. 117, no. 1, pp. 175–184, 2007.

[14] L. Chen, R. Chen, H. Wang, and F. Liang, "Mechanisms linking inflammation to insulin resistance," *International Journal of Endocrinology*, vol. 2015, Article ID 508409, 9 pages, 2015.

[15] K. Oeser, C. Schwartz, and D. Voehringer, "Conditional IL-4/IL-13-deficient mice reveal a critical role of innate immune cells for protective immunity against gastrointestinal helminths," *Mucosal Immunology*, vol. 8, no. 3, pp. 672–682, 2015.

[16] S. Agrawal and R. G. Townley, "Role of periostin, FENO, IL-13, lebrikzumab, other IL-13 antagonist and dual IL-4/IL-13 antagonist in asthma," *Expert Opinion on Biological Therapy*, vol. 14, no. 2, pp. 165–181, 2014.

[17] H. Kwon, S. Laurent, Y. Tang, H. Zong, P. Vemulapalli, and J. E. Pessin, "Adipocyte-specific IKK$\beta$ signaling suppresses adipose tissue inflammation through an IL-13-dependent paracrine feedback pathway," *Cell Reports*, vol. 9, no. 5, pp. 1574–1583, 2014.

[18] P. Darkhal, M. Gao, Y. Ma, and D. Liu, "Blocking high-fat diet-induced obesity, insulin resistance and fatty liver by overexpression of Il-13 gene in mice," *International Journal of Obesity*, vol. 39, no. 8, pp. 1292–1299, 2015.

[19] S. Rutti, C. Howald, C. Arous, E. Dermitzakis, P. A. Halban, and K. Bouzakri, "IL-13 improves beta-cell survival and protects against IL-1beta-induced beta-cell death," *Molecular Metabolism*, vol. 5, no. 2, pp. 122–131, 2016.

[20] L. Q. Jiang, N. Franck, B. Egan et al., "Autocrine role of interleukin-13 on skeletal muscle glucose metabolism in type 2 diabetic patients involves microRNA let-7," *American Journal of Physiology Endocrinology and Metabolism*, vol. 305, no. 11, pp. E1359–E1366, 2013.

[21] H. Q. Qu, Q. Li, A. R. Rentfro, S. P. Fisher-Hoch, and J. B. McCormick, "The definition of insulin resistance using HOMA-IR for Americans of Mexican descent using machine learning," *PLoS One*, vol. 6, no. 6, article e21041, 2011.

[22] J. Zhu, "T helper 2 (Th2) cell differentiation, type 2 innate lymphoid cell (ILC2) development and regulation of interleukin-4 (IL-4) and IL-13 production," *Cytokine*, vol. 75, no. 1, pp. 14–24, 2015.

[23] H. Madhumitha, V. Mohan, M. Deepa, S. Babu, and V. Aravindhan, "Increased Th1 and suppressed Th2 serum cytokine levels in subjects with diabetic coronary artery disease," *Cardiovascular Diabetology*, vol. 13, no. 1, p. 1, 2014.

[24] T. K. Nestvold, E. W. Nielsen, J. K. Ludviksen, H. Fure, A. Landsem, and K. T. Lappegard, "Lifestyle changes followed by bariatric surgery lower inflammatory markers and the cardiovascular risk factors C3 and C4," *Metabolic Syndrome and Related Disorders*, vol. 13, no. 1, pp. 29–35, 2015.

[25] D. O. Minchenko, V. V. Davydov, O. A. Budreiko et al., "The expression of *CCN2, IQSEC, RSPO1, DNAJC15, RIPK2, IL13RA2, IRS1,* and *IRS2* genes in blood of obese boys with insulin resistance," *Fiziologicheskiĭ Zhurnal*, vol. 61, no. 1, pp. 10–18, 2015.

[26] K. J. Stanya, D. Jacobi, S. Liu et al., "Direct control of hepatic glucose production by interleukin-13 in mice," *The Journal of Clinical Investigation*, vol. 123, no. 1, pp. 261–271, 2013.

[27] Y. Nishimura, T. Inoue, T. Nitto, T. Morooka, and K. Node, "Increased interleukin-13 levels in patients with chronic heart failure," *International Journal of Cardiology*, vol. 131, no. 3, pp. 421–423, 2009.

[28] U. Amit, D. Kain, A. Wagner et al., "New role for interleukin-13 receptor $\alpha$1 in myocardial homeostasis and heart failure," *Journal of the American Heart Association*, vol. 6, no. 5, article e005108, 2017.

[29] S. A. Westphal, "Obesity, abdominal obesity, and insulin resistance," *Clinical Cornerstone*, vol. 9, no. 1, pp. 23–31, 2008.

[30] D. C. Berry, D. Stenesen, D. Zeve, and J. M. Graff, "The developmental origins of adipose tissue," *Development*, vol. 140, no. 19, pp. 3939–3949, 2013.

[31] F. M. Schmidt, J. Weschenfelder, C. Sander et al., "Inflammatory cytokines in general and central obesity and modulating effects of physical activity," *PLoS One*, vol. 10, no. 3, article e0121971, 2015.

[32] P. Nehete, E. R. Magden, B. Nehete, P. W. Hanley, and C. R. Abee, "Obesity related alterations in plasma cytokines and metabolic hormones in chimpanzees," *International Journal of Inflammation*, vol. 2014, Article ID 856749, 11 pages, 2014.

[33] V. Marks, "Temporary removal: rebirth of the incretin concept; its conception and early development," *Peptides*, 2017, In press.

[34] P. D. Mitchell, B. M. Salter, J. P. Oliveria et al., "Glucagon-like peptide-1 receptor expression on human eosinophils and its regulation of eosinophil activation," *Clinical & Experimental Allergy*, vol. 47, no. 3, pp. 331–338, 2017.

[35] P. Lu, Y. Xu, Z. Su, and H. Xu, "Enhanced ILC2 activity contributes to metabolic syndrome multicomponent aggregation state in patients with type 2 diabetic nephropathy," *Xi Bao Yu Fen Zi Mian Yi Xue Za Zhi*, vol. 33, no. 6, pp. 820–825, 2017.

[36] L. H. Tangeras, M. Austdal, R. B. Skrastad et al., "Distinct first trimester cytokine profiles for gestational hypertension and preeclampsia," *Arteriosclerosis, Thrombosis, and Vascular Biology*, vol. 35, no. 11, pp. 2478–2485, 2015.

[37] J. Surendar, V. Mohan, M. M. Rao, S. Babu, and V. Aravindhan, "Increased levels of both Th1 and Th2 cytokines in subjects with metabolic syndrome (CURES-103)," *Diabetes Technology & Therapeutics*, vol. 13, no. 4, pp. 477–482, 2011.

[38] C. H. Tsao, M. Y. Shiau, P. H. Chuang, Y. H. Chang, and J. Hwang, "Interleukin-4 regulates lipid metabolism by inhibiting adipogenesis and promoting lipolysis," *Journal of Lipid Research*, vol. 55, no. 3, pp. 385–397, 2014.

[39] M. M. van Greevenbroek, C. G. Schalkwijk, and C. D. Stehouwer, "Obesity-associated low-grade inflammation in type 2 diabetes mellitus: causes and consequences," *The Netherlands Journal of Medicine*, vol. 71, no. 4, pp. 174–187, 2013.

[40] M. Chalubinski, E. Luczak, K. Wojdan, P. Gorzelak-Pabis, and M. Broncel, "Innate lymphoid cells type 2 - emerging immune regulators of obesity and atherosclerosis," *Immunology Letters*, vol. 179, pp. 43–46, 2016.

[41] S. K. Chang, A. C. Kohlgruber, F. Mizoguchi et al., "Stromal cell cadherin-11 regulates adipose tissue inflammation and diabetes," *The Journal of Clinical Investigation*, vol. 127, no. 9, pp. 3300–3312, 2017.

[42] A. Pilatz, C. Hudemann, J. Wolf et al., "Metabolic syndrome and the seminal cytokine network in morbidly obese males," *Andrology*, vol. 5, no. 1, pp. 23–30, 2017.

[43] J. P. Sikora, W. Kuzanski, and E. Andrzejewska, "Soluble cytokine receptors sTNFR I and sTNFR II, receptor antagonist IL-1ra, and anti-inflammatory cytokines IL-10 and IL-13 in the pathogenesis of systemic inflammatory response syndrome in the course of burns in children," *Medical Science Monitor*, vol. 15, no. 1, pp. CR26–CR31, 2009.

[44] I. Matia-García, J. Muñoz-Valle, Z. Reyes-Castillo et al., "Correlation between cytokine profile and metabolic abnormalities in young subjects," *International Journal of Clinical and Experimental Medicine*, vol. 9, no. 8, pp. 16596–16604, 2016.